INFORMATION TO USERS

This manuscript has been reproduced from the microfilm master. UMI films the text directly from the original or copy submitted. Thus, some thesis and dissertation copies are in typewriter face, while others may be from any type of computer printer.

The quality of this reproduction is dependent upon the quality of the copy submitted. Broken or indistinct print, colored or poor quality illustrations and photographs, print bleedthrough, substandard margins, and improper alignment can adversely affect reproduction.

In the unlikely event that the author did not send UMI a complete manuscript and there are missing pages, these will be noted. Also, if unauthorized copyright material had to be removed, a note will indicate the deletion.

Oversize materials (e.g., maps, drawings, charts) are reproduced by sectioning the original, beginning at the upper left-hand corner and continuing from left to right in equal sections with small overlaps.

Photographs included in the original manuscript have been reproduced xerographically in this copy. Higher quality 6" x 9" black and white photographic prints are available for any photographs or illustrations appearing in this copy for an additional charge. Contact UMI directly to order.

ProQuest Information and Learning
300 North Zeeb Road, Ann Arbor, MI 48106-1346 USA
800-521-0600

UMI®

University of Alberta

MODELLING WATER, CARBON, AND NITROGEN DYNAMICS IN CLASS – CANADIAN LAND SURFACE SCHEME

BY

SHUSEN WANG ©

A thesis submitted to the Faculty of Graduate Studies and Research in partial fulfillment of the requirements for the degree of

Doctor of Philosophy

Department of Renewable Resources

Edmonton, Alberta

Fall, 2000

National Library
of Canada

Acquisitions and
Bibliographic Services

395 Wellington Street
Ottawa ON K1A 0N4
Canada

Bibliothèque nationale
du Canada

Acquisitions et
services bibliographiques

395, rue Wellington
Ottawa ON K1A 0N4
Canada

Your file Votre référence

Our file Notre référence

The author has granted a non-exclusive licence allowing the National Library of Canada to reproduce, loan, distribute or sell copies of this thesis in microform, paper or electronic formats.

L'auteur a accordé une licence non exclusive permettant à la Bibliothèque nationale du Canada de reproduire, prêter, distribuer ou vendre des copies de cette thèse sous la forme de microfiche/film, de reproduction sur papier ou sur format électronique.

The author retains ownership of the copyright in this thesis. Neither the thesis nor substantial extracts from it may be printed or otherwise reproduced without the author's permission.

L'auteur conserve la propriété du droit d'auteur qui protège cette thèse. Ni la thèse ni des extraits substantiels de celle-ci ne doivent être imprimés ou autrement reproduits sans son autorisation.

0-612-59692-3

Canada

University of Alberta

Library Release Form

Name of Author:	Shusen Wang
Title of Thesis:	Modelling Water, Carbon, and Nitrogen Dynamics in CLASS – Canadian Land Surface Scheme
Degree:	Doctor of Philosophy
Year this Degree Granted:	2000

Permission is hereby granted to the University of Alberta Library to produce single copies of this thesis and to lend or sell such copies for private, scholarly or scientific research purpose only.

The author reserves other publication rights, neither the thesis nor extensive extracts from it may be printed or otherwise reproduced without the author's prior written permission.

Permanent address:

610C, Michener Park
Edmonton, Alberta, T6H 5A1
Canada

Date: May 17, 2000

University of Alberta

Faculty of Graduate Studies and Research

The undersigned certify that they have read, and recommend to the Faculty of Graduate Studies and Research, for acceptance, a thesis entitled **Modelling Water, Carbon, and Nitrogen Dynamics in CLASS – Canadian Land Surface Scheme** submitted by **Shusen Wang** in partial fulfillment of the requirements for the degree of **Doctor of Philosophy**.

Robert Grant

R.F. Grant (Supervisor)

Noorallah G- Juma

N.G. Juma

R.W. Wein

J.D. Wilson

T. A. Black.

T.A. Black (External)

Date: May 15, 2000

ABSTRACT

Land surface schemes in atmospheric General Circulation Models (GCMs) significantly affect the predicted surface climate. Over the past decade, several "second-generation" land surface schemes have emerged and dominated the modelling studies of climate by GCMs; CLASS, the Canadian Land Surface Scheme which was developed at the Canadian Climate Center for the Canadian GCM, is one of them. While it greatly improved the evaluations of land surface processes over its earlier version of the "first-generation" land surface scheme, it was realized recently that improperly prescribed vegetation parameters were the largest source of error in climate modelling.

These limitations were addressed in this thesis research by developing three modules in the current version of CLASS V2.6: *SVATC* – a carbon-coupled water transfer module in the soil-vegetation-atmosphere system; *PLANTC* – a dynamic plant module designed to simulate plant carbon and nitrogen processes including photosynthesis, respiration, growth and litterfall, etc.; and *SOILC* – a soil carbon and nitrogen module designed to simulate organic matter transformation processes in and on soil. This new version of CLASS physiologically couples plant water and carbon dynamics, implements plant litter and soil carbon biogeochemical cycles, emphasizes the role of nitrogen in land surface processes, and feeds back dynamically based vegetation parameters to the GCM. The CLASS has been improved by including carbon dioxide (CO_2) flux between land surfaces and the atmosphere, thus making the predictions of climate change more realistic.

Simulations were implemented on deciduous trees. Data from the Old Aspen (*Populus tremuloides*) site in the Southern Study Area (SSA-OA) of the Boreal Ecosystem-Atmosphere Study (BOREAS) were used to initialize and drive the model. Comparisons show that annual root mean square error and correlation coefficient between model output and measurements for daily evapotranspiration were 0.71 mm H_2O d^{-1} and 0.87, and for carbon exchange were 1.10 g C m^{-2} d^{-1} and 0.93. The model predicted this aspen ecosystem was a net carbon sink of 163.6 g C m^{-2} y^{-1} and 203.2 g C m^{-2} y^{-1} for 1994 and 1996, respectively. It accounted for about 16.7% of the total gross primary production (GPP) on average for the two years.

ACKNOWLEDGMENTS

A project this extensive could not have happened without the assistance from a lot of people and resources. I'd like to thank my supervisor, Dr. R. F. Grant for the assistance and guidance he has provided me over the years. Thanks also go to other members of my committee, Dr. N. G. Juma and Dr. R. W. Wein, for support and constructive suggestions. I am also grateful to my departmental reader, Dr. J.D. Wilson, for his advice, interest, and encouragement during the completion of this dissertation.

Special thanks to Dr. T. A. Black, my external examiner, and the related scientific researchers and data managers in the BOREAS project. They kindly helped me with some comprehensive datasets for the model run and tests. Dr. D. L. Verseghy, the CLASS project leader, provided me the original CLASS code of version 2.6. Without their help, this thesis research cannot have done.

I am indebted to Meteorological Service of Canada for funding my graduate studies and this research. Accolades must also go to Mike Abley, SIS lab of the Department of Renewable Resources, and CNS of the University of Alberta for computing support, and to fellow grad students – Una, Paolo, Bei, Shampa, Isacc, Zhaozhan, ... for adding another dimension to the tedious coding work.

To my parents, my wife, and my son I am most grateful; for the love, support and encouragement over the years. They have been the tower of moral support through this period. A chapter of life is closing and another must begin. I will always fondly remember my time as a graduate student and have gained many friendships as well as knowledge.

TABLE OF CONTENTS

Chapter 1 Introduction **1**

References 6

Chapter 2 General Model Structure **9**

2.1 Outline of Current Version of CLASS Model – V2.6 9

2.2 Discussion and Strategy on the New Developments in CLASS 16

2.3 Model Used Dataset 22

References 25

Chapter 3 Modelling Energy and Water Exchanges between Canopy and the Atmosphere in CLASS – the *SVATC* Module **29**

3.1 Introduction 29

3.2 Module Description 34

3.3 Parameterization, Simulation Results and Tests 42

3.4 Sensitivity Analyses 62

3.5 Conclusions and Discussion 65

References 67

Chapter 4 Modelling Plant Carbon and Nitrogen Processes in CLASS – the *PLANTC* Module **73**

4.1 Introduction 73

4.2 Module Description 75

4.3 Parameterization, Simulation Results and Tests 93

4.4 Sensitivity Analyses 114

4.5 Conclusions and Discussion 118

References 122

Chapter 5 Modelling Soil and Ecosystem Carbon and Nitrogen Processes in CLASS – the *SOILC* Module and the Overall Model Evaluation . **128**

5.1 Introduction 128

5.2 Module Description 131

5.3 Parameterization, Simulation Results and Tests 139

5.4 Sensitivity Analyses 154
5.5 Conclusions and Discussion 157
References 160

Chapter 6 General Conclusions and Discussion 164

References 170

Appendixes

A. Controlling Equations for the State Variables in the *PLANTC* Module 171
B. Controlling Equations for the State Variables in the *SOILC* Module 172

LIST OF TABLES

Table 3.1 Parameters Used in the *SVATC* Module. 44

Table 4.1 Parameters Used in the *PLANTC* Module 94

Table 4.2 Annual Carbon Budgets for Plant and the Ecosystem Simulated by the Model and Estimated by Other Researchers 113

Table 5.1 Parameters Used in the *SOILC* Module. 140

LIST OF FIGURES

Figure 2.1 Schematic diagram of CLASS version 2.6 10

Figure 2.2 The new model structure for CLASS 20

Figure 3.1 Schematic diagram for water and CO_2 processes around a stomate 36

Figure 3.2 Water flow processes in the soil-plant-atmosphere system implemented in the *SVATC* module 39

Figure 3.3 Simulated and tower measured half-hourly fluxes of net radiation, sensible heat and latent heat over the aspen canopy in the early growing season 47

Figure 3.4 The corresponding meteorological conditions during the comparison week in the early growing season 48

Figure 3.5 Simulated and tower measured half-hourly fluxes of net radiation, sensible heat and latent heat over the aspen canopy in the mid-growing season 49

Figure 3.6 The corresponding meteorological conditions during the comparison week in the mid-growing season 50

Figure 3.7 Simulated and tower measured half-hourly fluxes of net radiation, sensible heat and latent heat over the aspen canopy in the late growing season 51

Figure 3.8 The corresponding meteorological conditions during the comparison week in the late growing season 52

Figure 3.9 Linear regression relationship between simulated and tower measured half-hourly net radiation 55

Figure 3.10 Linear regression relationship between simulated and tower measured daily evapotranspiration 56

Figure 3.11 Diurnal pattern of plant root water uptake and transpiration under wet soil conditions 58

Figure 3.12 Diurnal pattern of plant root water uptake and transpiration under dry soil conditions 59

Figure 3.13 Sensitivity of simulated evapotranspiration to the variations of temperature, precipitation and CO_2 concentration 63

Figure 4.1 Schematic diagram of the *PLANTC* module 76

Figure 4.2 Schematic diagram of the components in the *PLANTC* module 77

Figure 4.3 Simulated and measured responses of leaf CO_2 exchange to radiation, CO_2, and temperature 98

Figure 4.4 Simulated and measured responses of leaf stomatal conductance to radiation, CO_2, and temperature 100

Figure 4.5 Diurnal changes of simulated plant gross photosynthesis, mainenance respiration, growth respiration, and net primary production........ 103

Figure 4.6 Annual distributions of simulated daily plant gross photosynthesis, maintenance respiration, and growth respiration for 1994 and 1996....... 106

Figure 4.7 Annual distributions of measured daily mean shortwave radiation, air temperature, and daily total precipitation in 1994............................. 107

Figure 4.8 Annual distributions of measured daily mean shortwave radiation, air temperature, and daily total precipitation in 1996............................. 108

Figure 4.9 Annual distributions of simulated daily net primary production for 1994 and 1996 110

Figure 4.10 Simulated and measured leaf area index for 1994 and 1996 111

Figure 4.11 Sensitivity of simulated gross primary production, autotrophic respiration, and net primary production to the variations of temperature, precipitation, and CO_2 concentration 115

Figure 5.1 Schematic diagram of the *SOILC* module 132

Figure 5.2 Impacts of soil water content on microbial decomposition rate 136

Figure 5.3 Impacts of microbial C:N ratio on the decomposition rate of lignin and cellulose 136

Figure 5.4 Diurnal changes of simulated heterotrophic respiration in winter and in summer, and the corresponding temperatures of the first soil layer 141

Figure 5.5 Annual courses of simulated daily heterotrophic respiration for 1994 and 1996 142

Figure 5.6 Simulated and measured annual courses of daily CO_2 fluxes on the soil surface 143

Figure 5.7 Simulated and measured half-hourly CO_2 exchanges between ecosystem and the atmosphere in winter and spring 145

Figure 5.8 Simulated and measured half-hourly CO_2 exchanges between ecosystem and the atmosphere in the middle and late growing season 146

Figure 5.9 Annual courses of simulated and tower measured daily CO_2 exchanges between ecosystem and the atmosphere for 1994 and 1996 151

Figure 5.10 Linear regression relationship between simulated and tower measured daily CO_2 exchanges between ecosystem and the atmosphere 152

Figure 5.11 Simulated annual carbon budgets for the Old Aspen ecosystem in the Southern Study Area 153

Figure 5.12 Sensitivity of simulated heterotrophic respiration to the variations of temperature, precipitation, and CO_2 concentration 155

Figure 5.13 Sensitivity of simulated net ecosystem production to the variations of temperature, precipitation, and CO_2 concentration 156

LIST OF SYMBOLS[*]

Symbol	**Definition**
Γ	compensation point for CO_2 fixation (μM)
Λ	leaf area index ($m^2\ m^{-2}$)
ψ_c	canopy water potential (m H_2O)
ψ_s	soil water potential (m H_2O)
$\alpha_{L+C,X}$	C:N ratio of lignin + cellulose in litter (kg C kg^{-1} N)
$\alpha_{S,X}$	C:N ratio in litter of tissue X (kg C kg^{-1} N)
Λ_{shaded}	leaf area index under shaded ($m^2\ m^{-2}$)
Λ_{sunlit}	leaf area index under sunlit ($m^2\ m^{-2}$)
b	path length for root water uptake (m)
C_a	CO_2 concentration of the air ($\mu mol\ mol^{-1}$)
$C_{L,X}$	substrate C in tissue X per unit ground area (kg C m^{-2})
$C_{S,X}$	structural C in tissue X per unit ground area (kg C m^{-2})
$[C_{L,X}]$	substrate C concentration in tissue X (kg C kg^{-1} C)
D_Y^C	C transformation of pool Y (kg C $m^{-2}\ s^{-1}$)
D_Y^N	N transformation of pool Y (kg N $m^{-2}\ s^{-1}$)
E	ratio of CO_2 fixation to electron transport (mol mol^{-1})
$F_{Y,X}^C$	litter partitioning of C to pool Y (kg C $m^{-2}\ s^{-1}$)
$F_{Y,X}^N$	litter partitioning of N to pool Y (kg N $m^{-2}\ s^{-1}$)
G_X^C	synthetic rate of substrate C to structural C (kg C $m^{-2}\ s^{-1}$)
G_X^N	synthetic rate of substrate N to structural N (kg N $m^{-2}\ s^{-1}$)
G_M^C	microbial biomass-C growth (kg C $m^{-2}\ s^{-1}$)

---

[*] Symbols for parameters used in the model are defined in Table 3.1, Table 4.1, and Table 5.1, and they are not included here.

G_M^N	microbial biomass-N growth (kg N m^{-2} s^{-1})
f_I	fraction of radiation intercepted by canopy (unitless)
h_s	relative humidity of the air (unitless)
I	absorbed photosynthetic active radiation (μmol m^{-2} s^{-1})
I_N	atmosphere N deposition (kg N m^{-2} s^{-1})
J	electron transport rate (μmol m^{-2} s^{-1})
LAI	leaf area index (m^{2} m^{-2})
L_d	root length density (m m^{-2})
L_R	root length (m)
$L_{L,X}^C$	litterfall of substrate C in tissue X (kg C m^{-2} s^{-1})
$L_{L,X}^N$	litterfall of substrate N in tissue X (kg N m^{-2} s^{-1})
$L_{S,X}^C$	litterfall of structural C in tissue X (kg C m^{-2} s^{-1})
$L_{S,X}^N$	litterfall of structural N in tissue X (kg N m^{-2} s^{-1})
N_I	inorganic N in soil (kg N m^{-2})
N_l	leaf nitrogen content (kg N kg^{-1} C)
$N_{L,X}$	substrate N in tissue X per unit ground area (kg N m^{-2})
$N_{S,X}$	structural N in tissue X per unit ground area (kg N m^{-2})
$[N_{L,X}]$	substrate N concentration in tissue X (kg N kg^{-1} C)
O_N	N output from soil (kg N m^{-2} s^{-1})
Q_N^d	nitrogen diffusive flow in soil (kg N m^{-2} s^{-1})
Q_N^m	nitrogen mass flow in soil (kg N m^{-2} s^{-1})
Q_N^u	root nitrogen uptake (kg N m^{-2} s^{-1})
$R_{a,X}$	autotrophic respiration rate of tissue X (kg C m^{-2} s^{-1})
$R_{g,X}$	growth respiration rate of tissue X (kg C m^{-2} s^{-1})
R_h	heterotrophic respiration (kg C m^{-2} s^{-1})
$R_{m,X}$	maintenance respiration rate of tissue X (kg C m^{-2} s^{-1})
r_c	canopy stomatal resistance (m^{2} s mol^{-1})

r_l	leaf stomatal resistance (m^2 s mol^{-1})
r_r	root radial resistance (s)
r_s	soil rhizosphere resistance (s)
r_x	root axial resistance (s)
T_c	canopy temperature (^{o}C)
$T^{C}_{X,Y}$	substrate C transport between tissue X and Y (kg C m^{-2} s^{-1})
$T^{N}_{X,Y}$	substrate N transport between tissue X and Y (kg N m^{-2} s^{-1})
$t^{N}_{L,X}$	substrate N retranslocation of tissue X (kg N m^{-2} s^{-1})
$t^{N}_{S,X}$	structural N retranslocation of tissue X (kg N m^{-2} s^{-1})
t_N	N retranslocation coefficient (unitless)
V_d	leaf dark CO_2 fixation rate (μmol m^{-2} s^{-1})
V_e	leaf light CO_2 fixation rate (μmol m^{-2} s^{-1})
V_l	leaf photosynthesis (μmol m^{-2} s^{-1})
WAI	wood area index (m^2 m^{-2})
X_C	root carbon exudation (kg C m^{-2} s^{-1})

Chapter 1 Introduction

Global climate change is one of the most complex and perplexing environmental issues of the present age. It has been studied intensively by scientists for several decades now. One of the central features of this research has been the development of numerical models – and, in particular, the powerful computer-based representation of the global climate system known as the General Circulation Model (GCM). Though it is just around 30 years old, it has become the essential tool in the practice of applied climatology and been widely considered to be the "best science" for the study of future climate change (Thompson and Perry, 1997).

A very important component of any GCM is the process coupling the land surface to the atmosphere – the land surface scheme. The land surface areas of the Earth represent significant sources, sinks, and reservoirs of heat, water, and carbon with respect to the atmosphere. In recent years, along with the proliferation of climate change studies using GCMs, the construction and refinement of land surface schemes suitable for coupling to GCMs has received increasing attention. With the recognition of their importance and the proliferation of land surface schemes, the Project for Inter-comparison of Land-surface Parameterization Schemes (PILPS) was conducted (Henderson-Sellers *et al.*, 1993). It was concluded that simulations of the surface climate by GCMs in terms of hydrological variables, temperature, heat fluxes, and circulations are very much dependent on the formulation of their land surface schemes. With the same atmospheric forcing data, different land surface schemes and parameters can achieve quite different annual equilibria of climate.

Recent examples that show the importance of land surface schemes in GCMs can be found from the improvements on climate predictions brought by the more realistic estimations of land surface albedo and water flux. It was found from the Boreal Ecosystem-Atmosphere Study (BOREAS) that the wintertime albedo of the boreal coniferous forest was measured to be much lower than the values used by a number of GCMs. Most land surface schemes treat snow albedo effects over the forest in the same way as for grass-covered or agricultural surfaces where the vegetation can be completely covered by snow to give a very high surface reflectance. In fact, forest vegetation usually projects above the snow, and even bare deciduous trees can present a very dark surface to the solar radiation (Betts and Ball, 1997). Shortwave radiation is therefore efficiently intercepted by the forest and largely converted into sensible heat flux and outgoing longwave radiation during the winter. Omission of this effect, for example, in the ECMWF (European Center for Medium-Range Weather Forecasting) model, which carried a winter albedo of around 0.8 as opposed to a value of around 0.25 as observed in the field, resulted in the systematic underestimation of near-surface winter air temperatures by up to 15°C during the BOREAS 1996 winter field campaign. By incorporating more representative winter albedo, the model has been greatly improved in the prediction of the near-surface air temperature, resulting in reduced lower tropospheric temperature biases and improved forecast scores over the North Pacific and North Atlantic (Sellers *et al.*, 1997a).

Water fluxes between the land surface and the atmosphere, as another example, were observed low at the above BOREAS forest sites and are not represented correctly in most atmospheric models. Due to low stomatal conductance, the transpiration rates are significantly depressed in the middle of the growing season. This makes the boreal forest a surprisingly strong source of sensible heat and a weak source of latent heat (Baldocchi *et al.*, 1997; Jarvis *et al.*, 1997), compared with temperate grassland sites (Sellers and Hall, 1992) and tropical forests (Shuttleworth *et al.*, 1984a, b). This situation often results in the generation of a very dry, warm lower troposphere with a deep and turbulent atmospheric boundary layer over the forest during the growing season, more typical of a lower-latitude arid zone than would be expected for a high-latitude biome supplied with plentiful water. In the ECMWF model, the systematic overestimation of the latent heat flux over the boreal forest resulted in over prediction of precipitation and cloudiness within the region during the BOREAS 1994 growing season (Sellers *et al.*, 1995). Again, improvements of the land surface water flux based on BOREAS measurements have had an immediate impact on the ECMWF performance (Sellers *et al.*, 1997b).

In the earlier land surface schemes, in order to avoid undue computational expense, land surfaces were treated as simple, finite reservoirs of heat and moisture – the so-called bucket schemes (Manabe, 1969; Carson, 1982), or the "first-generation" land surface schemes. For the surface thermal regime, the methods used included the assumption of zero heat capacity for the soil; the setting of the ground heat flux equal to a constant fraction of the surface net radiation; the "slab" approach for soil heat storage; and the force-restore approach of Deardorff (1978) for soil temperature. For the surface moisture regime, nearly all GCMs modelled a near-surface layer of soil as a bucket that could be filled by precipitation and snow melt (if any) and emptied by evaporation and by runoff; the latter occurred only when the bucket was full. The evaporation rate was a linear function of the amount of water in the bucket below some critical value. In these early models vegetation was not modelled as separate from the soil; its only effect was to change the surface roughness and albedo.

Over the past decade, with the advent of larger and faster computers and the increase of GCM spatial resolutions, several "second-generation" land surface schemes of varying complexity have been proposed. The marked difference between these two generations was the inclusion of the soil-vegetation-atmosphere transfer schemes (SVATs). In SVATs, vegetation is treated as a separate layer. Soil is divided into different layers and soil heat and moisture movement is simulated dynamically between these layers. The key elements of the surface calculations in most of the current land surface schemes include canopy conductance, aerodynamic resistance, albedo, water holding capacity and runoff. The first two land surface models of this type to be developed were the Biosphere-Atmosphere Transfer Scheme (BATS) (Dickinson *et al.*, 1986, 1992), and the Simple Biosphere scheme (SiB) (Sellers *et al.*, 1986). Some other schemes rapidly followed, such as the Goddard Institute for Space Studies (GISS) Model (Abramopoulos *et al.*, 1988), the Bare Essentials of Surface Transfer (BEST) (Pitman, 1988; Pitman *et al.*, 1991; Yang, 1992), and the Interaction

Soil-Biosphere-Atmosphere (ISBA) (Noilhan and Planton, 1989). In Canada, model development has been focused on the Canadian Land Surface Scheme "CLASS" (Verseghy, 1991, 2000; Verseghy *et al.*, 1993).

In recent years, it has been found that in current land surface schemes the neglect of dynamic biological processes of vegetation and climatic feedbacks on them is likely the largest error in climate modelling (Dickinson, 1995). Therefore much current work at the interface of climatology, geophysics, environmental physics and ecology is aimed at understanding such processes and feedbacks and including them in GCMs (Shackley *et al.*, 1998; Bounoua *et al.*, 1999). Sellers *et al.* (1997b) discussed the development for the "third-generation" land surface models which can be marked by including the coupled water-carbon cycles in plants. Nutrient conditions of the terrestrial ecosystems can also play important roles in the land surface processes. As observed at the BOREAS forest sites, the depressed transpiration rates in the middle of growing season are due to the low stomatal conductance associated with the low photosynthetic rates of these species, which are supposed to be the results of nutrient limitations, particularly nitrogen. However, to the best of the author's knowledge, most of the land surface schemes to date still do not have coupled water, carbon and nitrogen simulations. Impacts of nitrogen on the carbon processes, and thus on the water and energy processes, of vegetated land surfaces, have rarely been addressed. In addition, most of these schemes have focused on the momentum, radiation, sensible heat, and water vapour exchanges interactions between land surface and the atmosphere. The most important inducers of climate change, greenhouse gases such as CO_2, have not been involved.

To address these shortcomings and limitations, my research is focused on developing coupled water, carbon and nitrogen processes within the current version of CLASS – V2.6, which is a second-generation land surface model. Through physiological and biogeochemical simulations of the vegetated land surface, I try to improve the current energy and water calculations in CLASS, and enhance its ability by including the exchanges and interactions of greenhouse gas (CO_2), carbon, and nitrogen between the earth's terrestrial ecosystem and the atmosphere. Three new modules were developed for the purpose in this research, namely *SVATC* – a carbon coupled soil-vegetation-atmosphere water transfer module, *PLANTC* – a plant module for simulating the plant carbon and nitrogen processes, and *SOILC* – a soil module for simulating the plant litter and soil organic matter transformation processes. These three modules are closely linked with each other and with the calculations in the current CLASS model. Important outputs from this new version of CLASS include ecosystem CO_2 exchange with the atmosphere, gross primary production, net primary production, autotrophic respiration, heterotrophic respiration, plant tissue growth, litterfall production, root nitrogen uptake, and the revised energy balance and transpiration.

While a general introduction has been given in this chapter, the general model structure is introduced in Chapter 2. The main calculations in the current version of the CLASS model, V2.6, are outlined first, with emphasis on the parts that I am going to modify. The general scheme for the new development and improvement is discussed and sketched afterwards. At the end of Chapter 2, the main dataset used for driving and testing the model is briefly introduced. Chapter 3 describes the strategy and algorithm for the calculations in the *SVATC* module. The model outputs for energy and water exchanges based on the above calculations are then tested against measurements. Relationships between plant transpiration and root water uptake are also discussed. Sensitivity analyses of the model against some environmental variables are presented afterward. Chapters 4 and 5 follow the same format as Chapter 3, and give model descriptions, test, and sensitivity analyses for the *PLANTC* and *SOILC* modules, respectively. Also in Chapter 5, after all the three modules and their tests are finished, the overall model behavior on the carbon exchanges at the ecosystem level is evaluated. Chapter 6 gives some general conclusions from the model results and discussion on future developments.

References

Abramopoulos, F., Rosenzweig, C., and Choudhury, B., 1988. Improved ground hydrology calculations for global climate models (GCMs): Soil water movement and evapotranspiration. J. Climate, 1: 921-941.

Baldocchi, D.D., Vogel, C.A., and Hall B., 1997. Seasonal variation of energy and water vapor exchange rates above and below a boreal jack pine forest canopy. Journal Geophysical Research, 102, D24: 28,939-28952.

Betts, A.K. and Ball J.H., 1997. Albedo over the boreal forest. Journal of Geophysical Research, 102, D24: 28,901-28909.

Bounoua, L., Collatz, G.J., Sellers, P.J., Randall, D.A., Dazlich, D.A., Los, S.O., Berry, J.A., Fung, I., Tucker, C.J., Field, C.B., and Jensen, T.G., 1999. Interactions between vegetation and climate: radiative and physiological effects of doubled atmospheric CO_2. Journal of Climate, 12: 309-324.

Carson, D.J., 1982. Current parameterizations of land-surface processes in atmospheric general circulation models. In: Land Surface Processes in Atmospheric General Circulation Models, P.S. Eagleson (ed.), Cambridge University Press, Cambridge, 560pp.

Deardorff, J.W., 1978. Efficient prediction of ground surface temperature and moisture, with inclusion of a layer of vegetation. J. Geophys. Res., 83: 1889-1903.

Dickinson, R.E., 1995. Land surface processes and climate modeling, Bulletin of the American Meteorological Society, Vol. 76: 1445-1448.

Dickinson, R.E., Henderson-Sellers, A., Kennedy, P.J., and Wilson, M.F., 1986. Biosphere-Atmosphere Transfer Scheme (BATS) for the NCAR Community Climate Model, National Center for Atmospheric Research, Boulder, CO, Tech Note/TN-275+STR.

Dickinson, R.E., Henderson-Sellers, A., Kennedy, P.J., and Giorgi, F., 1992. Biosphere-Atmosphere Transfer Scheme (BATS) Version 1e as coupled to the NCAR Community Climate Model, National Center for Atmospheric Research, Boulder, CO, Tech Note.

Henderson-Sellers, A., Yang, Z.-L., and Dickinson, R.E., 1993. The project for intercomparison of land-surface parameterization schemes. Bulletin of the American Meteorological Society 74(7): 1335-1349.

Jarvis, P.G., Massheder, J.M., Hale, S.E., Moncrieff, J.B., Rayment, M., and Scott, S.L., 1997. Seasonal variation of carbon dioxide, water vapor, and energy exchanges of a boreal black spruce forest. Journal Geophysical Research, 102, D24: 28,953-28966.

Manabe, S., 1969. Climate and the ocean circulation: 1, the atmospheric circulation and the hydrology of the earth's surface. Mon. Wea. Rev., 97: 739-805.

Noilhan, J., and Planton, S., 1989. A simple parameterization of land surface processes for meteorological models. Mon. Wea. Rev., 117: 536-549.

Pitman, A.J., 1988. The development and implementation of a new land surface scheme for use in general circulation models, Ph.D. thesis, University of Liverpool, 481 pp.

Pitman, A.J., Yang, Z.-L., Cogley, J.G., and Henderson-Sellers, A., 1991. Description of Bare Essentials of Surface Transfer for the Bureau of Meteorology Research Center AGCM, BMRC Research Report No. 32, Melbourne, Victoria, 132 pp.

Sellers, P.J., Mintz, Y., Sud, Y.C., and Dalcher, A., 1986. A simple biosphere model (SiB) for use within general circulation models. J. Atmos. Sci., 43: 505-531.

Sellers, P.J. and Hall, F.G ., 1992. FIFE in 1992: Results, scientific gains, and future research directions. Journal of Geophysical Research, 97: 19,091-19,109.

Sellers, P.J., Hall, F., Margolis, H., Kelly, B., Baldocchi, D., den Hartog, G., Cihlar, J., Ryan, M.G., Goodison, B., Crill, P., Ranson, K.J., Lettenmaier, D., and Wickland, D.E., 1995. The Boreal Ecosystem-Atmosphere Study (BOREAS): An overview and early results from the 1994 field year. Bull. Am. Meteorol. Soc., 76: 1549-1577.

Sellers, P.J., Hall, F.G., Kelly, R.D., Black, A., Baldocchi, D., Berry, J., Ryan, M., Ranson, K.J., Crill, P.M., Lettenmaier, D.P., Margolis, H., Cihlar, J., Newcomer, J., Fitzjarrald, D., Jarvis, P.G., Gower, S.T., Halliwell, D., Williams, D., Goodison, B., Wichland, D.E., and Guertin, F.E., 1997a. BOREAS in 1997: Experiment overview, scientific results, and future directions. Journal of Geophysical Research, 102, D24: 28,731-28769.

Sellers, P.J., Dickinson, R.E., Randall, D.A., Betts, A.K., Hall, F.G., Berry, J.A., Collatz, G.J., Denning, A.S., Mooney, H.A., Nobre, C.A., Sato, N., Field, C.B., and Henderson-Sellers, A., 1997b. Modeling the exchanges of energy, water, and carbon between continents and the atmosphere. Science, 275: 502-509.

Shackley, S., Young, P., Parkinson, S., and Wynne, B., 1998. Uncertainty, complexity and concepts of good science in climate change modelling: are GCMs the best tools? Climatic Change 38: 159-205.

Shuttleworth, J.W., Gash, J.H.C., Lloyd, C.R., Moore, C.J., Roberts, J., *et al.*, 1984a. Eddy correlation of energy partition for Amazonian forest. Q. J. R. Meteorol. Soc., 110: 1143-1162.

Shuttleworth, J.W., Gash, J.H.C., Lloyd, C.R., Moore, C.J., Roberts, J., *et al.*, 1984b. Observations of radiation exchange above and below Amazonian forest. Q. J. R. Meteorol. Soc., 110: 1163-1169.

Thompson, R.D. and Perry, A., 1997. Applied Climatology – Principles and Approach. Routledge, London and New York. 36-48 pp.

Verseghy, D.L., 1991. CLASS - A Canadian land surface scheme for GCMs. I. Soil model. International Journal of Climatology 11: 111-113.

Verseghy, D.L., 2000. The Canadian Land Surface Scheme (CLASS): 1987–1997. Atmosphere-Ocean, (in press).

Verseghy, D.L., McFarlane, N.A., and Lazare, M., 1993. CLASS - A Canadian land surface scheme for GCMs. II. Vegetation model and coupled runs. International Journal of Climatology 13: 347-370.

Yang, Z.-L., 1992. Land surface processes in 3-dimensional climate models, Ph.D. thesis, Macquarie University, 437 pp.

Chapter 2 General Model Structure

The CLASS model is a second-generation land surface scheme that began to be developed in 1987 at the Canadian Climate Center (CCC) (Verseghy, 1991; Verseghy *et al.*, 1993). It is used to replace the former land surface scheme in the CCC GCM (McFarlane *et al.*, 1985, 1992), which like many older schemes, treated the soil as one layer and incorporated the force-restore method for the soil thermal regime and a "bucket" approach for the moisture regime. This new scheme incorporates three soil layers with physically-based calculations of heat and moisture transfers at the surface and across the layer boundaries. CLASS also developed the algorithms for heat transfer in snow distinguished from that in the soil. Another important development in CLASS is the treatment of vegetation. It includes physically-based calculation of energy and moisture fluxes from the canopy as well as radiation and precipitation cascades through it, and incorporates explicit thermal separation of the vegetation from the underlying ground.

The CLASS model has been developed to its version 2.6, with which my code will be developed and executed. The development phases of CLASS over the past ten years were traced by Verseghy (2000). In this chapter, the CLASS model is briefly outlined first in section 2.1, with emphasis on the parts that I am going to modify. Further details can be found in Verseghy (1991) and Verseghy *et al.* (1993). In section 2.2, the limitations in the current CLASS model are discussed first, followed by the strategy for the new model developments. Section 2.3 gives the background information about the main datasets used for the model initialization, boundary control and result test.

2.1 Outline of Current Version of CLASS Model – V2.6

Figure 2.1 shows the schematic diagram of the CLASS model organisation. Each modelled grid cell can have up to four subareas, representing bare soil, vegetation-covered, snow-covered and snow-and-vegetation covered "patches" of

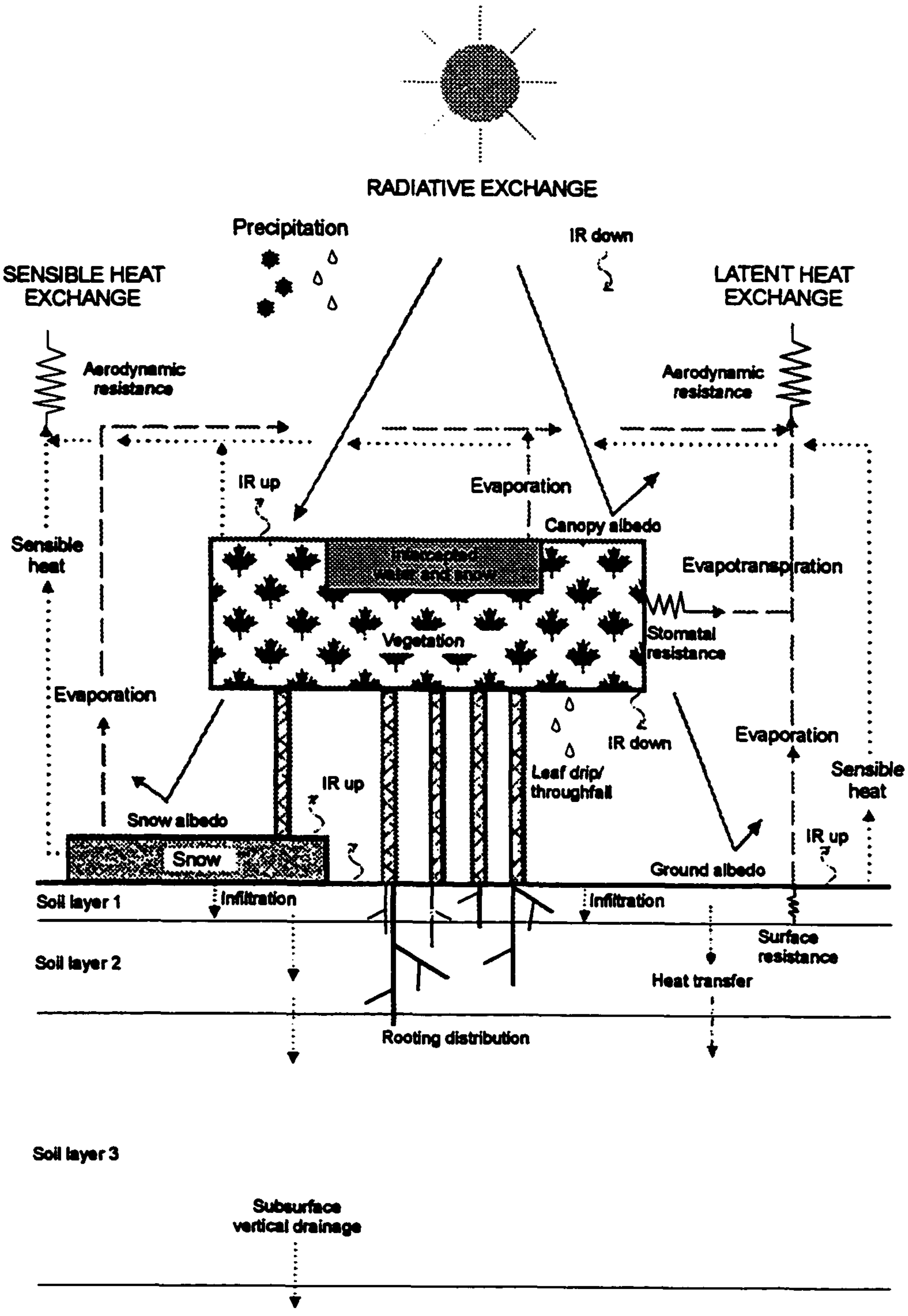
RADIATIVE EXCHANGE
Precipitation
IR down
SENSIBLE HEAT EXCHANGE
LATENT HEAT EXCHANGE
Aerodynamic resistance
Aerodynamic resistance
IR up
Evaporation
Canopy albedo
Sensible heat
Intercepted water and snow
Evapotranspiration
Vegetation
Stomatal resistance
Evaporation
IR down
Leaf drip/ throughfall
IR up
Evaporation
Sensible heat
Snow albedo
Snow
IR up
Ground albedo
Soil layer 1
Infiltration
Infiltration
Surface resistance
Soil layer 2
Heat transfer
Rooting distribution
Soil layer 3
Subsurface vertical drainage

Figure 2.1 Schematic diagram of CLASS version 2.6 (Verseghy, 2000)

the landscape. Inputs of meteorological variables at the bottom of the atmosphere are used to drive the energy and moisture balances for each of the subareas, and the resulting fluxes to the atmosphere are passed back to the GCM. The driving variables include the total incoming shortwave radiation, the incoming (or net) longwave radiation at the surface, the precipitation rate, the air temperature, the wind speed, the surface pressure, and the specific humidity of the air. The time step can be 30 minutes or shorter. In this research, it was set to 30 minutes.

The main calculations conducted in the model include energy balance, temperature regime, and water transfers of soil, snow and vegetation on the land surface.

2.1.1 Soil

CLASS represents three non-over lapping soil layers with the layer thicknesses of 0.10 m, 0.25 m, and 3.75 m. Soil layer temperatures and liquid and frozen moisture contents are carried as prognostic variables and are stepped forward in time. The change of average soil temperature $\overline{T}$ over one time step Δt of each layer i is calculated by applying the following finite-difference form of the one-dimensional heat conservation equation (Verseghy, 1991):

$$\overline{T}_i(t+1)=\overline{T}_i(t)+[G(z_{i-1},t)-G(z_i,t)]\frac{\Delta t}{C_i\Delta z_i}+S_i \tag{2.1}$$

where $G(z_{i-1},t)$ and $G(z_i,t)$ are the heat fluxes at the top and bottom of the layer, C_i is the volumetric heat capacity of the soil, Δz_i is the layer depth, and S_i is a correction term applied in case of freezing or thawing, or the percolation of ground water.

The heat fluxes between adjacent soil layers are calculated using the soil layer temperatures obtained in the previous time step. These two sets of variables are related by assuming that the temperature in each layer is a quadratic function of depth. Expressions for the average temperatures $\overline{T}_i$ are obtained by integrating $T(z)$ over each layer. G is then obtained by making use of Fourier's law for heat conduction in one dimension

$$G(z) = -\lambda(z)\left.\frac{dT}{dz}\right|_z \tag{2.2}$$

where $\lambda(z)$ is the thermal conductivity.

By assuming dT/dz at the bottom of the deepest layer is zero we can obtain a system of three linear equations in the unknown G, the surface temperature $T(0)$, and the known layer temperatures. Thus, if $T(0)$ is found, the heat flux terms can be evaluated.

Soil surface temperature can be obtained by combining the above system of equations for soil heat flux with the energy balance equation on the soil surface:

$$K_* + L_* + Q_{H,s} + Q_{E,s} = G(0) \tag{2.3}$$

where K_* and L_* are, respectively, the net shortwave and net longwave radiation absorbed at the surface, $Q_{H,s}$ and $Q_{E,s}$ are the sensible and latent heat fluxes at the soil-atmosphere interface, and $G(0)$ is the surface heat flux into the ground. In this equation, K_* and L_* are evaluated from the observed incoming shortwave and longwave radiation and the surface conditions, such as the albedo and temperature $T(0)$. $Q_{H,s}$ and $Q_{E,s}$ can be expressed as functions of surface temperature $T(0)$ and some atmospheric and surface conditions. Finally, the system of equations in the soil heat flux and surface energy balance is a function only of $T(0)$, certain atmospheric variables supplied by the GCM, and a set of known surface and soil properties. $T(0)$ can thus be evaluated by solving the above equations iteratively and substituted back to determine the energy balance terms, the heat fluxes between soil layers, and ultimately the layer temperatures for the next time step.

The average volumetric liquid and frozen moisture content, $\bar{\theta}_{l,i}$ and $\bar{\theta}_{f,i}$, are modelled for the same three soil layers as for the soil temperature, to allow coupling between soil temperature and water content. The change in $\bar{\theta}_{l,i}$ over a time step is calculated using the conservation equation analogous to temperature:

$$\bar{\theta}_{l,i}(t+1) = \bar{\theta}_{l,i}(t) + [F(z_{i-1},t) - F(z_i,t)]\frac{\Delta t}{\Delta z_i} + Q_{r,i} \tag{2.4}$$

where $F(z_{i-1},t)$ and $F(z_i,t)$ represent the liquid water flow rates at the top and bottom of the layer, respectively, evaluated using Darcy's equation. In the case of infiltration, the Green-Ampt method is used. If the infiltration capacity is exceeded, water is allowed to pond on the surface up to a maximum surface retention capacity which varies according to land cover. On the soil surface, $F(0)$ is given by the surface evaporation rate $Q_{E,s}/(L_v\rho_w)$ (L_v = latent heat of water evaporation, ρ_w = water density). When there is rain and its rate exceeds the evaporation rate, $F(0)$ is set to the infiltration rate. At the bottom of the third layer, $F(3)$ is calculated by the assumption of zero gradient of soil water potential ($d\psi_s/dz = 0$). The term $Q_{r,i}$ in the above equation represents plant root water uptake in the soil layer. It was not included in the original publication.

2.1.2 Snow

In CLASS, the snow pack is modelled as a fourth, variable-depth layer distinguished from the soil. The same set of equations for heat fluxes and surface energy balance as in the soil part are used for the snow calculations. The snow albedo and density are assumed to vary with time according to simple exponential decay functions and the calculated result for snow density is used to evaluate the snow heat capacity and thermal conductivity. The shortwave transmission within snow is calculated according to Beer's law using a constant extinction coefficient. Melting of the snow pack is simulated either when the solution of the surface energy balance equation results in a value of snow surface temperature greater than 0°C, or by conduction of heat from the soil underlying the snow pack, which may result in a soil temperature above zero. In this case, the excess energy is used to melt part of the snowpack and the temperature is set back to 0°C. Melted water percolates into the pack and refreezes until the temperature of the snowpack reaches the freezing point; any further melt is then allowed to reach the soil. The snow cover is assumed to be complete as long as the modelled snow depth does not fall below 0.10 m. When this occurs, the depth is reset to 0.10 m and a fractional snow coverage is calculated through the employment of conservation of snow mass.

2.1.3 Vegetation

In CLASS, the vegetation is treated as a single layer with up to two separate subareas in each grid square: vegetation-covered and vegetation-and-snow covered. Four broad vegetation groups are recognised within each canopy-covered subarea: needleleaf trees, broadleaf trees, crops and grass. Each of these vegetation types is characterised by a distinctive form of canopy architecture. They are therefore treated separately, and their effects are averaged to obtain "composite canopy" values of albedo, transmissivity, roughness length, unstressed stomatal resistance, standing mass, and rooting depth, etc. The canopy interception capacity of precipitation is calculated as a function of the leaf area index. Rain or snow which does not fall through gaps in the canopy fills the interception store until the capacity is exceeded, at which point any excess is allowed to run off and reach the ground.

The canopy is treated as a big leaf. Since the absorptivity, albedo, transmissivity, and other radiative properties of vegetation can show marked dependence on the wavelength and the angle of incoming radiation, CLASS uses different strategies for canopy radiation calculations under different wavelength (visible and near-infrared) and weather conditions (clear and cloudy skies). As shown later, CLASS is extremely successful in radiation estimations after it is modified.

Sensible and latent heat fluxes between the canopy and the atmosphere, $Q_{H,c}$ and $Q_{E,c}$, are modelled using the bulk aerodynamic approach which can be written as:

$$Q_{H,c} = \rho_a c_p \frac{T_a - \overline{T}_c}{r_a} \tag{2.5}$$

$$Q_{E,c} = \rho_a L_v \frac{q_a - q_{sat}(\overline{T}_c)}{r_a + r_c} \tag{2.6}$$

where ρ_a, c_p, T_a, and q_a represent the density, specific heat, temperature, and specific humidity respectively of the air at a reference height Z_R above the vegetation,

$q_{sat}(\overline{T}_c)$ is the saturation specific humidity at the canopy temperature $\overline{T}_c$, and r_a and r_c are the aerodynamic resistance and canopy stomatal resistance, respectively. When the canopy surface is covered with a film of intercepted precipitation, evaporation or sublimation takes place at the potential rate ($r_c = 0$) until the intercepted rain or snow is completely consumed.

Stomatal resistance is assumed to be affected by the environmental factors of the incoming solar radiation $K_{\downarrow}$, the air vapor pressure deficit Δe, the soil water suction ψ_s in the rooting zone (as a surrogate for leaf water potential since it is not calculated in the model, the value of ψ_s takes the minimum value of soil moisture suction found for the soil layers contained within the rooting zone), and the air temperature T_a. The effects of these factors are treated as multiplicative. Making use of the assumption that leaf resistance acts in parallel, r_c is obtained as:

$$r_c = r_{c,\min} f_1(K_{\downarrow}) f_2(\Delta e) f_3(\psi_s) f_4(T_a) \frac{\Lambda_{\max}}{\Lambda} \qquad (2.7)$$

where $r_{c,min}$ is a minimum resistance representing dense, green, unstressed canopies and $\Lambda_{\max}$ and Λ are the maximum and actual leaf area indices of the canopy.

To account for seasonal variations in the morphological characteristics of the four major canopy types, a growth index γ is carried for each. It has a value of 1 during periods when the vegetation is mature and/or fully leafed, and a value of 0 during dormant and leafless periods; the transition between the two is taken to be linear. With the prescribed parameters of maximum canopy height ($H_{\max}$), maximum standing mass, maximum vegetation rooting depth, and maximum and minimum leaf area index, the roughness length for momentum, the standing biomass, the rooting depth, and the leaf area index at each time step can thus be calculated using γ based linear equations. For example, the canopy leaf area index Λ for needleleaf and broadleaf trees is calculated according to the following equation:

$$\Lambda = \Lambda_{\min} + \gamma(\Lambda_{\max} - \Lambda_{\min}) \qquad (2.8)$$

2.2 Discussion and Strategy on the New Developments in CLASS

2.2.1 Physiology in Land Surface Processes

The inclusion of vegetation in land surface schemes as a layer distinct from soil in energy and water calculations in the CLASS model is a marked difference from the earlier generation schemes. However, as we can see from the model outline above, the vegetation is treated only as an additional physical layer in the model. There have been no dynamic plant physiological processes included yet. Some important parameters and processes of the vegetation, such as the stomatal resistance and plant leaf area index, are strongly controlled by plant physiological activities. But in the current model, these parameters or processes are fitted by prescribed curves or calculated from empirical equations. In fact, all of the second-generation land surface schemes coupled with GCMs represent poorly the physiological processes of vegetation. For example, in BATS (Dickinson *et al.*, 1986, 1992), canopy resistance is a function of minimum stomatal resistance, maximum stomatal resistance, visible solar radiation, leaf temperature, vapor pressure deficit, and soil moisture. As in CLASS, these limit factors are expressed in a multiplicative form. The same approach has been followed in BEST (Pitman, 1988; Pitman *et al.*, 1991; Yang, 1992) and in ISBA (Noilhan and Planton, 1989). In the GISS (Abramopoulos *et al.*, 1988), a bulk canopy stomatal resistance is given by r_{min}/LAI_e, where LAI_e is the effective leaf area index used to account for the attenuation of radiation as light passes through the canopy and the coincident decrease in plant surface that is actively transpiring. In the UKMO (Warrilow *et al.*, 1986), a constant value of the stomatal resistance is used. In SiB (Dorman and Sellers, 1989), a more elaborate formulation of r_c is used in which a sophisticated account of PAR (Photosynthetic Active Radiation) flux within the canopy is considered. In all of these schemes above, the physiological and biochemical controlling mechanisms on r_c are not considered.

Physiological processes of vegetation play important roles in determining the land surface processes and affecting the climate. Changes in the resistance from the soil-root-canopy system have profound impacts on shaping the energy partitioning of ecosystem. For example, the sensible heat flux over the boreal forest was observed to be unexpectedly high in the spring (Baldocchi *et al.*, 1997; Jarvis *et al.*, 1997). This seems to be due to late thawing of the soil, so the root systems remain frozen, which leads to a very high soil rhizosphere-root resistance to the water flow and canopy transpiration is thus cut off. In the middle of the growing season, the transpiration was also depressed, which was speculated to be due to the low stomatal conductance caused by the nutrient-poor environments. These small-scale physiological processes greatly impact the land surface processes and can have large-scale consequences. For example, observations from the BOREAS project have shown that the boundary layer depth over the boreal coniferous forest is similar to that measured over the Arabian desert even though the boreal landscape is wet (Margolis and Ryan, 1997). Through analyses and comparisons of the currently available GCMs, it was found that the largest source of error for determining climate over land is from the neglect of the resistance by stomata to water flux (Dickinson, 1995). It is therefore expected that better representations of this resistance and its dependencies on biological and environmental factors will provide further improvements to climate models, which may only be obtained by developing more physiologically-based models.

On the other hand, only with the inclusion of physiological processes can a climate model reflect the mechanisms of the many climatic feedbacks on the terrestrial ecosystems. Changes in the physical climate system can bring changes in the ecological functioning of the biome. It is anticipated that these may be accompanied by alterations in the biophysical characteristics of the surface; namely albedo, surface roughness, plant phenology, etc. Any changes in these may have feedback effects on the near-surface climatology, such as temperature, humidity, precipitation and cloudiness fields (Sato *et al.*, 1989).

2.2.2 Carbon and Nitrogen Biogeochemical Cycle in Land Surface Processes

The biogeochemical processes of terrestrial ecosystems, such as the carbon and nitrogen cycles, also interact with climate to a great extent. Temperature and precipitation anomalies have been compared with seasonal variations in atmospheric

CO_2 concentration. It is found that warm years over the northern continents are associated with a net terrestrial carbon sink, while cold and/or dry years are associated with a net source of terrestrial carbon (Keeling *et al.*, 1995; Ciais *et al.*, 1995; Denning *et al.*, 1995). It was estimated that the standing stocks of soil carbon in the top 1 m are three times as large as all of the standing crop biomass carbon in the global terrestrial biomes (Houghton *et al.*, 1985) and twice the 750 Pg carbon present in the atmosphere as CO_2 (Eswaran *et al.*, 1993). The soil and plant carbon dynamics and thereby the evolution of the principal greenhouse gases, namely carbon dioxide, methane, and nitrous oxide, are strongly controlled by climatic conditions, such as temperature and humidity. The extent of involvement of the terrestrial ecosystems in the evolution of greenhouse gases now becomes one of the major concerns of scientists interested in global change.

On the other hand, the feedbacks of climatic change on primary production and then on soil carbon stocks, are very large. Many results from experiments show that CO_2 enrichment can significantly increase the photosynthetic rate of plants, especially C_3 plants. Plant derived inputs are the primary source of organic substrate to soils, and such inputs, both from turnover of dead material and release of organic compounds from growing roots, are likely to increase at elevated CO_2. In addition, several studies have indicated that the biochemical composition of plant tissue is altered at elevated CO_2 (Curtis *et al.*, 1989; Conroy, 1992; Smart *et al.*, 1994), thus altering the quality of substrate entering soil. Typically, tissue C:N ratios increase at elevated CO_2 and the rate of microbial decomposition of both shoot and root material in soil is reduced (Couteaux *et al.*, 1991; Gorissen *et al.*, 1995). Concurrent with increased organic input from plants, uptake of mineral nutrients from soil to support growth is likely to increase. Therefore, the nutritional status of the soil is likely to shift in response to elevated atmospheric CO_2 concentration. Nutrients such as nitrogen can significantly affect the carbon cycles in the terrestrial ecosystems. This shift in soil nutrient status will in turn affect the land surface processes through their impacts on plant physiological processes.

Another point that illustrates the importance of developing the algorithms on biogeochemical cycles in land surface models is that only by completing the carbon and nitrogen biogeochemical cycles can we achieve the net carbon estimations in a ecosystem, such as the CO_2 flux between the land surface and the atmosphere. CO_2 is a very important variable in GCM simulations and climate studies. Improving the land surface scheme by including a CO_2 flux which is a dynamic result of the interactions between climate and ecosystem will significantly enhance the capabilities for climate simulations.

Recently, Sellers *et al.* (1996) revised their land surface scheme (SiB) into a new version (SiB2) by linking the stomatal resistance with photosynthesis, thus coupling water process with carbon process. This new scheme of coupling water and carbon has been proposed as the "third-generation" land surface models (Sellers *et al.*, 1997a), which has caused much interest in land surface modelling research. However, in the available land surface schemes coupled with GCMs to date, systematically addressed physiological and biogeochemical processes have not been included yet. With the realisation of the importance of the terrestrial ecosystems in the global climate change, there is a rapidly growing interest in coupling these processes with climate models (Dickinson *et al.*, 1998).

2.2.3 Proposed Model Development

In the research of this thesis, I intend to implement plant physiological algorithms that control the land surface energy and water processes, and biogeochemical algorithms that control the plant and soil carbon and nitrogen dynamics and their interactions with the atmosphere. Three modules (*SVATC*, *PLANTC*, and *SOILC*) and one interface (*CLASSC*) were developed in CLASS for this purpose as shown by the dotted part in Figure 2.2.

SVATC is a carbon coupled water transfer module in the soil-vegetation-atmosphere system designed to improve the energy balance calculations of the canopy in CLASS. A series of hydraulic resistances in the soil rhizosphere and plant root systems, the stomatal resistance coupled with carbon calculations using the Ball-

Berry model (Ball *et al*, 1987), and the plant water capacitance were explicitly calculated in this module. The canopy temperature and water potential were used as the prognostic variables and obtained by iteratively solving the energy and water balance equations. Energy and water exchanges between vegetated land surfaces and the atmosphere are directly determined by this module.

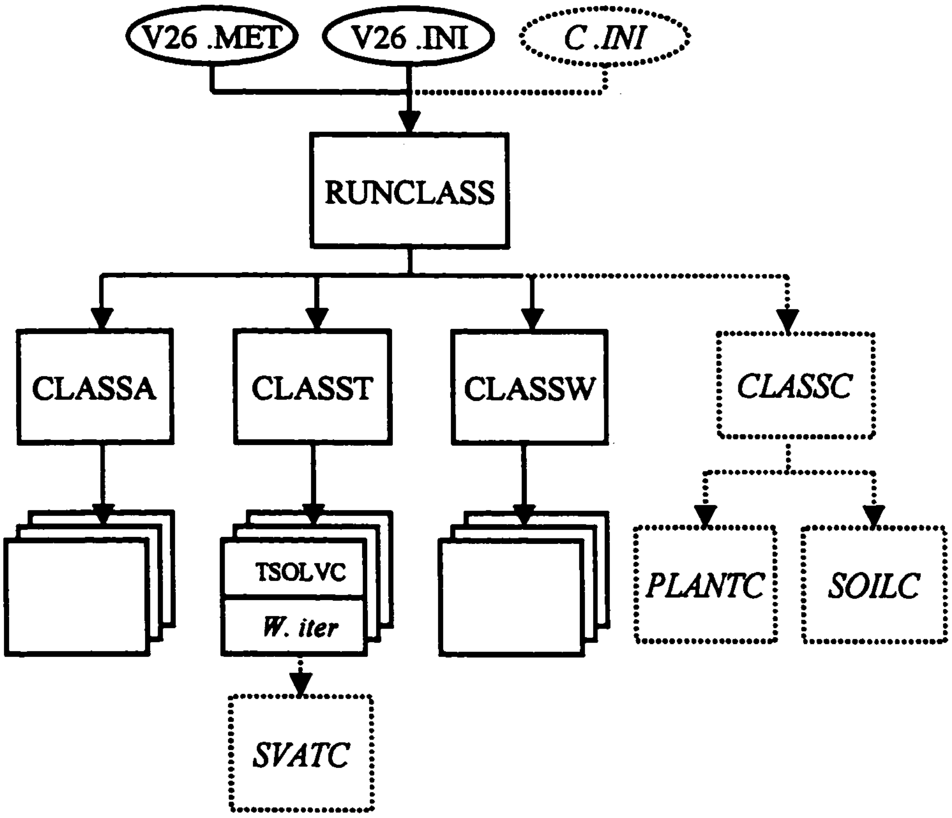

Figure 2.2 The new model structure for CLASS

(RUNCLASS – a driver programme which effectively takes the place of the GCM in the stand-alone or point version of CLASS. It feeds the initialization data and the meteorological data to the model;

CLASSA – the main subroutine controlling albedo and radiation calculations;

CLASST – the main subroutine controlling temperature and energy balance calculations;

CLASSW – the main subroutine controlling calculations associated with water budget;

CLASSC – the newly developed subroutine controlling carbon related calculations;

V26.MET, V26.INI, and *C.INI* represent the inputs of meteorological and initialization data.)

PLANTC is a plant module for simulating the plant carbon and nitrogen processes. Canopy photosynthesis was calculated first in this module by the method proposed by Farquhar *et al.* (1980). Root nitrogen uptake was simulated according to the mass movement of nitrogen with root water uptake and its diffusion in the soil solution. Other processes simulated in this module include the translocation of carbon and nitrogen substrates between sources and sinks within the plant, tissue growth, maintenance and growth respiration, and plant litterfall, etc. *PLANTC* plays the determining role in the whole model. Main outputs from this module include CO_2 exchanges between plant and its environment estimated from photosynthesis and autotrophic respiration, internal vegetation parameters such as plant leaf area index, and litterfall which is the main carbon and nitrogen input for the *SOILC* module.

SOILC is a soil carbon and nitrogen module designed to calculate the biogeochemical processes in soil. Plant litterfall is first partitioned into different pools according to the biochemical constituents of the litter. Together with the soil organic matter that already exists in the soil, decomposition of these organic materials is calculated using first-order kinetics. While heterotrophic respiration simulated in this module contributes to the CO_2 exchanges between the ecosystem and the atmosphere, nitrogen mineralised during the decomposition process is used as the main N source for the plant root uptake which plays important roles for plant simulation in the *PLANTC* module.

The three modules above are closely linked with each other and can be used to address the many climatic feedbacks on the biological processes that are not currently included in GCMs (Shackley *et al.*, 1998). Together they enhance the model by including the CO_2 exchanges between the land surface and the atmosphere. They provide the dynamically based internal parameters to other calculations in CLASS, such as canopy water potential, plant leaf area index, canopy stomatal resistance, and plant root distribution, etc., so prescriptions of these parameters as inputs are no longer required. Additional outputs from this new version of CLASS include revised ecosystem evapotranspiration, gross primary production, net primary production, net ecosystem production, autotrophic respiration, heterotrophic respiration, plant tissue growth, litterfall production, and soil carbon dynamics, etc. Detailed discussions on these three modules are given in Chapter 3, Chapter 4, and Chapter 5, respectively.

CLASSC is designed as an interface between the driver programme (RUNCLASS) and the new subroutines (*PLANTC* and *SOILC*). It initializes arrays and updates the vegetation and soil characteristics at the current time step. It also handles the scaling up calculations for each individual sub-land surface and vegetation type to the grid cell level after *PLANTC* and *SOILC* are invoked. Since it is more technique in code programming than scientific in research, it is not discussed in this thesis.

2.3 Datasets Used by the Model

To accommodate GCMs for the global run, CLASS was developed to include up to four vegetation types in each grid cell, namely evergreen tree, deciduous tree, crop, and grass. This research is focused on the vegetation type of deciduous trees. The main datasets that were used to initialise, drive and test the model are from the observations in the Boreal Ecosystem-Atmosphere Study (BOREAS) project at the Old Aspen (OA) site in the Southern Study Area (SSA).

BOREAS was a large-scale international interdisciplinary experiment in the northern boreal forests of Canada. Its goal was to improve our understanding of the boreal forests, particularly their interactions with the lower atmosphere, such as the exchanges of radiative energy, sensible heat, water, CO_2 and trace gases. Primary objectives of BOREAS were to collect the data needed to improve computer simulation models of the important processes controlling these exchanges so that the effects of global change on the biome can be anticipated, in particular the effects of altered temperature and precipitation, as well as to provide GCMs with better land surface process schemes and data sets for the boreal zone. The field phase of the experiment extended from 1993 to 1997 and included two series of intensive field campaigns in 1994 and 1996, which two years data were used in the present model development and testing. A detailed experimental overview and result summary was given by Sellers *et al.* (1997b).

The Southern Study Area (SSA) in BOREAS was placed near the southern ecotone of the biome and, together with the Northern Study Area (NSA), comprises the two BOREAS study areas. It is located near Prince Albert, Saskatchewan, Canada. The SSA relief is gentle, with a elevation of 550 m to 730 m. Soils range from gray wooded to degraded black classified as Brunisolic, Gleysolic, Chernozemic, Luvisolic and Organic soil orders. There are two major vegetation zones in the study area, the mixed wood section of the boreal forest region and the aspen grove section.

The Old Aspen (OA) site in the SSA is about 50 km Northwest of Prince Albert (106.196°W, 53.628°N). It is in an extensive stand of aspen (*Populus tremuloides*) about 70-years old that naturally established after a forest fire. The mean height of the trees was 21 m, while that of the canopy base was 15 m. Average tree diameter at the 1.5 m height was 17 cm and the stand density was 830 stems ha^{-1}. The understorey was mainly composed of hazelnut (*Corylus cornuta* Marsh.) about 2 m tall with occasional clumps of alder (*Alnus crispa* (Ait.) Pursch). A variety of shrubs (*e.g.*, prickly rose, *Rosa acicularis* Lindl.) occurred sparsely on the forest floor. The soil is an Orthic Gray Luvisol with an 8-10 cm deep surface organic layer. The mineral soil has a silty-clay texture. Further information on the site can be found in Black *et al.* (1996) and Blanken *et al.* (1997).

The BOREAS project has provided us with very comprehensive data covering almost all components of the ecosystem-atmosphere interactions. Observations were made at different scales and from different view points of scientific disciplines which included Airborne Fluxes and Meteorology (AFM), Tower Fluxes (TF), Terrestrial Ecology (TE), Trace Gas Biogeochemistry (TGB), Hydrology (HYD), and Remote Sensing Science (RSS) (Sellers *et al.*, 1997). Most of the data used in the model initialization, boundary control, and output test were obtained from these data sets. Soil background information for the model initialisation, such as bulk density, texture, organic carbon and nitrogen content, was mainly obtained from the observations published by Huang and Schoenau (1996). Data sets used for the plant initialisation such as plant root biomass and length, plant stem and sapwood volume, and plant N content, etc, were mainly obtained from Lavigne and Ryan (1997), Steele *et al.* (1997), and Gower *et al.* (1997).

The most important data used in this research were the meteorological observations for the model boundary control and tower flux measurements for the model tests. Meteorological observations include incoming shortwave radiation, incoming long wave radiation, air temperature, humidity, precipitation, wind speed, and atmospheric pressure. Tower flux measurements used in the model test include the sensible heat, latent heat, and CO_2 over the aspen canopy. These fluxes were measured using eddy-correlation at the 39.5 m height on a 37 m walk-up scaffold tower. Three-dimensional sonic anemometer-thermometers were used for the wind speed and temperature measurements. Fluctuations in CO_2 and water vapor concentration were measured using the closed-path approach with temperature-controlled infrared gas analysers. Half-hour fluxes were calculated on-line. Corrections were made for the effect of fluctuations in air density on the fluxes of CO_2 and water vapor. Canopy airspace CO_2 storage was approximated using the half-hour average CO_2 concentrations measured at the 39 m and 4 m level by the eddy correlation gas analysers. Storage within the hazelnut canopy was found to be small and was neglected. Both of the meteorology and flux data sets were provided by Dr. Black and his research group, namely the Tower Fluxes team 1 (TF1) – "Boreal Forest Atmosphere Interactions: Exchanges of Energy, Water vapor and Trace Gases (SSA-OA)". Detailed information on the measurements such as the instrumentation and quality control can be found in Black *et al.* (1996), Blanken *et al.* (1997), and Chen *et al.* (1999), or traced from there. Other data sets that were used for the model comparisons and analyses in this research are acknowledged later in the text.

References

Abramopoulos, F., Rosenzweig, C., and Choudhury, B., 1988. Improved ground hydrology calculations for global climate models (GCMs): Soil water movement and evapotranspiration. J. Climate, 1: 921-941.

Baldocchi, D.D., Vogel, C.A., and Hall B., 1997. Seasonal variation of energy and water vapor exchange rates above and below a boreal jack pine forest canopy. Journal Geophysical Research, 102, D24: 28,939-28952.

Ball, J.T., Woodrow, I.E. and Berry, J.A., A model predicting stomatal conductance and its contribution to the control of photosynthesis under different environmental conditions. In: Biggens J. (ed.). Progress in Photosynthesis Research, Vol. 4, pp. 221-224. Martinus-Nijhoff., Dordrecht, Netherlands, 1987.

Black, T.A., den Hartog, G., Neumann, H.H., Blanken, P.D., Yang, P.C., Russell, C., Nesic, Z., Lee, X., Chen, S.G., and Staebler, R., 1996. Annual cycles of water vapor and carbon dioxide fluxes in and above a boreal aspen forest. Global Change Biol. 2: 219-229.

Blanken, P.D., Black, T.A., Yang, P.C., Neumann, H.H., Nesic, Z., Staebler, R., den Hartog, G., Novak, M.D., and Lee, X., 1997. Energy balance and canopy conductance of a boreal aspen forest: Partitioning overstory and understory components. J. Geophysical Research, 102, No. D24: 28,915-28,927.

Chen, W.J., Black, T.A., Yang, P.C., Barr, A.G., Neumann, H.H., Nesic, Z., Blanken, P.D., Novak, M.D., Eley, J., Ketler, R.J., and Cuenca, R., 1999. Effects of climatic variability on the annual carbon sequestration by a boreal aspen forest. Global Change Biology, 5: 41-53.

Ciais, P., Tans, P.P., White, J.W.C., Trolier, M., Francey, R.J., Berry, J.A., Randall, D.R., Sellers, P.J., Collatz, J.G., and Schimel, D.S., 1995. Partitioning of ocean and land uptake of CO_2 as inferred by $\delta^{13}C$ measurements from the NOAA Climate Monitoring and Diagnostics Laboratory Global Air Sampling Network. J. Geophys. Res., 100: 5051-5070.

Conroy, J.P., 1992. Influence of elevated CO_2 concentrations on plant nutrition. Australian Journal of Botany. 40: 445-463.

Couteaux, M.M., Mousseau, M., Celerier, M.L., and Bottner, P., 1991. Increased atmospheric CO_2 and litter quality: decomposition of sweet chestnut leaf litter with animal food webs of different complexities. Oikos 61: 54-64.

Curtis, P.S., Drake B.G., and Whigham, D.F., 1989. Nitrogen and Carbon dynamics in C_3 and C_4 estuarine marsh plants grown under elevated CO_2 in situ. Oecologia 78: 297-301.

Denning, A.S., Fung, I., and Randall, D.A., 1995. Strong simulated meridional gradient of atmospheric CO_2 due to seasonal exchange with the terrestrial biota. Nature, 376: 240-243.

Dickinson, R.E., 1995. Land surface processes and climate modeling, Bulletin of the American Meteorological Society, Vol. 76: 1445-1448.

Dickinson, R.E., Henderson-Sellers, A., Kennedy, P.J., and Wilson, M.F., 1986. Biosphere-Atmosphere Transfer Scheme (BATS) for the NCAR Community Climate Model, National Center for Atmospheric Research, Boulder, CO, Tech Note/TN-275+STR.

Dickinson, R.E., Henderson-Sellers, A., Kennedy, P.J., and Giorgi, F., 1992. Biosphere-Atmosphere Transfer Scheme (BATS) Version 1e as coupled to the NCAR Community Climate Model, National Center for Atmospheric Research, Boulder, CO, Tech Note.

Dickinson, R.E., Shaikh, M., Bryant, R., and Graumlich, L., 1998. Interactive canopies for a climate model. J. Climate, 11: 2823-2836.

Dorman, J.L., and Sellers, P.J., 1989. A global climatology of albedo, roughness length and stomatal resistance for atmospheric general circulation models as represented by the simple biosphere model (SiB). J. Appl. Meteorol., 28: 833-855.

Eswaran, H., Van Den Berg, E., and Reich, P., 1993. Organic carbon in soils of the world. Soil Science Society of America Journal, 57: 192-194.

Farquhar, G.D., von Caemmerer, S., and Berry, J.A., 1980. A biochemical model of photosynthetic CO_2 assimilation in leaves of C_3 species. *Planta*. 149: 78-90.

Gorissen, A., van Ginkel, J.H., Keurentjes J.J.B., and van Veen, J.A., 1995. Grass root decomposition is retarded when grass has been grown under elevated CO_2. Soil Biology & Biochemistry 27: 117-120.

Gower, S.T., Vogel, J.G., Norman, J.M., Kucharik, C.J., Steele, S.J., and Stow, T.K., 1997. Carbon distribution and aboveground net primary production in aspen, jack pine, and black spruce stands in Saskatchewan and Manitoba, Canada. Journal of Geophysical Research, 102: 29,029-29,041.

Huang, W.Z. and Schoenau, J.J., 1996. Forms, amounts and distribution of carbon, nitrogen, phosphorus and sulphur in a boreal aspen forest soil. Can. J. Soil Sci., 76: 373-385.

Houghton, R.A., Schlesinger, W.H., Brown S., and Richards, J.F., 1985. Carbon dioxide exchange between the atmosphere and terrestrial ecosystems. In: Atmospheric Carbon Dioxide and the Global Carbon Cycle (ed. J. R. Trabalka), pp. 113-140. US Department of Energy, DOE/ER-0239, Washington, DC.

Jarvis, P.G., Massheder, J.M., Hale, S.E., Moncrieff, J.B., Rayment, M., and Scott, S.L., 1997. Seasonal variation of carbon dioxide, water vapor, and energy exchanges of a boreal black spruce forest. Journal Geophysical Research, 102, D24: 28,953-28966.

Keeling, C.D., Whorff, T.P., Wahlen, M., and van der Piicht, J., 1995. Interannual extremes in the rate of rise of atmospheric carbon dioxide since 1980. Nature, 375: 666-670.

Lavigne, M.B. and Ryan, M.G., 1997. Growth and maintenance respiration rates of aspen, black spruce and jack pine stems at northern and southern BOREAS sites. Tree Physiology, 17: 543-551.

Margolis, H.A. and Ryan, M.G., 1997. A physiological basis for biosphere-atmosphere interactions in the boreal forest: an overview. Tree Physiology 17: 491-499.

McFarlane, N.A., and Laprise, R., 1985. Parameterization of sub-grid scale processes in the AES/CCC spectral GCM. Atmospheric Environmental Service, Downsview, Ontario, No. 85-12 CCRN 17, 70pp.

McFarlane, N.A., Boer, G.L., Blanchet, J-P., and Lazare, M., 1992. The Canadian Climate Center second generation general circulation model and its equilibrium climate. J. Climate, 5: 1013-1044.

Noilhan, J. and Planton, S., 1989. A simple parameterization of land surface processes for meteorological models. Mon. Wea. Rev., 117: 536-549.

Pitman, A.J., 1988. The development and implementation of a new land surface scheme for use in general circulation models, Ph.D. thesis, University of Liverpool, 481 pp.

Pitman, A.J., Yang, Z.-L., Cogley, J.G., and Henderson-Sellers, A., 1991. Description of Bare Essentials of Surface Transfer for the Bureau of Meteorology Research Center AGCM, BMRC Research Report No. 32, Melbourne, Victoria, 132 pp.

Sato, N., Sellers, P.J., Randall, D.A., Schneider, E.K., Shukla, J., Kinter III, J.L., Hou, Y-T. and Albertanzi, E., 1989. Effects of implementing the simple biosphere model in a global circulation model. J. Atmos. Sci., 46: 2757-2782.

Sellers, P.J., Randall, D.A., Collatz, G.J., Berry, J.A., Field, C.B., Dazlich, D.A., Zhang, C., Collelo, G.D., and Bounoua, L., 1996. A revised land surface parameterization (SiB2) for atmospheric GCMs. Part I: Model formulation. J. Climate, 9: 676-705.

Sellers, P.J., Dickinson, R.E., Randall, D.A., Betts, A.K., Hall, F.G., Berry, J.A., Collatz, G.J., Denning, A.S., Mooney, H.A., Nobre, C.A., Sato, N., Field, C.B., and Henderson_Sellers, A., 1997a. Modeling the exchanges of energy, water, and carbon between continents and the atmosphere. Science, 275: 502-509.

Sellers, P.J., Hall, F.G., Kelly, R.D., Black, A., Baldocchi, D., Berry, J., Ryan, M., Ranson, K.J., Crill, P.M., Lettenmaier, D.P., Margolis, H., Cihlar, J., Newcomer, J., Fitzjarrald, D., Jarvis, P.G., Gower, S.T., Halliwell, D., Williams, D., Goodison, B., Wichland, D.E., and Guertin,F.E., 1997b. BOREAS in 1997: Experiment overview, scientific results, and future directions. Journal of Geophysical Research, 102, D24: 28,731-28,769.

Shackley, S., Young, P., Parkinson, S., and Wynne, B., 1998. Uncertainty, complexity and concepts of good science in climate change modelling: are GCMs the best tools? Climatic Change 38: 159-205.

Smart, D.R., Chatterton, N.J., and Bugbee, B., 1994. The influence of elevated CO_2 on non-structural carbohydrate distribution and fructan accumulation in wheat canopies. Plant, Cell, and Environment 17: 435-442.

Steele, S.J., Gower, S.T., Vogel, J.G., and Norman, J.M., 1997. Root mass, net primary production and turnover in aspen, jack pine and black spruce forests in Saskatchewan and Manitoba, Canada. Tree Physiology, 17: 577-587.

Verseghy, D.L., 1991. CLASS - A Canadian land surface scheme for GCMs. I. Soil model. International Journal of Climatology 11: 111-113.

Verseghy, D.L., 2000. The Canadian Land Surface Scheme (CLASS): 1987–1997. Atmosphere-Ocean (in press).

Verseghy, D.L., McFarlane, N.A., and Lazare, M., 1993. CLASS - A Canadian land surface scheme for GCMs. II. Vegetation model and coupled runs. International Journal of Climatology 13: 347-370.

Warrilow, D.A., Sangster, A.B., and Slingo, A., 1986. Modelling of land surface processes and their influence on European climate, Dynamic Climatology Tech. Note. No. 38, Meteorological Office, METO20, Bracknell, UK, 94 pp.

Yang, Z.-L., 1992. Land surface processes in 3-dimensional climate models, Ph.D. thesis, Macquarie University, 437 pp.

Chapter 3 Modelling Energy and Water Exchanges between Canopy and the Atmosphere in CLASS – the *SVATC* Module

3.1 Introduction

Calculations of the energy and water exchanges between land surface and the atmosphere are the primary objective of land surface schemes coupled with atmospheric GCMs. The fluxes of energy and water estimated from land surface schemes and passed back to GCMs can significantly affect the equilibrium surface climate simulated by GCMs. It is therefore very important to design the modelling algorithms that control these exchanging processes in the actual ecosystems. Much of the current work at the interface of climatology, geophysics, environmental physics and ecology is aimed at understanding such processes, and trying to include them in GCMs and improve the accuracy of the simulations has always been the main effort on the research of the land surface scheme.

On vegetated land surfaces, the dynamic vegetation processes play the controlling roles in determining the energy balance and water flux between the canopy and the lower atmosphere. Biophysical characteristics of the surface, such as albedo and surface roughness which are determined by the vegetation types and growing conditions, control the radiation balance and strongly affect the momentum transfer and the near surface boundary-layer structure. Physiological characteristics of the surface, such as the canopy stomatal resistance, the plant water storage capacity and root water up-take ability, control the plant water movement and transpiration processes and strongly affect the energy partitioning between sensible heat and latent heat. Treating vegetation separately from soil in the land surface schemes has brought land surface schemes up to the new stage which is recognised as the "second generation" model. However, nearly all of them use very simple and empirical schemes in calculating the plant processes, and these processes are usually focused on the physical aspect of the vegetation. Very rarely have the physiological and biochemical processes of the plant been involved.

Models that attempt to predict stomatal resistance (r_c) directly from factors of the environment, while making no attempt to address the fundamental underlying mechanisms, are presently the approach of choice in constructing models of transpiration and energy balance of land surfaces. Of the models available, most of the calculations of r_c are based on the empirical relationships regressed from direct observations on leaf stomatal resistance and environment factors, either under controlled or natural conditions (Jarvis, 1976; Avissar *et al.*, 1985; Jones and Higgs, 1989). For example, in CLASS, canopy stomatal resistance is calculated using the method proposed by Jarvis (1976), which uses a minimum value for the unconstrained r_c, multiplied by a series of dimensionless factors representing the effects imposed by each environmental variable known to affect stomatal resistance (equation 2.7). There are some shortcomings with these models. First, they tend to be specific to particular vegetation-climate systems (*e.g.*, Gash *et al.*, 1989; Jones and Higgs, 1989). Parameters such as the minimum stomatal resistance, or the sensitivity of stomatal resistance to the air vapour pressure deficit, must be readjusted to fit a particular vegetation type, or prevailing conditions. Second, the interactions of different environmental variables on stomatal resistance are difficult to determine, and may not be multiplicative. Such a non-mechanistic technique for calculating canopy resistance may cause inaccuracy in the simulation of energy partitioning on the land surface and limitations on the application of land surface schemes.

The physiological and biochemical mechanisms governing stomatal resistance have been widely studied by plant physiologists in the last two decades. The most interesting theory can be attributed to the feedback hypothesis on the stomatal aperture proposed by Wong *et al.* (1979). They claimed that stomatal aperture may be determined by the capacity of the mesophyll tissue to fix carbon and by some sort of communication from the photosynthetic mechanism to the stomatal control system. This theory attracted great attention and has been developed in detail by many researchers (Cowan, 1982; Farquhar and Sharkey, 1982; Ball and Berry, 1982; Wong *et al.*, 1985a, b, c; Ball *et al.*, 1987; Collatz *et al.*, 1991, 1992). These works led to the concept that the responses of stomata to changes in the environment conditions can be partitioned into components that are dependent on photosynthesis and others that are independent of photosynthesis (CO_2 and H_2O concentrations of the air). Details about this analysis were described by Ball (1988). In my research, the model used for the stomatal resistance calculations is based on this theory, which includes an implicit dependence of stomatal resistance on photosynthesis.

Resistance to water movement from soil to plant root is another important factor in controlling the canopy transpiration and energy balance. In the soil-vegetation-atmosphere transfer system, the catenary hypothesis or Ohm's Law analogue for water movement has provided an important conceptual framework for the study of crop water relations. This hypothesis was first proposed by van den Honert (1948) and could be described by an equation of the form

$$Q = -\frac{\psi_l - \psi_s}{R_{l,s}} \tag{3.1}$$

where Q is the water flux between any two points (from s to l) within the system, ψ_l and ψ_s are the water potentials (negative) at the points l and s, and $R_{l,s}$ is the hydraulic resistance of the pathway between the two points. For the soil-plant system, ψ_l and ψ_s can be regarded as the plant leaf water potential and soil water potential, respectively, $R_{l,s}$ then represents the total resistance from the soil rhizosphere and plant, and Q thus refers to the plant root water uptake. If Q is less than transpiration, the plant will be subjected to a net water loss, which will eventually lead to the closure of stomata and finally decrease canopy latent heat exchange. On the other hand, higher Q than transpiration will increase the plant water content and hence canopy water potential, which may lead to the opening of stomata and increase of canopy water loss.

Resistance from the soil rhizosphere and the plant is strongly dependent on soil water potential, plant root length density and its spatial distribution characteristics. Pioneer modelling work on the calculations of soil and plant root resistance can be attributed to Gardner (1960) and Cowan (1965). They predicted, on the basis of mathematical models, that the rhizosphere resistance could be appreciable when the soil matric potential is a few bars below zero. However, in a later study, Newman (1969) analysed the importance of root length and suggested that for most herbaceous and some woody species, the rhizosphere resistance will remain smaller than the plant resistance (and for some species will not even become appreciable) until the soil reaches near or beyond its permanent wilting point. A general agreement can be gleaned from all the studies that the hydraulic resistance from soil and plant root system are important in determining the water transfer processes in ecosystems at least under dry soil conditions. It is therefore necessary to explicitly implement these calculations in the land surface schemes.

Equation (3.1) can be seriously at fault because of its reliance upon a single number to represent soil water potential. For example, because of spatial variation in soil water potential, resistance from soil rhizosphere and plant root may vary with plant water conditions. When plant transpiration demand is small and leaf water potential is relatively high, roots extract water mainly from those regions of the soil profile where soil water potential is also high (usually deep in the profile). As plant transpiration demand is high and leaf water potential becomes more negative, roots begin removing water from regions of the profile where soil water potential is more negative. Hence the total length of roots actually taking up water at a particular time, and therefore its corresponding resistance, may vary with the plant water and environmental conditions (Reid and Huck, 1990). In addition, the carbon partition in the root profile or the root growth rates in different soil layers may also change with the changing conditions. Variations of plant resistance may also happen in other parts of the plants, as suggested by Boyer (1974), or by other mechanisms, as suggested by Dalton *et al.* (1975), Fiscus (1975), Jones (1978), and Biscoe *et al.* (1976). So, it is important to divide the soil and plant into different segments and treat them separately according their local conditions. CLASS divides the soil profile into three layers for the soil temperature and moisture calculations. By developing a dynamic plant root growth scheme which is driven by the local soil microclimate conditions and the internal plant characteristics, and implementing it in each soil layer, we can effectively simulate the root growth pattern in the soil profile and the actual water flow processes under changing conditions.

Plant water storage affects plant water conditions and alters the daily pattern of transpiration. For canopies with large biomass, water stored in the canopy can significantly adjust the relationship between transpiration and root water uptake, which can be marked by the time lag between these two fluxes as observed at this SSA-OA site (Hogg and Hurdle, 1997; Saugier *et al.*, 1997). Directly coupling equation (3.1) with transpiration calculations may bring errors in the temporal distribution of transpiration calculations. CLASS is developed for GCM studies and it is run at a short time step (30 minutes or less). Therefore I included plant water capacity calculations and coupled it in the water transfer scheme in this study.

Recently, the physiological processes controlling the stomatal resistance have been considered in the land surface schemes of SiB (Sellers *et al.*, 1996) and BATS (Dickinson and Shaikh, 1998). The soil-plant water dynamic processes are still a vacant area and have not been dealt with in any available land surface schemes. Without explicit calculation of plant water conditions, the estimation of soil rhizosphere and plant root resistances have to be ignored or evaluated in a very unrealistic way. In addition, some important parameters used for calculating the stomatal resistance, such as the leaf water potential, have to be replaced by other variables, such as the soil water content. As discussed above, these will bring considerable limitations to the application of the model.

In this chapter, the dynamic water transfer module *SVATC* is developed. Model algorithms are described first, which include the explicit calculations of stomatal resistance, soil rhizosphere resistance, plant root resistance, and plant water storage change within each time step. The dynamic water transport process in this soil-plant system is then coupled with the energy balance calculations of the land surface. The canopy surface temperature and canopy water potential are used as the prognostic variables and solved in each time step using an iterative technique. Results are then used for the energy and water flux calculations as well as for other calculations on the physiological and biogeochemical processes discussed in the next two chapters. Model predictions of net radiation, sensible heat and latent heat fluxes are compared with the tower flux measurements. Relationships between canopy transpiration and root water uptake are also discussed. Finally, the model sensitivity of evapotranspiration to the variations in climatic drivers is analysed.

3.2 Module Description

3.2.1 Resistances to Water Flow in Soil-Plant-Atmosphere System

The widely accepted approach to date for water movement studies in the soil-plant-atmosphere system is based on the concept that soil, plant, and atmosphere form a physically unified and dynamic system like links in a chain. Water flow takes place along the water potential gradient in the chain (Cowan, 1965; Philip, 1966). The flow path includes the water movement in the soil toward the roots, absorption into the roots, transport in the roots to the stems and through the xylem to the leaves, evaporation in the intercellular air space of the leaves, vapor diffusion through the stomata and finally transport to the external atmosphere. Resistances in this path are one of the major factors in determining the water flow rate. Under most circumstances, the highest resistance is believed to occur between the leaf and the atmosphere, a resistance which is controlled mainly by stomata. Resistances from the soil rhizosphere and plant root can also play significant role in the total resistance when the soil water content is low. In the water transfer model, the resistances from stomata, soil, and plant root are simulated explicitly. Boundary-layer resistance in CLASS is formulated by Abdella and McFarlane (1996) based on the Monin-Obukhov similarity theory, but with modifications in my calculations under stable atmospheric stratification. Resistances from other parts of the soil-plant-atmosphere system, such as the plant stem, are not considered in the model.

Stomatal resistance of a plant leaf r_l[†] is calculated according to the model proposed by Ball *et al.* (1987) as follows:

[†] Hereafter, the term "stomatal conductance", g_l, is occasionally used, which refers to the inverse of r_l.

$$r_l = (m\frac{h_s V_l}{C_a} + b)^{-1} \tag{3.2}$$

where h_s and C_a are the relative humidity and CO_2 concentration of the air near the leaf surface, and V_l is the CO_2 assimilation rate. V_l is controlled by leaf dark and light reaction rates and affected by leaf water and nutrient conditions. The relevant biochemical calculations will be discussed in the next chapter. The parameter m represents the composite sensitivity of stomatal conductance to carbon assimilation, CO_2 concentration, and relative humidity. The parameter b is found to be very close to zero and here I take it to be the cuticle conductance of the leaf when the stomata are completely closed. Figure 3.1 shows the processes related to the r_l calculations.

Scaling stomatal resistance at the leaf level (r_l) up to the canopy (r_c) and coupling it with the boundary layer resistance (r_a) can be complicated. One line of thinking leads to the development of single-layer models, or big-leaf models, which ignore the detailed and complex spatial structure of the actual canopy and treat it as no more than a partly wet plane at the lower boundary of the atmosphere. The total resistance is then calculated as the sum of a physiological canopy resistance (r_c) and an aerodynamic boundary-layer resistance (r_a). This scaling method is very simple, but it carries substantial problems in estimating r_c, especially for vegetation of large scale like forest. Another line of thinking considers the details of the canopy structure and microclimate conditions explicitly. Attention is usually focused on the vertical distributions of the canopy leaves and/or microclimatic conditions and this leads to the so-called multi-layer models. Multi-layer models address the reality of the transport processes of a scalar entity (*e.g.*, water), but calculations are much more complicated than for the single-layer models. For example, scalar turbulent fluxes in single-layer models are usually based on the gradient-diffusion hypothesis. However, accumulated evidence shows that this hypothesis frequently fails inside and just above plant canopies, i.e. counter-gradient fluxes for heat, water vapor, and CO_2 can occur within forest canopies (Denmead and Bradley, 1985, 1987). One option in dealing with the situation is by replacing the gradient-diffusion hypothesis with the

Lagrangian approach (Taylor, 1921) and implementing this in the multi-layer models (Wilson *et al.*, 1981; Raupach, 1987, 1989a, 1989b). This approach gives us very good theoretical estimation of scalar entity fluxes as well as the detailed spatial structure of the scalar entities within the canopy. On the other hand, it involves more parameters and greatly increases the computing time.

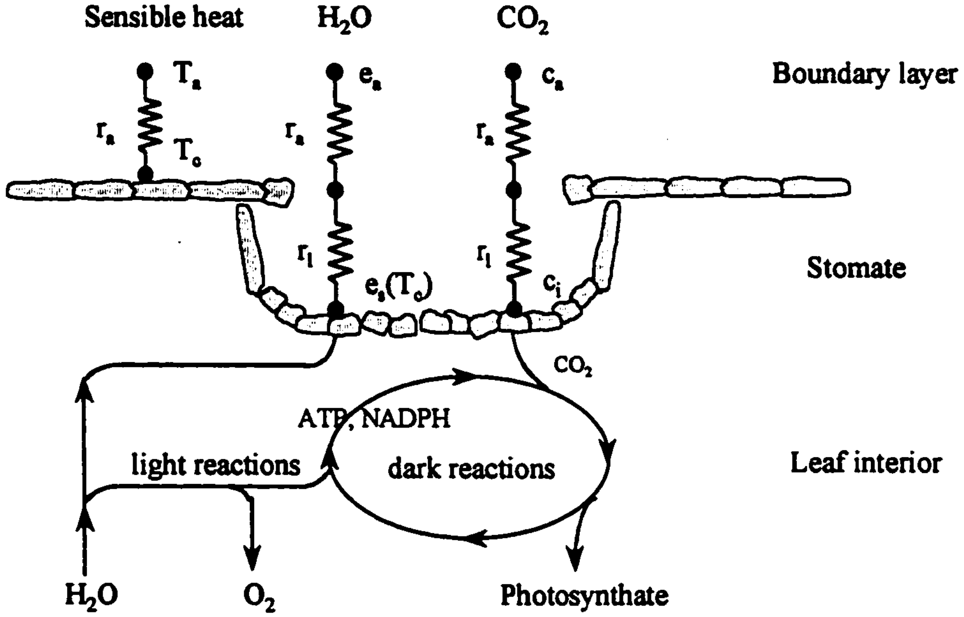
Sensible heat
H_2O
CO_2
T_a
r_a
T_c
e_a
r_a
c_a
r_a
Boundary layer
r_l
$e_s(T_c)$
r_l
c_i
Stomate
CO_2
ATP, NADPH
light reactions
dark reactions
Leaf interior
H_2O
O_2
Photosynthate

Figure 3.1 Schematic diagram for water and CO_2 processes around a stomate

Since CLASS is intended to function within atmospheric GCMs, it is concerned with vegetation essentially as a permeable lower boundary to the atmosphere. In this system, the length scale is much larger than that of the vegetation itself, which gives us the opportunity to pay less attention to the canopy and microclimate structures. Therefore, I developed a simple scheme in scaling up leaf stomatal resistance to the canopy level which can be regarded as a modified two-layer model. Since the physiological activities of plant leaves, and therefore their stomatal resistance, may differ markedly when they are sunlit or shaded, I first divided the total canopy leaves into two "layers" of functional types: sunlit and shaded, rather than dividing them according to their spatial (vertical) distributions. This is more consistent with the r_l scheme in the model. From equation (3.2) we can see that leaf stomatal resistance is mainly controlled by photosynthesis rate V_l. For different leaves within a canopy, the biggest difference of microclimatic conditions that affect their photosynthesis rates is usually the light interception intensity. The differences of other factors, such as temperature and humidity, are usually minor.

The segregation of the canopy into sunlit and shaded leaves begins by calculating the fraction (f_l) of radiation intercepted by the total canopy (Sinclair and Lemon, 1974)

$$f_l = 1.0 - e^{-\frac{kA}{\sin\beta}} \tag{3.3}$$

where k is the extinction coefficient, β is the solar elevation, and A is the total leaf area index obtained from plant growth simulations implemented in the *PLANTC* module. This equation has been well established as describing the geometry of radiation interception for a canopy with leaves randomly dispersed in the horizontal plane. For leaf canopies where the leaf area index approaches 3 or more, this equation has been shown to depict radiation interception well (*e.g.*, Sinclair and Knoerr, 1982). From basic geometrical considerations, the amount of leaf area that actually intercepts the direct-beam radiation, A_{sunlit}, can be calculated as

$$A_{sunlit} = f_l \sin\beta / k \tag{3.4}$$

By simple difference, the remaining leaf area is regarded as the shaded part (A_{shaded}) that intercepts only diffusive and scattered radiation.

$$A_{shaded} = A - A_{sunlit} \tag{3.5}$$

Leaf stomatal resistance r_l for both the sunlit ($r_{l,sunlit}$) and shaded ($r_{l,shaded}$) leaves is explicitly calculated. The total canopy stomatal resistance r_c is then scaled up based on the assumption of parallel resistance.

$$\frac{1}{r_c} = \frac{A_{sunlit}}{r_{l,sunlit}} + \frac{A_{shaded}}{r_{l,shaded}} \tag{3.6}$$

In general, the model is like a 2-layer model, but I recognize leaf "layer" according to its functionality instead of vertical placement (on which most multi-layer models are based). Compared with the big-leaf models, this segregation scheme provides a considerable advantage and improvement in the scale-up calculations from leaf to canopy (Boote and Loomis, 1991), while still keeping the question relatively simple. However, limitations apply to the process studies within the canopy, since neither explicit calculation of the diffusive processes within the canopy nor spatial distributions of the microclimatic conditions (except radiation) are included.

The hydraulic resistance of the soil and plant root system is modelled as the sum of three components: soil rhizosphere resistance r_s, root radial resistance r_r, and root axial resistance r_x, as shown in Figure 3.2. The resistance r_s is a property of the soil around each individual root. It differs from the resistance to water movement from one part of the soil to another (the pararhizal resistance) (Newman, 1969). In the model, r_s is simulated for each soil layer i following single root radial flow theory and the steady rate approximation (Gardner, 1960; Passioura and Cowan, 1968):

$$r_{s,i} = \frac{\ln(b_i / a)}{2\pi K_i L_{d,i} \Delta z_i} \tag{3.7}$$

where a is root radius, K_i is the soil hydraulic conductivity, $L_{d,i}$ is the root length density (total root length in a unit soil volume), and Δz_i is the soil layer depth. Total root length is converted from root biomass which is obtained from the result of root growth simulated in the *PLANTC* module. b_i is the path length for water uptake (half distance between adjacent roots) approximated by:

$$b_i = (\pi L_{d,i})^{-0.5} \tag{3.8}$$

The resistance to water flow radially across the roots into the plant, within soil layer i, $r_{r,i}$, is estimated from

$$r_{r,i} = \frac{r_r'}{L_{d,i} \Delta z_i} \tag{3.9}$$

where r_r' is root radial resistivity (resistance per unit root length). Some authors (*e.g.*, Herkelrath *et al.*, 1977) modify the above calculation by the degree of soil water saturation to account for the fraction of the root surface not in contact with water filled soil pores, and hence unable to conduct water. This factor is not included in my calculation, considering that the modelling site (SSA-OA, BOREAS) is dominated by relatively high soil water content during most of the time.

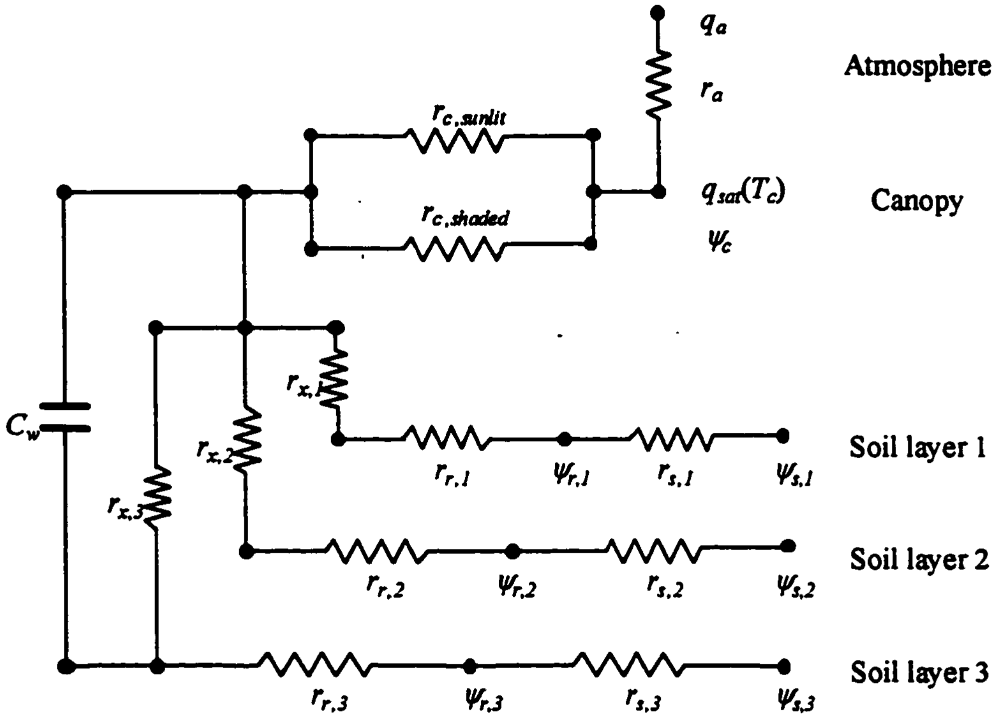
q_a
r_a
Atmosphere
$r_{c,sunlit}$
$r_{c,shaded}$
$q_{sat}(T_c)$
ψ_c
Canopy
C_w
$r_{x,1}$
$r_{x,2}$
$r_{x,3}$
$r_{r,1}$
$\psi_{r,1}$
$r_{s,1}$
$\psi_{s,1}$
Soil layer 1
$r_{r,2}$
$\psi_{r,2}$
$r_{s,2}$
$\psi_{s,2}$
Soil layer 2
$r_{r,3}$
$\psi_{r,3}$
$r_{s,3}$
$\psi_{s,3}$
Soil layer 3

Figure 3.2 Water flow processes in the soil-plant-atmosphere system implemented in the *SVATC* module

The axial resistance to water flow from a soil layer to the stem base, $r_{x,i}$, is difficult to estimate accurately because of the complicated rooting pattern. Here I follow the method proposed by Klepper *et al.* (1983)

$$r_{x,i} = \frac{r_x' z_{d,i}}{0.5 f L_{d,i}} \tag{3.10}$$

where r_x' is the root axial resistivity, $z_{d,i}$ is the depth of the midpoint of the soil layer i, and f represents the fraction of the number of roots which connect directly to the stem base to the total number of roots crossing a horizontal plane at that depth.

3.2.2 Plant Water Capacity

Water flow in the soil-plant-atmosphere system is an transient process most of the time. Water needs of plants are at least partly fulfilled by water stored in leaves, stems and roots when root water uptake can not meet the requirement for transpiration. Hysteresis between plant transpiration and soil water potential, which can be attributed to the changes in plant water storage, has been observed in many studies of plant-water relations (*e.g.*, Jarvis, 1976; Wallace and Biscoe, 1983). For vegetation with large biomass, water storage capacity can be very high. For example, the total water storage capacity of a *pseudotsuga menziesii* (Douglass-fir) forest was estimated at 270 m^3 ha^{-1} (26.7 mm) (Kozlowski, 1982). This large water reservoir can significantly affect the short-term (*e.g.*, hourly) pattern of the latent heat exchange between canopies and the atmosphere. As a land surface scheme to be coupled with GCMs, CLASS is run at a time step no longer than 30 minutes and is sensitive to the short-term distributions of energy partitioning. Therefore, it is necessary to implement the internal plant water adjusting mechanism within the whole water transfer scheme in the soil-plant-atmosphere system.

To simulate this process, the plant water capacity (C_w) is introduced into the model, as shown in Figure 3.2. It is defined as the rate of change of plant stored water θ_c with canopy water potential ψ_c

$$C_w = \frac{d\theta_c}{d\psi_c} \tag{3.11}$$

Water storage can occur in plants by different mechanisms. Therefore C_w can be very different when plants are at different water conditions. Here the hypothesis and experimental results by Tyree and Yang (1990) are adopted, and C_w is calculated in three phases. The first phase is capillary water stored at a high capacity and at high plant water potential (ψ_c from 0 to about -0.5 MPa). It represents a substantial fraction of the water use in wet environments. The second phase is an elastic storage component of minimum storage capacity at ψ_c values of about -0.5 to -3.0 MPa. This is the normal "operating" range of ψ_c in terms of trees during summer. The last phase of stored water is water released by cavitation events. It is a high capacity component that is released at about $\psi_c < -3.0$ MPa and occurs when stomata are likely to be closed and water uptake from soil is at a minimum. Specific parameter values are listed in Table 3.1.

3.2.3 Coupling Water Balance with Energy Balance

Plant water dynamics include three processes: canopy transpiration, root water uptake, and plant water storage change. If the amount of water used in the biochemical reactions is neglected, these three items should add up to zero in each time step in order to keep the water balanced. Taking canopy water potential (ψ_c) as the prognostic variable and using the resistance and capacitance calculations discussed above, we can write the plant water balance equation as

$$\frac{\rho_a[q_a - q_{sat}(T_c)]}{r_a + r_c} - \sum_{i=1}^{IG} \frac{\psi_c - \psi_{s,i}}{r_{r,i} + r_{s,i} + r_{x,i}} - C_w C_S \frac{\partial \psi_c}{\partial t} = 0 \qquad (3.12)$$

where IG represents the total number of soil layers included in the model ($IG = 3$ for CLASS), C_S is the plant biomass (see Chapter 4). Definitions for other variables can be found in the discussions above and in equation (2.6) of Chapter 2. The three items on the left side of this equation represent canopy transpiration, total plant root water uptake from each soil layer, and the change in plant water content, respectively.

In equation (3.12), canopy stomatal resistance r_c is related to carbon fixation V_l according to equation (3.2) and (3.6). Since V_l can be affected by ψ_c through equation (4.8) and (4.9) which are implemented in the *PLANTC* module and discussed latter in Chapter 4, r_c is thus finally related to ψ_c. The canopy temperature T_c is also affected by ψ_c through its impact on the energy partition between sensible and latent heat exchanges of the canopy. While transpiration (the first item) decreases with decreasing ψ_c through the effect of ψ_c on r_c, root water uptake (the second item) will increase through the effect of the difference between ψ_c and the soil water potential ψ_s. Plant water content (the third item) also changes with ψ_c. There is therefore a unique solution for ψ_c under any combination of soil and atmospheric conditions at which the difference between canopy transpiration and root uptake during any time step equals the difference in plant water storage between the current time step and the previous one.

There are two unknown prognostic variables in equation (3.12), ψ_c and T_c. To close the problem, we introduce the canopy energy balance.

$$Q_{H,c} + Q_{E,c} + Q_{S,c} + R_{N,c} = 0 \tag{3.13}$$

where $Q_{H,c}$ and $Q_{E,c}$, represent sensible and latent heat exchanges between canopy and the atmosphere, and are calculated according to equation (2.5) and (2.6), $Q_{S,c}$ represents the canopy heat storage change, and $R_{N,c}$ represents the canopy net radiation (longwave + shortwave). The detailed formulations of $Q_{S,c}$ and $R_{N,c}$ can be found in Verseghy *et al.* (1993) and are not discussed here. All of the four items in equation (3.13) can be finally expressed as functions of a set of known boundary conditions and two unknown prognostic variables the same as those in equation (3.12), that is, ψ_c and T_c. Therefore if we couple equation (3.12) with (3.13), we have two equations with those two unknown variables, and they can then be solved. Since these two equations are highly non-linear, an iterative technique is used. After ψ_c and T_c are obtained in each time step, the canopy net radiation, sensible heat and latent heat exchanges, root water uptake, and the canopy storage change of water and heat can then be calculated.

3.3 Parameterization, Simulation Results and Tests

3.3.1 Parameterization

To be consistent with the overall design of CLASS, the *SVATC* module is parameterized generally to the functional type of deciduous trees, or the second vegetation type recognised in CLASS. Specific parameters for aspen are only taken when it is considered significantly different with other deciduous trees and easily available. The main parameters are adopted from research that is independent of the model used datasets. This strategy is also used in the parameterization of the *PLANTC* and *SOILC* modules discussed in the next two chapters.

Some state variables and driving variables that are important to this module, such as the plant leaf area, plant root length, and photosynthetic rate, etc., are determined by other modules in the model and will be discussed in the next two chapters. The independent parameters used in this module, their values and references are listed in Table 3.1.

3.3.2 Simulation Results and Tests

(1) Energy Balance

Tower measurements of net radiation R_n, sensible heat flux density H, and latent heat flux density LE above the aspen canopy for 1994 and 1996 were compared with the model outputs. Other energy items, such as canopy heat storage change, soil heat flux, and snow melt and re-freezing, were also simulated in the model to balance energy at each time step. Since these items can be regarded as the residue of R_n, H, and LE, and usually have relatively small values, they are not discussed in the following energy comparisons. Another reason for not including them in the comparisons is that the calculations for these energy items were not specifically addressed and therefore not modified in this research; all of their algorithms were kept the same as the original CLASS version 2.6.

Continuous comparisons of measured versus simulated half-hourly R_n, H, and LE for three weeks in 1994 are shown in Figure 3.3, 3.5 and 3.7, respectively. These three weeks were selected in order to cover the model responses in different growing seasons (early, middle and late) and in different weather conditions (clear, cloudy and rainy). The main driving variables corresponding to these comparison periods are plotted in Figure 3.4, 3.6 and 3.8, respectively. It can be found that the modelled energy exchanges between the atmosphere and canopy successfully traced the diurnal variations of the measured values. In the early growing season as shown in Figure 3.3, both the simulated and measured values show that the radiative energy received by the canopy during daytime was mainly dissipated as sensible heat exchange. The amount of latent heat exchange was very small. At this stage, the leaf emergence had

Table 3.1 Parameters Used in the *SVATC* Module.

Symbol	*Equation*	*Value*	*Units*	*Reference*
C_a	3.2	350	ppm	
m	3.2	9.00 [#]	unitless	Ball *et al.*, 1987
b	3.2	1.0×10^{-4} [&]	m s^{-1}	Kozlowski, 1997
k	3.3	0.5 [§]	unitless	Sinclair, 1991
a	3.7	2.0×10^{-3}	m	Steele *et al.*, 1997
r_r'	3.9	4.9×10^{11} [†]	s m^{-1}	Reid and Huck, 1990
r_x'	3.10	3.5×10^{10} [†]	s m^{-3}	Reid and Huck, 1990
f	3.10	0.22	Unitless	Reid and Huck, 1990
C_w	3.12	0.694, ($\psi_c > -0.5$ MPa)	kg MPa^{-1} kg^{-1} DW*	Tyree and Yang, 1990
		0.014, ($-0.5 > \psi_c > -3.0$ MPa)	kg MPa^{-1} kg^{-1} DW*	Tyree and Yang, 1990
		0.046, ($\psi_c < -3.0$ MPa)	kg MPa^{-1} kg^{-1} DW*	Tyree and Yang, 1990

[#] The slope parameters were observed very close to each other for the plants with the same photosynthetic pathway. For C_3 plants, m ≈ 9, and for C_4 plants, m ≈ 4.

[&] The *b* parameter represents the minimum conductance of the leaves when stomata are closed. Its role in total conductance is limited and neglected in some model applications. Here I assign it the value of cuticle conductance of deciduous tree leaves.

[§] Spherical leaf-angle distribution, random. The extinction coefficient depends on leaf angle and solar elevation angle β. It varies by a factor of $1.0/\sin\beta$ with the solar position changes as represented by equation (3.3). Variations in leaf angle also have a large effect on *k* because less light is intercepted when leaves are displayed obliquely to the direct beam. An assumption of randomness approximates most crop canopies. Departures are noticeable in clumped, regular, and solar-tracking communities.

[†] Root radial and axial resistivity may change significantly within different parts of root and with the environmental conditions. For example, the values for root tips were reported smaller than other parts of the root. Here I use an intermediate value to represent the average of the whole root systems.

[*] DW = dry wood biomass.

just begun and plant branches and stems mainly composed the canopy. Since r_c was simulated inversely proportional to leaf area index *LAI* (equation 3.6), small *LAI* contributed to the high canopy resistance on the ground area basis, even though the resistance on the leaf area basis (r_l) was within the normal range. This made the low ratio of r_a / (r_a+r_c) at the early growing season, which finally led to the large partitioning of radiative energy into sensible heat.

Net radiation during this period reached about 600 W m^{-2} under clear weather conditions. In the original version of CLASS, R_n tends to be underestimated in wintertime and in the early growing season which is due to the neglect of the impact of plant stems and twigs on the energy balance. In the non-growing season or when the *LAI* is very small, land surface albedo in the deciduous forest is still quite low even if the ground surface is covered by snow, which is due to the covering by plant wood. After the variable of "wood area index" (*WAI*) (discussed in Chapter 4) was added to the model, there was a significant improvement on the net radiation simulations in the model as can be seen from Figure 3.3. Due to the high net radiation and depressed evapotranspiration of the ecosystem, sensible heat exchange was simulated as high as about 400 W m^{-2} under clear weather conditions, such as day 131, and 133 to 135, similar to the magnitude of measurements.

During night time in the early growing season, while simulated latent heat exchange agreed well with the observations and was close to zero, negative net radiation and downward sensible heat flux tended to be exaggerated (up to 40 W m^{-2}) by the model. It was found that these discrepancies occurred mostly during clear nights. In addition, comparisons among different growing seasons show that these discrepancies diminished when the above ground biomass got larger in the middle and late growing season. These simulation errors were due to over-estimation of canopy temperatures, probably due to underestimation of boundary-layer resistance under stable atmospheric stratification. During clear nights, along with the decrease of land surface temperature, stable atmospheric stratification dominated most of the time which caused significant increase in boundary layer resistance r_a. Lower estimates of r_a under this condition led to the over estimation of downward sensible heat flux, which would retard the surface temperature drop and thus cause higher emission of longwave radiation. When the canopy biomass and *LAI* were high, such as at the full growing period of the aspen forest, heat capacity of the canopy was also high, which could weaken the degree of atmosphere stability during night. Therefore the errors in R_n and H estimations were decreased. The calculation of boundary-layer resistance under stable atmospheric conditions in the CLASS model was formulated by Abdella and McFarlane (1996) following Beljaars and Holtslag (1991). Unfortunately, its output for r_a under stable conditions was unreasonable. I modified r_a calculations according to Webb (1970) and Pruitt *et al.* (1973) which significantly improved its estimation. But problems with lower estimation under strongly stable conditions still need to be solved. Detailed calculations of r_a is beyond the focus of this thesis and will not be discussed.

The comparisons in the mid-growing season are shown in Figure 3.5. Plant *LAI* at this stage was simulated to be around 4.5-5.0 which was close to the modelled and observed peak values (see Figure 4.10 in Chapter 4). Plant and soil water potentials at this time were still relatively high and not strong limiting factors for transpiration. As a result, modelled latent heat exchange was significantly increased and exceeded sensible heat exchanges during most of the daytime. The tower flux measurements on H and LE also show this seasonal shift in energy partitioning. For different weather cases, day 182 was clear in the daytime with very high solar radiation. The observed net radiation around the noontime was about 650 W m^{-2}. Day 183 was a cloudy day with the net radiation lower than 100 W m^{-2} during most of the daytime. On day 185 there were some shower in the afternoon which caused the sharp decreases of observed R_n at these times. It can be seen that the modelled R_n traced the observations extremely well under all these weather conditions. The modelled H and LE also successfully reflected the general pattern of observations on day 183 and 185. However, large discrepancies occurred in the afternoon on day 182. Reasons for these differences may be limited to this specific situation since it did not happen

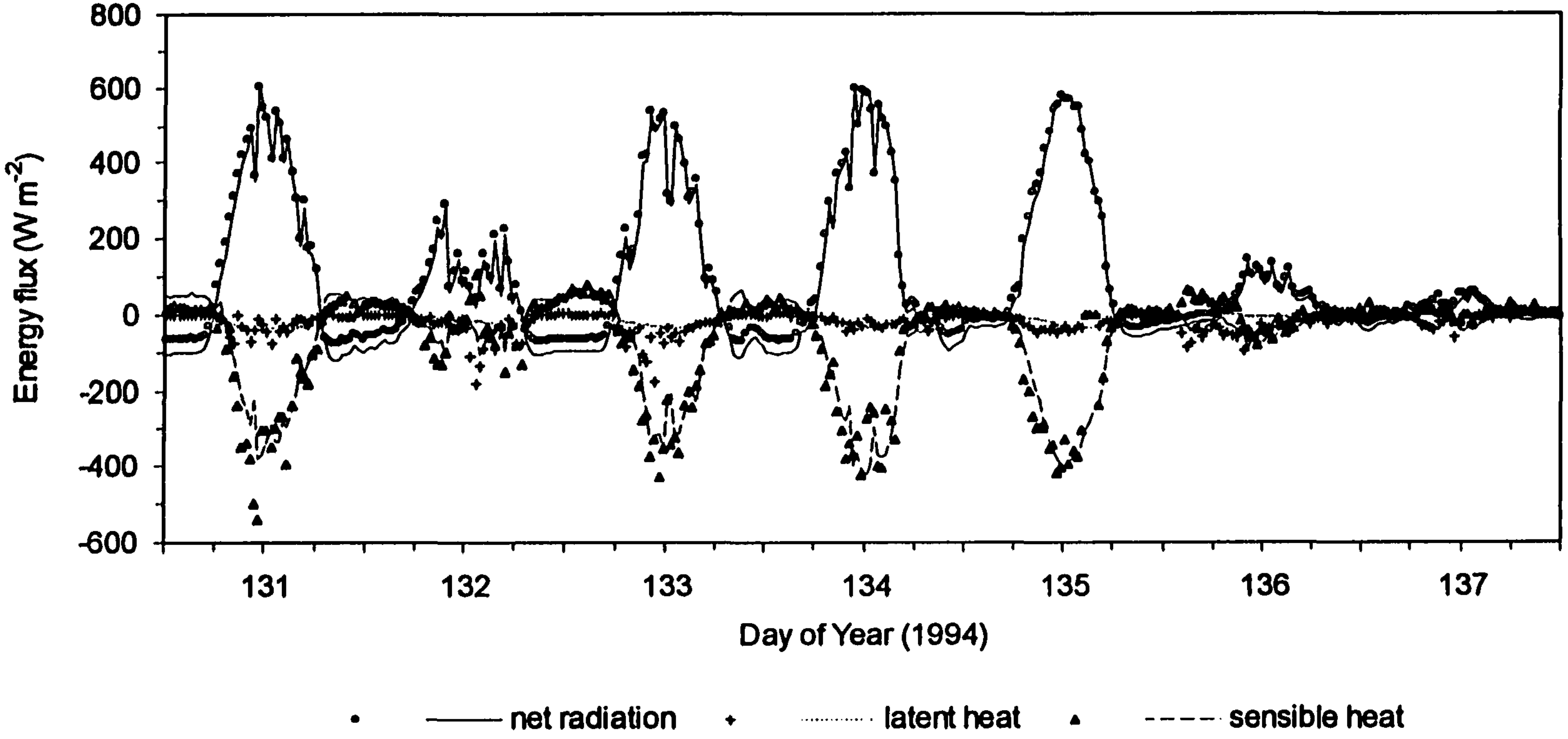

Figure 3.3 Simulated (lines) and tower measured (symbols) half-hourly fluxes of net radiation, sensible heat and latent heat over the aspen canopy in the early growing season

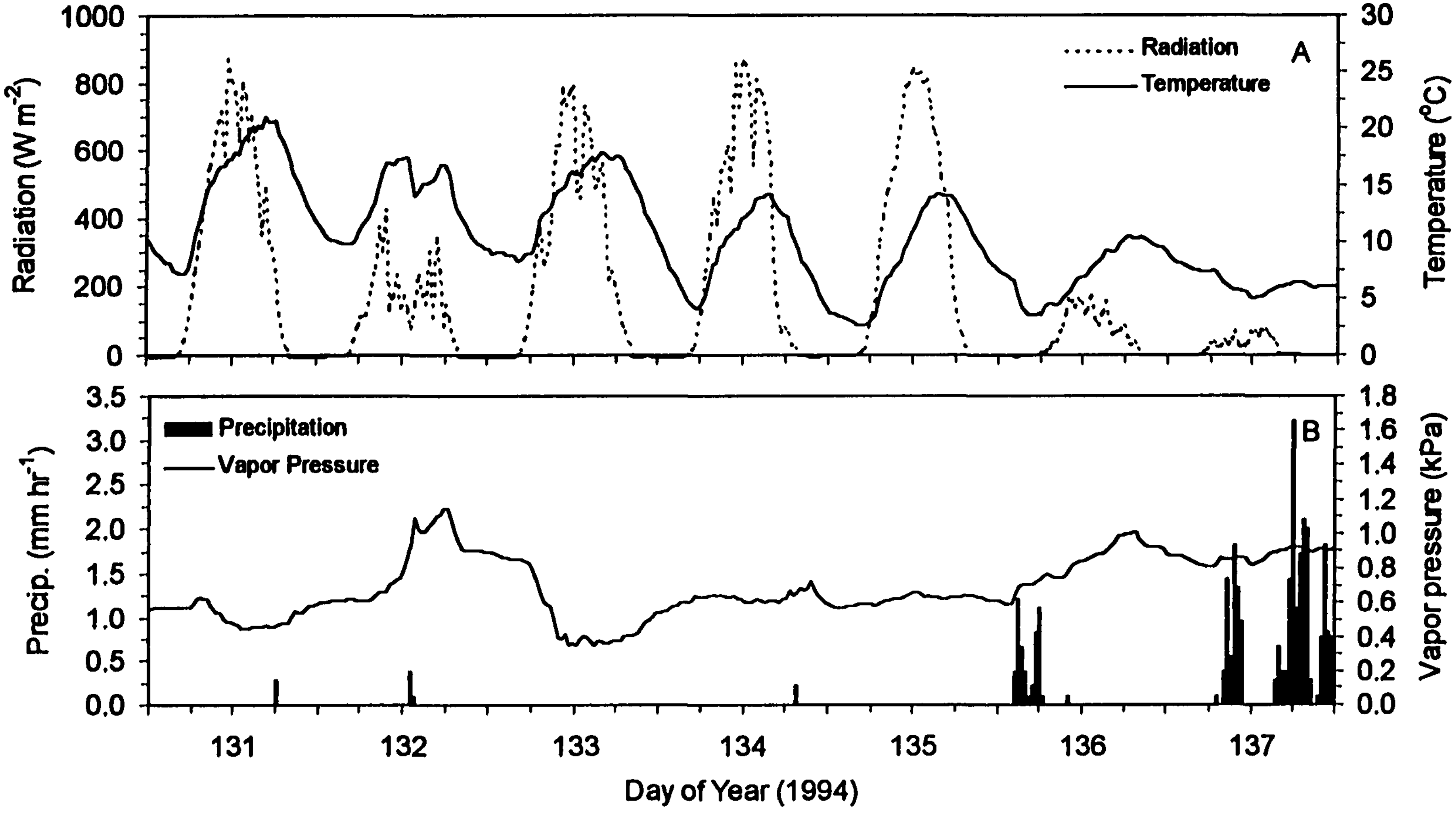

Figure 3.4 The corresponding meteorological conditions during the comparison week in the early growing season

A: shortwave radiation R_s and air temperature T_a, B: precipitation P and water vapor pressure e_a

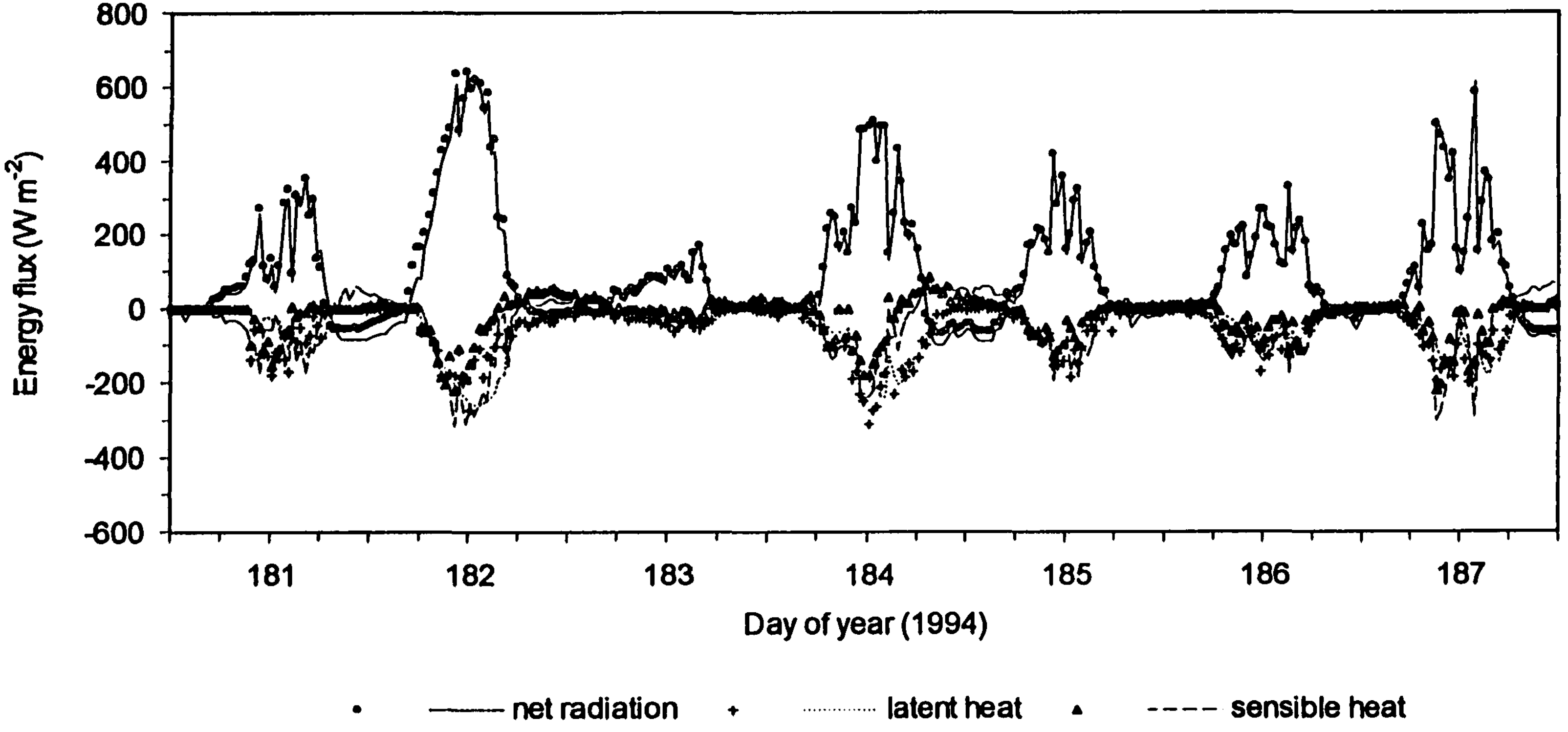

Figure 3.5 Simulated (lines) and tower measured (symbols) half-hourly fluxes of net radiation, sensible heat and latent heat over the aspen canopy in the mid-growing season

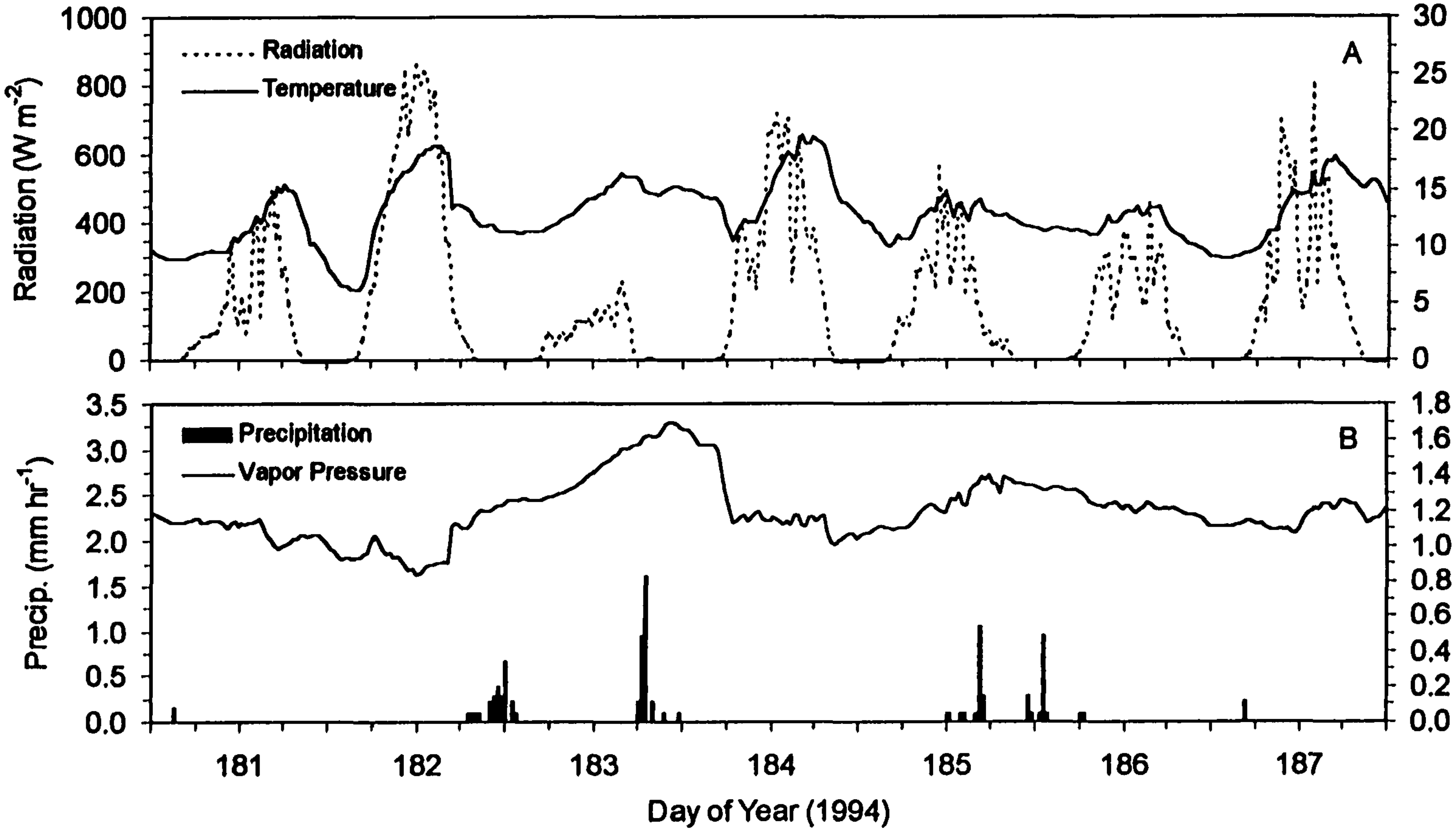

Figure 3.6 The corresponding meteorological conditions during the comparison week in the mid-growing season

A: shortwave radiation R_s and air temperature T_a, B: precipitation P and water vapor pressure e_a

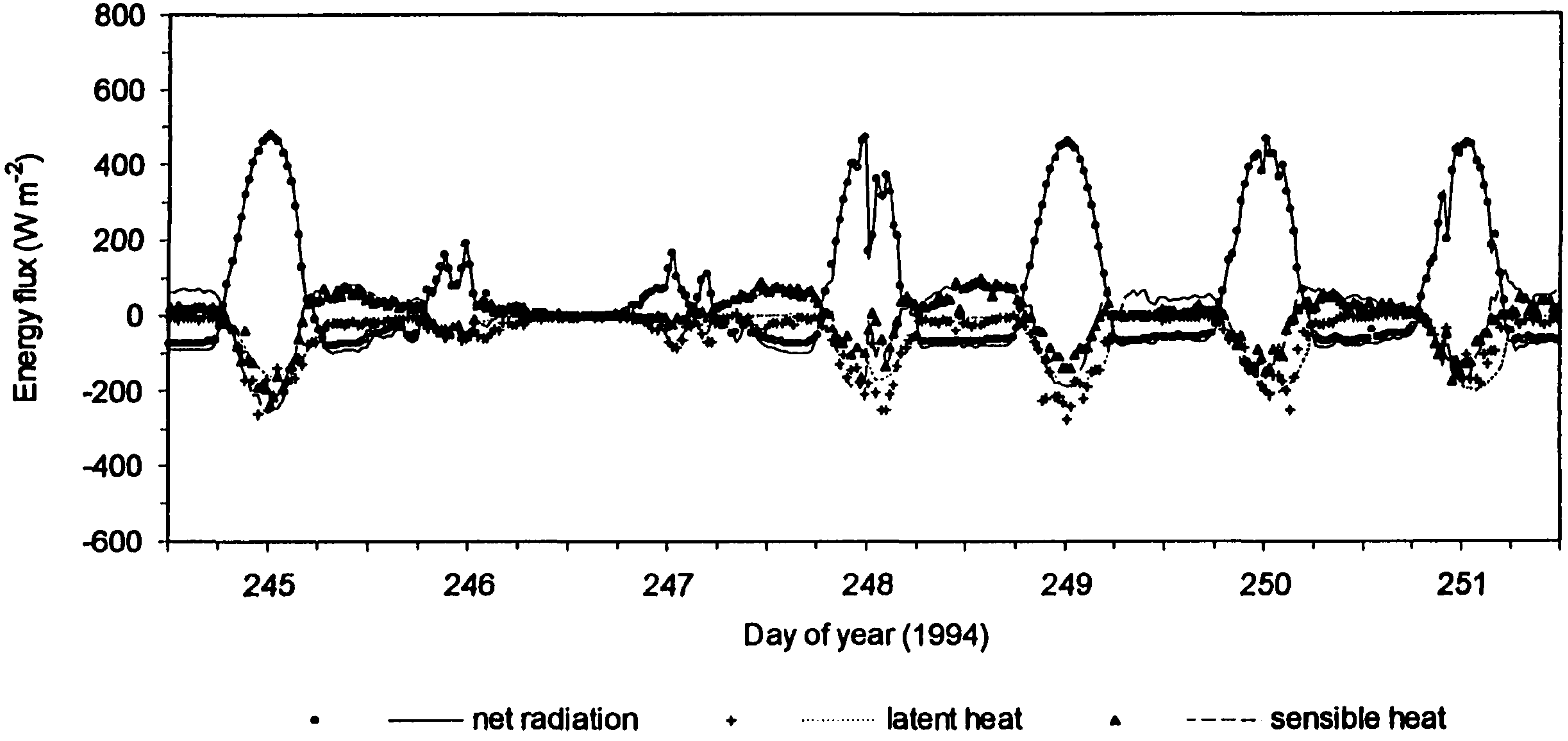

Figure 3.7 Simulated (lines) and tower measured (symbols) half-hourly fluxes of net radiation, sensible heat and latent heat over the aspen canopy in the late growing season

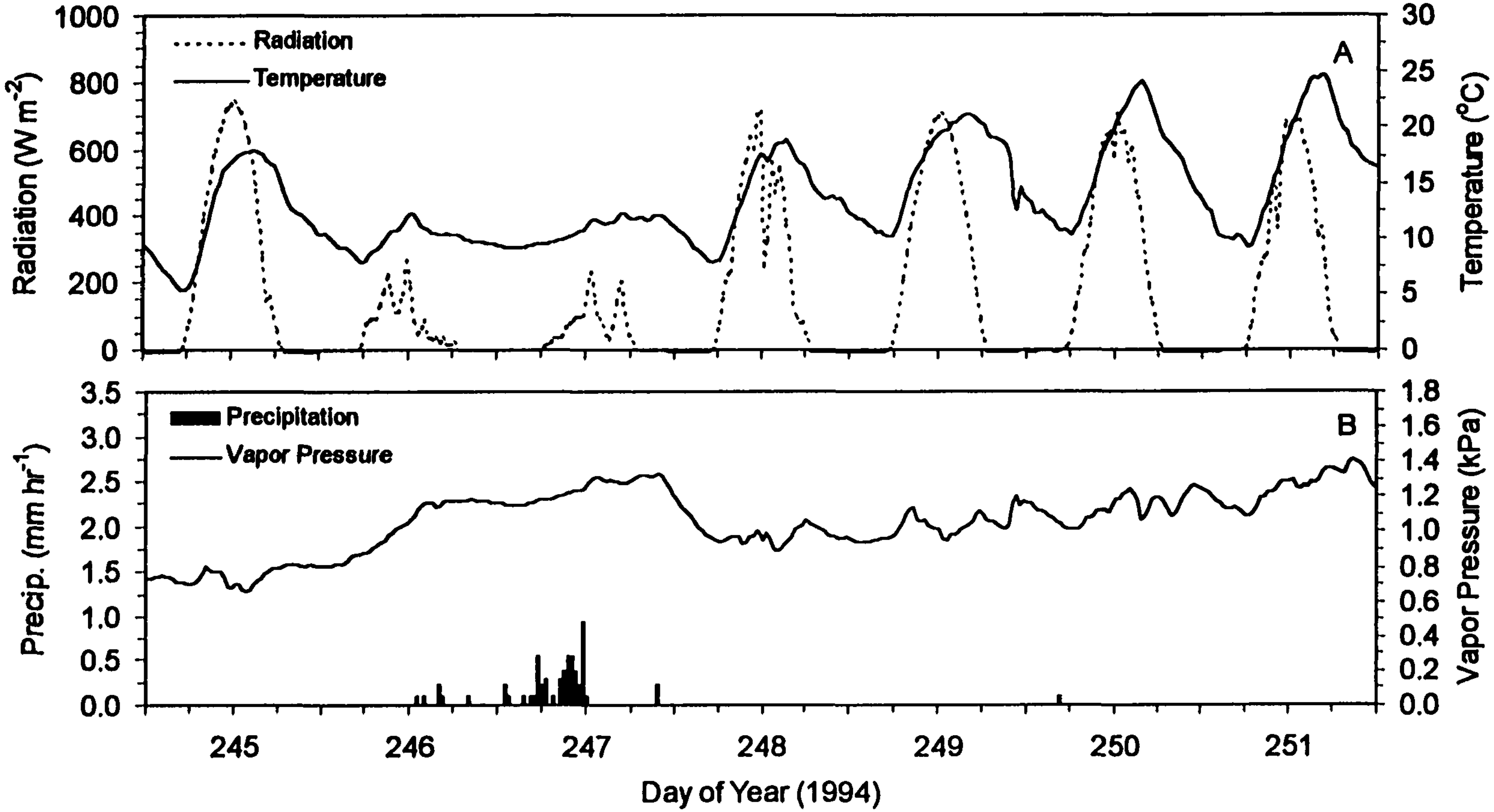

Figure 3.8 The corresponding meteorological conditions during the comparison week in the late growing season

A: shortwave radiation R_s and air temperature T_a, B: precipitation P and water vapor pressure e_a

systematically on other clear days. On cloudy nights such as the nights of day 183-184 and 185-187, high incoming longwave radiation slowed down the decrease in canopy temperatures thus prevented the formation of strong atmospheric inversion. Both the simulated and observed energy fluxes of R_n, H, and LE were close to zero under these conditions. During clear nights such as the nights of day 181-182 and 184-185, the model overestimated the negative net radiation and downward sensible heat flux as discussed above. However, the discrepancies were less than those in the early growing season as shown in Figure 3.3, which was likely due to the impact of the increased canopy heat capacity on the r_a estimations.

Patterns of energy exchanges in the late growing season before leaf senescence are illustrated in Figure 3.7. On day 245 the soil was relatively dry and both the observed and modelled results reflected this water stress by having higher H than LE around the noontime. In the next two days (day 246-247), there was a 10.7 mm rainfall. Both the measured and modelled latent heat exchanges were significantly increased and exceeded the sensible heat fluxes after this rain event in the following 4 clear days (day 248-251). It is also worth noting that large negative R_n and downward H (about 80 W m^{-2}) were both observed and simulated during the clear nights of this period (*e.g.*, day 245-246, 247-249), thus making the differences between modelled and observed values much smaller than those in the early growing season (Figure 3.3). Overall, the net radiation received by the ecosystem during this time period had significantly decreased due to the decrease in solar radiation, which also caused the decreases in the intensity of sensible heat and latent heat exchanges between the ecosystem and the atmosphere.

Even though there is a considerable increase in the fraction of R_n going to LE as the forest leaf area developed, we can still find significant sensible heat exchanges during the middle to late growing season in this aspen forest. Blanken *et al.* (1997) compared the seasonal pattern of daily mean H and LE at this site and it was indicated that H was much lower than LE after the canopy was leafed. Since there was considerable amount of downward H in cloud-free nights as shown in Figure 3.7, Bowen ratio β ($\beta = H/LE$) based on daily means of H and LE can be significantly lower than the daytime values when the energy exchange on the land surface is most intensive. If we calculate β for each 30 minutes during the daytime, we find that for most of the time during the middle and late growing seasons it was over 0.5. For example, the average β around the noontime (11 a.m. - 1 p.m.) for the five clear days shown in Figure 3.7 was observed to be 0.71. This number is significantly higher than Bowen ratios observed in tropical forests (*e.g.*, Shuttleworth *et al.*, 1984), irrigated crops under different climatic regions (*e.g.*, Wang and Chen, 1993; Wang *et al.*, 1994; Wang *et al.*, 1996), and grassland (*e.g.*, Fritschen and Qian, 1992; Smith *et al.*, 1992) under similar soil water conditions to this aspen forest. Higher Bowen ratio has been recognised as an important characteristic in the boreal forest which is found to have significant effects on the land surface-atmosphere interactions, such as the observed high boundary layer depth over the northern boreal forest (Margolis and Ryan, 1997). Some explanations for the occurrence of high β values for this ecosystem will be given in the next two chapters based on the plant and soil simulations.

Net radiation is the most important driving variable for almost all of the processes in ecosystems. Therefore its simulation plays a critical role in ecosystem modelling. Only with good estimations in radiation can a model have the potential to explore correctly other processes of an ecosystem. After the new modules were developed and a few bugs were fixed in the original program regarding radiation calculations, CLASS performs extremely well in radiation simulations throughout all the seasons of a year. Figure 3.9 gives an example of the correlation between the simulated and observed half-hourly R_n. There are, for each year in 1994 and 1996, 30 days data randomly selected from the three growing seasons in this plot, with ten days in each growing season (May, July, September). The simulated results for 1994 in the positive region (the first quadrant) are extremely good; only a few data sets in the low value region were scattered away. There is a systematic error in the high negative region which causes the data to deviate down from the 1:1 line. This error is mainly caused by the overestimation of negative R_n during nighttime in the early growing season as discussed above. The results for 1996 are a little more scattered compared with that 1994. A slight underestimation in the high radiation region can be noticed in this year. Overall, the slope and intercept obtained from least-squares linear regression are 0.98 and -11.02 W m^{-2}, respectively. The correlation coefficient between modelled and observed R_n for the more than three thousand data samples shown in Figure 3.9 is 0.993. The root mean square error (RMSE) is only 27.2 W m^{-2}.

Unlike the simulations on radiation which has solid physical laws underlying it and less parameters in simulation, latent heat or evapotranspiration estimation is much more complicated and many processes are still empirical. Figure 3.10 shows the regression relationship of simulated daily evapotranspiration to the measured results during the growing seasons of both 1994 and 1996. The data in this graph include all

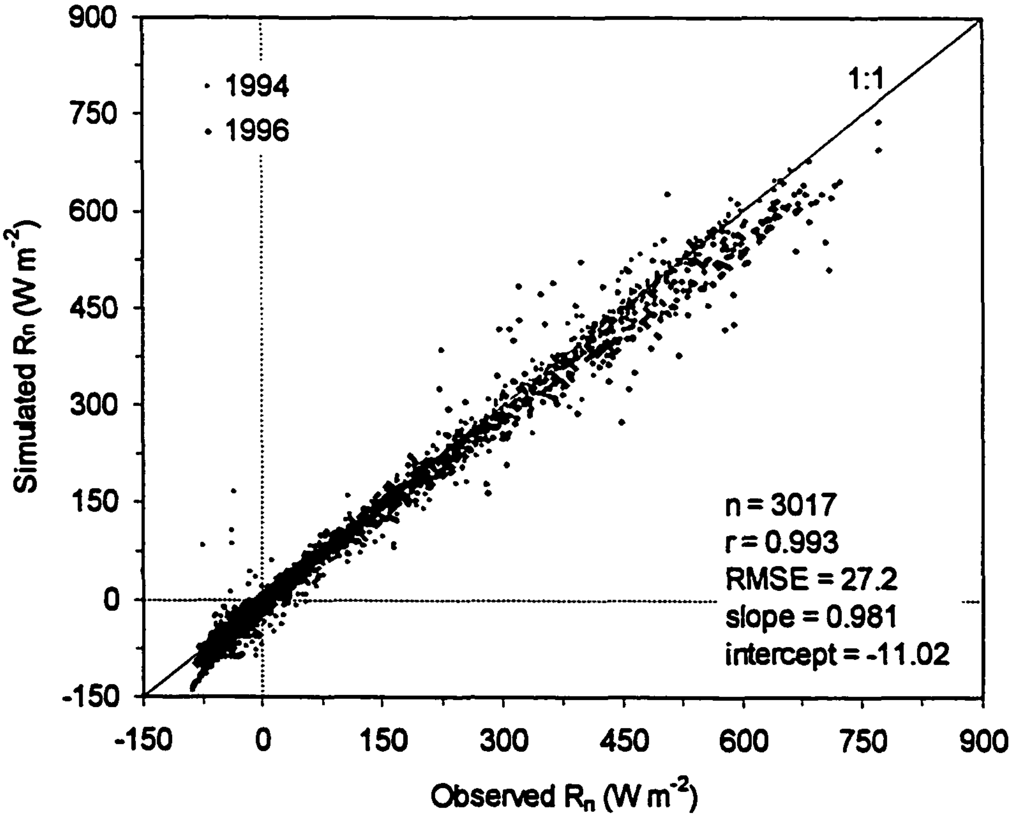

Figure 3.9 Linear regression relationship between simulated and tower measured half-hourly net radiation

the days (188 days) that have 24-hour continuous observations in 1994 (66 days) and 1996 (122 days). While underestimation of evapotranspiration in the low values can be found in 1994, there is no significant systematic deviation for 1996. The slope and intercept from linear regression of the two years' data are 0.94 and -0.14 mm H_2O day^{-1}. The RMSE and correlation coefficient are 0.71 mm day^{-1} and 0.866.

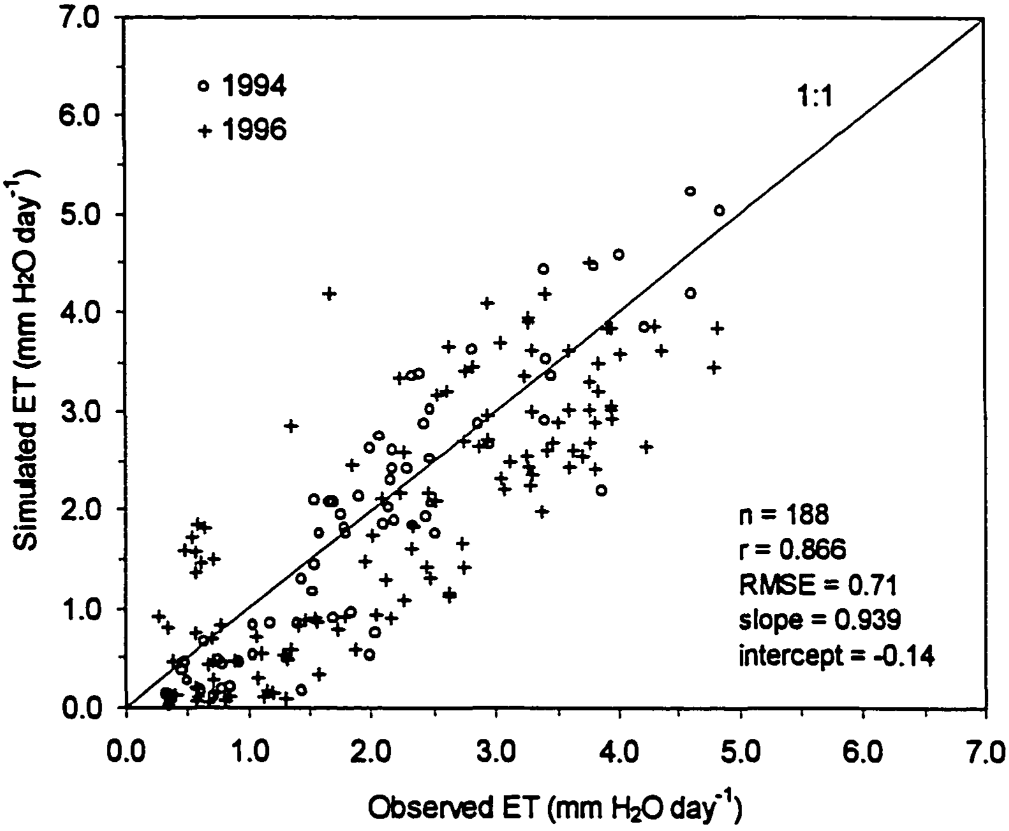

Figure 3.10 Linear regression relationship between simulated and tower measured daily evapotranspiration

Discrepancies between simulated and tower measured energy fluxes were probably a result of several factors. The model was initialised and driven by data measured from a specific site, while tower flux measurements represented the general results from a certain sized area. So the prerequisite for their comparisons is the homogeneity of land surface characteristics, such as the stand depth, stand structure, *LAI*, soil water content, and topography, etc. However, these conditions can be hardly met. Stand conditions at the SSA-OA sites were both spatially and temporally diverse and were composed of different age types, biomass densities and species compositions (Baldocchi and Vogel, 1996; Black *et al.*, 1996). Site heterogeneity may be an important factor responsible for the discrepancies between measured and modelled results.

There was a large proportion of biomass distributed in the understory plants that might contribute a significant amount of transpiration in this boreal forest (Black *et al.*, 1996). The understory plants that adapted to the shaded environment may behave quite differently from the overstory aspen with respect to the relationship between stomatal activity and the plant and microclimatic conditions. The model does not treat the overstory and understory plants separately. This may be another source causing the scattering of the simulated results.

Discrepancies could also be induced by inaccurate model parameterisations. Use of realistic site parameters is essential to model evaluations with measurements. However, most of the model parameters in this research were adopted to let the model behave as a functional vegetation type of deciduous tree rather than the aspen at the specific site. While this generalisation makes it easy for the coupled run with GCMs in the global scale, it could cause disagreement with specific site measurements.

Another reason for the discrepancies was related to the quality of the measurements. As shown in Figures 3.3, 3.5 and 3.7, the observed fluxes often revealed a pronounced "saw-blade" pattern in both *LE* and *H*. The sudden "up" and "down" in *LE* and *H* was physically unrealistic since there were no coincidental changes in any of the variables known to promote such changes (Blanken *et al.*, 1997). Detailed analyses on the data quality in flux measurements introduced by eddy correlation can be found in Blanken *et al.* (1997) and it is not addressed here.

(2) Root Water Uptake and Transpiration

By coupling plant water capacity into the dynamic water flow processes, we can use the model to explore the relationship between root water uptake Q_r and transpiration $Q_{E,c}$. Two typical patterns of Q_r with $Q_{E,c}$ are given in Figure 3.11 and Figure 3.12, together with their corresponding soil water potential ψ_s (simulated) and canopy water potential ψ_c (simulated). Changes in canopy water potential indicate whether the plant is losing water faster than it can replace losses by uptake from the soil. When leaf water loss exceeds root water uptake rates, both plant water content and canopy water potential decline. Recovery occurs when the root water uptake exceeds the rate of water loss from the leaves.

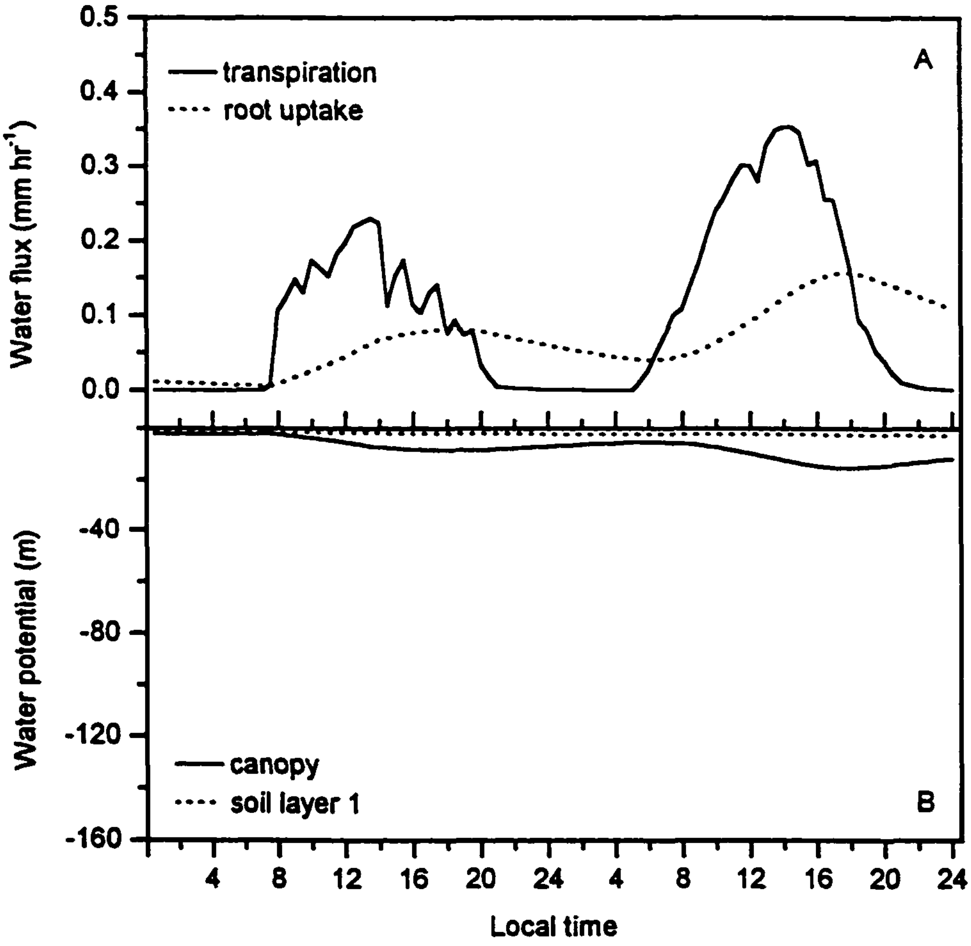

Figure 3.11 Diurnal pattern of plant root water uptake and transpiration under wet soil conditions (June 17 and 18, 1994)

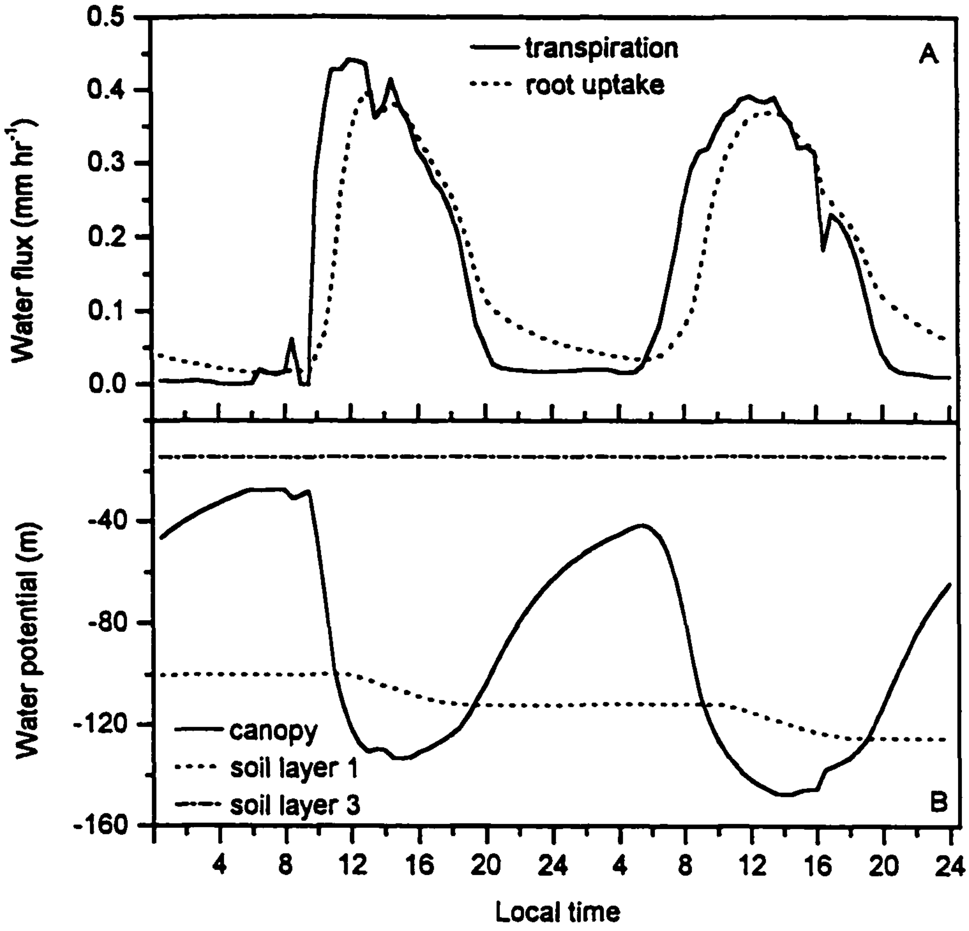

Figure 3.12 Diurnal pattern of plant root water uptake and transpiration under dry soil conditions (August 1 and 2, 1994)

Under wet soil conditions as shown in Figure 3.11 (June 17 and 18, 1994), the plant water capacity C_w (Table 3.1) was high. Transpiration under these conditions caused small decrease in ψ_c. Therefore there was a large time lag in Q_r with respect to $Q_{E,c}$ (3-4 hours). Due to the small gradient of water potential between soil and plant leaf (Figure 3.11B), the difference between the maximum transpiration rate and root uptake rate was also very large as shown in Finger 3.11A. Water lost in the plant during the daytime was replenished gradually with the onset of darkness until the next day when transpiration began to climb up with sunrise. This recovery phase was closely related to the ability of soil-root systems to transport water into the leaves. When ψ_s was high, ψ_c became quite close to ψ_s in the early morning. In the two days shown in Figure 3.11, transpiration reached its peak of 0.23 mm per hour on June 17 and 0.35 mm per hour on June 18 around 2 p.m., while the peak values for Q_r were around 6 p.m., with the respective values of only 0.08 mm per hour and 0.16 mm per hour, about 35% and 47% of the maximum $Q_{E,c}$.

Figure 3.12 shows another pattern when the soil was relatively dry (August 1 and 2, 1994). Soil water potential in the first soil layer where the major part of plant root was distributed had dropped to -100—-125 m H_2O on the two days (Figure 3.12B). Under these conditions, C_w was low. Water loss in this range can cause significant decrease in ψ_c and therefore increase the water potential gradient between leaf and soil. Both the time lag of Q_r with $Q_{E,c}$ and the difference of peak values between Q_r and $Q_{E,c}$ under these conditions were much smaller than those under wet soil conditions discussed above. Another characteristic was the peak values of transpiration appeared earlier when soil was dry. As shown in Figure 3.12A, $Q_{E,c}$ reached its maximum value around 12 a.m. on both August 1 and August 2, two hours earlier than that on June 17 and June 18 on Figure 3.11A. Maximum Q_r under the drier soil conditions was increased to about 90% and 95% of maximum $Q_{E,c}$. The time lags of Q_r with $Q_{E,c}$ on these two days were only about 1 hour. The deep soil layer on these two days was still quite wet as shown in Figure 3.12B, but a very limited amount of plant roots were distributed at this depth and this constrained the root water uptake rate. Therefore, even with the water replenishment after a whole night, the canopy water potential in the early morning was still significantly lower than the soil water potential.

Another point that can be addressed from the results is the duration of water availability in the dry soil layers. During night and in the early morning, ψ_c was even higher than the ψ_s in the first soil layer. Therefore the trees could not extract water from the dry top soil. The functioning roots for water uptake at this time were only those distributed in the deep and wet soil layers (*e.g.*, layer 3 in Figure 3.12B), which was only a small fraction of the total root system. Since the root hydraulic resistance and soil rhizosphere resistance are formulated directly as a function of root length in the model (equation 3.7, 3.9, and 3.10), we can speculate that the total resistance from plant roots and soil was high during this time period which retarded water replenishment at night. In the daytime from around 11 a.m. to 7 p.m. on these two days, ψ_c had dropped lower than the ψ_s of the top soil layer which made the water in this dry soil layer available to plant. This change also greatly increased the total functioning root amount and hence decreased its hydraulic resistance. Therefore there was a diurnal change in the hydraulic resistance of the soil-plant systems. This phenomenon has been observed in studies on crops (*e.g.*, Biscoe *et al.*, 1976; Jones, 1978; Choudhury and Idso, 1985; Reid and Huck, 1990).

The simulated results on the relationship between root water uptake and transpiration can be supported by the field observations from BOREAS. Simultaneous measurements were made in aspen at this study site by Hogg and Hurdle (1997) on sap flow, determined by the heat pulse method at a height of about 1.3 m above the ground, and transpiration rate, determined by eddy correlation. It was indicated that sap flow measurements showed a diurnal time lag of about 1 hour relative to aspen canopy transpiration. In another study at the BOREAS site, Saugier *et al.* (1997) analysed the time lag observations of a boreal pine forest. It was found that a half-hour time lag clearly gave a hysteresis loop in the plot of sap flow against transpiration measured by branch bag, whereas there was a better fit for the 1 h and 1.5 h time lag. It was also indicated that the time lag was not constant (see also Loustau *et al.*, 1996). For instance, on cloudy days the time lag was found to be in excess of 2 hours. The model outputs on the length of time lag were consistent with these observations. Under wet soil conditions, longer time lags were simulated than those observed. This was probably because the observed data were a result of changes in water storage within the tree above the point of sap flow measurement (1.3 m above ground), whereas the simulated data represented the changes in the water content of the whole trees including roots.

3.4 Sensitivity Analyses

Sensitivity tests can help quantify the general variability in modelled responses to changing climate and other model inputs and parameters. In this thesis, sensitivity analyses are focused on the model response to the variations in climate drivers. A series of sensitivity simulations were performed by changing a single climate driver in separate model runs. These individual sensitivity runs were not intended to model scenario studies, which can be defined as using physically consistent, simultaneous changes or variations in all drivers or site parameters. This strategy for model sensitivity tests was also used in Chapter 4 and Chapter 5.

Three climate variables were selected for the model sensitivity tests, namely, air temperature T_a, precipitation P, and atmospheric carbon dioxide concentration CO_2. The variations for these drivers were prescribed principally to be large enough to identify and isolate the major differences in model responses, while also remaining within the range of variability that the boreal forest ecosystem may be exposed to over a time period of about 50 to 100 years (Potter *et al.*, 2000; Kattenberg *et al.*, 1996; Kirschbaum *et al.*, 1996). The changes included: i), T_a±2.0°C – add or subtract 2.0°C to T_a in each time step; ii), P±50% – multiply the amount in each precipitation event by 50% or 150%, so the total number of rain events in a year remained the same; and, iii), CO_2±100 ppm – that is, CO_2=250 ppm or CO_2=450 ppm. To test the model responses and predictions with the changes of these environmental factors, model evapotranspiration *ET* was selected as the prognostic variable.

Figure 3.13 shows the sensitivity results represented by the relative changes of *ET* from the model runs. Variations in temperature brought the most significant changes in *ET*. A raise in air temperature by 2.0°C increased *ET* by 34.6%. This change was probably an integrated result attributed by several processes that directly or indirectly acted on *ET*. Temperature increase caused atmospheric potential evapotranspiration increase which could significantly increase the actual *ET* if the ecosystem was not water limited. This direct impact of temperature increase was represented in the model by an augmented humidity gradient between the air inside the stomata and the atmosphere. Some indirect impacts can also play important roles. Increase in the growing season length due to the T_a rise could help explain this change to some extent. Temperature increase at this boreal site also improved the conditions for plant photosynthesis and growth, and hence the canopy tended to have large *LAI*. According to Ball-Berry model (equation 3.2) and the scaling up formulations for canopy resistance (equation 3.6), both increase in photosynthesis and *LAI* will decrease r_c and finally increase *ET*. Soil temperature was also higher when air temperature was increased. Decomposition of the huge amount of soil organic matter will be accelerated under high soil temperatures which will cause more release of mineral nitrogen and improve the plant nutrient condition and therefore its growth. In addition, some increase in *ET* could be attributed to the higher snow sublimation and soil water evaporation under increased air temperature.

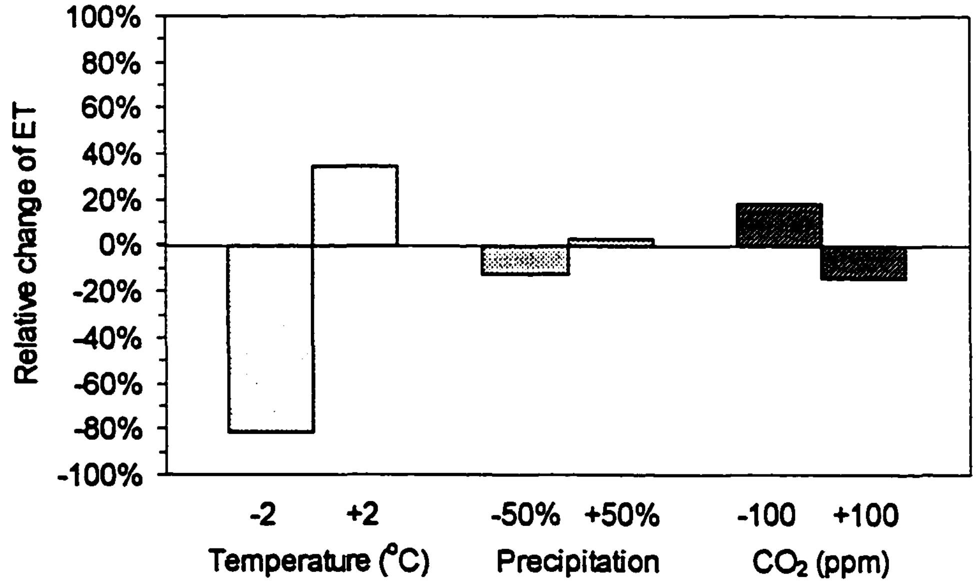

Figure 3.13 Sensitivity of simulated evapotranspiration (*ET*) to the variations of temperature, precipitation and CO_2 concentration

Decrease in air temperature affects all of the above processes in the other direction. A prescribed decline of 2.0°C in air temperature decreased *ET* by 81.7%

according to the model. Significant delay in leaf emergence date and earlier senescence of the plant contributed to the *ET* decrease to a large extent. It was also found that after T_a was decreased by 2°C, plant growth was apparently inhibited. A point that needs to be noted is that when the air temperature was decreased by 2°C, other climate drivers such as atmosphere water content were not changed. This may cause some unrealistic conditions that lead to the overestimation of atmospheric relative humidity (sometimes above 100%), which will decrease the *ET* estimations and may even cause the formation of condensation. The decrease of *ET* can be exaggerated by the model due to these improper variations in climate conditions.

There was no severe water stress found during most of the time in the two-year's simulations. This was consistent with observations by Black *et al.* (1996). Therefore increase in precipitation did not affect the simulated *ET* very much in the sensitivity test. A 50% increase in annual precipitation only slightly increased ecosystem *ET* by about 2.6%. However, a decline of 50% precipitation caused water stresses sometime in August and September. The simulated *ET* was dropped by 6.3% under this test. Small response of simulated *ET* to the variations in precipitation indicates that the model predicted the ecosystem as not strongly water limited. It is also worthwhile to note that the small response may be attributed partly to improper model initializations. For example, CLASS treats the soil profile to a depth of 4.1 m. The huge amount of water stored in this soil column can compensate the water shortage brought by the decreased precipitation amount and therefore lessen the model response to the prescribed drier conditions.

CO_2 concentration in the atmosphere can affect the *ET* estimation in two different ways. Leaf photosynthesis was enhanced under high CO_2 concentration (simulated in the next chapter) and plant growth can then be accelerated. Plants thus tended to have large *LAI* under enriched CO_2 conditions. This process can increase the *ET* of ecosystems. On the other hand, stomatal resistance was increased proportionally with CO_2 concentration of the air following equation (3.2). Increase in r_l by this process could significantly decrease transpiration rate. As a result, the integrated effects simulated by the model show that an increase of 100 ppm CO_2 finally decreased *ET* by 14.3%, and a decrease of 100 ppm CO_2 finally increased *ET* by 18.4%. Therefore under elevated CO_2 conditions, plants tend to conserve water which may benefit water-limited ecosystems. These trends of simulated effects have been observed on many CO_2 enrichment experiments on crops (Strain and Cure, 1985; Wang and Yu, 1993; Yu *et al.*, 1993).

3.5 Conclusions and Discussion

Canopy stomatal resistance plays a key role in determining plant transpiration. Field and laboratory studies have documented tight linkage between leaf photosynthesis and stomatal resistance. Theoretical work also shows that stomata function so as to maximise the plant water use efficiency. The relationship established by Ball-Berry model (equation 3.2) can be successfully used to couple the plant water and carbon processes and implemented in land surface schemes. It has some advantages over older schemes such as equation (2.7). First, though equation (3.2) is still an empirical equation, it is more biologically realistic in coupled water and carbon calculations. Second, it needs few parameters and is very applicable to the large scale generalised simulations like land surface schemes in GCMs. Third, other processes in the plant such as nutrient conditions can be included in the stomatal resistance calculations. For example, N is regarded as an important stress factor in the boreal forest. This nutrient limitation on stomatal resistance and hence on mass and energy exchange can be represented by the effects of N deficits on plant CO_2 fixation.

Plant water storage can greatly affect the temporal distributions of transpiration and root water uptake. Since land surface schemes coupled with GCMs are usually run at short time steps, this buffering process has practical significance. Coupling plant water capacity in the water transfer models in the soil-plant system can successfully simulate this impact.

The diagnostic variables of surface temperatures (canopy, ground, or snow) are the most important variable in the whole model. Their simulated results directly determine the amount and direction of mass and energy exchanges between land surfaces and the atmosphere. Therefore, the correctness in simulating surface temperatures determines the whole model behaviour to a great extent. For vegetated land surfaces, canopy temperature plays the key role in controlling the energy balance of the ecosystem. In this revised version of CLASS, canopy energy balance is coupled with the water transfer dynamics in the soil-plant system in which another diagnostic variable of canopy water potential is added. Since canopy temperature is the main factor in determining the net radiation calculations in the model, extremely good estimations in net radiation during the daytime by the model implies the correctness in the canopy temperature and water potential simulations. Boundary-layer resistance can affect surface temperature by controlling the intensity of latent and sensible heat exchanges. Unrealistic high r_a happened in the original model when the atmosphere is under stable stratification. Modified calculations in r_a were used in this research which greatly improved the model outputs. However, errors in the simulations during the nighttime of winter and early growing season still exist. Further work on the r_a formulation is required.

Sensitivity analyses show that evapotranspiration from this boreal ecosystem is most sensitive to changes in temperature and least sensitive to precipitation. Higher air temperatures can significantly increase the ecosystem water loss, while lower temperatures can greatly decrease this amount, though the number generated by the model may be exaggerated. CO_2 concentrations can also significantly affect the water budgets of ecosystems by altering the canopy stomatal resistance and plant growth. It was simulated that for the C_3 plant of the deciduous tree, elevated atmospheric CO_2 can help the ecosystems conserve water, which will benefit water-limited ecosystems.

References

Abdella, K., and McFarlane, N.A., 1996. Parameterization of the surface-layer exchange coefficients for atmospheric models. Boundary-layer meteorology. 80: 223-248.

Avissar, R., Avissar, P., Mahrer, Y., and Bravdo, B.A., 1985. A model to simulate response of plant stomata to environmental conditions. Agric. For. Meteorol., 34: 21-29.

Ball, J.T., 1988. An analysis of stomatal conductance. Ph.D. Thesis, Stanford University. CA. 89 pp.

Ball, J.T. and Berry, J. A., 1982. The c_i/c_s ratio: A basis for predicting stomatal control of photosynthesis. Carnegie Institute Washington Yearbook. 81: 88-92.

Ball, J.T., Woodrow, I.E. and Berry, J.A., 1987. A model predicting stomatal conductance and its contribution to the control of photosynthesis under different environmental conditions. In: Biggens J. (ed.). Progress in Photosynthesis Research, Vol. 4, pp. 221-224. Martinus-Nijhoff., Dordrecht, Netherlands.

Beljaars, A.C.M. and Holtslag, A.A.M., 1991. Flux parameterization over land surfaces for atmospheric models. J. Applied Meteorol., 30: 327-341.

Biscoe, P.V., Cohen, Y., and Wallace, J.S., 1976. Daily and seasonal changes of water potential in cereals. Philos. Trans. R. Soc. London Ser. B. 273: 565-580.

Baldocchi, D.D., and Vogel, C.A., 1996. Energy and CO_2 flux densities above and below a temperate broad-leaved forest and a boreal pine forest. Tree Physiol. 16: 5-16.

Black, T.A., den Hartog, G., Neumann, H.H., Blanken, P.D., Yang, P.C., Russell, C., Nesic, Z., Lee, X., Chen, S.G., and Staebler, R., 1996. Annual cycles of water vapor and carbon dioxide fluxes in and above a boreal aspen forest. Global Change Biol. 2: 219-229.

Blanken, P.D., Black, T.A., Yang, P.C., Neumann, H.H., Nesic, Z., Staebler, R., den Hartog, G., Novak, M.D., and Lee, X., 1997. Energy balance and canopy conductance of a boreal aspen forest: Partitioning overstory and understory components. J. Geophysical Research, 102, No. D24: 28,915-28,927.

Boote, K.J. and Loomis, R.S., 1991. The prediction of canopy assimilation. In: Boote, K.J. and Loomis, R.S., (eds) Modelling Crop Photosynthesis – from Biochemistry to Canopy. CSSA Special Publication No.19, pp109-140.. Madison, Wisconsin, USA.

Boyer, J.S., 1974. Water transport in plants: Mechanism of apparent changes in resistance during absorption. Planta, 117: 187-207.

Choudhury, B.J. and Idso, S.B., 1985. Evaluating plant and canopy resistances of filed-grown wheat from concurrent diurnal observations of leaf water potential, stomatal resistance, canopy temperature, and evapotranspiration flux. Agric. For. Meteorol., 34: 67-76.

Collatz, G.J., Ball, J.T., Grivet, C., and Berry, J.A., 1991. Physiological and environmental regulation of stomatal conductance, photosynthesis and transpiration: A model that includes a laminar boundary layer. Agric. For. Meteorol., 54: 107-136.

Collatz, G.J., Ribas-Carbo, M., and Berry, J.A., 1992. Coupled photosynthesis-stomatal conductance model for leaves of C_4 plants. Aust. J. Plant Physiol., 19: 519-538.

Cowan, I.R., 1965. Transport of water in the soil-plant-atmosphere system. J. Appl. Ecol., 2: 221-239.

Cowan, I.R., 1982. Regulation of water use in relation to carbon gain in higher plants. Encycl. Plant Physiol., New Ser. 12B: 535-562.

Dalton, F.N., Raats, P.A.C., and Gardner, W.R., 1975. Simultaneous uptake of water and solutes by plant roots. Agron. J. 67: 334-339.

Denmead, O.T., and Bradley, E.F., 1985. Flux-gradient relationships in a forest canopy. In: The Forest-Atmosphere Interaction. (Eds. B.A. Hutchison and B.B. Hicks) pp. 421-42. Reidel: Dordrecht.

Denmead, O.T., and Bradley, E.F., 1987. On scalar transport in plant canopies. Irrigation Science, 8: 131-149.

Dickinson, R.E. and Shaikh, M., 1998. Interactive canopies for a climate model. J. Climate, 11: 2823-2836.

Farquhar, G.D. and Sharkey, T.D., 1982. Stomatal conductance and photosynthesis. Annu. Rev. Plant Physiol. 33: 317-345.

Fiscus, E.L., 1975. The interaction between osmotic- and pressure-induced water flow in plant roots. Plant Physiol. 55: 917-922.

Fritschen, L. and Qian, P., 1992. Variation in energy balance components from six sites in a native prairie for three years. Journal of Geophysical Research, 97: 18,651-18,661.

Gardner, W.R., 1960. Dynamic aspects of water availability to plants. Soil Sci., 89: 63-73.

Gash, J.H.C., Shuttleworth, W.J., Lioyd, C.R., Andre, J-C. and Goutorbe, J-P., 1989. Micrometeorological measurements in Les Landes forest during HAPEX-MOBILHY. Agric. For. Meteorol., 46: 131-147.

Herkelrath, W.N., Miller, E.E., and Gardner, W.R., 1977. Water uptake by plants: II. The root contact model. Soil Sci. Soc. Am. Proc. 41: 1039-1043.

Hogg, E.H. and Hurdle, P.A., 1997. Sap flow in trembling aspen: implications for stomatal responses to vapor pressure deficit. Tree Physiology. 17: 501-509.

Jarvis, P.G., 1976. The interpretation of the variation in leaf water potential and stomatal conductance found in canopies in the field. Philosophical Transactions of the Royal Society of London. Ser. B 273: 593-610.

Jones, H.G., 1978. Modelling diurnal trends of leaf water potential in transpiring wheat. J. Appl. Ecol. 15: 613-626.

Jones, H.G. and Higgs, K.H., 1989. Empirical models of the conductance of leaves in apple orchards. Plant Cell Environ., 12: 301-308.

Kattenberg, A., Giorgi, F., Grassl, H., Meehl, G.A., Mitchell, J.F.B., Stouffer, R.J., Tokioka, T., Weaver, A.J., and Wigley, T.M.L., *et al.*, 1996. Climate models - Projections of future climate. In: Climate Change 1995 – The Science of Climate Change: Contribution of Working Group I to the Second Assessment of the Intergovernmental Panel on Climate Change, J. T. Houghton, L. G. Meira Filho, B. A. Callender, N. Harris, A. Kattenberg and K. Maskell (Eds.), Cambridge University Press, UK. pp. 285-357.

Kirschbaum, M.U.F., Fischlin, A., *et al.*, 1996. Climate Change Impacts on Forests. In: Climate Change 1995 - Impacts, Adaptations and Mitigation of Climate Change: Scientific-Technical Analyses. Contribution of Working Group II to the Second Assessment of the Intergovernmental Panel on Climate Change, R.T. Watson, M. C. Zinyowera, and R. H. Moss, (Eds.), Cambridge University Press, UK. pp.95-129.

Klepper, B., Rickman, R.W., and Taylor, H.M., 1983. Farm management and the function of field crop root system. Agric. Water Manage. 7: 115-141.

Kozlowski, T.T., 1982. Water supply and tree growth. Part I, Water deficits. Forestry Abstracts, 43: 57-83.

Kozlowski, T.T., and Pallardy, S.G., 1997. Physiology of Woody Plants. Second edition. Academic Press, San Diego.

Loustau, D., Berbigier, P., Roumagnac, P., Arruda-Pacheco, C., David, J.S., Ferreira, M.I., Pereira, J.S., and Tavares, R., 1996. Transpiration of a 64-year-old maritime pine stand in Portugal. 1. Seasonal courses of water flux through maritime pine. Oecologia, 107: 33-42.

Margolis, H.A. and Ryan, M.G., 1997. A physiological basis for biosphere-atmosphere interactions in the boreal forest: an overview. Tree Physiology, 17: 491-499.

Newman, E.I., 1969. Resistance to water flow in soil and plant. I Soil resistance in relation to amounts of root: theoretical estimates. Journal of Applied Ecology 6: 1-12.

Passioura, J.B. and Cowan, I.R., 1968. On solving the non-linear diffusion equation for the radial flow of water to the roots. Agricultural Meteorology, 5: 129-134.

Philip, J.R., 1966. Plant water relations: Some physical aspects. Ann. Rev. Plant Physiol. 17: 245-268.

Potter, C., Amthor, J., King, A., Nikolov, N., Chen, J., Frolking, S., Grant, R., Wang, S., Kimball, J., Running, S., McGuire, D., and Clein, J., 2000. Comparison of boreal ecosystem model sensitivity to variability in climate and forest site parameters. (To be published).

Pruitt, W.O., Morgan, D.L., and Lourence, F.J., 1973. Momentum and mass transfers in the surface boundary layer. Quart. J. R. Met. Soc., 99: 370-386.

Raupach, M.R., 1987. A Lagrangian analysis of scalar transfer in vegetation canopies. Quartly Journal of the Royal Meteorological Society. 113: 107-120.

Raupach, M.R., 1989a. A practical Lagrangian method for relating scalar concentrations to source distributions in vegetation canopies. Quarterly Journal of the Royal Meteorological Society, 115: 609-632.

Raupach, M.R., 1989b. Applying Lagrangian fluid mechanics to infer scalar source distributions from concentration profiles in plant canopies. Agricultural and Forest Meteorology, 47: 85-108.

Reid, J.B. and Huck, M.G., 1990. Diurnal variation of crop hydraulic resistance: a new analysis. Agron. J. 82: 827-834.

Saugier, B., Granier, A., Pontailler, J.Y., Dufrene, E, and Baldocchi, D.D., 1997. Transpiration of a boreal pine forest measured by branch bag, sap flow and micrometeorological methods. Tree Physiology, 17: 511-519.

Sellers, P.J., Randall, D.A., Collatz, G.J., Berry, J.A., Field, C.B., Dazlich, D.A., Zhang, C., Collelo, G.D., and Bounoua, L., 1996. A revised land surface parameterization (SiB2) for atmospheric GCMs. Part I: Model formulation. J. Climate, 9: 676-705.

Shuttleworth, W.J., *et al.*, 1984. Eddy correlation measurements of energy partition for Amazonian forest. Quart. J. R. Met. Soc., 110: 1143-1162.

Sinclair, T.R., 1991. Canopy carbon assimilation and crop radiation-use efficiency dependence on leaf nitrogen content. In: Boote, K.J. and Loomis, R.S., (eds) Modelling Crop Photosynthesis – from Biochemistry to Canopy. CSSA Special Publication No.19, pp. 95-108. Madison, Wisconsin, USA.

Sinclair, T.R. and Lemon, E.R., 1974. Penetration of photosynthetically active radiation in corn canopies. Agron. J., 66: 201-205.

Sinclair, T.R. and Knoerr, K.R., 1982. Distribution of photosynthetically active radiation in the canopy of a loblolly pine plantation. J. Appl. Ecol., 19: 183-191.

Smith, E.A., Hsu, A.Y., Crosson, W.L., Field, R.T., Fritschen, L.J., Gurney, R.J., Kanemasu, E.T., Kustas, W.P., Nie, D., Shuttleworth, W.J., Stewart, J.B., Verma, S.B., Weaver, H.L., and Wesely, M.L., 1992. Area-averaged surface fluxes and their time-space variability over the FIFE experimental domain. Journal of Geophysical Research, 97: 18,599-18,622.

Steele, S.J., Gower, S.T., Vogel, J.G., and Norman, J.M., 1997. Root mass, net primary production and turnover in aspen, jack pine and black spruce forests in Saskatchewan and Manitoba, Canada. Tree Physiology. 17: 577-587.

Strain, B.R. and Cure, J.D., 1985. Direct effects of increasing carbon dioxide on vegetation. Carbon Dioxide Res. Div., U. S. Dep. Energy, DOE/ER-0238, Washington, D.C.

Taylor, G.I., 1921. Diffusion by continuous movements. Proc. Lond. Math. Soc. Ser. 2, 20: 196-212.

Tyree, M.T. and Yang, S., 1990. Water-storage capacity of *Thuja*, *Tsuga* and *Acer* stems measured by dehydration isotherms. Planta. 182: 420-426.

Van den Honert, T.H., 1948. Water transport in plants as a catenary process. Faraday Soc. Discuss. 3: 146-153.

Verseghy, D.L., McFarlane, N.A., and Lazare, M., 1993. CLASS - A Canadian land surface scheme for GCMs. II. Vegetation model and coupled runs. International Journal of Climatology 13: 347-370.

Wallace, J.S., and Biscoe, P.V., 1983. Water relations of winter wheat. J. Agric. Sci., 100: 591-600.

Wang, S. and Chen, F., 1993. Experimental study on energy balance and CO_2 flux of spring wheat field near the edge of oasis. In: Proceedings of International Symposium on HEIFE. Kyoto Japan.

Wang, S. and Yu, H., 1993. Direct Impacts of increasing atmosphere CO_2 concentration on crop growth and development. In: Effects of Increasing CO_2 on Agriculture of China. Beijing Science & Technology Press.

Wang, S., Sun, S., Zhu, Z., and Chen, F., 1994. Energy and water budgets over wheat field in different climatic regions. In: Proceedings of the International Symposium on the Global Energy and Water Cycle Experiment (GEWEX) in Asia - GAME. Beijing University, Beijing.

Wang, S., Zhu, Z., and Sun, X., 1996. Characteristics of energy and mass exchanges in the wheat field of Lhasa, Xizang (Tibet). *Science in China (Series D)*, Vol 39: 418-424.

Webb, E.K., 1970. Profile relationships: the log-linear range, and extension to strong stability. Quart. J. R. Met. Soc., 96: 67-90.

Wilson, J.D., Thurtell, G.W., and Kidd, G.E., 1981. Numerical simulation of particle trajectories in inhomogeneous turbulence, II: Systems with variable turbulent velocity scale. Boundary-layer Meteorol., 21: 423-441.

Wong, S.C., Cowan, I.R., and Farquhar, G.D., 1979. Stomatal conductance correlates with photosynthetic capacity. Nature (London), 282: 424-426.

Wong, S.C., Cowan, I.R. and Farquhar, G.D., 1985a. Leaf conductance in relation to rate of CO_2 assimilation. I. Influence of nitrogen nutrition, phosphorous nutrition, photon flux density and ambient partial pressure of CO_2 during ontogeny. Plant Physiol., 78: 821-825.

Wong, S.C., Cowan, I.R. and Farquhar, G.D., 1985b. Leaf conductance in relation to rate of CO_2 assimilation. II. Effects of short term exposure to different photon flux densities. Plant Physiol., 78: 826-829.

Wong, S.C., Cowan, I.R., and Farquhar, G.D., 1985c. Leaf conductance in relation to rate of CO_2 assimilation. III. Influence of water stress and photoinhibition. Plant Physiol., 78: 830-834.

Yu, H., Wang, S., and Deng, G., 1993. Study on the effects of carbon dioxide concentration doubling on the yield of field crops. In: "Proceedings of International Symposium on Climatic Change, Natural Disasters and Agricultural Strategies". China Meteorological Press. Beijing.

Chapter 4 Modelling Plant Carbon and Nitrogen Processes in CLASS – the *PLANTC* Module

4.1 Introduction

The terrestrial biosphere plays several important roles in determining the global climate system. The physical part of the land surface processes, such as energy and water exchanges, can be strongly affected by the plant physiology, such as the stomatal control in canopy transpiration discussed in Chapter 3. These plant physiology also controls some other important processes in the land surfaces. For example, as a main greenhouse gas affecting global change, net CO_2 flux between ecosystems and the atmosphere is largely determined by a combined result of plant photosynthesis and autotrophic respiration. Moreover, plant litter production and root carbon exudation are the main soil organic matter inputs. Both their quantity and quality drive the heterotrophic respiration and control the CO_2 flux between soil and the atmosphere. Carbon exchange between the terrestrial ecosystem and the atmosphere is the dominant processe in atmosphere CO_2 budgets. Small shifts in the C fixation ability of the ecosystems may bring significant change in the atmospheric CO_2 conditions, which is expected to impact the climate system of the earth.

In second-generation land surface schemes, plant processes at the physiological level have not been considered. The CO_2 exchanges between land surfaces and the atmosphere are thus not included. Atmospheric CO_2 conditions in GCMs are usually prescribed as model inputs, instead of being calculated based on the atmosphere and land surface interactions. Energy and water calculations are treated independently of the plant carbon processes. Some vegetation parameters that are important to the land surface processes, such as canopy resistance and plant leaf area index (*LAI*), are usually treated simply and obtained from prescribed formulations (Henderson-Sellers *et al.*, 1993).

There are some disadvantages with these kinds of simplifications in land surface schemes. First, the dynamic characteristics of the plant growth and development are in reality driven by the physiological activities of the plants themselves. Many factors including the intrinsic characteristics of the plants and their interactions with the environmental factors control the plant status at a specific time. To prescribe these parameters and processes in a model is not a realistic way to reflect the dynamic aspect of plant biological processes and their potential interactions with the climate system. Second, feedbacks of the canopy changes induced by climatic change can not be easily implemented in the model. It is anticipated that climate changes may cause alterations in the biophysical characteristics of the surface; namely albedo, surface roughness and the biophysical control of evapotranspiration (surface and internal resistance). Any changes in these may have feedback effects on the near-surface climatology, such as temperature, humidity, precipitation and cloudiness fields.

Recently, some efforts have been made to overcome these disadvantages. In the land surface scheme of BATS (Dickinson and Shaikh, 1998), simple methods on plant carbon uptake, allocation between plant tissues, and respiration loss were implemented; so the seasonal growth of plant leaf area was inferred from these calculations. In IBIS (Foley, 1996), the vegetation dynamics which reflect the transient changes in vegetation cover in response to environmental conditions were addressed. The annual carbon balance was estimated and used to predict changes in the leaf area index and biomass.

In this chapter, I developed a physiologically based plant module – *PLANTC*, for the dynamic plant growth and development simulations. It is focused on the carbon and nitrogen dynamics of the plant and provides the basis for the coupled water and carbon calculations in the land surface scheme as discussed in Chapter 3. The main physiological processes developed in this module include plant photosynthesis, root nitrogen uptake, respiration, substrate C and N translocation and plant tissue growth, and plant litter production, etc. This module is closely related to other modules in the CLASS model. Some important variables and parameters used in other parts of the model, such as the carbon fixation rate used for the stomatal resistance calculations (V_l in equation 3.2), *LAI*, and root distributions in different soil layers, are obtained from the calculations in this module. Therefore these parameters and processes no longer need to be prescribed by the model as independent inputs. This module also provides carbon and nitrogen influx to the *SOILC* module through plant litter and root exudation calculations.

4.2 Module Description

4.2.1 General Module Structure

Figure 4.1 shows the general structure of the *PLANTC* module that represents the plant system. The plant is divided into three different functional parts: foliage, sapwood of branch, stem and coarse root, and fine root. Carbon and nitrogen in each of these three physiologically active parts are considered to comprise the plant dry matter. They are assumed to exist in two different states: substrate and structural. Substrate C refers to the carbon fixed during leaf photosynthesis and substrate N is obtained by root uptake from soil. Both substrate C and N can be either transported between or stored within different plant parts according to the source-sink strength relations. Structural C and N represents the outcome of plant growth by chemical and/or biochemical conversions of the substrate C and N and it forms the main part of the plant biomass. The structural C and N pools for plant fine root are further divided into three sub-pools, with each sub-pool representing the amount of structural C and N of the root in that specific soil layer. Heartwood is also recognised as the fourth part of plants in the module, but it is treated as physiologically inactive.

The inputs to the *PLANTC* module include carbon fixed in photosynthesis which is directly added to the substrate C pool of the foliage, and nitrogen extracted from each soil layer which is added to substrate N pool of the fine root (Figure 4.1). The outputs of the module include the CO_2 production from the substrate C pools of each plant part due to autotrophic respiration, the root carbon exudation from root substrate C pool, and the plant litterfall produced from both the substrate and structural C and N pools of each plant part. Plant litterfall and root carbon exudation will be used as the main C and N inputs in the *SOILC* module discussed in Chapter 5. The translocation of substrate C and N between adjacent plant parts is formulated according to their concentration gradient and transfer resistance. Heartwood growth is estimated by the senescence rate of structural sapwood.

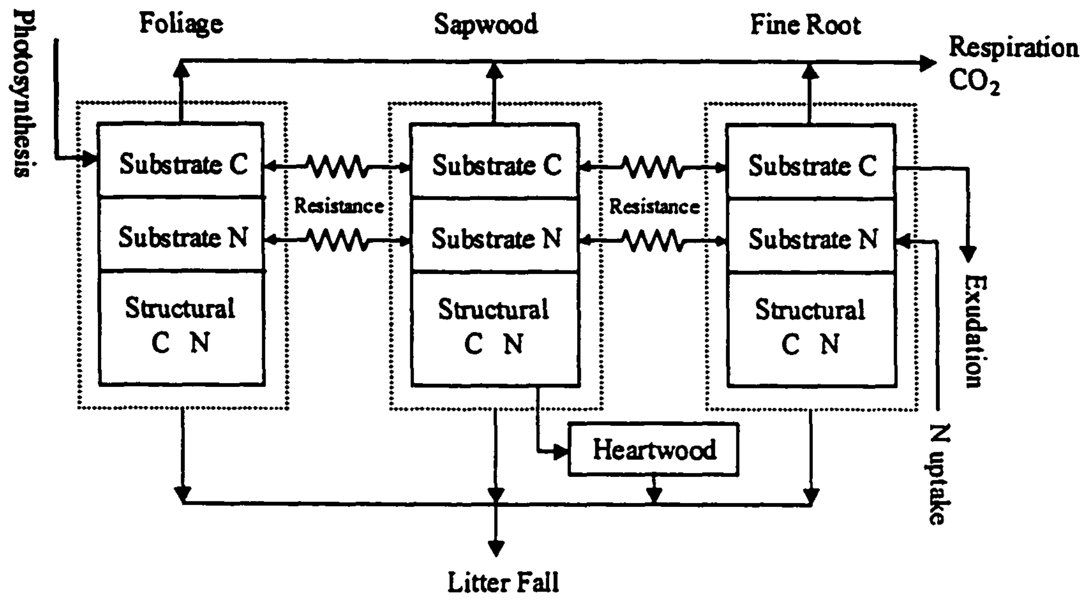
Photosynthesis
Foliage
Sapwood
Fine Root
Respiration
CO2
Substrate C
Substrate N
Structural
C N
Resistance
Resistance
Substrate C
Substrate N
Structural
C N
Substrate C
Substrate N
Structural
C N
Exudation
N uptake
Heartwood
Litter Fall

Figure 4.1 Schematic diagram of the *PLANTC* module

Processes included in each of these three physiologically active plant parts are shown in Figure 4.2. It is assumed that the substrate C in each plant part is consumed by maintenance respiration which is required to maintain the biological integrity of the plant. The remaining substrate C and the substrate N are then used for the translocation and tissue growth calculations. In case the storage of substrate C is less than the requirement for maintenance respiration, remobilization of C and N in structural materials is assumed to happen. Nitrogen remobilized during this process is assumed to return to the local substrate N pool. Before litter fall, a fraction of N is considered to translocate back to the local substrate N pool to represent the plant N biochemical cycles.

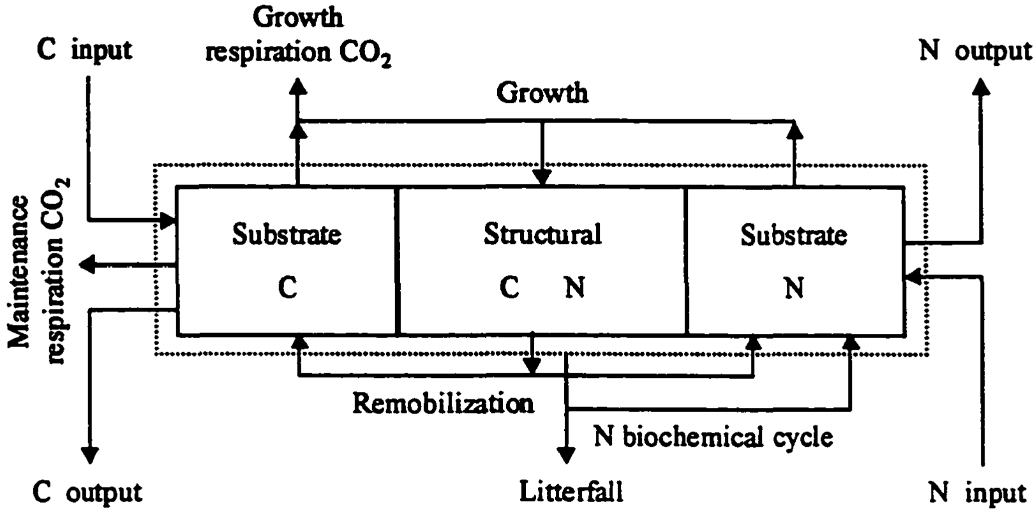
C input
Growth respiration CO_2
N output
Growth
Maintenance respiration CO_2
Substrate C
Structural C N
Substrate N
Remobilization
N biochemical cycle
C output
Litterfall
N input

Figure 4.2 Schematic diagram of the components in the *PLANTC* module

4.2.2 Plant Photosynthesis

Photosynthesis involves the interception of light energy and its conversion to chemical energy in intermediates of high chemical potential, which are then used to drive the catalytic fixation of CO_2 into sugars and other compounds. Canopy photosynthesis plays the key role in the land surface processes and ecosystem simulations. In the coupled water-carbon hypothesis it is one of the main factors in determining leaf stomatal resistance (equation 3.2) which significantly shapes the energy partitioning patterns of the vegetated land surfaces. Photosynthesis is also the main process in forming the gross primary production of terrestrial ecosystems. All of the biological processes in plants and biogeochemical processes in ecosystems are ultimately driven by the products of photosynthesis. Traditionally, plant photosynthesis is estimated using regressive relationships with the environmental conditions, *e.g.*, light, temperature, and soil moisture, etc. These kinds of methods are useful in the general evaluations of plant productivity or in analysing the agro-climatic characteristics of ecosystems. However, they are not applicable to the land surface schemes in GCMs which address the physical interactions and processes between vegetation and the atmosphere in a short time step.

In the past two decades, mechanistic methods for calculating photosynthesis have been formulated. The biochemical model developed by Farquhar *et al.* (1980) has been of particular interest. Since its publication, considerable experimental evidence has been obtained that substantiates much of the theory and has enriched the detail of the underlying biochemical mechanism of the model. It describes CO_2 assimilation by chloroplasts as rate-limited by the enzyme kinetics (dark reaction), specifically the amount and cycle time of the carboxylating enzyme Rubisco, and the electron transport (light reaction), which is a function of incident photosynthetic active radiation (PAR) (see Figure 3.1). This theory has been widely recognised and used in many studies (*e.g.*, Farquhar and Caemmerer, 1982; Evans and Farquhar, 1991; Gutschick, 1991; Norman and Arkebauer, 1991; Collatz *et al.*, 1991; Foley *et al.*, 1996; Sellers *et al.*, 1996). I will follow this theory and implement it in the carbon fixation calculations. Detailed formulations used in this research are discussed below.

For C_3 plants, leaf photosynthesis under unconstrained conditions of water and nutrients, V_L, is expressed as the minimum of two potential capacities to fix carbon.

$$V_L = \min(V_d, V_e) \tag{4.1}$$

where V_d represents the dark reaction rate which is limited by the efficiency of the photosynthetic enzyme system (Rubisco-limited), and V_e represents the light reaction rate which is limited by the electron transport rate and its utilization efficiency.

The dark reaction rate for each leaf can be calculated according to Farquhar *et al.* (1980)

$$V_d = \frac{V_{d,\max}(C_i - \Gamma)}{C_i + k_c(1 + O_i / k_o)} \tag{4.2}$$

where $V_{d,max}$ is the maximum capacity of Rubisco to perform the carboxylase function under saturated CO_2 conditions, C_i and O_i represent the liquid concentrations of CO_2 and O_2 in the chloroplasts, Γ is the compensation point for CO_2 fixation at current C_i

and O_i, and k_c and k_o are the Michaelis-Menten constants for CO_2 and O_2. Values of C_i and O_i are calculated from the intercellular gaseous concentrations of CO_2 and O_2 using temperature-dependent solubility functions (Wilhelm *et al.*, 1977) assuming that mesophyll resistance to CO_2 diffusion is negligible. Intercellular CO_2 concentration is set to be a constant fraction of the atmospheric CO_2 concentration (0.7 for C_3 plants). The value of Γ is calculated as:

$$\Gamma = \frac{0.5 V_{o,\max} k_c O_i}{V_{d,\max} k_o} \tag{4.3}$$

where $V_{o,max}$ is the maximum O_2-saturated rate of oxygenation. It is assumed to be 0.21 of $V_{d,max}$ according to Farquhar *et al.* (1980).

The light CO_2 fixation rate V_e is given by:

$$V_e = JE \tag{4.4}$$

where J is the electron transport rate at ambient irradiance and temperature, and E is the ratio of CO_2 fixation to electron transport which is estimated as (Farquhar and von Caemmerer, 1982):

$$E = \frac{C_i - \Gamma}{\varepsilon C_i + 10.5\Gamma} \tag{4.5}$$

The term ε is the electron requirement for CO_2 fixation.

The electron transport rate J is obtained using a nonrectangular hyperbolic equation (Evans and Farquhar, 1991):

$$J = \frac{\alpha I + J_{\max} - [(\alpha I + J_{\max})^2 - 4\beta \alpha I J_{\max}]^{0.5}}{2\beta} \tag{4.6}$$

where α is the quantum efficiency, I is the absorbed photosynthetically active radiation, and J_{max} is the maximum rate of electron transport. The parameter β is a curvature factor, $0 \le \beta \le 1$, which determines how quickly the transition is made from the region of maximum quantum yield to the light-saturated rate. Detailed analysis of the use of this nonrectangular hyperbola for predicting photosynthetic response to PPFD (photosynthetic photon flux density) can be found in Johnson and Thornley (1984).

The maximum dark reaction rate $V_{d,max}$ and electron transport rate J_{max} in the above equations (4.2, 4.3, and 4.6) are highly temperature dependent. Here they are modified according to the following Arrhenius temperature equation (Sharpe and DeMichelle, 1977):

$$f(T_c) = \frac{T_c e^{(A - \frac{H_a}{RT_c})}}{1 + e^{\frac{H_{dl} - ST_c}{RT_c}} + e^{\frac{ST_c - H_{dh}}{RT_c}}} \tag{4.7}$$

where T_c is the canopy temperature, A is a parameter selected such that $f(T_c) = 1.0$ at $T_c = 30°\mathrm{C}$, R is the universal gas constant, S is the change in entropy, H_a is the energy of activation, H_{dh} is the energy of high temperature deactivation, and H_{dl} is the energy of low temperature deactivation.

Leaf photosynthesis rate V_L obtained by light and dark reaction rates (equation 4.1) is a function of absorbed PAR, leaf temperature, carbon dioxide concentration within the leaf, and the Rubisco enzyme capacity for photosynthesis. The actual photosynthetic rate of plant leaves can also be affected by some other factors, particularly the plant water and nutrient conditions. To account for the impacts from water and nitrogen limitations on photosynthesis, V_L is modified according to the following equation for the actual carbon fixation (V_l) calculations.

$$V_l = V_L f(\psi_c) f(N_l) \tag{4.8}$$

where $f(\psi_c)$ and $f(N_l)$ are the functions of canopy water potential ψ_c and leaf nitrogen concentration N_l, representing the constraints of water and N nutrition on leaf photosynthesis, respectively.

Limitations of CO_2 fixation with decreasing plant water potential have been widely observed. Comprehensive reviews on their relationship can be found in Kozlowski (1982) and Larcher (1995). It is pointed out that the curves of photosynthesis vs. plant leaf water potential show two critical points: the threshold between full photosynthetic capacity and reduced capacity and the null point for gas exchange. The threshold is reached when water stress is such that the stomata begin to close. The null point is determined by the total or near total closure of the stomata and by the direct effect of water deficiency on the protoplasm; it is reached only when dehydration of the leaves is well advanced. The sensitivity of CO_2 fixation to water shortage, which is reflected by the positions of the two critical values described above, is to a large extent a characteristic feature of plant species, which can be classified into hydrophytes, mesophytes, and xerophytes according to their adaptations to water stress (Kimmins, 1997). Here the above concept is used for the water impact formulations.

$$f(\psi_c) = \begin{cases} 0.0 & \psi_c \le \psi_{c,\min} \\ \dfrac{\psi_c - \psi_{c,\min}}{\psi_{c,\max} - \psi_{c,\min}} & \psi_{c,\min} < \psi_c < \psi_{c,\max} \\ 1.0 & \psi_c \ge \psi_{c,\max} \end{cases} \tag{4.9}$$

where $\psi_{c,min}$ and $\psi_{c,max}$, respectively, represents the null point and threshold point of canopy water potential for photosynthesis. Their values for mesophytes are taken in this research and are listed in Table 4.1. Canopy water potential ψ_c at each time step is obtained from the coupled energy and water convergence solutions obtained in equation (3.12) of Chapter 3.

Nitrogen deficiency occurs commonly and usually decreases photosynthesis more than deficiencies of other nutrients. Since the soluble proteins of the Calvin cycle and thylakoid membranes contain most of the leaf N, strong linear correlations between the rate of photosynthesis and leaf N content have been demonstrated in a wide variety of plants (*e.g.*, Field, 1983; Evans, 1989; Leuning *et al.*, 1991; Harley *et al.*, 1992; Abrams and Mostoller, 1995). In this research, a linear relationship

$$f(N_l) = \begin{cases} 0.0 & N_l \le N_{l,\min} \\ \dfrac{N_l - N_{l,\min}}{N_{l,\max} - N_{l,\min}} & N_{l,\min} < N_l < N_{l,\max} \\ 1.0 & N_l \ge N_{l,\max} \end{cases} \tag{4.10}$$

is assumed, where $N_{l,\min}$ is a threshold value of N_l below which there is no photosynthesis, and when N_l exceeds $N_{l,\max}$, it is assumed that there is no N constraint on photosynthesis. The N constraint factor $f(N_l)$ moves linearly from 0 to 1 as the foliage nitrogen concentration changes from $N_{l,\min}$ to $N_{l,\max}$.

Leaf photosynthesis calculated from equation (4.1) – (4.10) is controlled significantly by several environmental factors, *e.g.*, radiation intensity on the leaf surface (equation 4.6), temperature (equation 4.7), leaf water potential (equation 4.9), and leaf N concentration (equation 4.10), etc. If we neglect the temperature difference within the canopy and assume that all leaves experience the same water and N conditions, the differences of photosynthesis among plant leaves are then caused mainly by the differences in radiation. Since the radiation intensity on the leaf surface may differ markedly when they are sunlit and shaded, the canopy leaves are first separated into two categories: sunlit and shaded (see Chapter 3, equation 3.3 – 3.5). The radiation intensity for each category is calculated from solar zenith angle and by assuming random leaf inclination distribution (Campbell, 1977). The photosynthesis calculations discussed above are then executed separately on both sunlit and shaded leaves. The resulting CO_2 fixation rates $V_{l,sunlit}$ and $V_{l,shaded}$ (equation 4.8) are thereafter used for the stomatal resistance estimations according to equation (3.2), and for the canopy gross photosynthesis V_c estimations through multiplication by their respective leaf areas.

$$V_c = \Lambda_{sunlit} V_{l,sunlit} + \Lambda_{shaded} V_{l,shaded} \qquad (4.11)$$

where Λ_{sunlit} and Λ_{shaded} are the plant leaf areas for the sunlit and shaded leaves.

4.2.3 Root Nitrogen Uptake

Among the macronutrients, nitrogen is especially important. Many carbon processes in plants, such as photosynthesis, are dependent on nitrogen-containing compounds such as chlorophyll. Therefore the nitrogen conditions of a canopy can not only affect the ecosystem primary production, but also alter canopy transpiration and then the energy exchanges between the ecosystem and the atmosphere by controlling the stomatal resistance (equation 3.2). For example, in the boreal region, most of the forested areas are thought to be poor in soil nutrients, especially nitrogen. It is speculated that this nitrogen limitation may contribute to the high stomatal resistance observed (Sellers *et al.*, 1997). To explore the roles of nitrogen in the ecosystem production and land surface processes, algorithms for the root nitrogen uptake from the soil are developed based on mechanistic processes. These algorithms also provide a framework for including other mineral nutrients. Mineral nitrogen extracted by plant roots is coupled with the substrate carbon fixed by photosynthesis to drive plant growth and other physiological processes in the model. Though a small amount of nitrogen can enter through the surface of plant shoots, I only include the process of root uptake here since this is regarded as the main mechanism for terrestrial species to acquire their mineral substances.

The nitrogen uptake rate of roots from the soil (Q_N) is dependent on two factors, the N supply characteristics of the soil, and the N uptake kinetics of the root. Research in the last two decades on nutrient flux into plant roots growing in soil has greatly increased our understanding of the processes involved. A series of mechanistic mathematical models describing these processes have been developed (*e.g.*, Claassen and Barber, 1976; Barber and Cushman, 1981; Siddiqi and Glass, 1982; Läuchli, 1984; Barber, 1995). In the model of N uptake, I explicitly calculate the N diffusion and mass flow processes in soil using the methods proposed by Barber and Silberbush (1984). These two processes are then dynamically coupled to root N uptake formulated according to Siddiqi and Glass (1982), which follows Michaelis-Menten kinetics with negative feedback from uptake products.

Nitrogen flows in soil to the root surface either by mass flow with the root water absorption which is mainly driven by plant transpiration, or by diffusion according to the N concentration gradient in the soil solution. The amount of mass flow in soil layer *i*, $Q^m_{N,i}$, is related to the water extracted and N concentration of that water. It can be calculated as

$$Q^m_{N,i} = Q_{r,i} C_{Ns,i} = Q_{r,i} \frac{N_{l,i}}{\theta_{l,i}} \tag{4.12}$$

where $Q_{r,i}$ and $C_{Ns,i}$ are the root water uptake and the concentration of mineral nitrogen in the soil solution, respectively, in soil layer *i* within a time step. $C_{Ns,i}$ is calculated from the ratio of mineral N amount ($N_{l,i}$) and the liquid soil water content

($\theta_{l,i}$). In this equation, $Q_{r,i}$ is obtained in the water convergence solutions according to equation (3.12). $N_{l,i}$ is obtained through soil organic matter decomposition calculations implemented in the *SOILC* module in Chapter 5. $\theta_{l,i}$ is obtained from the original CLASS calculations as illustrated by equation (2.4) in Chapter 2.

When mass flow does not supply the root with sufficient quantities of N, continued uptake reduces the concentration of available N in the soil at the root surface. This in turn causes a concentration gradient perpendicular to the root surface, with nutrients subsequently diffusing along the gradient toward the root surface. The amount of N transported by diffusion in soil layer *i*, $Q_{N,i}^{d}$, is calculated as:

$$Q_{N,i}^{d} = D_e b_p A_{r,i} \frac{\partial C_{N_{s,i}}}{\partial r} = \frac{2\pi D_e b_p L_{d,i} \Delta z_i}{\ln(b_i / a)} (C_{N_{s,i}} - C_{N_{o,i}}) \tag{4.13}$$

where D_e is the effective diffusion coefficient for nitrogen, b_p is the buffer power representing a mean value describing the changes of N concentration on solid phase with the changes of N concentration in soil solution, $A_{r,i}$ is the root surface area, and r is the distance to the root axes. Its approximate form shown in the right side of the equation is obtained from Campbell (1985), where $C_{No,i}$ represents the N concentration in the soil solution at the root surface, $L_{d,i}$ is the root length density, Δz_i is the soil layer depth, a is root radius, and b_i is the path length for nitrogen uptake (half distance between adjacent roots).

Knowledge about the mechanisms of root nutrient uptake has led to the carrier concept of ion transport through root cell membranes. It is postulated that carrier-mediated transport of an ion is analogous to the process of enzyme-mediated catalysis of a substrate and follows the Michaelis-Menten kinetics. It is also found from observations that ion uptake is profoundly influenced by the nutrient status of the root. Influx of ions appears to be negatively correlated with the tissue concentration of the particular ion (Cram, 1973; Glass, 1975). Here I take tissue N concentration into consideration and use equation (4.14) for the root N uptake calculations. This equation is modified from Siddiqi and Glass (1982) which is an extension of the Michaelis-Menten equation.

$$Q^u_{N,i} = \max(U_{N\max})e^{-sC_{Nr,i}} A_{r,i} f(T_{s,i}) \frac{C_{No,i} - C_{N\min}}{\min(K_m)e^{s'C_{Nr,i}} + C_{No,i} - C_{N\min}} \tag{4.14}$$

where $Q^u_{N,i}$ is the N influx at a given tissue N concentration $C_{N\,r,i}$, $U_{N\,max}$ is the maximum transport rate per unit root surface area, K_m the Michaelis-Menten constant, max($U_{N\,max}$) and min(K_m) are the maximum $U_{N\,max}$ and minimum K_m when they are determined at varying tissue concentration, respectively, s is the slope relating $U_{N\,max}$ and s' is the slope relating K_m to the tissue concentration, and $C_{N\,min}$ is the N concentration in the soil solution at the root surface when the net influx equals to 0. The same Arrhenius equation $f(T_{s,i})$ as equation (4.7) is used to describe the sensitivity of $Q^u_{N,i}$ to soil temperature.

There is an unknown variable ($C_{N\,o,i}$) in both equation (4.13) and (4.14) so the nitrogen flow can not be solved directly. Making assumption that N uptake by plant roots equals to the sum of N fluxes of mass flow and diffusion in the same soil layer in each time step, we have

$$Q^u_{N,i} = Q^m_{N,i} + Q^d_{N,i} \tag{4.15}$$

Substituting for the three terms in (4.15) by equations (4.12), (4.13), and (4.14), we can obtain an equation with only one unknown variable, $C_{N\,o,i}$. Root N uptake rate can thus be calculated by solving for $C_{N\,o,i}$ first. Total N uptake by plant roots Q_N is taken as the sum of $Q^u_{N,i}$ in each soil layer.

$$Q_N = \sum_{i=1}^{IG} Q^u_{N,i} \tag{4.16}$$

where *IG* represents the total soil layers in the model.

4.2.4 Substrate Transport and Plant Growth

The C fixed in photosynthesis V_c (equation 4.11) and N extracted by plant roots Q_N (equation 4.16) are added to the foliage substrate C pool and root substrate N pool, respectively, as shown in Figure 4.1. These two substrates are then used to drive the plant growth and other processes. Simulation of plant growth has been a widely researched topic. Some quite comprehensive reviews have been given by Wilson (1988), Dixon *et al.* (1990), Ågren *et al.* (1990), Marcelis (1993), and Cannell and Dewar (1994). Empirically based models may work well in fitting the patterns of observed data. However, it is difficult to extend such models to topics that are of concern to the short term interactions with climate conditions or the plant physiological processes. Thornley (1972) developed a mechanistic model based on the transport-resistance approach for shoot:root partitioning in relation to the availability of C and N on crops. A similar model was constructed later on forest growth and partitioning based on the same theory (Thornley, 1991b). In this approach substrate sources are connected with transport resistances to substrate sinks where chemical/biochemical conversions take place. The substrate allocation is the outcome of the processes of substrate supply, transport, and utilization. This approach is described as 'irreducible' because transport and chemical conversion are processes which must take place in order that allocation is accomplished, although how these processes are controlled is arguable (Thornley, 1997). Many model applications have employed this method since it was proposed (*e.g.*, Wann *et al.*, 1978; Mäkelä and Sievänen, 1987; Rastetter *et al.*, 1991; Minchin *et al.*, 1993).

In *PLANTC*, the concept of this transport-resistance hypothesis for the plant substrate allocation is adopted. Transport of substrate (*L*) C and N between plant tissues is driven by the concentration gradient of the substrates. It is also dependent on the conductivity of the tissues. Conductivity is scaled according to the tissue sizes represented by their structural (*S*) C pools as shown in equation (4.17) to (4.20)[†].

[†] The scaling term for the conductivity of a substrate flow between tissue X and Y, $\frac{C_{S,X}C_{S,Y}}{C_{S,X}+C_{S,Y}}$, is used to make the product of $([C_{L,X}]-[C_{L,Y}])\frac{C_{S,X}C_{S,Y}}{C_{S,X}+C_{S,Y}}$ the maximum amount that the substrate can transport in a time step. The maximum amount of a substrate transport, $T_{X,Y\,\max}$, is assumed to be the amount that makes the substrate concentration in the two tissues equal, which has the relation: $\frac{C_{L,X}-T_{X,Y\,\max}}{C_{S,X}}=\frac{C_{L,Y}+T_{X,Y\,\max}}{C_{S,Y}}$. If we rearrange this equation we can obtain the expression: $T_{X,Y\,\max}=([C_{L,X}]-[C_{L,Y}])\frac{C_{S,X}C_{S,Y}}{C_{S,X}+C_{S,Y}}$.

$$T^{C}_{F,S}=D^{C}_{FS}([C_{L,F}]-[C_{L,S}])\frac{C_{S,F}C_{S,S}}{C_{S,F}+C_{S,S}} \tag{4.17}$$

$$T^{C}_{S,R}=D^{C}_{SR}([C_{L,S}]-[C_{L,R}])\frac{C_{S,S}C_{S,R}}{C_{S,S}+C_{S,R}} \tag{4.18}$$

$$T^{N}_{R,S}=D^{N}_{RS}([N_{L,R}]-[N_{L,S}])\frac{C_{S,S}C_{S,R}}{C_{S,S}+C_{S,R}} \tag{4.19}$$

$$T^{N}_{S,F}=D^{N}_{SF}([N_{L,S}]-[N_{L,F}])\frac{C_{S,F}C_{S,S}}{C_{S,F}+C_{S,S}} \tag{4.20}$$

where $T^{C}_{F,S}$, $T^{C}_{S,R}$, $T^{N}_{R,S}$, and $T^{N}_{S,F}$ are the substrate C and N transport rates between the two tissues represented by their subscript (*F*=foliage, *S*=sapwood, *R*=fine root), and $D^{C}_{FS}, D^{C}_{SR}, D^{N}_{RS}$, and D^{N}_{SF} are their corresponding transport coefficients. The substrate C and N concentrations of the tissues, $[C_{L,X}]$ and $[N_{L,X}]$ ($X=F, S, R$), are expressed as the amount of substrate C ($C_{L,X}$) or N ($N_{L,X}$) per unit of structural C ($C_{S,X}$).

$$[C_{L,X}]=\frac{C_{L,X}}{C_{S,X}} \tag{4.21}$$

$$[N_{L,X}]=\frac{N_{L,X}}{C_{S,X}} \tag{4.22}$$

The structural C pool for the fine root in the above equations $C_{S,R}$ is the sum of the sub-pools of root structural C in all of soil layers.

$$C_{S,R}=\sum_{i=1}^{IG}C_{S,R,i} \tag{4.23}$$

Plant tissue growth are simulated according to the bisubstrate, Michaelis-Menten equation, but modified to simulate the changes of C:N ratio in the newly formed material with that of the substrate C and N availability (Rastetter *et al.*, 1991).

$$G^{C}_{X}=g_{X}f(T_{X})C_{S,X}\frac{[C_{L,X}][N_{L,X}]}{a_{X}([C_{L,X}]+b_{X}A_{X}[N_{L,X}])+[C_{L,X}][N_{L,X}]+k_{X}} \tag{4.24}$$

$$G^{N}_{X}=\frac{g_{X}}{A_{X}}f(T_{X})C_{S,X}\frac{[C_{L,X}][N_{L,X}]}{a_{X}(b_{X}[C_{L,X}]+A_{X}[N_{L,X}])+[C_{L,X}][N_{L,X}]+k_{X}} \tag{4.25}$$

where $X = F, S, R$, G_X^C and G_X^N represent the amounts of substrate C and N used in constructing structural materials in tissue X, g_X is the maximum growth rate, b_X is the C to N range parameter, A_X is the non-restricted C:N ratio, a_X and k_X are parameters derived from the Michaelis-Menten constants of C and N, and $f(T_X)$ is the temperature impact function with the same form as equation (4.7). If $X = R$, growth calculations for fine root will be conducted for each individual soil layer according to its own structural C sub-pool size in that layer and its respective soil layer temperature.

This growth scheme allows the C:N ratios of the newly constructed biomass to be controlled by the availability of substrate C and N in the plant tissue. From equation (4.24) and (4.25) we have

$$\lim_{[N]\to 0} \frac{G_X^C}{G_X^N} = A_X b_X \tag{4.26}$$

$$\lim_{[C]\to 0} \frac{G_X^C}{G_X^N} = \frac{A_X}{b_X} \tag{4.27}$$

which means that when the plant is under N limitation (equation 4.26), it tends to construct structural materials with a higher C:N ratio. On the other hand, when substrate N is not constrained but substrate C is limited (equation 4.27), the newly constructed materials will have lower C:N ratios.

4.2.5 Plant Respiration

The substrate carbon stored in each plant tissue is used first for respiration to meet the plant requirement for energy. It has become common to consider respiration as consisting of two separate components, the maintenance respiration associated with protein turnover and the growth respiration considered to involve the use of energy to synthesize new tissue (Amthor, 1986). Maintenance respiration R_m has been reported to vary with temperature, protein content, atmospheric CO_2 concentration, pollutants and general physiological activity (Amthor, 1989, 1991; Ryan, 1991). While R_m is considered to be proportional to the amount of tissue biomass in most models, tissue N mass is used in this model for estimating R_m because, typically, most of the nitrogen in plant cells is associated with protein. A better relationship between R_m and N content than that between R_m and dry biomass has been reported in some studies (Ryan, 1995; Ryan *et al.*, 1996). Another consideration in using a nitrogen-based model for R_m is that it would link respiration dynamically with other processes, such as photosynthesis, carbon allocation, litter quality and decomposition, etc. The maintenance respiration rate of tissue X, $R_{m,X}$ ($X = F, S, R$), is calculated as:

$$R_{m,X} = r_{m,X} f_r(T_X) N_{S,X} \tag{4.28}$$

where $r_{m,X}$ is the maintenance respiration coefficient at the reference temperature T_{ref}, and $f_r(T_X)$ is a dimensionless temperature function representing the impact of the tissue temperature on its respiration rate, which can be expressed by the Q_{10} function.

$$f_r(T_X) = Q_{10,X}^{\frac{T_X - T_{ref}}{10}} \tag{4.29}$$

Growth respiration of tissue X ($R_{g,X}$) is assumed to be a constant proportion of tissue growth from equation (4.24). This is the method adopted by most modelling and observational studies.

$$R_{g,X} = r_{g,X} G_X^C \tag{4.30}$$

where $r_{g,X}$ is the growth respiration coefficient.

If $X = R$, both $R_{m,X}$ and $R_{g,X}$ are calculated separately for each soil layer according to the structural N amount of the root, soil temperature, and root growth rate in that specific soil layer.

Finally, the autotrophic respiration of the ecosystem R_a is evaluated as the sum of plant maintenance and growth respiration:

$$R_a = \sum_{X=F,S,R} (R_{m,X} + R_{g,X}) \tag{4.31}$$

4.2.6 Plant Litterfall

The rate and time of litterfall production of a plant tissue is mainly controlled by the size of the tissue and the plant phenological characteristics. Knowledge of phenology, even today, is based on the observation of externally visible stages of development. Calculations of litter production rates are usually treated simply as a constant percentage of the existing tissue biomass (Thornley, 1991a; Rastetter *et al.*, 1991). There is no intention in this research to explore the controlling mechanisms on litterfall production. Litter production rates of plant tissues are modelled according to a phenologically modified first order kinetics.

$$L^C_{L,X} = p_X l_X C_{L,X} \tag{4.32}$$

$$L^C_{S,X} = p_X l_X C_{S,X} \tag{4.33}$$

$$L^N_{L,X} = p_X l_X (1-t_N) N_{L,X} \tag{4.34}$$

$$L^N_{S,X} = p_X l_X (1-t_N) N_{S,X} \tag{4.35}$$

where $L^C_{L,X}$ and $L^C_{S,X}$ are the litterfall rates of carbon produced from the substrate (*L*) and structural (*S*) pools of each plant tissue *X*, $L^N_{L,X}$ and $L^N_{S,X}$ are the corresponding N contents in the litterfall, p_X represents the impact of plant phenology, l_X is the litterfall rate constant for tissue *X*, and t_N is the N retranslocation coefficient. It is assumed that a proportion of N (t_N) in the litterfall from both the substrate and structural N pools is retranslocated back to the plant at the time of senescence. This internal redistribution of nutrients in plants, or the biochemical cycle, has been recognized as an important mechanism by which plants conserve nutrients. Observations show that t_N can vary significantly with different plant species and be affected by environmental factors such as the availability of N in the soil. Data for deciduous trees show that t_N may vary from 1% – 52% (Kimmins, 1997). In this research, t_N is taken to vary within this range according to the foliage N concentration N_l which is assumed to be an indicator in representing the soil nutrient conditions in N.

$$t_N = \begin{cases} 0.01 & N_l \geq N_{l,\max} \\ 0.01 + 0.51\dfrac{N_{l,\max} - N_l}{N_{l,\max} - N_{l,\min}} & N_{l,\min} < N_l < N_{l,\max} \\ 0.52 & N_l \leq N_{l,\min} \end{cases} \tag{4.36}$$

where $N_{l,\min}$ and $N_{l,\max}$ are the leaf N concentration parameters that are assumed to take the same values as those used for photosynthesis calculations in equation (4.10).

This scheme let the retranslocation coefficient vary linearly from 1% when the leaf N concentration reaches $N_{L\max}$ or above to 52% when it is below $N_{L\min}$.

The phenological impact parameter p_X takes the value of 0.0–1.0 and is controlled by the plant growth index γ as introduced in Chapter 2. The formulation for γ was originally developed in CLASS based on time. However, index formulated on temperature is usually considered to represent the plant growth and phenological stages better than that based on time. For example, the time of the onset of phenophases in the first half of the year depends primarily on certain temperature thresholds for the plants in the temperate zone. Phenological dates falling in the second half of the year, such as leaf fall, can be affected by many environmental conditions that delay or accelerate the processes of maturation and ageing. However, temperature is still of the greatest significance. Therefore I modified γ by using accumulated temperature in this research instead of using time as in the original model. One advantage of using accumulated temperature over time is that it is sensitive to the changes of environmental factors which can affect plant physiological processes. This modification on γ is important in the model sensitivity studies.

Plant litterfall provides the main source for the soil C and N. Another source of C input into the soil that is included in the model is root exudation. Knowledge of this process is still very limited. In the *ecosys* model (Grant, 1993), it is simulated as a radial flux driven by concentration gradients of soluble C between roots and the soil solution. In this model, root C exudation (X_C) is simply treated as a constant proportion (c_R) of root growth rate.

$$X_{C,i} = c_R G^C_{R,i} \tag{4.37}$$

Simulated exudation rate is thus sensitive to temperature, radiation and water conditions, as reported experimentally (Hale and Moore, 1979).

4.2.7 Plant State Variables

Plant state variables of substrate and structural C and N for each of the plant parts recognised in the model are obtained at the end of each time step according to the flux calculations formulated above and the controlling equations listed in Appendix A. Some important parameters of plants used in other parts of the model, such as plant leaf area index (*LAI*), root length and distributions in each soil layer, can then be calculated based on the respective pool size.

Leaf area change is assumed proportional to the change of the foliage structural C ($C_{S,F}$). Plant *LAI* is calculated by simply converting $C_{S,F}$ using the specific leaf area (*SLA*) parameter.

$$LAI = SLA \times C_{S,F} \tag{4.38}$$

SLA may change significantly with plant phenology stage and environmental conditions as observed in this aspen site by Middleton *et al.* (1997). In the early growing stage or under shaded environment, plants tend to have high *SLA* values. To make the model simple, *SLA* is treated as a constant value in this research.

Similar to *LAI*, plant wood area index (*WAI*) is also calculated in the model by converting the structural carbon of stem sapwood ($C_{S,S}$) plus heartwood carbon (C_H) using a simple parameter of 'specific wood area (*SWA*)'

$$WAI = SWA \times C_{S,S} \tag{4.39}$$

Wood area here refers to the hemi-surface area of the stems and twigs. Therefore there are two area indexes related the vegetation after the CLASS model is revised, *LAI* and *WAI*. For the simulations such as radiation balance, the total area index of *LAI* plus *WAI* is used, while for the simulations such as stomatal resistance and carbon fixation, only the parameter of *LAI* is used. Plant *WAI* is an important parameter in the energy balance calculations particularly during the non-growing season. It significantly affects the land surface albedo and therefore greatly changes the radiation calculations.

Plant fine root length in soil layer *i*, $L_{R,i}$, is converted from its root structural C pool $C_{S,R,i}$

$$L_{R,i} = \frac{C_{S,R,i}}{\pi c \rho_R a^2} \tag{4.40}$$

where *c* and ρ_R are the carbon concentration and density of the root biomass, and *a* is the root radius.

4.3 Parameterization, Simulation Results and Tests

4.3.1 Parameterization

Parameters used in the *PLANTC* module are listed in Table 4.1.

4.3.2 Simulation Results and Tests

The *PLANTC* module plays an important role in the whole model. Its outputs determine the behaviour of the *SVATC* and *SOILC* modules and can significantly affect the whole model outputs. For example, the results of energy distribution and evapotranspiration of the canopy calculated in *SVATC* module are directly controlled by the canopy resistance (equation 3.6), which is determined by carbon fixation rate (equation 3.2) and plant leaf area index (equation 3.3 - 3.5) obtained in the *PLANTC* module (equation 4.8 and 4.38, respectively). Litterfall production (equation 4.32 - 4.35), as another example, is the main input of organic matter to the soil that drives the soil biochemical transformation processes implemented in the *SOILC* module (discussed in Chapter 5). Therefore, to some extent, the *PLANTC* module has been tested by the results of energy and water exchanges discussed in the previous chapter and will be tested by the litterfall decomposition results discussed in the next chapter. The CO_2 exchange of the plant with its environment is another key part of test for this module. Since the tower measurements of CO_2 flux between the ecosystem and the atmosphere include the CO_2 fluxes from both the plant and soil, the test for plant CO_2 dynamics against this dataset will be conducted after the *SOILC* module is introduced.

(1) Model Responses at Leaf Level

The model predictions of CO_2 exchange and stomatal conductance were first tested at the leaf level. Measurements of response curves of leaf CO_2 exchange and stomatal conductance to light, CO_2, and temperature were made by the BOREAS TE

Table 4.1 Parameters Used in the *PLANTC* Module

	Equation	*Value*	*Units*	*Reference*
Photosynthesis				
$V_{d,max}$	(4.2–4.3)	57.0	μmol m^{-2} s^{-1}	Kozlowski and Pallardy, 1997
k_c	(4.2–4.3)	12.5	μM	Douglas and Ogren, 1984
k_o	(4.2–4.3)	500.0	μM	Douglas and Ogren, 1984
ε	(4.5)	4.5	mol e$^-$ mol^{-1} CO_2	Farquhar and von Caemmerer, 1982
J_{max}	(4.6)	127.0	μmol m^{-2} s^{-1}	Kozlowski and Pallardy, 1997
α	(4.6)	0.5	mol e$^-$ mol^{-1} quanta	Evans and Farquhar, 1991
β	(4.6)	0.8	unitless	Evans and Farquhar, 1991
A	(4.7)	18.02	unitless	
S	(4.7)	710.0	J mol^{-1} K^{-1}	
H_a	(4.7)	57500.0	J mol^{-1}	
H_{dl}	(4.7)	190000.0	J mol^{-1}	
H_{dh}	(4.7)	214000.0	J mol^{-1}	
$\psi_{c,min}$	(4.9)	-200.0	m H_2O	Larcher, 1995; Kimmins, 1997
$\psi_{c,max}$	(4.9)	-100.0	m H_2O	Larcher, 1995; Kimmins, 1997
$N_{l,min}$	(4.10)	0.005	kg N kg^{-1} C	Thornley and Cannell, 1992
$N_{l,max}$	(4.10)	0.07	kg N kg^{-1} C	Thornley and Cannell, 1992
N uptake				
D_e	(4.13)	2.5×10^{-6}	cm^2 s^{-1}	Barber and Silberbush, 1984
b_p	(4.13)	1.0	unitless	Barber and Silberbush, 1984
$U_{N\,max}$	(4.14)	100.0	nmol m^{-2} s^{-1}	Barber and Silberbush, 1984
s	(4.14)	-0.025	unitless	Siddqi and Glass, 1982
s'	(4.14)	0.009	unitless	Siddqi and Glass, 1982
K_m	(4.14)	0.025	μmol cm^{-3}	Barber and Silberbush, 1984
$C_{N\,min}$	(4.14)	0.002	μmol cm^{-3}	Barber and Silberbush, 1984
C and N allocation and tissue growth				
D^C_{FS}, D^C_{SR}	(4.17–4.18)	5.78×10^{-5}	s^{-1}	Thornley, 1991a

D^N_{RS}, D^N_{SF}	(4.19–4.20)	$5.78\text{x}10^{-5}$	s^{-1}	Thornley, 1991a
g_X, $X = F, S, R$	(4.24–4.25)	$2.08\text{x}10^{-6}$	s^{-1}	calculated from Thornley, 1991b
a_F	(4.24–4.25)	$1.18\text{x}10^{-4}$	kg N_L kg^{-1} C_S	calculated
a_S	(4.24–4.25)	$2.95\ \text{x}10^{-5}$	kg N_L kg^{-1} C_S	calculated
a_R	(4.24–4.25)	$5.91\ \text{x}10^{-5}$	kg N_L kg^{-1} C_S	calculated
A_F	(4.24–4.25)	14.29	kg C kg^{-1} N	
A_S	(4.24–4.25)	57.16	kg C kg^{-1} N	
A_R	(4.24–4.25)	28.58	kg C kg^{-1} N	
b_X, $X = F, S, R$	(4.24–4.25)	2.86	unitless	
k_F	(4.24–4.25)	$1.99\ \text{x}10^{-7}$	kg C_L kg N_L k_g^{-2} C_S	calculated
k_S	(4.24–4.25)	$4.99\ \text{x}10^{-8}$	kg C_L kg N_L k_g^{-2} C_S	calculated
k_R	(4.24–4.25)	$9.98\ \text{x}10^{-8}$	kg C_L kg N_L k_g^{-2} C_S	calculated
Respiration				
$r_{m,X}$, $X = F, S, R$	(4.28)	$2.06\text{x}10^{-6}$	kg C kg^{-1} N s^{-1}	Ryan, 1995
T_{ref}	(4.29)	10	°C	Ryan, 1995
$Q_{10,F}$	(4.29)	2.1	unitless	Ryan *et al.*, 1997
$Q_{10,S}$	(4.29)	1.3	unitless	Ryan *et al.*, 1997
$Q_{10,R}$	(4.29)	1.9	unitless	Ryan *et al.*, 1997
$r_{g,X}$, $X = F, S, R$	(4.30)	0.29	unitless	Lavigne and Ryan, 1997
Litterfall				
l_F	(4.32–4.35)	$5.56\text{x}10^{-6}$	s^{-1}	calculated
l_S	(4.32–4.35)	$5.56\text{x}10^{-7}$	s^{-1}	calculated
l_R	(4.32–4.35)	$5.56\text{x}10^{-7}$	s^{-1}	calculated
c_R	(4.37)	0.1	unitless	estimated from Rovira, 1969
State variable				
SLA	(4.38)	22.5	m^2 kg^{-1} C	Kimball *et al.*, 1997
SWA	(4.39)	0.06	m^2 kg^{-1} C	Estimated from Gower *et al.*, 1997
c	(4.40)	0.45	unitless	Atjay *et al.*, 1977
ρ_R	(4.40)	250	kg biomass m^{-3}	Ryan *et al.*, 1997
a	(4.40)	$1\text{x}10^{-3}$	m	Steele *et al.*, 1997

04 team in the mid-August of 1994 using intact attached leaves of the aspen at this site (Berry *et al.*, 1998). Selected leaves near the top of the aspen canopy were enclosed in the cuvette of a portable gas exchange system with an infrared gas analyser and a dew point mirror which enabled precise control of CO_2, temperature, irradiance, and humidity at the leaf surface. These measurements were decoupled from the ambient environment. There was no direct correspondence between the temperature, light intensity, or other environmental conditions in the cuvette during these experiments and the ambient environmental conditions at the site of the measurements. In each measurement, chamber CO_2 concentration, incident flux density of photosynthetic active radiation, or chamber air temperature was varied while other factors were held constant. CO_2 responses were measured at a high photon flux density (PPFD = 1477 μmol m^{-2} s^{-1}), a high chamber relative humidity (76%), and a high temperature (T_a = 25.3°C). For light response curves, the leaf was preconditioned to 1000 μmol m^{-2} s^{-1}; light was then increased in increments of about 300 μmol m^{-2} s^{-1} until saturation was evident and then decreased in steps to zero. Temperature responses were measured by increasing the chamber temperature while PPFD was rate saturating and keeping the dew point temperature of inlet air constant. The starting temperature was low (about 15°C) and the chamber temperature was increased by about 2.5°C per step up to the highest chamber temperature that the gas exchange system could reach in field (about 38°C). This protocol was chosen to mimic the covariation of leaf temperature and vapor pressure deficit that occurs naturally on warm, dry days in this environment. Measurements of CO_2 flux and stomatal conductance were taken when steady state values were achieved (usually 30 minutes after conditions were changed).

The model outputs of net CO_2 exchange (V_l - $R_{m,F}$ - $R_{g,F}$) and stomatal conductance (g_l) of the sunlit leaf were used to test against the observations. The model was first run using actual boundary conditions from the first day of 1994 to the date of the leaf experiment. Boundary conditions driving the model were then changed artificially to mimic the treatments in the leaf experiments. Figure 4.3 shows the response curves of the observed and simulated leaf CO_2 exchanges to photon flux density, CO_2 concentration, and air temperature, respectively.

The response curve of simulated CO_2 exchange to PPFD fitted the measurements very well as shown in Figure 4.3A. The increasing rates of leaf photosynthesis decreased gradually with PAR until it became saturated around PPFD = 800 μmol m^{-2} s^{-1}. The light compensation point, when leaf CO_2 exchange reached zero, was simulated at about PPFD = 15 μmol m^{-2} s^{-1}. This behaviour was mainly controlled by the model formulations on the electron transport rate (equation 4.6). The shape of the curve represented by this nonrectangular hyperbola equation is mainly determined by the curvature factor β. When $\beta = 0$, the response curve becomes a rectangular hyperbola curve, while $\beta = 1$ describes the Blackman response of two straight lines representing light-dependent and light-saturated rates. A value between $\beta = 0.7 - 0.9$ is suggested by most of the evidence (*e.g.*, Marshall and Biscoe, 1980). In my model run I took the value of $\beta = 0.8$.

The response of simulated leaf CO_2 exchange to ambient CO_2 concentration is different from the observed values (Figure 4.3B). The modelled CO_2 exchange rates increased rapidly with increasing CO_2 under low CO_2 concentrations but levelled off when CO_2 exceeded 500 ppm, while the observed rates showed an almost constant increasing rate with CO_2 concentrations at least until it reached the maximum CO_2 concentration given in the experiment (729 ppm). According to the model, photosynthesis is mainly controlled by equation (4.2), when rubisco is limited, and equation (4.6), when electron transport is limited. Both of these equations give a response curve similar to a Michaelis-Menten function, that is, an almost linear response to increasing CO_2 under low CO_2 concentration and a less rapid response under high CO_2 concentration, as shown by the modelled curve in Figure 4.3B. This kind of photosynthetic response to CO_2 concentration has been widely demonstrated in experimental and modelling studies (*e.g.*, Evans and Farquhar, 1991; Harley and Tenhunen, 1991). Possible reasons for the observed response and the discrepancies with the model output are discussed later. For the comparison in magnitude, when

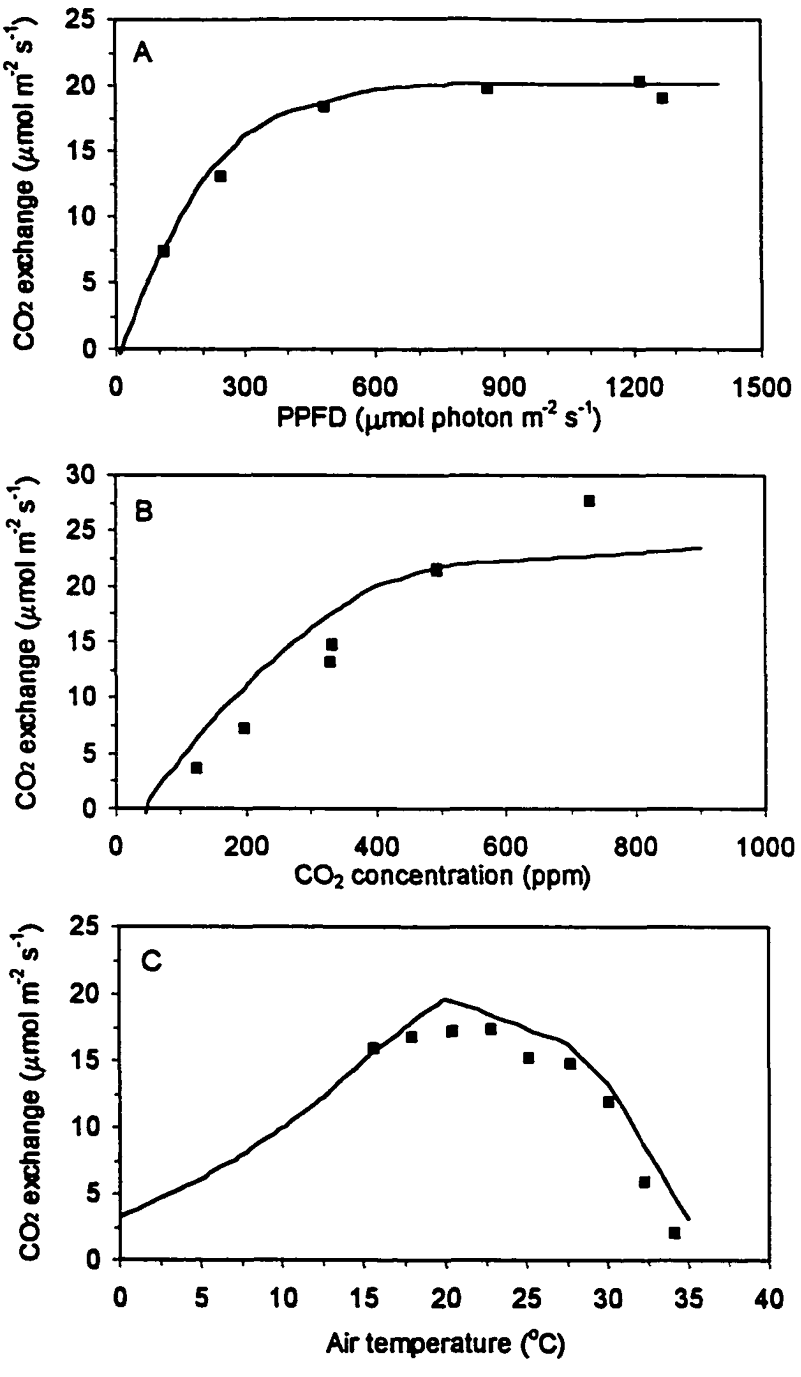

Figure 4.3 Simulated (line) and measured (symbols) responses of leaf CO_2 exchange to radiation (A), CO_2 (B), and temperature (C)

(A: $CO_2 = 344.4$ ppm; $T_a = 20.6$°C; $q_a = 0.012$ kg H_2O kg^{-1} air.
B: PPFD = 1477.3 μmol photon m^{-2} s^{-1}; $T_a = 25.3$°C; $q_a = 0.015$ kg H_2O kg^{-1} air.
C: PPFD = 1181.9 μmol photon m^{-2} s^{-1}; $CO_2 = 331.8$ ppm; $q_a = 0.009$ kg H_2O kg^{-1} air.)

CO_2 concentration was lower than 400–500 ppm, simulated CO_2 exchanges were slightly higher than the observed results. Under higher CO_2, the only one observation at 729 ppm showed it was significantly higher than the simulated results. Both the simulated and observed CO_2 compensation points were around 50 ppm.

The observed and modelled temperature responses are shown in Figure 4.3C. Leaf CO_2 exchange can be affected by temperature through several ways in the model, such as through respiration (equation 4.28 and 4.29) and the CO_2 solubility which affects the CO_2 concentration at the site of carboxylation C_i (equation 4.2). However, the dominant process of temperature in controlling leaf CO_2 exchanges during the photosynthetically active period is through its impact on the maximum carboxylation capacity and electron transport rate according to equation (4.7) in the model. The experiment was conducted at an air temperature range between 15°C – 35°C. The simulated CO_2 exchanges in this temperature range tended to be slightly higher than the observed values, but the changing pattern followed the observed results quite well.

Comparisons of the model predicted stomatal conductance (g_l) of the sunlit leaf versus the observed values from the leaf experiment are given in Figure 4.4. Since leaf stomatal conductance was formulated as a function of photosynthesis, relative humidity, and CO_2 concentration according to the Ball-Berry equation (3.2), simulated response of stomatal conductance to irradiance (Figure 4.4A, CO_2 and humidity remained constant under this scenario) showed a similar shape to that of photosynthesis (Figure 4.3A). Stomatal conductance increased more rapidly at low PPFD than at high PPFD levels, which was caused by the higher increase rate of photosynthesis at low irradiance conditions. There was no significant change with the simulated stomatal conductance when PPFD reached 800 $\mu mol\ m^{-2}\ s^{-1}$ or higher. For the observed values, only a slight increase of g_l can be noticed in the low PPFD level, while in the high PPFD level, the pattern was not clear.

Unlike the irradiance response curve, stomatal conductance changed with CO_2 concentration differently from the photosynthesis-CO_2 curve due to the direct impact

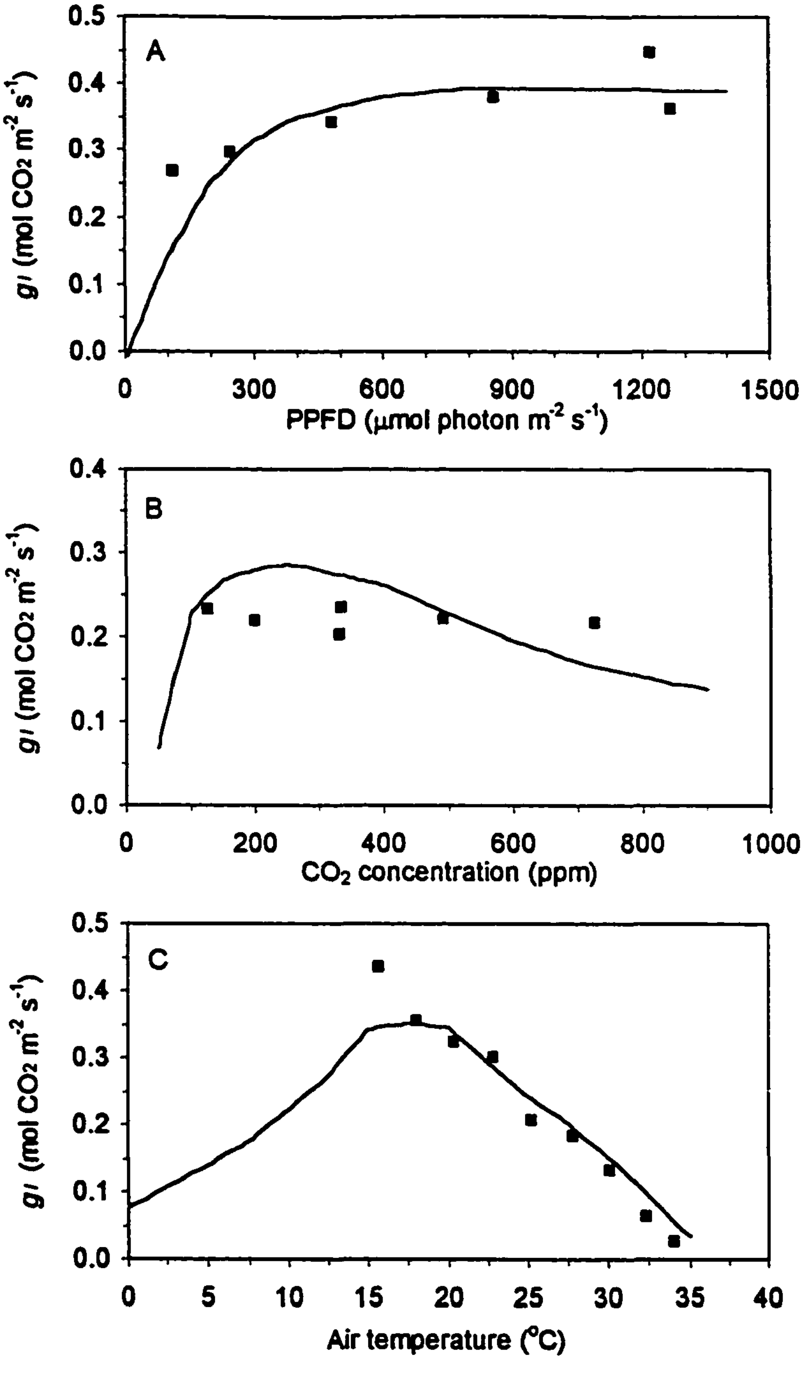

Figure 4.4 Simulated (line) and measured (symbols) responses of leaf stomatal conductance g_l to radiation (A), CO_2 (B), and temperature (C)

(A: $CO_2 = 344.4$ ppm; $T_a = 20.6$°C; $q_a = 0.012$ kg H_2O kg^{-1} air.

B: PPFD = 1477.3 μmol photon m^{-2} s^{-1}; $T_a = 25.3$°C; $q_a = 0.015$ kg H_2O kg^{-1} air.

C: PPFD = 1181.9 μmol photon m^{-2} s^{-1}; $CO_2 = 331.8$ ppm; $q_a = 0.009$ kg H_2O kg^{-1} air.)

of CO_2 concentration in controlling g_l (equation 3.2). When CO_2 concentration was above 250 ppm, increase of CO_2 led to the decrease of stomatal conductance. The simulated g_l decreased by half when CO_2 was increased from 250 ppm (0.286 mol CO_2 m^{-2} s^{-1}) to 900 ppm (0.138 mol CO_2 m^{-2} s^{-1}). However, stomatal conductance increased with CO_2 concentration under the extraordinary low levels when CO_2 was between 0–250 ppm. The reason for this model behaviour was that when CO_2 was very low, photosynthesis dropped rapidly. CO_2 produced by leaf respiration provided a larger part in the CO_2 requirement for gross photosynthesis. For example, when CO_2 = 200 ppm, the simulated gross photosynthesis of the sunlit leaf was 13.12 μmol CO_2 m^{-2} s^{-1}, the respiration rate was about 1.98 μmol CO_2 m^{-2} s^{-1}, about 15% of the total CO_2 requirement. The plant leaf thus needed to get most of the CO_2 (11.18 μmol CO_2 m^{-2} s^{-1}) diffused from ambient air through the stomata. Under CO_2 = 50 ppm, the gross photosynthesis decreased to 2.67 μmol CO_2 m^{-2} s^{-1} and the respiration keeps approximately the same. Therefore the CO_2 requirement by photosynthesis could be largely met by the CO_2 released from respiration by leaf itself (74%). Under this condition, CO_2 demand from the ambient air was low and the leaf was modelled to close its stomata, which would cause the decrease in leaf conductance as shown in Figure 4.4B. The pattern of the observed response of stomatal conductance to CO_2 was not clear; within the CO_2 range in the experiment (100 ppm–700 ppm), stomatal conductance did not show significant changes with CO_2 variations but remained around 0.22 mol CO_2 m^{-2} s^{-1}.

The temperature response curve (Figure 4.4C) of stomatal conductance shows a slightly different shape from the photosynthesis-temperature curve as shown in Figure 4.3C, which can be attributed mostly to the impact of temperature on the relative humidity of the air. In both the experiment and simulation run, the specific humidity of the air was held constant. Therefore when temperature was forced to change, the leaf underwent different conditions with relative humidity (h_s) which is strongly temperature dependent. Since stomatal conductance is proportional to h_s according to the Ball-Berry model (equation 3.2), the g_l vs. T_a curve can be regarded as the integrated impact of temperature on both photosynthesis (Figure 4.3C) and relative humidity of the air. The simulated g_l–T_a relationship corresponded with the observed values well except the measurement at 15°C. Unfortunately, temperature in the experiment was limited to above 15°C and there were no comparisons available at low temperature ranges which happened frequently to the forest at this site.

Limitations existed with the above comparisons. In the field experiment, the leaf was treated only about 30 minutes for each condition. Therefore the measurements can be regarded as the temporal or short-term response of the leaf to the specific conditions. While for the model run, parameters were usually adopted from studies that had a time scale much longer than 30 minutes. Since the short-term responses of plants to the environmental changes can be quite different from their long-term responses (Wang and Yu, 1993), direct comparisons between these two can lead to a disagreement to some extent. In addition, only a few leaves in a tree were sampled in the leaf experiment. In the model simulations, however, the whole sunlit leaf area of the canopy was assumed to experience the same conditions as those in the experiment. This can lead to the different plant statuses which indirectly affect the responses tested.

Discrepancies between the simulated and observed responses may also arise from improper parameterizations in the model and the uncertainties in the experiment. Many of the parameters were taken generally for C_3 woody plants instead for the aspen at this specific site, such as $V_{d,max}$ (equation 4.2), J_{max} (equation 4.6), and m (equation 3.2) etc., which played the key roles in simulating photosynthesis and stomatal conductance. Uncertainties in the experiments may include instrument noise and systematic calibration errors, and because of the somewhat different conditions the leaf experienced in the cuvette (*e.g.*, spectral composition or anisotropy of light) than it would in a natural environment (Berry *et al.*, 1998).

(2) Diurnal Patterns and Annual Courses of Plant Carbon Exchanges

Two successive days in 1994, July 1, a typical clear day, and July 2, a typical cloudy day, were chosen to show the modelled diurnal patterns of plant carbon

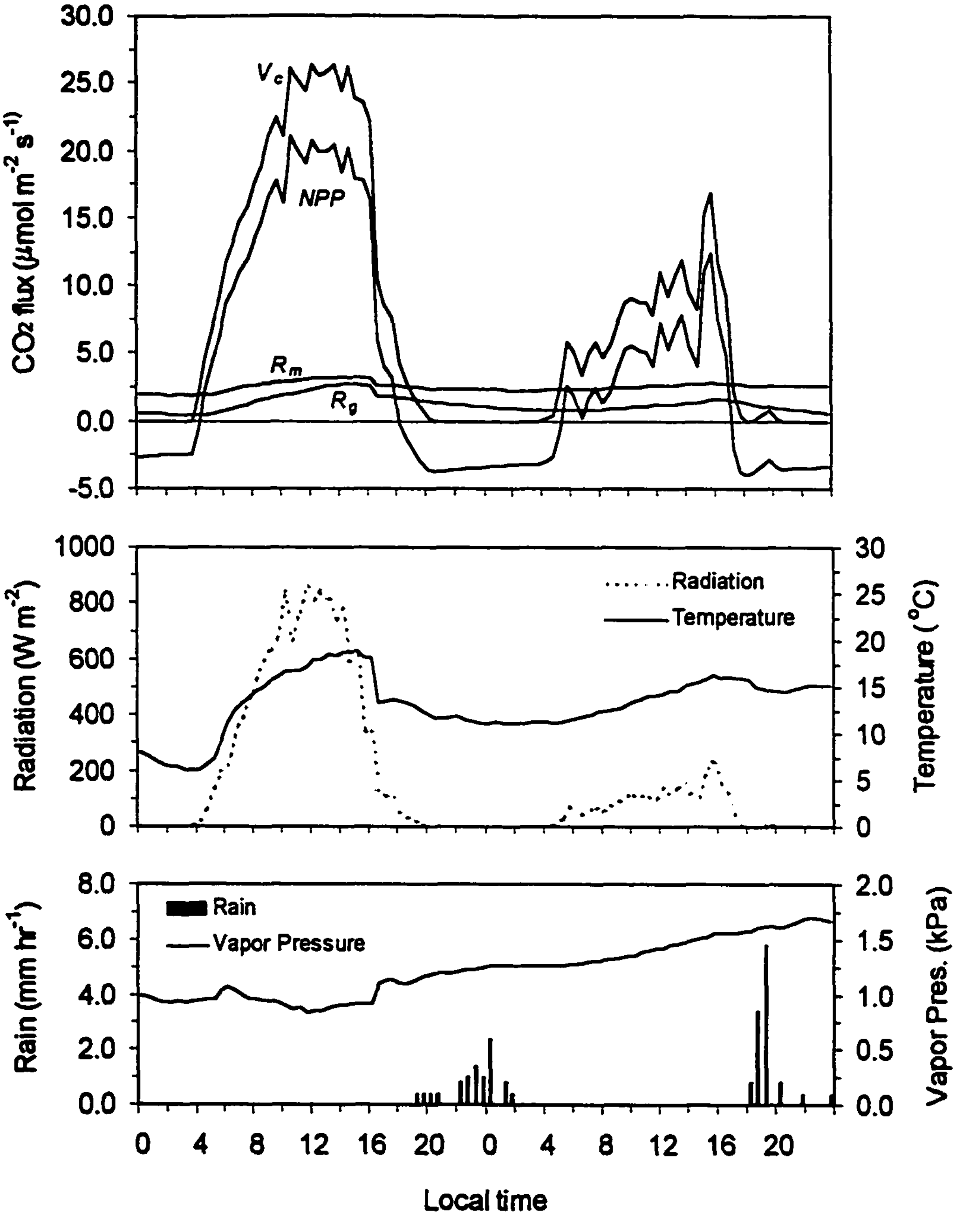

Figure 4.5 Diurnal changes of simulated plant gross photosynthesis V_c, maintenance respiration R_m, growth respiration R_g, and net primary production *NPP*

(The corresponding measurements of shortwave radiation R_s, air temperature T_a, humidity e_a, and precipitation are shown in the two figures below.
Date: July 1 and July 2, 1994).

exchanges under different weather conditions (Figure 4.5). The four carbon items (gross photosynthesis V_c, maintenance respiration R_m, growth respiration R_g, and net primary production *NPP*) were not directly measured in the field experiment, so only the model output were plotted and discussed. Verification of these simulations against the measured ecosystem CO_2 flux will be conducted after the soil heterotrophic respiration is introduced in the next chapter.

Similar shape between the curves of photosynthesis V_c and shortwave radiation R_{sw} indicated that the modelled V_c was strongly controlled by R_{sw}. Photosynthesis began very early in the morning at about 4 a.m. when shortwave radiation was available, and stopped very late at around 8 p.m. when the shortwave radiation dropped to zero. The total C fixation time in a day during this period of the year can be more than 16 hours. In the clear day when the solar radiation was high, gross photosynthesis of the canopy reached a maximum value of 26.1 μmol CO_2 m^{-2} s^{-1} (0.31 mg C m^{-2} s^{-1}) around noon. During the cloudy day, photosynthesis was apparently lower than that during the clear day, implying that C fixation rate was strongly constrained by the radiation intensity at this time. The accumulated gross photosynthesis (or gross primary production, *GPP*) in the cloudy day was simulated at 2.5 g C m^{-2} d^{-1}, only about 40% of the *GPP* in the clear day (6.2 g C m^{-2} d^{-1}).

Maintenance respiration R_m was strongly affected by temperature (equations 4.28 and 4.29). The simulated R_m during this time period was around 2.27 μmol CO_2 m^{-2} s^{-1} (0.027 mg C m^{-2} s^{-1}), and it changed mainly with temperature. High R_m values appeared in the afternoon when air temperature was high, and low values occurred in the early morning when temperature reached the lowest in a day. Growth respiration R_g was simulated as proportional to the growth rates of the plant tissues (equation 4.30), which were mainly determined by the amount of available C and N substrates and affected by temperature (equation 4.24). It can be found that there was a significant increase of R_g during the daytime particularly in the clear day, implying the enhancement of growth rate induced by the substrate C accumulation from photosynthesis. Growth respiration rate was lower than maintenance respiration rate on both the clear and the cloudy days. The simulated daily totals of CO_2 released from R_m and R_g were 1.47 g C m^{-2} d^{-1} and 0.82 g C m^{-2} d^{-1} on the clear day, and 1.48 g C m^{-2} d^{-1} and 0.64 g C m^{-2} d^{-1} on the cloudy day. It was worth noting that though the maximum intensity of R_m in the clear day was higher than that in the cloudy day, because of the higher daily maximum temperature, the daily sum of R_m of the clear day was smaller than that of the cloudy day, which was mainly due to the higher night temperature in the cloudy day than in the clear day.

Net primary production *NPP*, calculated as V_c-R_g-R_m, plays an important role in the carbon budget analysis of vegetation. Figure 4.5 shows that net carbon gain of the plant started about one hour later after photosynthesis began, and it ended 2 or 3 hours earlier than when photosynthesis stopped. The longer time difference in the afternoon was mainly due to the higher plant respiration rates in the late afternoon than in the early morning. On the clear day high gross photosynthesis greatly increased the net C gain of the plant. Under cloudy conditions when the solar radiation was very low, a large part of the C fixed during the daytime was consumed by plant respiration. The simulated daily sum of *NPP* for the clear day was 3.91 g C m^{-2} d^{-1}, while for the cloudy day it was only 0.39 g CO_2 m^{-2} d^{-1}, about 10 percent of the net carbon gain in the clear day.

The annual distributions of daily total V_c (or *GPP*), R_m, and R_g for 1994 and 1996 were plotted in Figure 4.6, followed by the corresponding distributions of three main meteorological variables (radiation, temperature, and precipitation) in Figure 4.7 and Figure 4.8 for the two years, respectively. Plant photosynthesis was simulated to begin during the middle of April when both the air temperature and the first soil layer temperature rose above zero. In the first month after the leaf emergence, photosynthesis rates remained low due to the small leaf area and cool temperature. Rapid increase in gross photosynthesis V_c (or *GPP*) occurred in late May, along with the rapid increase in leaf area, solar radiation, and air temperature. V_c reached its high values of above 12.0 g C m^{-2} d^{-1} in June, July, and early August. The maximum daily *GPP* in the model was 13.0 g C m^{-2} d^{-1} on July 13, 1994, and 13.1 g C m^{-2} d^{-1} on June

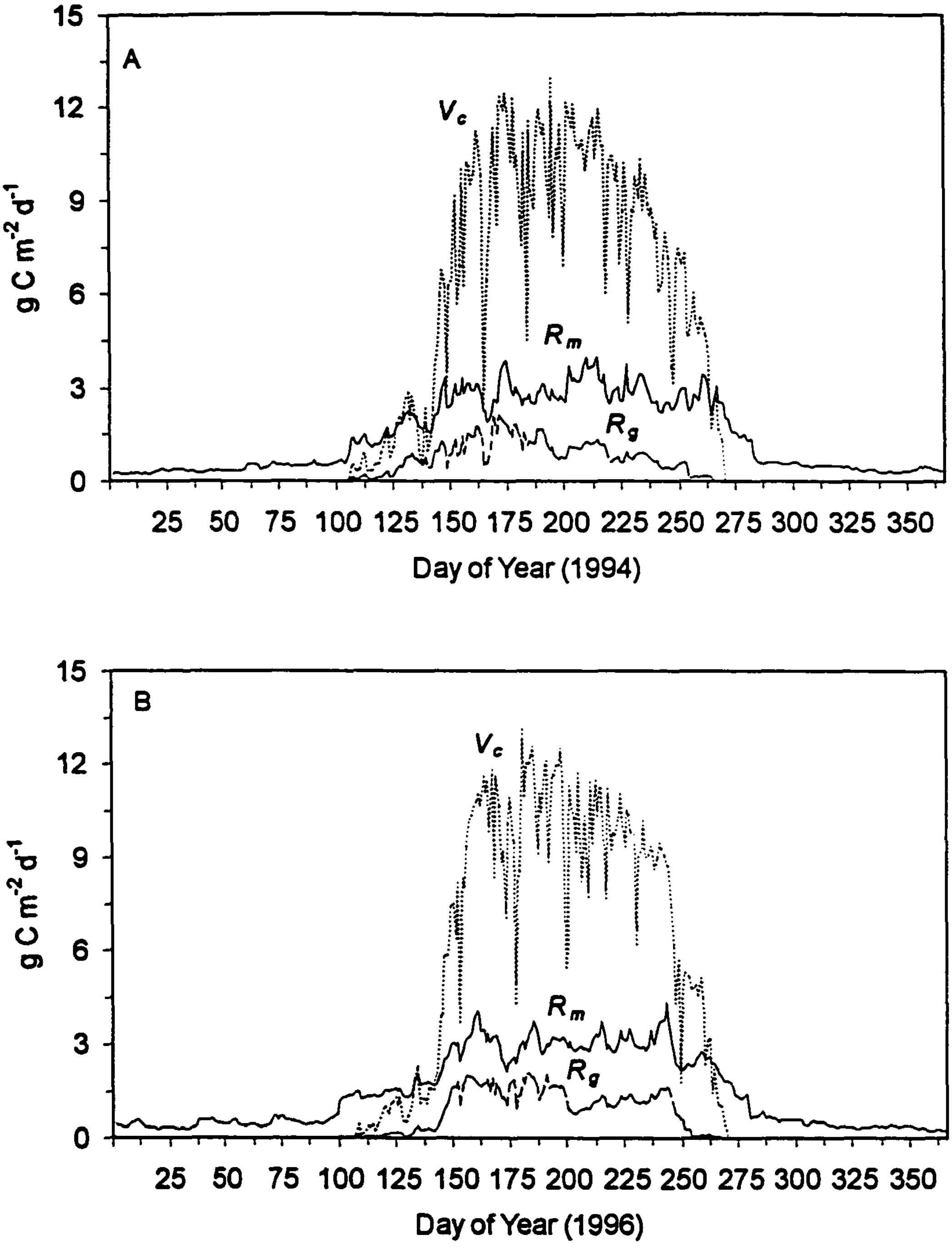

Figure 4.6 Annual distributions of simulated daily plant gross photosynthesis V_c, maintenance respiration R_m, and growth respiration R_g for 1994 and 1996

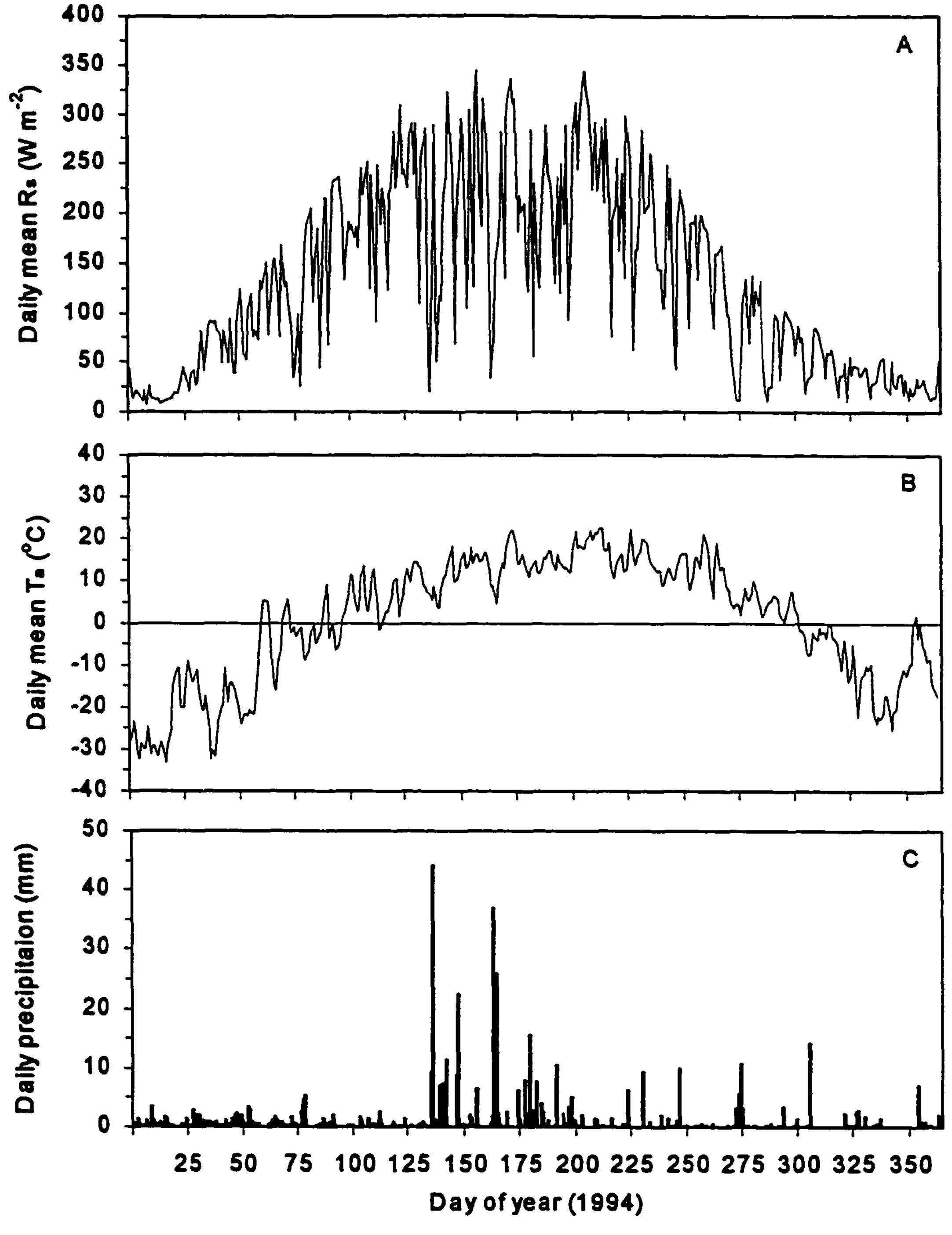

Figure 4.7 Annual distributions of measured daily mean shortwave radiation R_s (A), air temperature T_a (B), and daily total precipitation P (C) in 1994

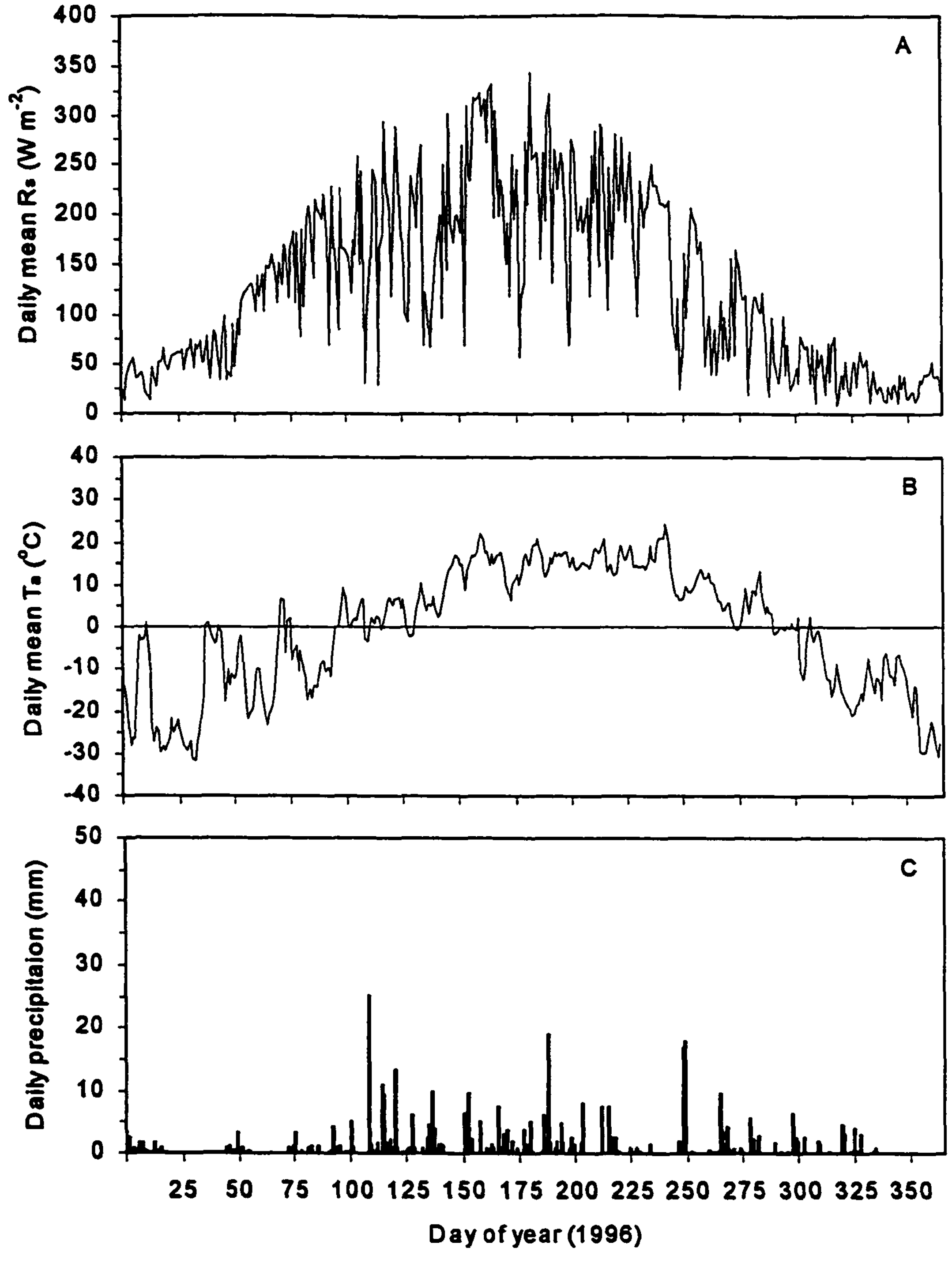

Figure 4.8 Annual distributions of measured daily mean shortwave radiation R_s (A), air temperature T_a (B), and daily total precipitation P (C) in 1996

29, 1996. Fluctuations of daily *GPP* were very significant, caused primarily by the fluctuations in solar radiation. Great decrease in *GPP* can be found in cloudy days. Senescence occurred mainly in September and the plant stopped its growth completely in early October. The modelled duration of plant growing period was 178 days for 1994 and 180 days for 1996.

Maintenance respiration was simulated to occur year round, with the exception of foliage in the non-growing season. During wintertime, R_m was very low due to the low air and soil temperatures, especially for December, January and February. R_m during these three months was simulated at around 0.23 g C m^{-2} d^{-1}. After leaf emergence, R_m increased rapidly due to the increase of temperature and plant biomass pools (equation 4.28 and 4.29), particularly the foliage C and N pools. The peak values obtained for R_m were around 4.0 g C m^{-2} d^{-1}, which lasted from June to early September. Growth respiration was assumed to be zero during the non-growing season, and it started with the leaf emergence. R_g was simulated lower than R_m year round. The peak values for R_g were around 2.0 g C m^{-2} d^{-1} in the model.

The annual distributions of simulated daily *NPP* were plotted separately in Figure 4.9. During the non-growing season, *NPP* remained negative which means the net C loss of the plant. The magnitude of *NPP* at this time was the same as R_m since R_g and V_c were treated as zero. Just after the plant started to grow, plant respiration rate increased rapidly and photosynthesis rate at that time was still small due to the small plant leaf area and cool temperature. Plant *NPP* thus showed a slight increase in C loss in the first month after the leaf emergence. Along with the increase of plant leaf area and more favourable weather conditions such as temperature and radiation (Figure 4.7 and Figure 4.8), plant photosynthesis increased rapidly and finally exceeded the sum of plant maintenance and growth respiration, which led to the net carbon gain (positive *NPP*) of the plant. The time when *NPP* went through zero from negative to positive was simulated on May 23 in 1994 and on May 24 in 1996, about six weeks after photosynthesis started. *NPP* increased rapidly in May and early June and reached its peak value around July. The simulated maximum daily *NPP* for 1994 and 1996 was 8.9 g C m^{-2} d^{-1} and 8.1 g C m^{-2} d^{-1}, respectively. On September 20 in both 1994 and 1996, about two weeks before the plant stopped its growth, *NPP* was simulated to go through zero back to negative values which means the start of net carbon loss of the plant. There was a negative peak for *NPP* at the end of September in both of the two years, showing the maximum carbon loss of the plant due to the relative high respiration and low photosynthesis rates at this time of the year. The simulated duration for positive *NPP* (carbon gain) was about 120 days in a year.

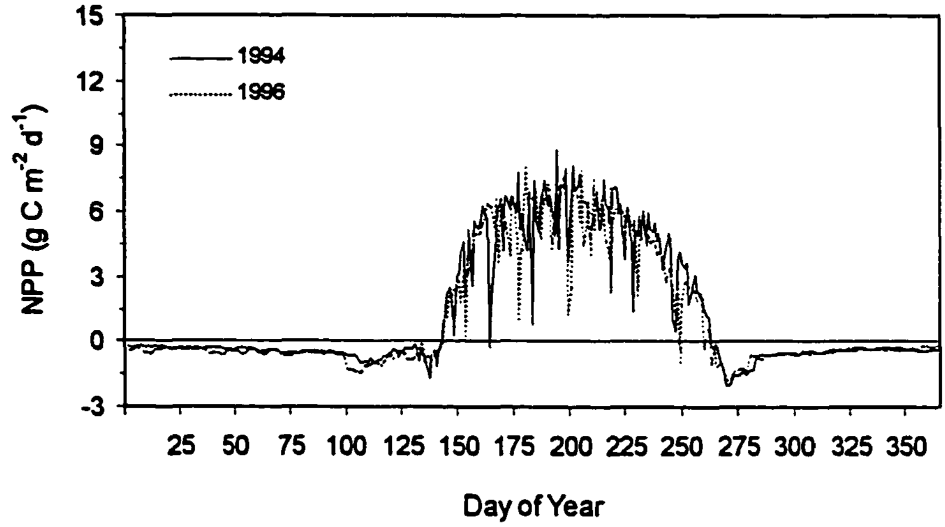

Figure 4.9 Annual distributions of simulated daily net primary production NPP for 1994 and 1996

The changing pattern of leaf area index *LAI* calculated from equation (4.38) was plotted in Figure 4.10. Leaf growth was simulated to start both from mid-April in 1994 and 1996. While the leafing date simulated for 1994 was close to the observations (Chen *et al.*, 1999), leafing date for 1996 was observed to be 24 days later than 1994 due to the late spring in 1996. This difference was not reflected in the model. However, much slower increase in *LAI* for 1996 than that for 1994 in the early growing season was obtained in the model caused mainly by the cool spring temperature in 1996. Rapid increase occurred from late May until it reached the maximum value in mid-July. The simulated maximum *LAI* during the full growth period was about 5.5 for 1994 and 5.0 for 1996, compared with the observed maximum of total *LAI* (aspen plus hazelnut) of about 5.6 for 1994 and 4.4 for 1996, respectively (Chen *et al.*, 1999). Decrease of *LAI* started earlier in 1994 than 1996 in the model, and both of them decreased rapidly in September until they reached zero at about the same time in early October. Observations, however, showed that growing period for 1996 ended 17 days later than that for 1994. The difference between modelled and observed growing dates was mainly due to the improper formulations and parameterizations on the plant phenology in the model.

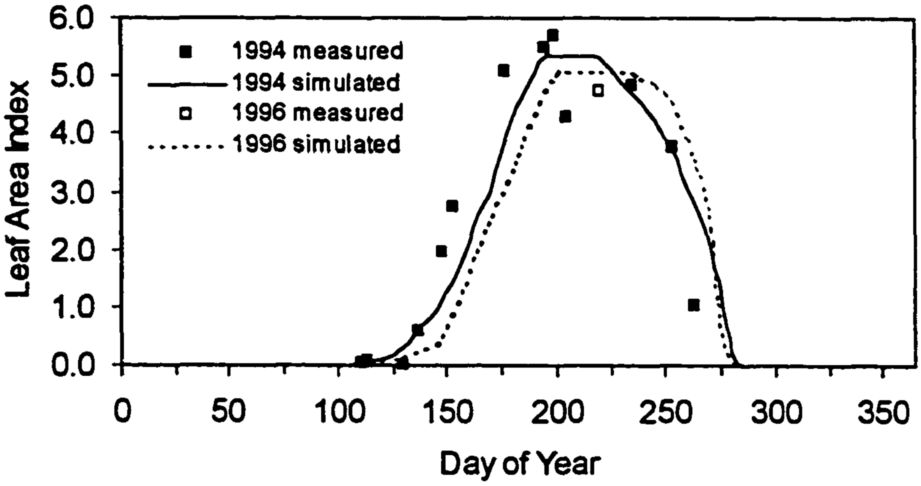

Figure 4.10 Simulated (line) and measured* (symbols) leaf area index (*LAI*) for 1994 and 1996
(* measured values are the sum of leaf area index of aspen plus hazelnut)

(3) Annual Budgets of Plant C Exchanges

Annual totals of C exchanges accumulated from half-hourly values in the model were summarised in Table 4.2. These results were compared with the estimations from CO_2 flux measurements according to Chen *et al.* (1999) and from chamber measurements according to Ryan *et al.* (1997). The simulated annual ecosystem gross primary production (*GPP*) was 1103.8 g C m^{-2} $year^{-1}$ for 1994 and 1091 g C m^{-2} $year^{-1}$ for 1996, about 1.5% lower and 5.9% higher than those estimated by Chen *et al.* (1999) for the two years, respectively. A decrease of 90 g C m^{-2} in 1996 compared with 1994 was obtained based on the flux measurement, which was mainly attributed to the combined effect of the late spring in 1996 and the asymmetrical distribution of incident PPFD over the growing season (Chen *et al.*, 1999). While in the model, since the simulated growing season for 1996 was similar to 1994, the simulated *GPP* for 1996 was only 13 g C m^{-2} lower than that for 1994.

Annual carbon cost in plant growth respiration R_g was simulated at 119.3 g C m^{-2} year^{-1} on the average for the two years, about 10.9% of *GPP*. Of this 10.9%, 6.0% was due to the foliage, 3.0% was due to the stem sapwood and coarse root, and 1.9% was due to the fine root growth respiration. Annual maintenance respiration R_m was much higher than R_g (515.2 g C m^{-2} year^{-1} vs. 119.3 g C m^{-2} year^{-1}) and it took 47% of *GPP*. Of this 47%, 21.9% was simulated from stem sapwood and coarse root, 14.9% from fine root, and 10.2% from foliage maintenance respiration. Annual aboveground respiration $R_{a,abv}$ was the sum of growth and maintenance requirements for all foliage and stem sapwood. $R_{a,abv}$ values of 324.6 g C m^{-2} year^{-1} and 303.3 g C m^{-2} year^{-1} in the model for 1994 and 1996, respectively, were slightly lower than their corresponding below-ground autotrophic respiration $R_{a,blw}$ (coarse root + fine root) of 332.2 g C m^{-2} year^{-1} and 309.0 g C m^{-2} year^{-1}. Similar results on aboveground and below-ground respiration have been estimated by Ryan *et al.* (1997) to be about 290 g C m^{-2} year^{-1} and 314 g C m^{-2} year^{-1} for 1994. Autotrophic respiration R_a, the sum of R_g and R_m or $R_{a,abv}$ and $R_{a,blw}$, amounted to be 656.73 g C m^{-2} year^{-1} and 612.3 g C m^{-2} year^{-1} for 1994 and 1996, respectively, which was 57.8% of the annual *GPP* on the average. This number was very close to the estimation from chamber measurement according to Ryan *et al.* (1997) which showed a carbon use efficiency (1.0 - R_a/GPP or NPP/GPP) of 42%. So more than half of the C fixed by plant during a year was consumed by plant respiration and released back to the soil and atmosphere as CO_2.

With a mean carbon use efficiency of 42.2% in the model, the simulated net primary production *NPP* was 462.88 g C m^{-2} year^{-1} on the average (447.0 g C m^{-2} year^{-1} for 1994 and 478.7 g C m^{-2} year^{-1} for 1996). *NPP* in 1994 has been estimated

Table 4.2 Annual Carbon Budgets for Plant and the Ecosystem Simulated by the Model and Estimated by Other Researchers (g C m^{-2} $year^{-1}$)

	Simulated				Other Estimations	
	1994	1996	Average	% *GPP*	1994	1996
GPP	1,104	1,091	1,097		1120 (± 60)[a]	1030 (± 60)[a]
R_g	132	107	119	11%		
R_m	525	506	515	47%		
$R_{a,abv}$	325	303	314	29%	290[b]	
$R_{a,blw}$	332	309	321	29%	314[b]	
R_a	657	612	635	58%	604[b]	
NPP	447	479	463	42%	440[b]	
LFP	338	356	347	32%	(123[c] + 46[d])	
Δ_{biom}	109	123	116	11%		
R_h[#]	284	276	280	26%		
R_{EOS}[#]	940	888	914	83%	920 (± 90)[a]	900 (± 90)[a]
NEP[#]	164	203	183	17%	200 (± 30)[a]	130 (± 30)[a]

Abbreviations: *GPP* = gross primary production; R_g = growth respiration; R_m = maintenance respiration; $R_{a,abv}$ = above ground autotrophic respiration; $R_{a,blw}$ = below ground autotrophic respiration; R_a = total autotrophic respiration (= $R_g + R_m$ or = $R_{a,abv} + R_{a,blw}$); *NPP* = net primary production (*GPP* - R_a); *LFP* = litterfall; Δ_{biom} = plant biomass change (*NPP* - *LFP*); R_h = heterotrophic respiration; R_{ECO} = total ecosystem respiration ($R_a + R_h$); *NEP* = net ecosystem production (*GPP* - R_{ECO}).

[#] Shaded values are obtained from the results simulated in Chapter 5.

[a] Chen *et al.* (1999), estimations based on CO_2 flux measurements using eddy correlation technique. Data gaps when flux was not measured were filled using regression relationships obtained between photosynthesis and respiration and various climatic and biological variables. The uncertainty (numbers in brackets) is estimated from the filling processes.

[b] Ryan *et al.* (1997), estimations based on chamber measurements.

[c] Gower *et al.* (1997), estimations for the aboveground littler fall from litter traps.

[d] Steele *et al.* (1997), estimations for the fine root C turnover from root growth measured in growth cores and a fine root turnover index.

by Ryan *et al.* (1997) to be about 440 g C m^{-2} $year^{-1}$. Among this net carbon gain, about 75% was simulated as plant litterfall and root carbon exudation (*LFP*), which was regarded as the input of organic matter into the soil. This carbon loss from plant to soil was greater than that measured from litter traps for aboveground litterfall according to Gower *et al.* (1997) plus root carbon turnover measured from root growth by growth cores and a fine root turnover index of between 1.5 and 2 calculated from minirhizotron measurements according to Steele *et al.* (1997) (338.1 g C m^{-2} $year^{-1}$ versus 159 g C m^{-2} $year^{-1}$ for 1994). Net plant growth, or the change in plant biomass Δ_{biom}, was calculated as the difference between *NPP* and *LFP*. The average Δ_{biom} for 1994 and 1996 was modelled at 115.9 g C m^{-2}, about 10.6% of the total *GPP*.

4.4 Sensitivity Analyses

The same strategy as used in Chapter 3 was used here to analyse the model sensitivity on the plant carbon simulations to the variation in climate drivers. Plant gross primary production (*GPP*), autotrophic respiration (R_a), and net primary production (*NPP*) were selected as the prognostic variables. Model behaviour under the variations of climate drivers are presented in Figure 4.11. As a general trend, modelled *GPP*, R_a, and *NPP* commonly decreased with the prescribed lower air temperature, precipitation, and CO_2 concentration, and increased with the prescribed higher values of these climate drivers, with the exception of *NPP* under higher precipitation which also showed a slight decrease.

The great response of *GPP* to temperature changes indicates that the model predicted the plant carbon fixation in this boreal forest as mainly temperature constrained. *GPP* was simulated to decrease 46.9% if the temperature was 2°C lower, and to increase 17.6% if the temperature was 2°C higher. The main processes that contributed to these changes included the direct impact of temperature on leaf photosynthetic rates, changes in growing season length and in the plant nutrient (N) conditions, etc. According to the meteorological observations at this aspen site (see

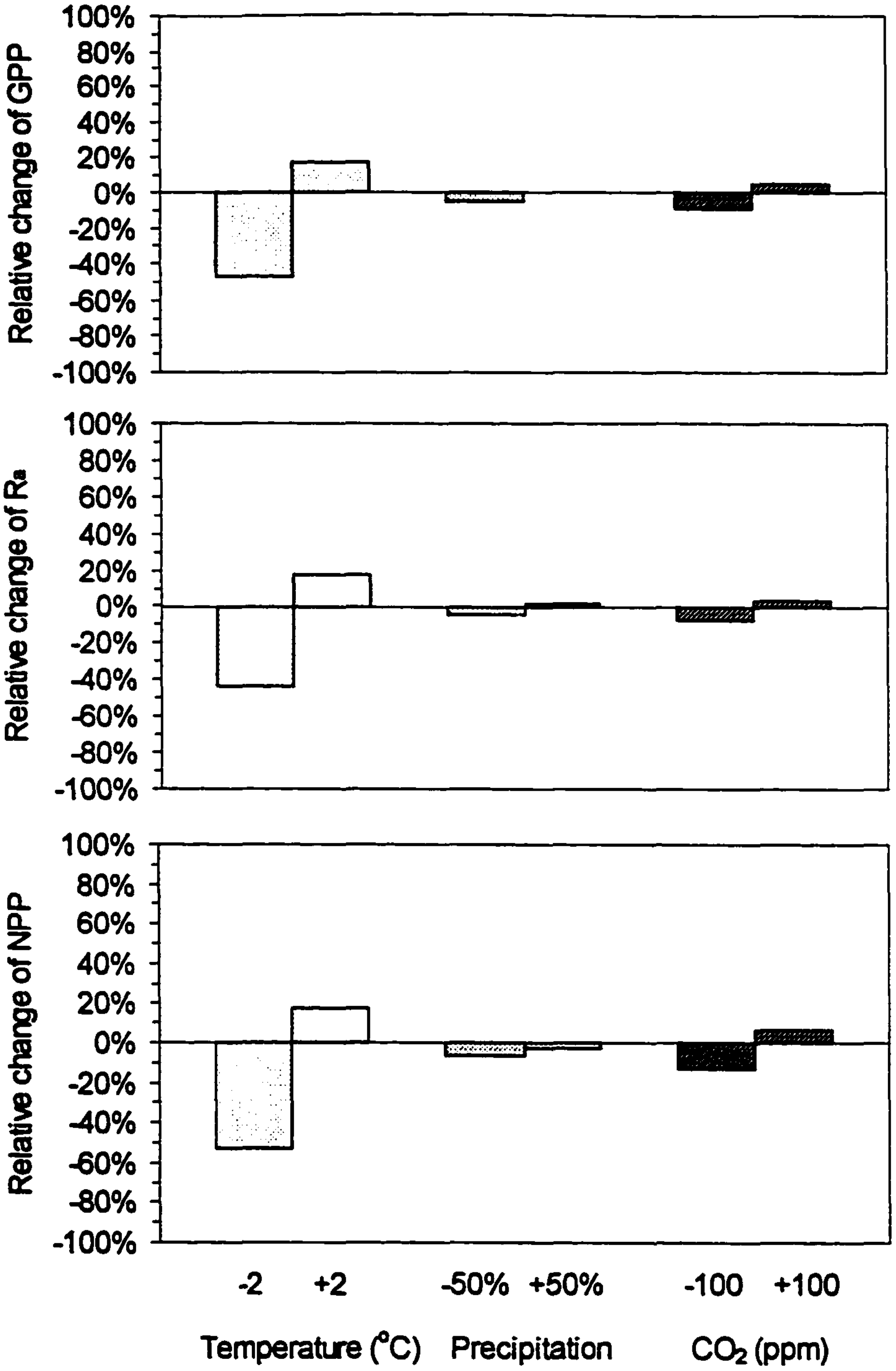

Figure 4.11 Sensitivity of simulated gross primary production GPP, autotrophic respiration R_a, and net primary production NPP to the variations of temperature, precipitation, and CO_2 concentration

Figure 4.7 and 4.8), temperature in the main growing period (May – August) was much lower than the optimum temperature according to the temperature response function for gross photosynthesis (equation 4.7). Therefore increase or decrease in temperature at this baseline would significantly increase or decrease the gross photosynthesis rate of per unit leaf area. Changes in temperature also caused the variation in growing season. Higher temperature resulted in earlier leaf emergence which allowed the plant to have longer time to gain carbon. Plant N conditions were also altered by the variations of temperatures according to the model. Higher temperature increased the decomposition rate of the huge soil organic matter pool (discussed in Chapter 5). As a result, mineral N release from the soil was increased which could accelerate the plant root N uptake. Since plant gross photosynthesis was formulated directly as a function of leaf N concentration (equation 4.8), improvement in plant N conditions would enhance its *GPP*.

The least response of *GPP* was to the variations in precipitation, particularly to the prescribed 50% increase in annual precipitation which caused only 0.3% increase. It indicates that the plant carbon fixation at this SSA-OA site was not predicted as being highly water limited during a near-average rainfall year represented by 1994 and 1996. Another reason for the smallest change in *GPP* with increasing precipitation was from the negative effect by the delay in plant leaf emergence. Precipitation increase in the model caused increase in the amount of snow during wintertime, which led to a late snowmelt prediction and therefore shortening the growing season. Decrease of precipitation by 50% caused water stress problems in this ecosystem according to the model, particularly in August and September. Even though less precipitation led to an earlier snow melt date and longer growing period, an overall decrease of 5.0% in annual *GPP* was predicted by the model under this prescribed drier conditions.

The effects of variation in CO_2 concentration were somewhere between those of temperature and precipitation. Modelled *GPP* increased 4.6% with 100 ppm higher CO_2 and decreased 9.6% with 100 ppm lower CO_2. The process that directly contributes to this response can be represented by the Farquhar equation (equation 4.2), which shows that changes in CO_2 strongly affect carbon fixation through Michaelis-Menten kinetics. Secondary effects such as larger *LAI* caused by the higher *GPP* also contributed to the changes to some extent.

Autotrophic respiration R_a is mainly determined by temperature. Plant growth rate also affects R_a by controlling R_g, but to a less extent according to the model. Similar magnitude of R_a response to temperature variations was obtained with those of *GPP*. R_a was increased 17.8% under 2°C higher temperature and decreased 43.8% under 2°C lower temperature. While higher temperature directly led to a higher plant maintenance respiration rate, growth respiration was also increased due to the higher plant growth rates, and vice versa. Another factor that attributed to this change was from the change in plant nitrogen content. Since plant maintenance respiration was calculated based on the plant N content (equation 4.28), the trees under lower temperatures tended to have lower amount of N due to the slower decomposition rates of soil organic matter.

Response of R_a to the variations in precipitation can be explained by the change in maintenance respiration and growth respiration. Slightly higher *GPP* with 50% increase in precipitation and lower *GPP* with 50% decrease in precipitation contributed to the similar changing pattern of growth respiration as those of R_a. It is noteworthy that the increase of R_a under 50% higher precipitation was larger than that of *GPP* (2.0% vs. 0.3%), while the decrease of R_a under 50% lower precipitation was smaller than that of *GPP* (4.3% vs. 5.0%). It can be explained by the change in maintenance respiration due to the difference in plant N content under the dry and wet conditions. Under wet conditions, decomposition of soil organic matter was more rapid than under dry conditions (discussed in Chapter 5), which would lead the plants to have higher N content and thus higher maintenance respiration. Under drier conditions, maintenance respiration tended to be small due to the lower N content of the plant.

Changes of R_a with CO_2 concentration were mainly caused by the variation of growth respiration. Increase of *GPP* with 100 ppm higher CO_2 and decrease of *GPP* with 100 ppm lower CO_2 determined the response of R_a to CO_2 variations. Maintenance respiration was not directly affected by the CO_2 concentration, except when we consider the altered root growth by CO_2 which may have some effect on plant N uptake.

Since *NPP* is calculated as the difference between *GPP* and R_a, response of *NPP* to the variations in climate drivers represents their integrated impacts on *GPP* and R_a. Due to the relatively larger decrease in *GPP* than in R_a with 2°C lower temperature, a decrease of 53.2% in *NPP* was obtained in the model under this cooler conditions, again indicating the temperature limitations to the plant carbon processes. Impacts of 2°C higher temperature on *GPP* and R_a were of similar magnitude, and led to the similar *NPP* increase of about 17.4%.

NPP was decreased for both the prescribed 50% decrease in precipitation and 50% increase in precipitation. *GPP* was decreased more than R_a under the drier conditions which led to a 6.2% decrease in *NPP*. While under the prescribed wetter conditions, more increase in R_a was obtained than in *GPP*, and it finally caused *NPP* to be decreased by 2.8%.

Increase in CO_2 concentration benefited *GPP* more than R_a. Therefore simulated sensitivity of *NPP* to CO_2 variation was relatively higher than those of *GPP* and R_a. A decrease of 12.8% in *NPP* was obtained under 100 ppm lower CO_2, and an increase of 6.7% was obtained under 100 ppm higher CO_2.

4.5 Conclusions and Discussion

Developing process based plant models in land surface schemes is still very new. Errors caused from ignoring the impacts of plant physiological processes on the water and energy exchange of vegetated land surfaces have been realized in this decade. The coupled water-carbon models have been proposed as the direction for the development of the "third-generation" land surface schemes. In some ecosystems, limitation of plant nutrient conditions largely constrains the plant carbon process.

This limitation may exert significant impacts on the land surface energy and water exchanges with the atmosphere, such as the nitrogen limitation in the boreal forest which is supposed to cause unexpectedly low stomatal conductance (Sellers *et al.*, 1997). However, implementation of coupled carbon and nutrition models in land surface schemes has not yet been realized, according to the knowledge of the author on the latest literature review.

In the *PLANTC* module developed for CLASS, explicit calculations of coupled carbon-nitrogen processes of photosynthesis, respiration, plant root N uptake, tissue growth, and litterfall production were explored. Just as the vegetation plays important roles in controlling the energy and water processes on the land surfaces and in determining the carbon biochemical and biogeochemical cycles in the terrestrial ecosystems, the *PLANTC* module has the decisive position in controlling the whole model behaviour and predictions. Simulation of photosynthesis and plant growth not only makes the coupled water-carbon calculations implemented in Chapter 3 possible, but also provides the basis for the estimation of plant parameters and ecosystem carbon budgets. Litterfall estimation, on the other hand, directly drives the carbon biochemical transformations occurring in the soil ecosystem and makes it possible to complete the carbon cycles in natural ecosystems.

A particular feature of the *PLANTC* module is the emphasis on the role of nitrogen in the plant carbon processes. The potential limitation of N on gross primary production is regarded to be of the same significance as that of water. This nitrogen scheme enables the effect of N deficits on stomatal resistance, and thereby on mass and energy exchange, to be represented by CLASS. Plant growth rates and biomass C:N ratios are also controlled by the availability of nitrogen. The C:N ratios of plant biomass determine the N concentration in the plant litterfall which is used as an index for representing the plant litter quality as discussed in Chapter 5.

Estimation of gross photosynthesis is extremely important in simulating both the energy balance and ecosystem C budgets. Separating canopy leaves into sunlit and shaded categories is mainly based on the consideration that radiation difference on the leaf surfaces is the most significant factor in causing the photosynthetic differences among leaves. While this can greatly improve the scaled-up results from leaf calculation to the canopy level, limitations may apply due to the influences from other factors. For example, many researchers have demonstrated that the N concentration is very different with respect to the leaf position within canopy (*e.g.*, Hirose and Werger, 1987; Schieving *et al.*, 1992; Evans, 1993), leaf age (*e.g.*, Middleton *et al.*, 1997), and PAR interception (Dang *et al.*, 1997), etc. Spatial inhomogeneities of leaf characteristics are not addressed in this model development, which may bring errors in the overall estimations.

Another simplification in the model that may cause improper estimations is the absence of canopy spatial structure and plant species difference. At the observation site, crown space of aspen is limited to the upper 5-6 m beneath which is a branchless trunk space. The understory is dominated by a uniform cover of hazelnut (*Corylus cornuta* Marsh.) with a mean height of 2 m. Wild rose (*Rosa woodsii*) and alder (*Alnus crispa*) are also found intermittently (Black *et al.*, 1996; Blanken *et al.*, 1997). *LAI* of the hazelnut at this site has the similar magnitude to that of the aspen. Hazelnuts in forest ecosystems may play important roles in altering the land surface energy, water and carbon processes. For example, Black and Kelliher (1989) summarized the research on evapotranspiration from understories in a wide range of forests and found that fraction of forest evapotranspiration contributed by understories varied from 10% to 65%. Since the overstory canopies and the understory canopies have acclimated to very different microclimatic environments, their physiological characteristics may be quite different. In the model, the whole canopy (overstory + understory) was treated the same and with common physiological characteristics. While this simplification greatly decreases the calculation requirements, it may cause errors in estimation and bring limitations to model application such as in the spatial analyses of energy, water and carbon dynamics within the canopy.

Since many processes developed in the *PLANTC* module are strongly dependent on the nitrogen condition of the plant, *e.g.*, gross photosynthesis and maintenance respiration, model outputs such as *NPP* can be very sensitive to the N variations. Unfortunately, knowledge and measurements of the ecosystem N dynamics are much less than those for carbon. This makes the model more difficult to validate against the N dynamics. Net N input or output rate into or out of the natural ecosystems are usually small and have limited effects on the model behaviour on a short time scale (months to years). However, it may have significant impacts on a long-term run (decades to century). Since the nitrogen budgets on the ecosystem level are treated simply (discussed in Chapter 5), we must be cautious in applying the modelled results particularly from the long-term point of view.

References

Abrams, M.D. and Mostoller, S.A., 1995. Gas exchange, leaf structure and nitrogen in contrasting successional tree species growing in open and understory sites during a drought. Tree physiology, 15: 361-370.

Ågren, G.I., McMurtrie, R.E., Parton, W.J., Pastor, W.J., and Ahugart, H.H., 1990. State-of-the-art of models of production-decomposition linkages in conifer and grassland ecosystems. Ecological Applications, 1: 118-138.

Amthor, J.S., 1986. Evolution and applicability of a whole plant respiration model. Journal of Theoretical Biology, 122: 473-490.

Amthor, J.S., 1989. Respiration and crop productivity. Springer-Verlag, New York.

Amthor, J.S., 1991. Respiration in a future, higher- CO_2 world. Plant, Cell and Environment, 14: 13-20.

Atjay, G.L., Ketner, P., and Duvigneaud, P., 1977. Terrestrial primary production and phytomass. In: Bolin, B.E., Degens, T., Kempe, S., and Ketner, P. (editors), The Global Carbon Cycle. Scope vol. 13, pp. 129-181. John Wiley, New York.

Barber, S.A., 1995. Soil Nutrient Bioavailability: A mechanistic approach. Second edition. John Wiley & Sons, New York.

Barber, S.A. and Cushman, J.H., 1981. Nitrogen uptake model for agronomic crops. p. 382-409. In: Iskandar, I.K. (ed.) Modeling wastewater renovation-land treatment. Wiley-Interscience, New York.

Barber, S.A. and Silberbush, M., 1984. Plant root morphology and nutrient uptake. In: Roots, Nutrient and Water Influx, and Plant Growth. ASA Special Publication Number 49. pp: 65-88.

Berry, J.A., Collatz, J., Gamon, J., Fu, W., and Fredeen, A., 1998. BOREAS TE-04 Gas Exchange Data from Boreal Tree Species. Available online at [http://www-eosdis.ornl.gov/] from the ORNL Distributed Active Archive Center, Oak Ridge National Laboratory, Oak Ridge, Tennessee, U.S.A.

Black, T.A. and Kelliher, F.M., 1989. Processes controlling understory evapotranspiration. Phil. Trans. Royal Soc. London B, 324: 207-231.

Black, T.A., den Hartog, G., Neumann, H.H., Blanken, P.D., Yang, P.C., Russell, C., Nesic, Z., Lee, X., Chen, S.G., and Staebler, R., 1996. Annual cycles of water vapor and carbon dioxide fluxes in and above a boreal aspen forest. Global Change Biol. 2: 219-229.

Blanken, P.D., Black, T.A., Yang, P.C., Neumann, H.H., Nesic, Z., Staebler, R., den Hartog, G., Novak, M.D., and Lee, X., 1997. Energy balance and canopy conductance of a boreal aspen forest: Partitioning overstory and understory components. Journal of Geophysical Research, 102, D24: 28915-28927.

Campbell, G.S., 1977. An Introduction to Environmental Biophysics. Springer-Verlag. N.Y.

Campbell, G.S., 1985. Soil physics with BASIC. Transport models for soil plant systems. Development in soil science 14. Elsevier Science Publishers, B.V., Amsterdam.

Cannell, M.G.R. and Dewar, R.C., 1994. Carbon allocation in trees: a review of concepts for modelling. Advances in Ecological Research, 25: 59-104.

Chen, W.J., Black, T.A, Yang, P.C., Barr, A.G., Neumann, H.H., Nesic, Z., Blanken, P.D., Novak, M.D., Eley, J., Ketler, R.J., and Cuenca, R., 1999. Effects of climatic variability on the annual carbon sequestration by a boreal aspen forest. Global Change Biology, 5: 41-53.

Claassen, N., and Barber, S.A., 1976. Simulation model for nutrient uptake from soil by a growing plant root system. Agron. J., 68: 961-964.

Collatz, G.J., Ball, J.T., Grivet, C., and Berry, J.A., 1991. Physiological and environmental regulation of stomatal conductance, photosynthesis and transpiration: a model that includes a laminar boundary layer. Agric. For. Meteorol., 54: 107-136.

Cram, W.J., 1973. Internal factors regulating nitrate and chloride influx. J. Exp. Bot., 24: 328-341.

Dang, Q.L., Margolis, H.A., Sy, M., Coyea, M.R., Collatz, G.J., and Walthall, C.L., 1997. Profiles of photosynthetically active radiation, nitrogen and photosynthetic capacity in the boreal forest: Implications for scaling from leaf to canopy. Journal of Geophysical Research, 102, D24: 28,845-28,859.

Dickinson, R.E. and Shaikh, M., 1998. Interactive canopies for a climate model. J. Climate, 11: 2823-2836.

Dixon, R.K., Meldahl, R.S., Ruark, G.A., and Warren, W.G., 1990. Process Modelling of Forest Growth Responses to Environmental Stress. 441 pp. Timeber Press, Portland, Oregon, USA.

Douglas, B.J. and Ogren, W.L. 1984. The CO_2/O_2 specificity of ribulose 1,5-biphosphate carboxylase / oxygenase. *Planta.* 161: 308-313.

Evans, J.R., 1989. Photosynthesis and nitrogen relationships in leaves of C_3 plants. Oecologia, 78: 9-19.

Evans, J.R., 1993. Photosynthetic acclimation and nitrogen partitioning within a lucerne canopy. II Stability through time and comparison with a theoretical optimum. Australian Journal of Plant Physiology, 20: 69-82.

Evans, J.R. and Farquhar, G.D., 1991. Modeling canopy photosynthesis from the biochemistry of the C_3 chloroplast. In: Modelling crop photosynthesis from biochemistry to canopy. K. J. Boote and R. S. Loomis (Eds), CSSA Special publication number 19. pp.1-15.

Farquhar, G.D., von Caemmerer, S., and Berry, J.A., 1980. A biochemical model of photosynthetic CO_2 assimilation in leaves of C_3 species. *Planta*. 149: 78-90.

Farquhar, G.D. and von Caemmerer, S., 1982. Modelling of photosynthetic response to environment. p. 549-587. In: Encyclopedia of plant physiology,. O. L. Lange *et al.* (Eds), New Ser. Vol. 12B. Physiological Plant Ecology II. Springer-Verlag, Berlin.

Field, C., 1983. Allocating leaf nitrogen for the maximisation of carbon gain: Leaf age as a control on the allocation program. Oecologia, 56: 341-347.

Foley, J.A., Prentice, I.C., Ramankutty, N., Levis, S., Pollard, D., Sitch, S., and Haxeltine, A., 1996. An integrated biosphere model of land surface processes, terrestrial carbon balance, and vegetation dynamics. Global Biogeochemical Cycles, 10: 603-628.

Glass, A., 1975. The regulation of potassium absorption in barley roots. Plant Physiol., 56: 377-380.

Gower, S.T., Vogel, J.G., Stow, T.K., Norman, J.M., Kucharik, C.J., and Steele, S.J., 1997. Carbon distribution and aboveground net-primary production in aspen, jack pine, and black spruce stands in Saskatchewan and Manitoba, Canada. J. Geophys. Res., 102 D24: 29029-29042.

Grant, R.F., 1991. The distribution of water and nitrogen in the soil-crop system: a simulation study with validation from a winter wheat field trial. Fertilizer Research 27: 199-213.

Grant, R.F., 1993. Rhizodeposition by crop plants and its relationship to microbial activity and nitrogen distribution. Modeling Geo-Biosphere Processes, 2: 193-209.

Gutschick, V.P., 1991. Modelling photosynthesis and water-use efficiency of canopies as affected by leaf and canopy traits. In: Modelling crop photosynthesis from biochemistry to canopy K. J. Boote and R. S. Loomis (Eds), CSSA Special publication number 19. pp.57-74.

Hale, M.G. and Moore, L.D., 1979. Factors affecting root exudation. II: 1970-1978. Adv. Agron., 31: 93-124.

Harley, P.C., and Tenhunen, J.D., 1991. Modelling the photosynthetic response of C_3 leaves to environmental factors. In: Modelling crop photosynthesis from biochemistry to canopy. K. J. Boote and R. S. Loomis (Eds), CSSA Special publication number 19. pp.17-40.

Harley, P.C., Thomas, R.B., Reynolds, J.F., and Strain, B.R., 1992. Modelling photosynthesis of cotton grown in elevated CO_2. Plant, Cell and Environment, 15: 271-282.

Henderson-Sellers, A., Yang, Z.-L., and Dickinson, R. E., 1993. The project for intercomparison of land-surface parameterization schemes. Bulletin of the American Meteorological Society 74(7): 1335-1349.

Hirose, T. and Werger, M.J.A., 1987. Maximising daily canopy photosynthesis with respect to the leaf nitrogen allocation pattern in the canopy. Oecologia, 72: 520-526.

Johnson, I.R. and Thornley, J.H.M., 1984. A model of instantaneous and daily canopy photosynthesis. J. Theor. Biol., 107: 531-545.

Kimball, J.S., Thornton, P.E., White, M.A., and Running, S.W., 1997. Simulating forest productivity and surface-atmosphere carbon exchange in the BOREAS study region. Tree Physiology, 17: 589-599.

Kimmins, J.P., 1997. Forest Ecology: A foundation for sustainable management. 2nd ed. Prentice Hall.

Kozlowski, T.T., 1982. Water supply and tree growth. Part I, Water deficits. Forestry Abstracts. 43: 57-95.

Kozlowski, T.T., and Pallardy, S.G., 1997. Physiology of Woody Plants. Second edition. Academic Press, San Diego.

Läuchli, A., 1984. Plant root morphology and nutrient uptake. In: Roots, Nutrient and Water Influx, and Plant Growth. ASA Special Publication Number 49. pp: 1-26.

Larcher, W., Physiological Plant Ecology. Third Edition. 1995. Springer, Austria. P117.

Lavigne, M.B. and Ryan, M.G., 1997. Growth and maintenance respiration rates of aspen, black spruce and jack pine stems at northern and southern BOREAS sites. Tree Physiology, 17: 543-551.

Leuning, R., Cromer, R.N., and Rance, S., 1991. Spatial distributions of foliar nitrogen and phosphorus in crowns of *Eucalyptus grandis*. Oecologia, 88: 504-510.

Mäkelä, A.A. and Sievänen, R.P., 1987. Comparison of two shot-root partitioning models with respect to substrate utilization and functional balance. Annals of Botany, 59: 129-140.

Marcelis, L.F.M., 1993. Simulation of biomass allocation in glasshouse crops - a review. Acta Horticulturae, 328: 49-67.

Marshall. B., and Biscoe, P.V., 1980. A model for C_3 leaves describing the dependence of net photosynthesis on irradiance. J. Exp. Bot., 31: 29-39.

Middleton, E.M., Sullivan, J.H., Bovard, B.D., Deluca, A.J., Chan, S.S., and Cannon, T.A., 1997. Seasonal variability in foliar characteristics and physiology for boreal forest species at the five Saskatchewan tower sites during the 1994 Boreal Ecosystem-Atmosphere Study. Journal of Geophysical Research, 102, D24, 28831-28844.

Minchin, P.E.H., Thorpe, M.R., and Farrar, J.F., 1993. A simple mechanistic model of phloem transport which explains sink priority. J. Exp. Botany, 44: 947-955.

Norman J.M. and Arkebauer, 1991. Modelling photosynthesis and water-use efficiency of canopies as affected by leaf and canopy traits. In: K. J. Boote and R. S. Loomis (Eds), Modelling crop photosynthesis from biochemistry to canopy. CSSA Special publication number 19. pp.75-94.

Rastetter, E.B., Ryan, M.G., Shaver, G.R., Melillo, J.M., Nadelhoffer, K.J., Hobbie, J.E., and Aber, J.D., 1991. A general biogeochemical model describing the responses of the C and N cycles in terrestrial ecosystems to changes on CO_2, climate, and N deposition. Tree Physiology, 9: 101-126.

Rovira, A.D., 1969. Plant root exudates. Bot. Rev., 35: 35-57.

Ryan, M.G., 1991. The effect of climate change on plant respiration. Ecological Applications, 1: 157-167.

Ryan , M.G., 1995. Foliar maintenance respiration of subalpine and boreal trees and shrubs in relation to nitrogen content. Plant, Cell and Environment, 18: 765-772.

Ryan, M.G., Hubbard, R.M., Pongracic, S., Raison, R.J., and McMurtrie, R.E., 1996. Foliage, fine-root, woody-tissue and stand respiration in *Pinus radiata* in relation to nitrogen status. Tree Physiology, 16: 333-343.

Ryan, M.G., Lavigne, M.B., and Gower, S.T., 1997. Annual carbon cost of autotrophic respiration in boreal forest ecosystems in relation to species and climate. Journal of Geophysical Research, 102, NO. D24: 28,871-28,883.

Schieving, F., Pons, T.L., Werger, M.J.A., and Hirose, T., 1992. The vertical distribution of nitrogen and photosynthetic activity at different plant densities in Carex acutiformis. Plant and Soil, 14:9-17.

Sellers, P.J., Randall, D.A., Collatz, G.J., Berry, J.A., Field, C.B., Dazlich, D.A., Zhang, C., Collelo, G.D., and Bounoua, L., 1996. A revised land surface parameterization (SiB2) for atmospheric GCMs. Part I: Model formulation. J. Climate, 9: 676-705.

Sellers, P.J., *et al.*, 1997. BOREAS in 1997: Experiment overview, scientific results, and future directions. Journal of Geophysical Research, 102, D24: 28,731-28,769.

Sharpe, P.S.H. and DeMichelle, D.W., 1977. Reaction kinetics of poikilothermic development. J. Theor. Biol., 64: 649-670.

Siddiqi, M.Y. and Glass, A.D.M., 1982. Simultaneous consideration of tissue and substrate potassium concentration in K^+ uptake kinetics: a model. Plant Physiol. 69: 283-285.

Steele, S.J., Gower, S.T., Vogel, J.G., and Norman, J.M., 1997. Root mass, net primary production and turnover in aspen, jack pine, and black spruce forests in Saskatchewan and Manitoba, Canada. Tree physiology, 17: 577-587.

Thornley, J.H.M., 1972. A balanced quantitative model for root:shoot ratios in vegetative plants. Annals of Botany, 36: 431-441.

Thornley, J.H.M., 1991a. A model of leaf tissue growth, acclimation and senescence. Annals of Botany, 67: 219-228.

Thornley, J.H.M., 1991b. A transport-resistance model for forest growth and partitioning. Annals of Botany, 68: 211-226 .

Thornley, J.H.M., 1997. Modelling allocation with transport/conversion processes. Silva Fennica, 31: 341-355.

Thornley, J.H.M. and Cannell, M.G.R., 1992. Nitrogen relations in a forest plantation - soil organic matter ecosystem model. Annals of Botany 70: 137-151.

Wang, S. and Yu, H., 1993. Direct Impacts of increasing atmosphere CO_2 concentration on crop growth and development. In: Effects of Increasing CO_2 on Agriculture of China. Beijing Science & Technology Press.

Wann, M., Raper, C.D., and Lucas, H.L. Jr., 1978. A dynamic model for plant growth: a simulation of dry matter accumulation for tobacco. Photosynthetica, 12: 121-136.

Wilhelm, E., Battino, R., and Wilcock, R.J., 1977. Low-pressure solubility of gasses in liquid water. Chemical Reviews, 77: 219-262.

Wilson, J.B., 1988. A review of evidence on the control of shoot:root ratio, in relation to models. Annals of Botany, 61: 433-449.

Chapter 5 Modelling Soil and Ecosystem Carbon and Nitrogen Processes in CLASS – the *SOILC* Module and the Overall Model Evaluation

5.1 Introduction

Carbon and nitrogen processes in the soil ecosystem can also affect land surface processes and the global climate system. Soil organic matter (SOM) constitutes a basic component of any terrestrial ecosystem, SOM being structurally and functionally integrated into fundamental ecosystem processes. Besides being closely associated with physical and chemical soil properties vital to plant growth, SOM also provides carbon and energy to the saprotrophic system responsible for nutrient cycling. During biological turnover, plant nutrients held in SOM may become mineralised and available for root uptake or loss via leaching from the root zone or gaseous losses to the atmosphere.

The CO_2 released during SOM turnover is one of the major contributors to the overall carbon exchange between terrestrial ecosystem and the atmosphere. In natural ecosystems, most of the carbon fixed by plants will finally go to the soil either as above ground litterfall or as below ground root residue and exudation. The carbon transferred to the soil then, together with the organic matter already in the soil, undergoes decomposition through which most of the carbon is returned to the atmosphere as CO_2. Estimates of the quantity of carbon held in SOM globally show it to be about twice the 750 Pg carbon present in the atmosphere as CO_2 (Eswaran *et al.*, 1993). Therefore even a small change in this large stock could cause a significant change in atmospheric CO_2 concentration which is responsible for 50-60% of the increase in radiative forcing arising from anthropogenic emissions of gases to the atmosphere (IPCC, 1995). The boreal forest biome covers approximately 11% of the planet's terrestrial surface and its soils are a major storehouse for organic carbon (Bonan and Shugart, 1989; Tans *et al.*, 1990; Schlesinger, 1991). Because of the size of the biome and the large amount of carbon stored in the soil, boreal forests are critically important to the global carbon cycle. Understanding the interactions between the soil carbon dynamics and climate change would enhance our ability to make climate change predictions.

Climate change can influence this stock of soil organic matter in several ways: i) through changes in soil temperature, moisture and other external abiotic factors which exert overall control over SOM dynamics; ii) by altering plant growth, thus altering the annual return of plant debris to the soil, both in quantity and quality; and, iii) through feedbacks such as changed nutritional conditions on plant productivity, etc. Changes in climate and in the properties of SOM present in natural soil ecosystems tend to occur slowly. In temperate regions it is common for changes in SOM content to be undetectable within 1 or 2 decades. It is generally impossible to conduct experiments that will provide results within a reasonable time scale. Similarly it is impossible to conduct experiments at sites covering all possible combinations of soil type, climate, vegetation, and climate change scenario, etc. Therefore SOM models are an essential tool in making projections of the likely trends in SOM, the interactions of SOM dynamics with the atmosphere and climate, and the related properties and processes in soil.

Modelling plant litter and soil organic matter dynamics has been undertaken for several decades. A large number of SOM models have been published at least since the 1940s. Jenny (1941) used a single state variable model form to represent the decline of organic C and N in cultivated soils. It has been recognised, however, that SOM has many components that vary in stability and decomposition rate, which led to the strategies for developing multicompartment models. For example, Campbell *et al.* (1978) improved upon Jenny's approach by dividing soil organic matter into two different compartments, which included stable organic matter and labile organic matter represented by different turnover rates. Van Veen and Paul (1981) made further improvements in their models by dividing the plant residue into recalcitrant and decomposable fractions and introducing the concept of physically protected soil organic matter which had a much lower decomposition rate than non-physically protected organic matter. Jenkinson (1990) and Paustian (1994) reviewed some published SOM models and found some common elements: i) dominance of first-order kinetics; ii) discrete SOM components with characteristic rates of decomposition; and, iii) interconnected dynamics of C and N. The time steps used in the models can be very different. Some focus on the long-term changes in soil organic matter and the time step is usually long, *e.g.* one month in the CENTURY model (Parton *et al.*, 1987). Another group of models use very short time step of hours (*e.g.*, Juma and Paul, 1981, Molina *et al.*, 1983) in which the dynamics of microbial biomass and the labile organic matter can be well represented. A comprehensive review and evaluation of some current models on soil organic matter can be found in Powlson *et al.* (1996).

In the available land surface schemes coupled with GCMs, process based calculations on the soil organic matter dynamics have not been included yet. However, with the realisation of the importance of soil carbon in climate change, there is a growing interest in coupling biogeochemical processes with the climate models. In fact, GCMs provide us the opportunity to develop the soil carbon processes within the land surface scheme since GCMs output the short-term variables that can be used to drive the soil biochemical reactions.

Transformation of organic matter in and on soil is mainly controlled by soil physical conditions (*e.g.*, temperature, moisture, and texture), chemical conditions (*e.g.*, pH), and biological and biochemical conditions (*e.g.*, substrate availability and quality), with numerous feedback mechanisms operating in a hierarchical manner. In the *SOILC* module developed in this chapter, the partitioning of plant litterfall into different kinetic compartments is first conducted according to its biochemical characteristics. The organic matter that already existed in soil is also divided into different compartments with different decomposition rates. Carbon and nitrogen transformations of these organic materials are then conducted for each soil layer. In addition, a surface layer is represented separately to account for the foliage and stem litterfall on the mineral soil surface. An individual microbial pool and mineral N pool are also included in each of the layers. All of the decomposition processes in the compartments follow the first-order reaction kinetics. Soil temperature and moisture simulated in the CLASS model are used to modify the reaction rates.

By finishing the carbon transformation processes in soil in this Chapter, I have covered the main carbon pathways in the terrestrial ecosystems. Therefore after the *SOILC* module is introduced and its main output of heterotrophic respiration discussed, I combine the carbon calculations for plants implemented in Chapter 4 with the soil results obtained in this chapter, which can be used to represent the carbon dynamics at the ecosystem level. The combined carbon fluxes simulated for the ecosystem are then compared with the tower flux measurements. Discussion and evaluation on the overall model behavior is given afterwards, followed by the model sensitivity analyses.

5.2 Module Description

5.2.1 General Module Structure

The structure of the *SOILC* module is shown in Figure 5.1. The pools for the newly formed plant litterfall and the soil organic matter (SOM) already in the soil were simulated for the same three soil layers as for the soil thermal and moisture regimes (see Chapter 2). In addition, a surface litter layer was recognized to account for the foliage and stem litterfall. The SOM carbon and nitrogen were divided into three compartments: i) an active compartment (C_A, N_A) consisted of SOM with a high turnover rate; ii) a slow compartment (C_S, N_S) that is physically protected and/or in chemical forms with more biological resistance to decomposition, with an intermediate turnover rate; and, iii) a humus compartment (C_H, N_H) that is chemically recalcitrant and that may also be physically protected, with the slowest turnover rate. This kind of classification scheme according to the decomposition ability of SOM has been widely adopted in modelling studies (*e.g.*, Juma and Paul, 1981; van Veen *et al.*, 1985; Parton *et al.*, 1987; and Verberne *et al.*, 1990).

Litterfall from the structural C and N pools of plant foliage, stem, and root (see Figure 4.1) was also partitioned into three compartments based on their

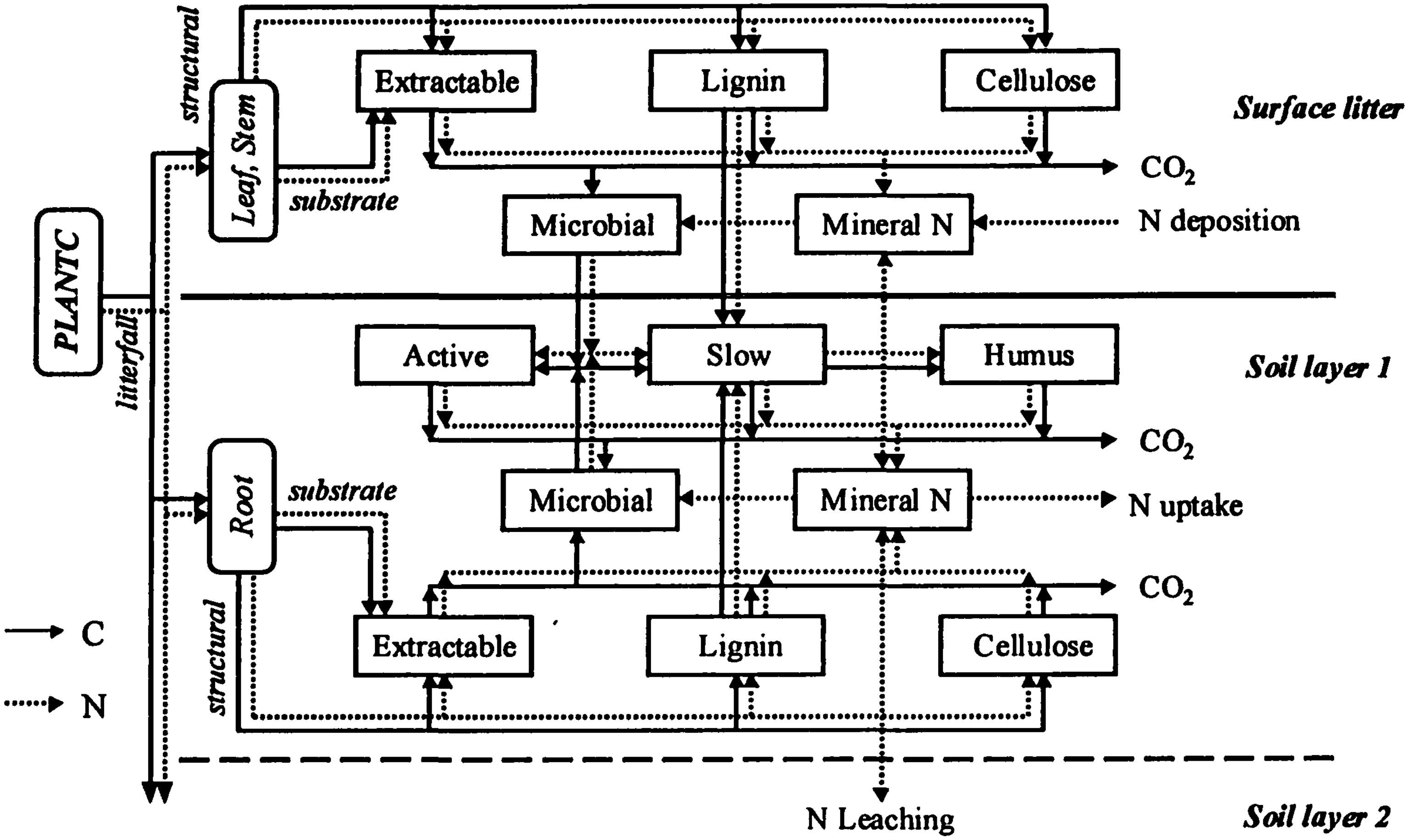
structural
Extractable
Lignin
Cellulose
Surface litter
Leaf, Stem
substrate
CO2
PLANTC
Microbial
Mineral N
N deposition
litterfall
Active
Slow
Humus
Soil layer 1
CO2
Root
substrate
Microbial
Mineral N
N uptake
CO2
structural
Extractable
Lignin
Cellulose
C
N
N Leaching
Soil layer 2

Figure 5.1 Schematic diagram of the *SOILC* module

biochemical characteristics. These were, with progressively more resistance to decomposition, i) extractable compartment (C_E, N_E), including carbohydrates and proteins; ii) cellulose and hemicellulose (C_C, N_C); and, iii) lignin (C_L, N_L). Litterfall from the substrate C and N pools of plant foliage, stem, and root was assumed to be all extractable. A microbial pool (C_M, N_M) and an inorganic nitrogen pool (N_I) were also included in each layer. Microbial pools acted as the main pathway for plant litter to be transformed into SOM. Inorganic N pools were the sink of mineralised N and source of immobilized N for all of the mineralization and immobilization processes simulated in the system. Plant litterfall production simulated in the *PLANTC* module was the main source of C and N for the *SOILC* module. Litterfall from foliage and stem was contributed to the surface litter pools, and the plant root residue and carbon exudation in each soil layer was added to the litter pools of its respective soil layer. Figure 5.1 gives the C and N transformation processes of the surface litter layer and the first soil layer. The processes in the other two soil layers are the same as the first soil layer, but without the C and N transport from the surface litter layer.

5.2.2 Litterfall Partitioning

The structural component in the plant litter is partitioned into extractable, cellulose, and lignin pools according to its N concentration and the assumed ratio of cellulose to lignin in the litterfall (Rastetter *et al.*, 1991). The C:N ratio of the structural component in the litterfall from tissue X, $\alpha_{S,X}$ ($X = F, S, R$), is calculated directly from its C and N content:

$$\alpha_{S,X} = \frac{L_{S,X}^{C}}{L_{S,X}^{N}} \tag{5.1}$$

where $L_{S,X}^{C}$ and $L_{S,X}^{N}$ are the litterfall from the structural C and N pools of tissue X (calculated in equation 4.33 and 4.35). The C:N ratio for the components of lignin plus cellulose, $\alpha_{L+C,X}$, in the litterfall can be calculated as

$$\alpha_{L+C,X} = \frac{(1+d_X)\alpha_L\alpha_C}{d_X\alpha_L + \alpha_C} \tag{5.2}$$

where d_X is the cellulose to lignin ratio, α_L and α_C are the given parameters representing the C:N ratios of lignin and cellulose, respectively. The partitioning of litterfall into different soil litter pools is then formulated from the two indexes of $\alpha_{S,X}$ and $\alpha_{L+C,X}$ obtained above:

$$F^C_{L,X} = \frac{L^C_{S,X}(\alpha_{L+C}\alpha_{S,X})}{(1+d_X)(w\alpha^2_{L+C} + \alpha^2_{S,X})} \tag{5.3}$$

$$F^C_{C,X} = d_X F^C_{L,X} \tag{5.4}$$

$$F^C_{E,X} = L^C_{L,X} + L^C_{S,X} - F^C_{L,X} - F^C_{C,X} \tag{5.5}$$

where $F^C_{L,X}$, $F^C_{C,X}$, and $F^C_{E,X}$ are the C fluxes from the litterfall of tissue X to the soil litter pools of lignin, cellulose, and extractable, respectively, w is the litterfall quality partitioning parameter according to Rastetter *et al.* (1991), and $L^C_{L,X}$ is the substrate component in the litterfall (calculated in equation 4.32). $L^C_{L,X}$ is assumed extractable and therefore added directly to $F^C_{E,X}$ as shown in equation (5.5). The above partitioning scheme allows that within the normal range of C:N ratios in the litterfall, increase in N content will decrease the fractions of lignin and cellulose and increase the extractable fraction. This agrees with the hypothesis that most of the nitrogen is contained in the easily decomposable materials such as protein.

The N partitioning of litterfall into lignin and cellulose, $F^N_{L,X}$ and $F^N_{C,X}$, is determined by the C fluxes ($F^C_{L,X}$ and $F^C_{C,X}$) obtained above divided by their corresponding C:N ratios (α_L and α_C). The N in the substrate component of the litterfall, $L^N_{L,X}$, together with the remaining N in the structural component, is assumed to be the N contained in the extractable materials. Therefore we have

$$F^N_{E,X} = L^N_{L,X} + L^N_{S,X} - F^N_{L,X} - F^N_{C,X} \tag{5.6}$$

where $F^N_{E,X}$ is the N flow into the extractable compartment, and $L^N_{S,X}$ is the total N content in the structural component of the litterfall from tissue X (calculated in equation 4.35).

5.2.3 Organic Matter Transformations

All transformations for the plant litter pools and SOM pools are considered to follow the first-order kinetics, on the assumption that the concentration of the material involved rather than the biological capacity is rate-limiting in decomposition. The transformation rates are then modified by multiplying three dimensionless functions of temperature $f(T_s)$, moisture $f(\psi_s)$, and microbial C:N ratio $f(\alpha_M)$

$$D_Y^C = k_Y C_Y f(T_s) f(\psi_s) f(\alpha_M) \tag{5.7}$$

where D_Y^C, k_Y, and C_Y are the carbon decomposition rate, first-order rate constant, and the total carbon amount of pool Y (Y represents: E = extractable, C = cellulose, L = lignin, A = active, S = slow, H = humus, and M = microbial), respectively. T_s and ψ_s are the soil temperature and water potential, and α_M represents the microbial C:N ratio. When $Y = M$, D_Y^C represents the microbial death rate. Each transformation in the different pools is given a specific decomposition rate constant.

The decomposition rate can be strongly affected by the climatic conditions. A great deal of information is available on the independent effect of climatic factors, but very little is known about the quantitative aspects of the combined effect. Expressing the effect of controlling factors by using reduction factors ranging from a value of 1, at optimum conditions, down to zero, depending on the particular environmental conditions, is now common in soil organic matter simulation models. The combined effect is then expressed by multiplying the reduction factors with each other (McGill *et al.*, 1981, Parton *et al.*, 1987). In the model as shown in equation (5.7), I follow the same method to express the impacts of soil temperature and moisture, which are assumed the two main climatic factors in constraining decomposition rate in most natural ecosystems.

The same Arrhenius equation form as equation (4.7) with slightly different parameter values (see Table 5.1) is used for the $f(T_s)$ formulation. The moisture function $f(\psi_s)$ is formulated according to Van Veen and Paul (1981) and Hunt (1977) (Figure 5.2), which shows that the maximum reaction rate of decomposition occurs around the soil water potential of -50 – -100 kPa. There is a rapid decrease when the soil is dried and it is assumed that decomposition nearly halts at -1500 kPa. The extension of the curve to zero at -4000 kPa allows for slight activity in very dry soil. Saturation of soil also causes lower reaction rate due to the limitation of oxygen in soil. Soil water potential in each soil layer is supplied by the water flow calculations in the original CLASS model.

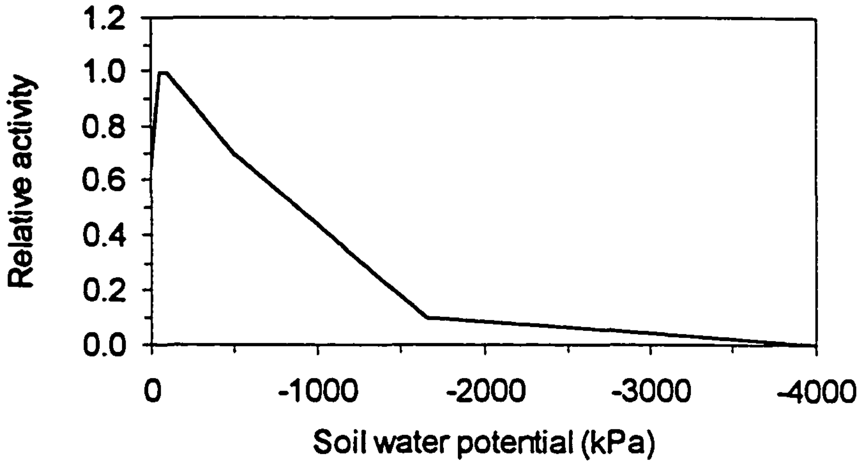

Figure 5.2 Impacts of soil water content on microbial decomposition rate

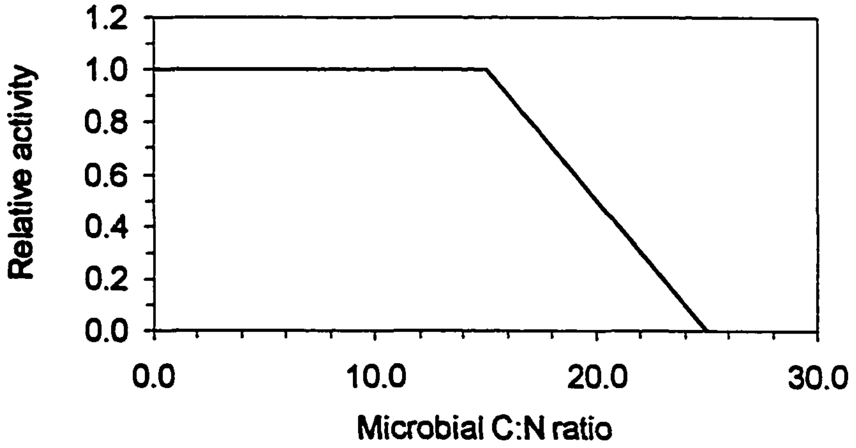

Figure 5.3 Impacts of microbial C:N ratio on the decomposition rate of lignin and cellulose

Decomposition of lignin and cellulose may be slowed if insufficient N is available for microbial growth (McGill *et al.*, 1981). Therefore another constraining factor, $f(\alpha_M)$, which is supposed to express the impact of N limitations on decomposition is added in equation (5.7) and it only applies to lignin and cellulose. It is formulated by microbial C:N ratio α_M ($= C_M / N_M$) following the relationship given in McGill *et al.* (1981) (Figure 5.3), which shows that there is a rapid decrease in the decomposition rate when the microbial C:N ratio exceeds 15 – 20.

Microorganisms use C compounds for biosynthesis forming new cellular or extracellular material and as energy supply. The fraction of the decomposing materials incorporated into microbial biomass is defined by the yield efficiency parameter β_Y. The remainder ($1 - \beta_Y$) is assumed to be respired and leaves the system as CO_2. Therefore the total growth rate of microbial biomass-C G_M^C and the total heterotrophic respiration rate R_h can be obtained by:

$$G_M^C = \sum_Y \beta_Y D_Y^C \quad (Y = E, C, L, A, S, H) \tag{5.8}$$

$$R_h = \sum_Y (1 - \beta_Y) D_Y^C \quad (Y = E, C, L, A, S, H) \tag{5.9}$$

While decomposing the lignin D_L^C (equation 5.7), a fraction (f_{LS}) is assumed to be directly transferred into the slow compartment of the SOM pools (T_{LS}^C). This enables the simulation of the role of ligneous compounds in the chemical stabilisation of organic matter in soil (Swift *et al.*, 1979).

$$T_{LS}^C = f_{LS} D_L^C \tag{5.10}$$

Transformation of the organic matter in the slow pool to the humus pools by chemical stabilisation, T_{SH}^C, is also included and assumed to follow first-order kinetics.

$$T_{SH}^C = k_{SH} C_S f(T_s) f(\psi_s) \tag{5.11}$$

where k_{SH} is the rate constant, and $f(T_s)$ and $f(\psi_s)$ are the temperature and moisture impact functions used in equation (5.7).

Microbial death D_M^C is also described by the first-order kinetics. Upon death microbial tissue is considered to split into two fractions: the material that decomposes rapidly and is freely accessible is partitioned to the active SOM pool (T_{MA}^C), and the material that is recalcitrant or physically protected against immediate microbial attack is added to the slow SOM pool (T_{MS}^C).

$$T_{MA}^C = r_{AS} D_M^C \tag{5.12}$$

$$T_{MS}^C = (1 - r_{AS}) D_M^C \tag{5.13}$$

where r_{AS} is the fraction of microbial products entering the active SOM pool.

The N fluxes in the decomposition processes D_Y^N are assumed to be proportional to the C fluxes. The rate of nitrogen release thus depends on the C:N ratio of the decomposed material α_Y.

$$D_Y^N = \frac{D_Y^C}{\alpha_Y} \tag{5.14}$$

The growth rate of microbial biomass-N G_M^N is calculated according to an optimum microbial C:N ratio ($\alpha_{M,O}$), and it is limited by the availability of the inorganic nitrogen N_l mineralized and stored in that soil layer.

$$G_M^N = Min(\frac{G_M^C}{\alpha_{M,O}}, N_l) \tag{5.15}$$

where G_M^C is the total growth rate of microbial C calculated in equation (5.8).

5.2.4 Mineral N Input and Output

Nitrogen input into the ecosystem I_N due to atmospheric deposition is assumed to be controlled by precipitation (Parton *et al.*, 1987).

$$I_N = c_N P_r \tag{5.16}$$

where c_N is the supposed concentration of N in the precipitation P_r. Other processes of N input such as from N bio-fixation are not considered in the model.

Nitrogen removal from the soil O_N is mainly determined by the plant root N uptake (Q_N) simulated in the *PLANTC* module (equation 4.16). Nitrogen loss from ecosystem also occurs as a result of leaching and volatilization of NH_3, N_2O and N_2. Here only the N leaching is considered and it is calculated by the product of downward water flux at the bottom of the soil column ($F_{w,IG}$) and the N concentration in the soil water of the bottom layer.

$$O_N = Q_N + F_{w,IG} \frac{N_{I,IG}}{\theta_{I,IG}} \tag{5.17}$$

where $N_{I,IG}$ and $\theta_{I,IG}$ are the mineral nitrogen and water content, respectively, of the bottom soil layer *IG*.

5.3 Parameterization, Simulation Results and Tests

5.3.1 Parameterization

Parameters used in the *SOILC* module are listed in Table 5.1.

5.3.2 Simulation Results and Tests

(1) Heterotrophic Respiration in Soil

Heterotrophic respiration R_h (equation 5.9) is one of the key variables in determining the soil ecosystem processes. The intensity of R_h directly controls the carbon source-sink relations of the soil. To show the changes of simulated half-hourly R_h, I plotted R_h for a two week period under extreme conditions, one in winter (DOY = 31 – 37) with low R_h and one in summer (DOY = 171 – 177) with high R_h (Figure 5.4A). In the winter week (the bottom line), R_h was simulated as low as 0.05 μmol CO_2 m^{-2} s^{-1}. This was mainly due to the low soil temperatures (the bottom line in Figure 5.4B) which remained below -8°C for the first soil layer. There was no apparent diurnal fluctuation of R_h found at this time period because of the stable soil temperatures. The magnitude of R_h from November through March was simulated under 0.07 μmol CO_2 m^{-2} s^{-1} for most of the time. Extremely low heterotrophic respiration rates during the wintertime that lasted about half of a year greatly

Table 5.1 Parameters Used in the *SOILC* Module.

Symbol	*Equation*	*Value*	*Units*	*Reference*
$d_{X (X=F,S,R)}$	(5.2–5.4)	2.35	Unitless	Calculated from Trofymow *et al.*, 1995
α_L	(5.2)	100.0	Unitless	Verberne *et al.*, 1990
α_C	(5.2)	150.0	Unitless	Verberne *et al.*, 1990
w	(5.3)	0.74	Unitless	Calculated from Trofymow *et al.*, 1995
k_E	(5.7)	4.60×10^{-3}	30min^{-1}	Calculated from van Veen and Paul, 1981
k_C	(5.7)	1.74×10^{-3}	30min^{-1}	Calculated from van Veen and Paul, 1981
k_L	(5.7)	2.09×10^{-4}	30min^{-1}	Calculated from van Veen and Paul, 1981
k_A	(5.7)	2.09×10^{-4}	30min^{-1}	Calculated from Verberne *et al.*, 1990
k_S	(5.7)	6.25×10^{-6}	30min^{-1}	Calculated from Verberne *et al.*, 1990
k_R	(5.7)	1.67×10^{-8}	30min^{-1}	Calculated from Verberne *et al.*, 1990
k_M	(5.7)	3.00×10^{-4}	30min^{-1}	Calculated from Juma and Paul, 1981
A	(4.7) (5.7)	17.24	unitless	
S	(4.7) (5.7)	710.0	$\text{J mol}^{-1}\text{ K}^{-1}$	
H_a	(4.7) (5.7)	57500.0	J mol^{-1}	
H_{dl}	(4.7) (5.7)	195000.0	J mol^{-1}	
H_{dh}	(4.7) (5.7)	220000.0	J mol^{-1}	
k_{SH}	(5.11)	6.25×10^{-8}	30 min^{-1}	Calculated from Juma and Paul, 1981
β_E	(5.8–5.9)	0.5	unitless	Verberne *et al.*, 1990
β_C	(5.8–5.9)	0.3	unitless	Verberne *et al.*, 1990
$\beta_L, \beta_S, \beta_H$	(5.8–5.9)	0.2	unitless	Verberne *et al.*, 1990
β_A	(5.8–5.9)	0.4	unitless	Verberne *et al.*, 1990
f_{LS}	(5.10)	1.0	unitless	
r_{AS}	(5.12–5.13)	0.5	unitless	Verberne *et al.*, 1990
α_S	(5.14)	15.0	unitless	Verberne *et al.*, 1990
α_H	(5.14)	10.0	unitless	Verberne *et al.*, 1990
$\alpha_{M,O}$	(5.15)	8.0	unitless	Verberne *et al.*, 1990
c_N	(5.16)	7.76×10^{-7}	$\text{kg N kg}^{-1}\text{ H}_2\text{O}$	Calculated from Kimmins, 1997

contributed to the soil carbon accumulation in the boreal forests.

In the summer week, R_h (the top line in Figure 5.4A) rose to about 1.0 – 2.5 μmol CO_2 m^{-2} s^{-1} due to the increase in soil temperatures (the top line in Figure 5.4B) which was observed between 10 – 23°C. There existed an apparent diurnal change in the CO_2 production which was similar to the diurnal change in soil temperature, indicating that soil temperature played the key roles in controlling heterotrophic respiration for this ecosystem. The daily maximum and minimum R_h values occurred a few hours after the noontime and midnight, respectively, following the same pattern as soil temperature variations. The magnitude of R_h in the summer was simulated between 1.0 – 2.5 μmol CO_2 m^{-2} s^{-1} for most of the time, with peak value reached about 3.5 μmol CO_2 m^{-2} s^{-1}.

Annual courses of daily R_h for 1994 and 1996 (Figure 5.5) show that R_h remained at high value of 1.0 – 2.0 g C m^{-2} d^{-1} for most of the days between May to September. Rapid increase of R_h occurred in April in 1994, while in 1996, it was

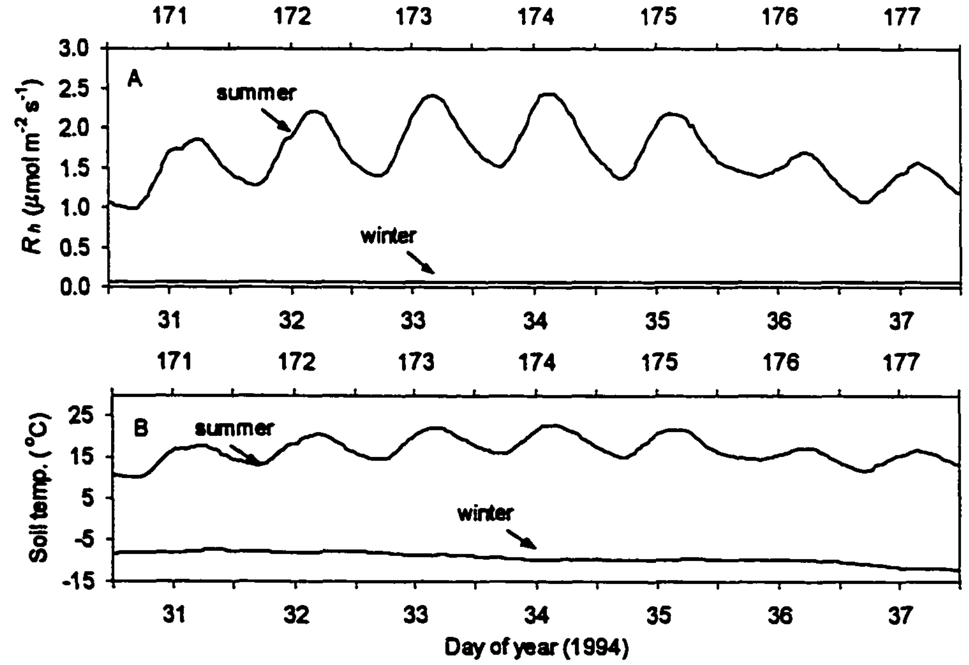

Figure 5.4 Diurnal changes of simulated heterotrophic respiration in winter and in summer (A), and the corresponding temperatures of the first soil layer (B)

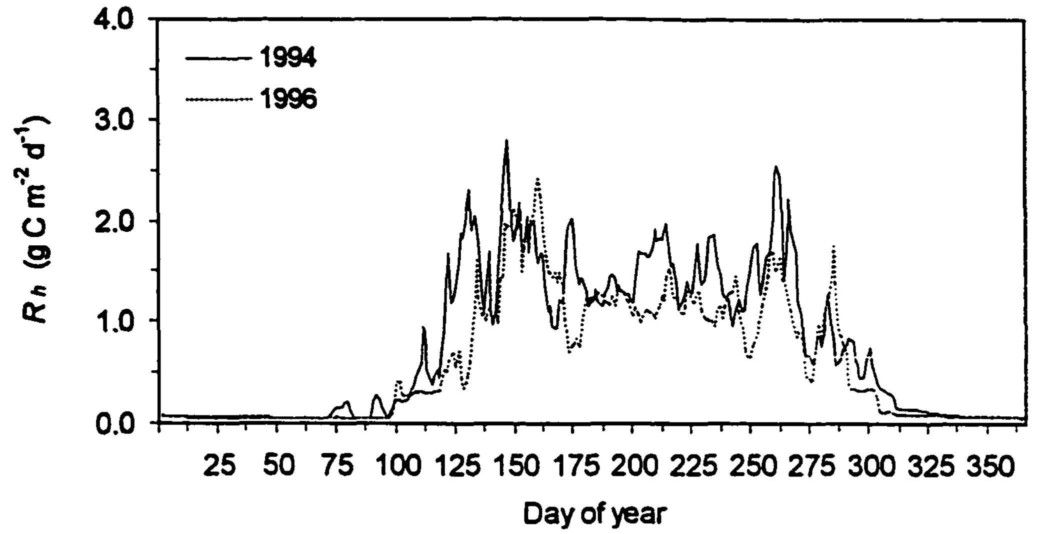

Figure 5.5 Annual courses of simulated daily heterotrophic respiration for 1994 and 1996

significantly delayed during to the late spring. According to the model, the annual courses of R_h at this aspen site were mainly determined by two factors: temperature and litterfall. While R_h from SOM decomposition was mainly controlled by soil temperature, R_h from litterfall decomposition could also be strongly affected by the quantity and quality of the litter pools, namely, extractable, cellulose and lignin. Since most of the litterfall was simulated to occur in September, this caused the significant increase in these three litter pools which contributed to the high R_h values around September. New litterfall produced during the senescence period also enhanced the SOM pools later along the litterfall decomposition in the model, which led to the high R_h values in May.

(2) Below-ground CO_2 Production

Heterotrophic respiration rate is very hard to determine separately from other processes occurring in soil that also produce CO_2 at the field conditions, such as the autotrophic respiration due to the plant root. In order to test the model against the CO_2 flux measurements at the soil surface, I added the simulated root respiration to the R_h in Figure 5.5. Comparisons (Figure 5.6) show that the simulated CO_2 fluxes at the soil surface ($R_h + R_{m,R} + R_{g,R}$; equation 5.9, 4.28 and 4.30, respectively) were only close to the chamber measurements[†] in April through June and in September during the growing period when observations were available. In July and August, however, the simulated values were significantly lower than the measurements. Peak values of CO_2 flux in summer at the soil surface were about 4.2 g C m^{-2} d^{-1} in the model, less than half of the measurements. The magnitude of measured CO_2 fluxes during this time period was similar to the total respiration rate simulated for the ecosystem, which also includes the plant leaf and stem respiration.

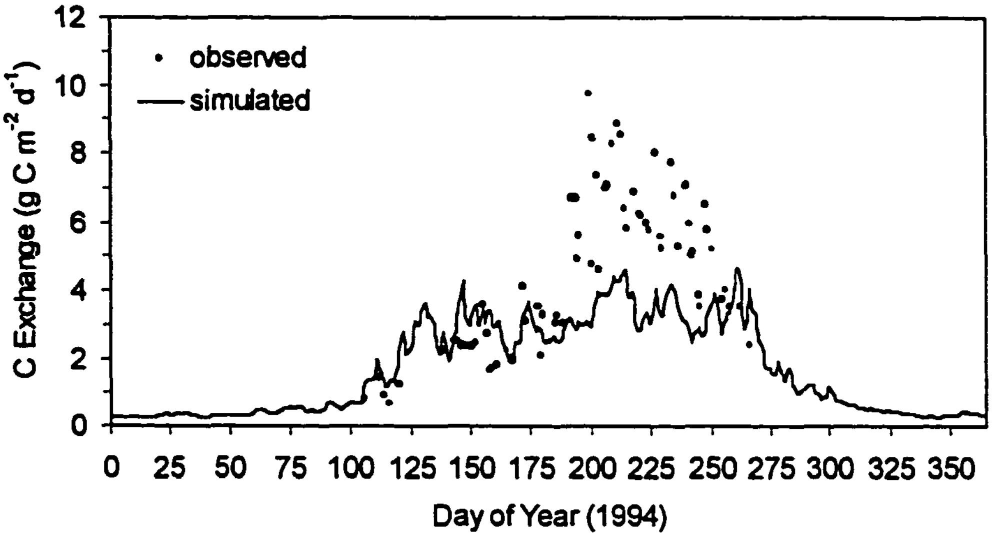

Figure 5.6 Simulated (line) and measured (symbols) annual courses of daily CO_2 fluxes on the soil surface

Comparisons between the chamber measurements and the total ecosystem respiration (soil + hazelnut + aspen) were also made by Black *et al.* (1996). It was found that in April through June the chamber measurements were less than the total ecosystem respiration, while in July and August there were no significant difference between them, which means that the total ecosystem respiration was mainly contributed from soil (including plant root). The model hypothesis is not in agreement with this observational result, since it is assumed that the respiration reactions of plant leaf and stem have the similar intensities with those from plant root and soil. As can be seen from model outputs listed in Table 4.2, the annual totals of the above ground autotrophic respiration had the similar magnitude to the belowground respiration.

[†] Measurements of CO_2 flux at the soil surface were made from soil chambers with a LI-Cor 6200 portable photosynthesis unit. Data are day-time averages of daily observations recorded between 10 a.m. and 4 p.m. local time. This data, considered to be final data, is a joint University of Guelph and University of British Columbia contribution.

The modelled results are similar to the corresponding values of 4.7 g C m^{-2} d^{-1} measured by Schlentner and Van Cleve (1985) from the forest floor of a mature aspen stand in interior Alaska using soda lime to absorb CO_2 that diffused from the soil into a chamber. Baldocchi and Vogel (1996) reported eddy-correlation fluxes approaching 3.5 g C m^{-2} d^{-1} from the forest floors of the oak-hickory-pine forest near Oak Ridge and the old jack pine forest near Nipawin. Amthor (2000) calculated the nighttime CO_2 fluxes from the forest floors of an old black spruce site in the northern study area of BOREAS according to the chamber measurements from Goulden and Crill (1997) (Daytime measurements were excluded because they included moss photosynthesis). It shows the annual peak values were around 3.3 g C m^{-2} d^{-1}. This number is expected to be lower than the actual daily CO_2 productions from soil and plant root because of slightly warmer temperatures during daytime.

(3) CO_2 Exchanges between the Ecosystem and the Atmosphere

CO_2 exchange between the ecosystem and the atmosphere represents the net ecosystem production (*NEP*) and is a key variable in understanding the carbon dynamics of the ecosystem. Instantaneous tower measurements on CO_2 flux above the aspen canopy were measured using eddy correlation technique (see Chapter 2). CO_2 concentration within the canopy space and therefore the storage of CO_2 was also observed and calculated. The sum of tower flux and storage change in each time step – the corrected tower flux, can be used to represent the combined carbon fluxes from both plant and soil. Modelled heterotrophic respiration in soil, together with the autotrophic respiration and photosynthesis simulations for plant implemented in Chapter 4, were integrated and compared with the corrected tower CO_2 flux measurements. Half-hourly comparisons at four different time periods of the year

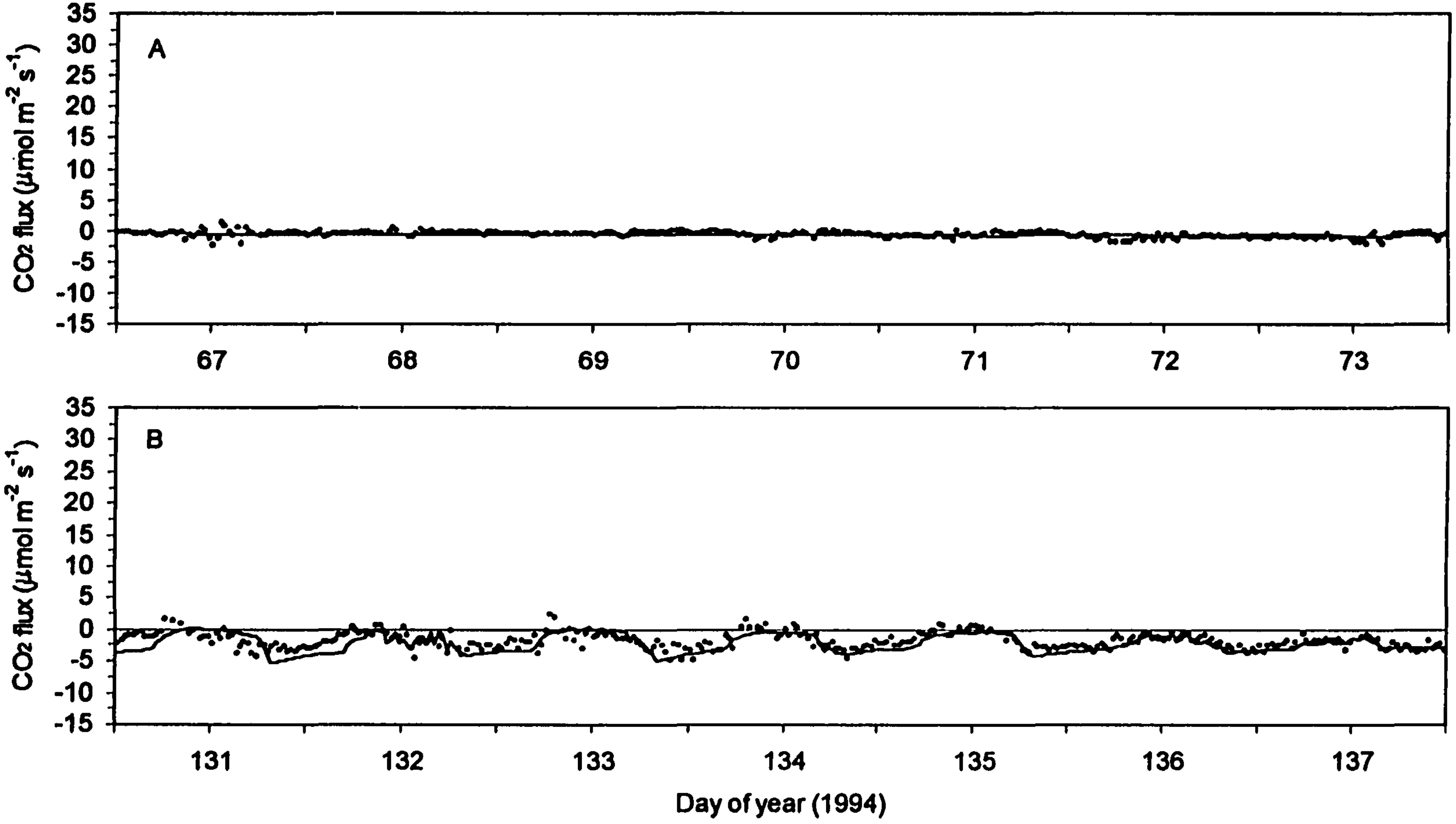

Figure 5.7 Simulated (line) and measured (symbols) half-hourly CO_2 exchanges between ecosystem and the atmosphere in winter (A) and spring (B, about two weeks after leaf emergence)

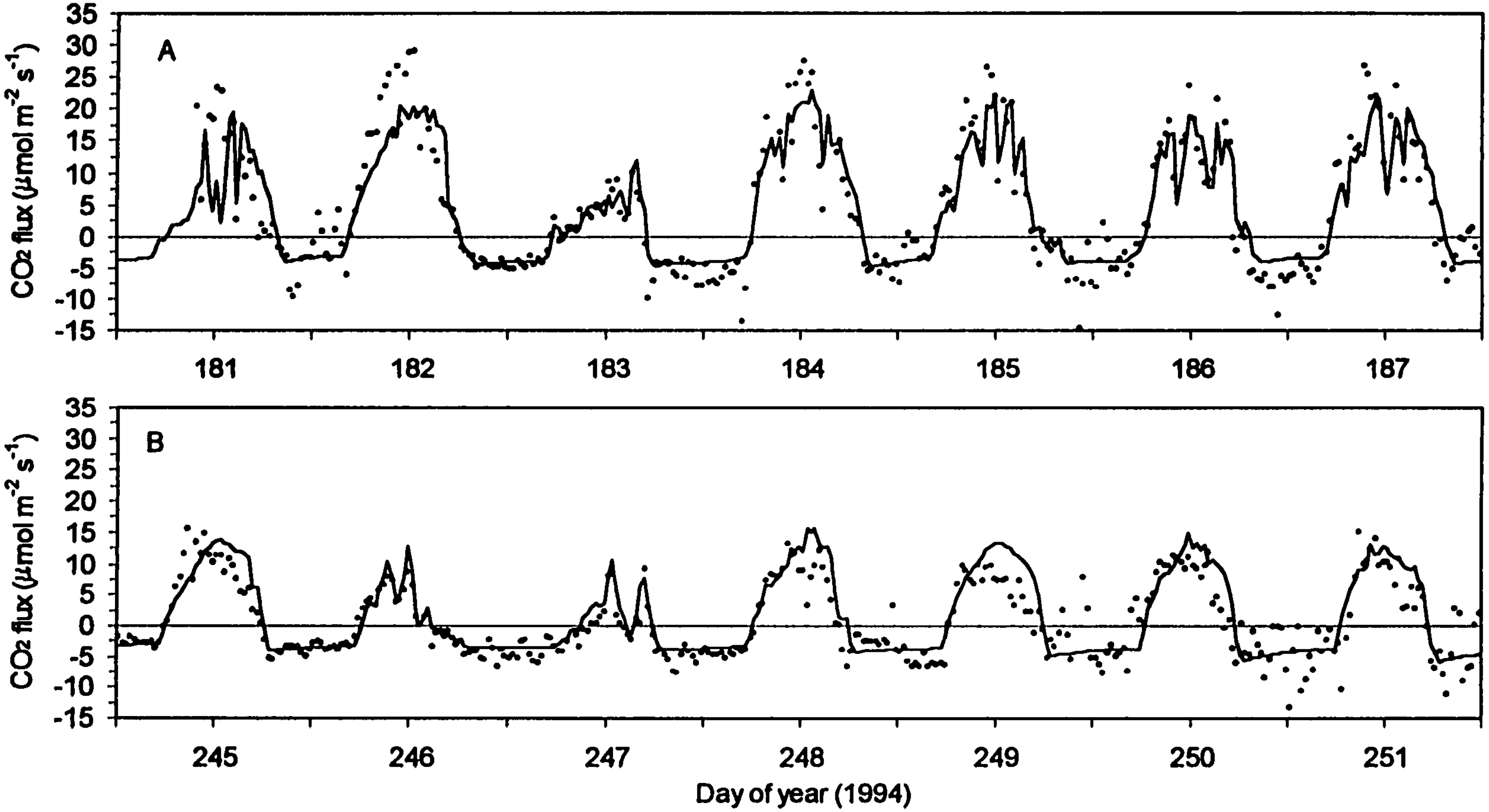

Figure 5.8 Simulated (line) and measured (symbols) half-hourly CO_2 exchanges between ecosystem and the atmosphere in the middle (A) and late (B) growing season

(winter, early, middle, and late growing season) are presented in Figures 5.7 and 5.8. The simulated and observed values at night or during the non-growing season represent the total ecosystem respiration which was the sum of autotrophic respiration by plant (equation 4.31) plus heterotrophic respiration from soil (equation 5.9). During daytime in the growing season, however, they were the difference between plant gross photosynthesis (equation 4.11) and the total ecosystem respiration.

During wintertime (Figure 5.7A) when there was no plant CO_2 fixation, CO_2 flux was negative (upward, representing carbon loss of the ecosystem) with very small numbers. Low soil and air temperatures were the main constraining factors for the low CO_2 flux in winter. Measurements were rather scattered with time when checked at an enlarged scale. There were no apparent patterns of diurnal change in both the measured and modelled CO_2 fluxes due to the stable soil temperature. The simulated CO_2 flux was around -0.57 μmol CO_2 m^{-2} s^{-1} and it was very close to the field measurements. Autotrophic respiration from the plant root was simulated to contribute the largest part in this carbon exchange, followed by that from plant sapwood. R_h from soil took the smallest fraction.

After about two weeks of the leaf emergence, solar radiation had risen to a very high value of above 800 W m^{-2} on clear days. Air temperature also increased to above 10°C during the daytime (see Figure 3.4). Both autotrophic respiration and heterotrophic respiration were greatly increased at this time. Plant photosynthesis had started, however, due to the small leaf area index and relatively low air temperature, the total canopy photosynthesis rate was low. As a result, both the measured and modelled CO_2 exchanges between the ecosystem and the atmosphere (Figure 5.7B) began to show diurnal changes and they were much more negative compared with those in wintertime, indicating an increased rate of carbon loss of the ecosystem. At night, CO_2 efflux was about eight times higher than the winter season, implying the increased plant maintenance respiration and soil heterotrophic respiration due to the increased air and soil temperatures and by the addition of plant growth respiration. CO_2 flux values became less negative during daytime due to the photosynthetic C fixation of the canopy, however, it was still less than the total ecosystem CO_2 production, even around noontime when V_c reached its maximum rate.

In the mid-growing season when the plant was of the largest leaf area, CO_2 exchanges between the ecosystem and the atmosphere can be characterized by the apparent diurnal fluctuations and large positive (downward) CO_2 fluxes during the daytime (Figure 5.8A). Temperature and water vapor pressure at this time (see Figure 3.6) were higher than that in the early growing season. Solar radiation on clear days still reached above 800 W m^{-2}. Favorable environmental conditions and large plant leaf area during this period of time led to the high canopy photosynthetic rate and thus high CO_2 influx to the ecosystem during daytime. Peak values of CO_2 influx under good weather conditions were simulated to exceed 20 μmol CO_2 m^{-2} s^{-1} (*e.g.*, day 182, 184, 185 and 187). Under cloudy weather conditions such as day 183, CO_2 influx was greatly decreased during the daytime due to the reduction in solar radiation. CO_2 exchange rates during nighttime remained around 4 μmol CO_2 m^{-2} s^{-1} in the model. It can be seen that the simulated results matched the measurements very well, both in amplitude and phase, or under different weather conditions.

Similar diurnal patterns in the ecosystem CO_2 flux can be found in the late growing season as represented by the measured and modelled results on day 245 – 251 (Figure 5.8B). However, the magnitudes of CO_2 flux during daytime had been significantly decreased compared with those in the mid-growing season. Peak values for CO_2 influx were simulated below 15 μmol CO_2 m^{-2} s^{-1} even under clear weather conditions (*e.g.*, day 245 and 248 – 251). This was mainly caused by the decrease in solar radiation and plant leaf area. Maximum intensity of solar radiation during this time period was observed around 700 W m^{-2} on clear days (see Figure 3.8). Plant leaf area index was simulated under 4.0 (see Figure 4.10). CO_2 flux at night had the similar magnitude with those in the mid-growing season, but with longer duration. As a result, the net carbon gain of the ecosystem was significantly decreased.

Unlike the bell shape of CO_2 influx during daytime, CO_2 efflux at night was rather stable, with a slight decrease from after sunset until photosynthesis began the next morning. This is because at daytime, the dominant component in *NEP* is the plant gross photosynthesis, which is mainly driven by the shortwave solar radiation and affected by the air temperature. Both the radiation and temperature posses the bell shapes during daytime, particularly under clear weather conditions. While at night, both air and soil temperatures decrease with time, which cause the plant maintenance respiration and soil heterotrophic respiration to decrease. Plant growth respiration rate also decreases with time at night, because the substrate C concentration in plant tissues is higher during early night due to daytime accumulation of photosynthesis and thus makes the tissue growth rates relatively high.

Scattering of the observed CO_2 fluxes and the discrepancies between measurements and simulations are probably a result of several factors. The magnitude of CO_2 flux during wintertime is quite small. Instrument noise and calibration errors may significantly affect the observation readings. Advection due to the site heterogeneity and other factors can also affect the representativeness of the measurements for the specific site. In addition, the comparisons between the corrected tower CO_2 flux measurements and the simulated CO_2 results can be affected by the CO_2 buffering in soil. The transport processes of CO_2 produced in soil by plant root and microbial respiration to the atmosphere can occur in both liquid and gas phases, and it can be affected by factors such as air temperature, soil temperature, and water content, etc. (Buyanovsky and Wagner, 1983; Buyanovsky *et al.*, 1986). Studies on the process-based simulations of CO_2 transport in soil can be found in Šimūnek and Suarez (1993a, 1993b). Considering that this process has limited significance in land surface models and climate change studies, I did not include any calculations on the CO_2 diffusion processes in soil. Therefore CO_2 production in a time step was treated the same as CO_2 efflux in the model. This approximation can cause discrepancies between tower measurements and the model outputs, particularly when comparing them in short time steps and when the magnitude of CO_2 production is small such as in the wintertime.

Comparisons based on the daily values[†] (24-h) of CO_2 exchange in 1994 and 1996 are given in Figure 5.9. It can be seen that the simulated annual courses of ecosystem carbon exchange successfully traced the general changing patterns of the measurements. The ecosystem reached its highest carbon sequestration rates around July, when LAI was high and climate conditions were favorable. The daily average CO_2 exchange in July was simulated at 4.87 g C m^{-2} d^{-1} in 1994 and 4.92 g C m^{-2} d^{-1} in 1996. Fluctuations of CO_2 exchanges in summer among different days were very significant and mainly due to the change in weather conditions. The maximum daily net CO_2 influxes into the ecosystem was simulated as high as 7.54 g C m^{-2} d^{-1} in 1994 and 6.85 g C m^{-2} d^{-1} in 1996. On the other hand, the minimum daily net CO_2 exchange in summer can be negative, such as on the very cloudy day of 183 in 1994 of which the net CO_2 exchange was simulated as -0.25 g C m^{-2} d^{-1}. It means that even during the summer time when plant is in full growth, the ecosystem may still act as a carbon source on a daily basis (24-h) under some extreme weather conditions.

CO_2 exchange of the ecosystem in winter was stable, small and negative (carbon source). The average daily CO_2 exchange for the five winter months from November through March was 0.48 g CO_2 m^{-2} d^{-1}, with 13% contributed by soil heterotrophic respiration and the rest from plant root and sapwood maintenance respiration. There were two peaks in terms of ecosystem carbon loss. These occurred in May and late September and were caused mainly by the high heterotrophic respiration rates. The simulated dates when the ecosystem switched between carbon source and carbon sink were May 25 and September 17 in 1994, and May 26 and September 16 in 1996. The duration for the ecosystem acting as a net carbon sink was therefore one week shorter than the plant net carbon fixation time (see Figure 4.9).

Regression analysis of daily CO_2 exchange between simulated and tower measured was conducted based on the measurements available in 1994 and 1996 (Figure 5.10). There were 243 days in total with complete measurements (48 records

---

[†] Daily values of the observed *NEP* were calculated by integrating the storage corrected tower CO_2 flux for each time step (30 minutes) in a day. Days with any missing observations were not included in the analysis.

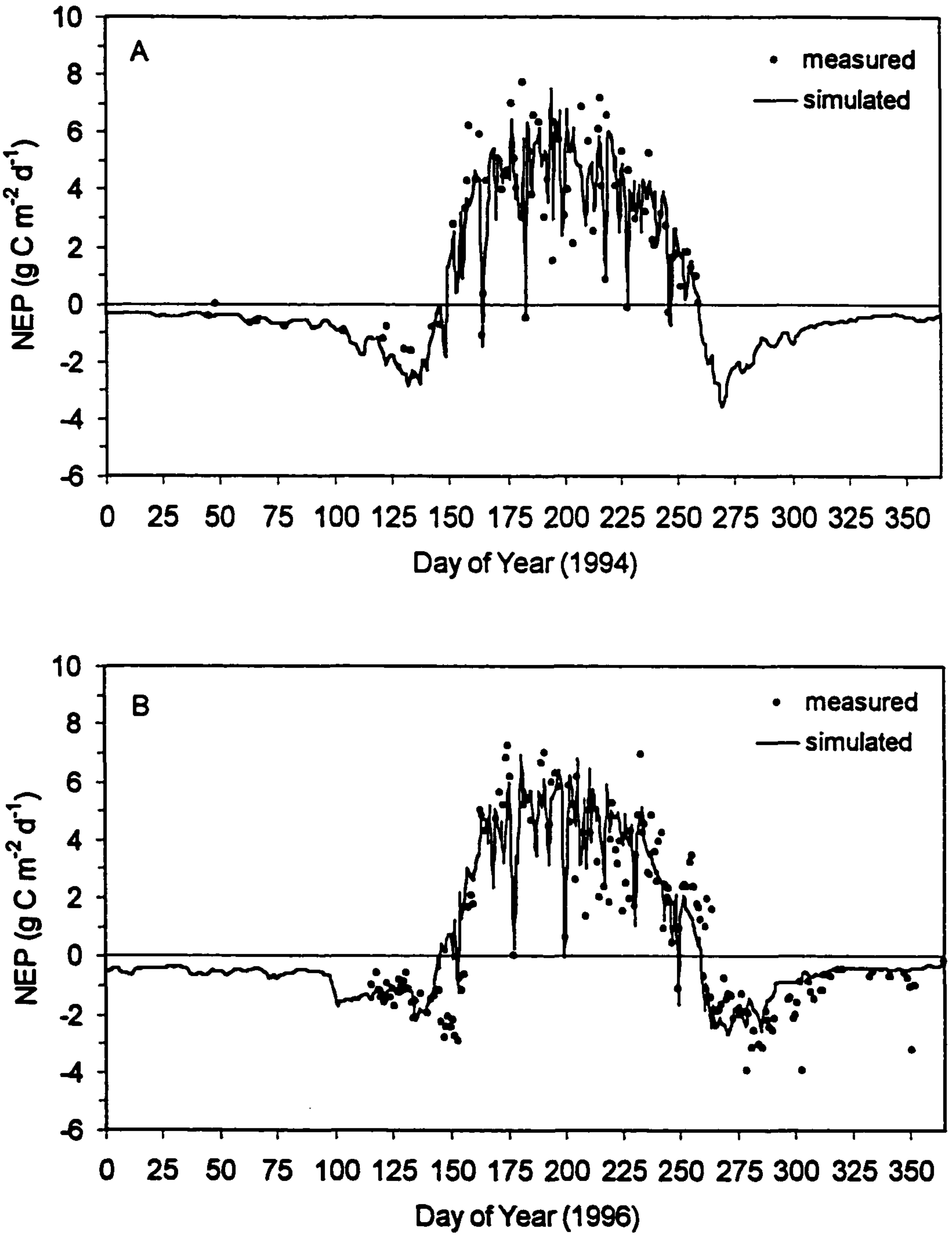

Figure 5.9 Annual courses of simulated (line) and tower measured (symbols) daily CO_2 exchanges between ecosystem and the atmosphere for 1994 and 1996

a day) (74 days in 1994 and 169 days in 1996). A good linear relationship with a correlation coefficient of 0.929 was obtained. The difference of daily means between the simulated (1.73 g C m^{-2} d^{-1}) and observed (1.52 g C m^{-2} d^{-1}) CO_2 exchange was only -0.21 g C m^{-2} d^{-1}. Root mean square error (RMSE) was 1.1 g C m^{-2} d^{-1}.

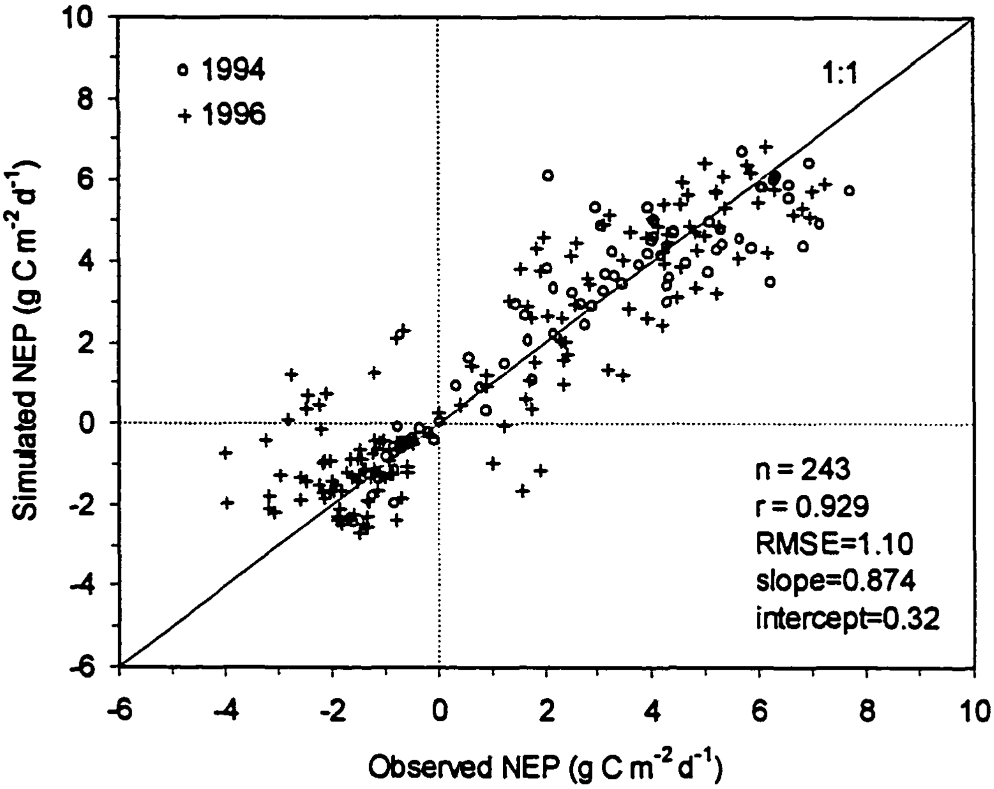

Figure 5.10 Linear regression relationship between simulated and tower measured daily CO_2 exchanges between ecosystem and the atmosphere

(4) Annual Carbon Budgets of the Ecosystem

The overall annual C behaviour of the ecosystem simulated by the model is presented in Figure 5.11 and Table 4.2. R_h represented a small component in the total ecosystem respiration. The annual accumulated amount of R_h was simulated at 280 g C m^{-2} year^{-1} on the average for 1994 and 1996, which was less than half of R_a and about one fourth of the total *GPP* (Table 4.2). Total ecosystem respiration, or the sum of R_a and R_h, was 940 g C m^{-2} year^{-1} for 1994 and 888 g C m^{-2} year^{-1} for 1996 in the model. These results were similar with the estimations of 920 g C m^{-2} year^{-1} and 900 g C m^{-2} year^{-1} for 1994 and 1996, respectively, according to Chen *et al.* (1999) based on eddy correlation measurements. On the average, annual C used for ecosystem respiration takes 83% in the model and 85% according to the estimation from flux measurements (Chen *et al.*, 1999) of the total C fixed in photosynthesis.

Annual *NEP* represents the net carbon change of the ecosystem in a year. The model predicted the ecosystem as a net carbon sink for both 1994 and 1996. Based on the meteorological conditions recorded at the tower site of SSA-OA in 1994 and 1996, a net carbon gain of 164 g C m^{-2} year^{-1} and 203 g C m^{-2} year^{-1} were obtained for the two years, respectively, in the model. It is worth noting that though *GPP* simulated for 1996 was 13 g C m^{-2} year^{-1} lower than that for 1994, *NEP* in 1996 was 40 g C m^{-2} year^{-1} more than that in 1994 due to the lower autotrophic respiration and heterotrophic respiration simulated for 1996. *NEP* estimated from flux measurements (Chen *et al.*, 1999) shows that there was a 70 g C m^{-2} year^{-1} decrease in 1996 compared with 1994 which was mainly caused by the 90 g C m^{-2} year^{-1} decrease in *GPP* estimated for 1996. On the average, *NEP* took about 17% of the total *GPP* in the model, which was 15% according to the estimation from flux measurements.

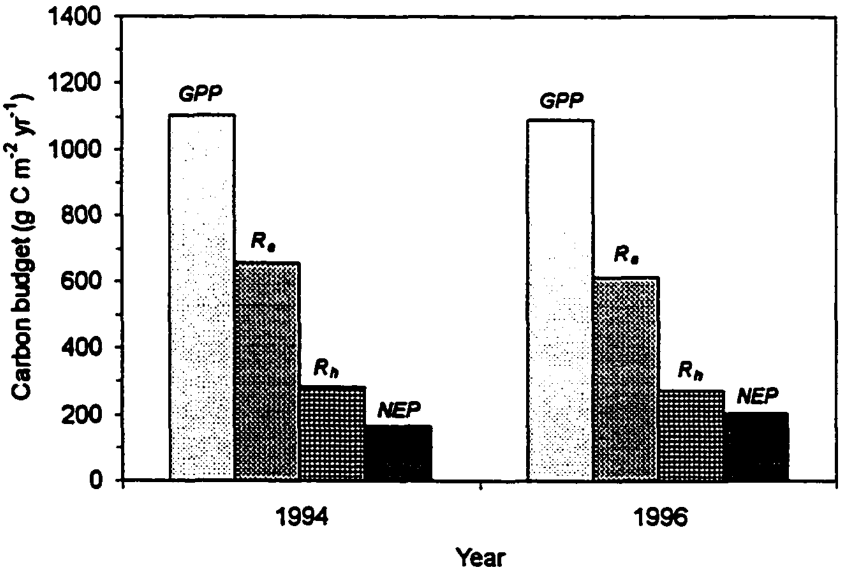

Figure 5.11 Simulated annual carbon budgets for the Old Aspen ecosystem in the Southern Study Area

5.4 Sensitivity Analyses

As the main carbon flux between soil ecosystems and their environment, heterotrophic respiration R_h is reported here as the prognostic variable in the model sensitivity analyses to variations in climate drivers. There were two environmental factors that were in direct control of the R_h rates according to the model (equation 5.7 and 5.9), namely soil temperature and moisture, which can be related to the tested climate drivers of air temperature and precipitation. There were some other processes that can indirectly affect the modelled R_h by changing climate drivers. For example, R_h was accounted for the microbial decomposition of both soil organic matter and the new plant litterfall. While the SOM pool was relatively stable, plant litterfall onto the soil surface from plant foliage and stem and into the soil layers from plant roots could be significantly altered under the variations of climate drivers as discussed in Chapter 4, which would lead to the change of modelled R_h.

Sensitivity test results for R_h was given in Figure 5.12. The model predicted a higher R_h (by 11.3%) under the prescribed T_a + 2°C conditions and a lower R_h (by 19.3%) under the prescribed T_a - 2°C conditions. Compared to the decrease of *GPP* or *NPP* with the lower T_a conditions (see Figure 4.11), the decrease of R_h under lower T_a was relatively small, even though there was a significant decrease in plant litter production. This was probably because of the less impact of N conditions on the microbial decomposition processes compared with those on plant photosynthesis and respiration.

Response of R_h to precipitation variations shows that R_h was more sensitive to the decrease in precipitation. Under the prescribed drier conditions, soil water content became a limiting factor in microbial decomposition sometime during the summer. Combined with the lower *NPP* and plant litterfall under these conditions, an overall decrease of 12.6% in annual R_h was obtained according to the model prediction. The increase of R_h with the prescribed wetter conditions was small, indicating that under the year with a normal amount of rainfall, soil water conditions was not ound to be a strong limiting factor in the microbial decomposition. Another reason for the small

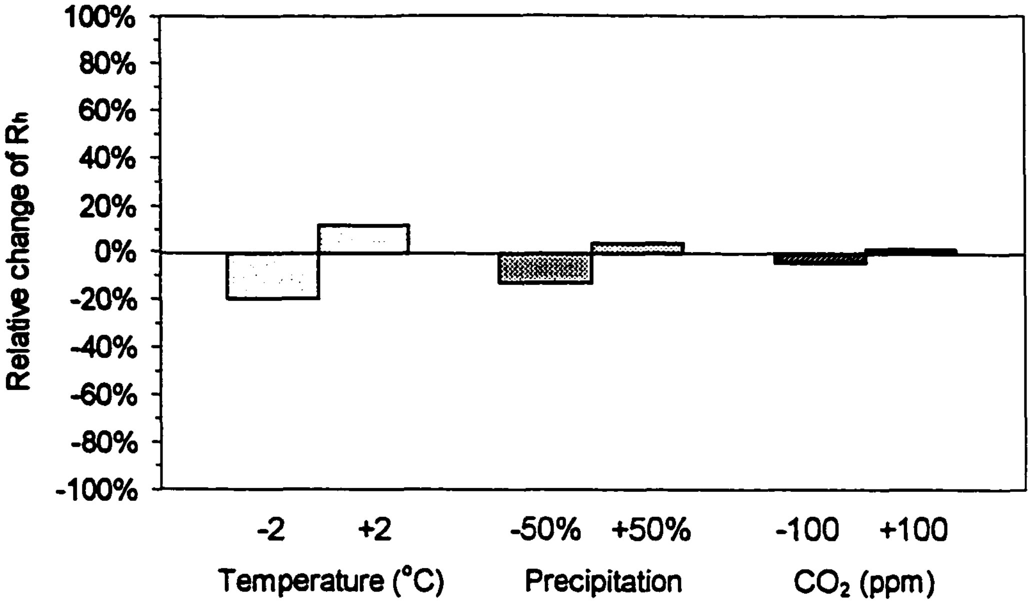

Figure 5.12 Sensitivity of simulated heterotrophic respiration (R_h) to the variations of temperature, precipitation, and CO_2 concentration

response may be due to the higher snowfall during winter, which can delay the time of snowmelt in spring and thus affect the soil temperature profiles.

CO_2 concentration did not directly affect the microbial decomposition processes in the model. However, variations in CO_2 did alter the modelled R_h, which was caused by the changes in plant litter production. Increased *NPP* under elevated CO_2 enhanced the carbon input to the soil from litterfall, and hence increasing R_h. Therefore the modelled sensitivity of R_h to CO_2 variations corresponded to that of *NPP* (see Figure 4.11).

For the overall model sensitivity analyses in terms of carbon exchange, the response of *NEP* to the variations in the three climate drivers was calculated. *NEP* is a secondary measurement derived from several primary carbon fluxes, and hence is more complex to interpret in its causal mechanisms. Because *NEP* by definition represents a small residual of the difference between much larger flux variables (*GPP* - R_a - R_h or *NPP* - R_h), any changes in model inputs that result in major changes in a single component of *NEP*, but not in the other component(s), can result in a comparatively large shift in predicted *NEP*.

Figure 5.13 shows that while a positive response of *NEP* (stronger carbon sink) to warmer (T_a + 2°C) conditions was predicted by the model, a large negative *NEP* response of over 100% was obtained in the model under the cooler (T_a - 2°C) conditions. (The absolute number was -57.1 g C m^{-2} $year^{-1}$). This was mainly due to the larger declines in predicted *NPP* than R_h under the cooler prescriptions (see Figure 4.11 and Figure 5.12). Therefore the ecosystem was simulated as a net carbon source if the temperature was decreased instead of net carbon sink as it was under current temperature conditions. This result is likely supported by the conclusions made from comparing temperature with seasonal variations in the atmospheric CO_2 concentration and isotope analyses, which show that warm years over the northern continents are associated with a net terrestrial carbon sink, while cold years are associated with a net terrestrial carbon source (Keeling *et al.*, 1995; Ciais *et al.*, 1995; Denning *et al.*, 1995).

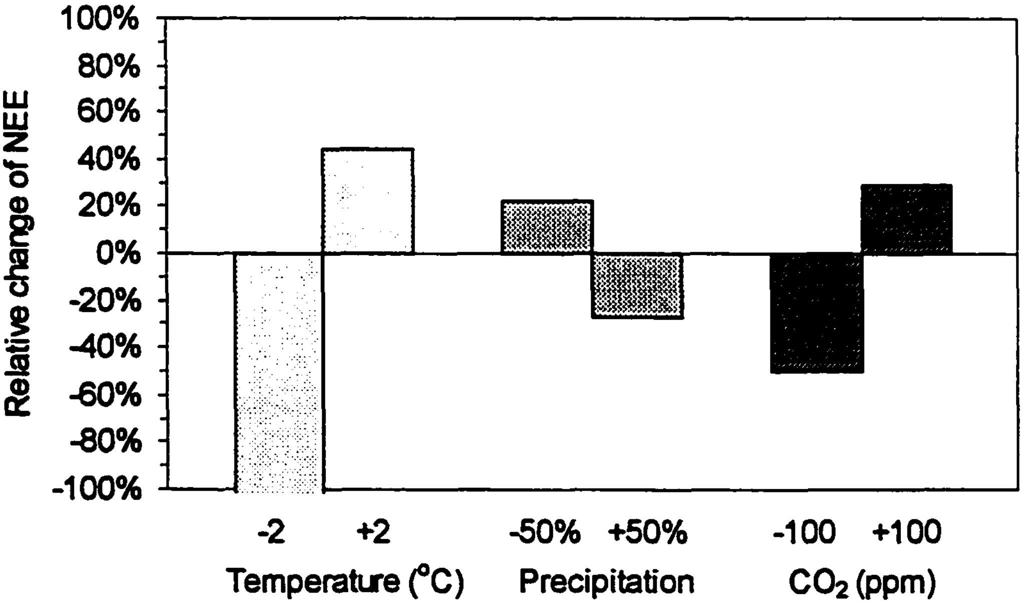

Figure 5.13 Sensitivity of simulated net ecosystem production (NEP) to the variations of temperature, precipitation, and CO_2 concentration

Unlike the response of *NPP* which was decreased under both +50% and -50% precipitation (see Figure 4.11), modelled *NEP* was increased under the drier conditions because of the relatively large decrease in R_h. The response of *NEP* to the variations in CO_2 concentration was with the similar pattern of *NPP*, which shows a decrease (by 49%) under CO_2 - 100 ppm and an increase (by 29%) under CO_2 + 100 ppm. As indicated above, since *NEP* represents a small residue in the carbon flux calculations, its relative change can be high even though the absolute change is small.

It is noteworthy that because of the huge pool size of the SOM and the small *NPP* in this ecosystem, difference in model algorithms for microbial decomposition can strongly affect the simulated *NEP* response (Potter *et al.*, 2000). For example, when models include the impact of oxygen availability as a limiting factor for microbial activity, decomposition may become slower under more saturated soil water conditions. Small changes in R_h may lead to a very different result for *NEP*. In ecosystem modelling studies, soil carbon processes are still very hard to validate against field conditions. Improper parameterization on soil carbon calculations may limit the model applications.

5.5 Conclusions and Discussion

Unlike the soil physical processes such as soil heat and water fluxes which directly affect the land surface processes of energy and water exchange, soil biological and biochemical processes such as the soil organic matter dynamics mainly affect these land surface processes indirectly, *e.g.* through its impacts on soil properties and nutrient conditions. However, soil organic matter dynamics directly interact with the global climate system through greenhouse gas exchanges. Modelled results suggest that for this boreal aspen ecosystem, carbon amount consumed by microbial decomposition took about 60% of annual net primary production. While water was not simulated as a strong limiting factor in the microbial activities, variations in temperature can cause significant change in the turnover rate of soil organic matter. Higher turnover rates brought by increased temperature can accelerate the N release in the organic matter which improves the soil nutrient conditions and thus enhances the plant growth.

Both the direct and indirect impacts of soil organic matter dynamics on the land surface processes and climate happen at a time scale much longer than other processes developed in the model. These slow processes and the complexity in soil organic matter dynamics bring the difficulties for model parameterization and validation. While some parameters and processes in the SOM models can be well validated against laboratory experiments, long term predictions using the models under natural conditions are still problematic. Even with the validation of the model against a long term run (decades or century), problems may still exist because reasonable state variables predicted by the model can also be produced by a set of false rates. This claim can be supported by the fact that in the large number of SOM models published, similar conclusions can be obtained but parameters such as the turnover rate of SOM compartments can be very different. Therefore particular attention should be paid when using the model for extrapolating from current knowledge in both time and space, such as climate change analysis. As indicated by Parton (1996) in a paper entitled "Ecosystem model comparison: Science or fantasy world?" from recent results of SOM model comparison activities: "there are substantial differences among models in predicted ecosystem impacts of altered climatic change scenarios in spite of the fact that the simulated model results are similar for current climatic conditions. These results suggest that there is substantial uncertainty about the ability of ecosystem models to simulate the effect of environmental changes on ecosystem dynamics and that it is risky to use results from only one ecosystem model".

Knowledge about the mechanisms of organic matter transformations in soil and the realistic schemes for soil organic matter fractionation is required for the further improvement in model development. While the multicompartment structure for soil organic matter has been widely accepted in model development, the conceptual pools in the model are artificially made to a great extent. A major limitation of the current multicompartment models of soil organic matter transformation is that most of the conceptual pools they contain do not correspond to the experimentally verifiable fractions (Christensen, 1996). Model design with better matches between the measurable soil organic matter fractions and conceptual pools should enhance the model abilities in both validation and application.

Another line of thinking is the development of another kind of model which is primarily different from the multicompartment models. Since the organic matter components are highly heterogeneous, they should be considered as a continuous distribution of organic materials rather than a set of discrete pools. It also means that the influence of quality on decomposition rate should be a continuous distribution rather than a set of prescribed rate constants for the conceptual pools in the model. Models developed toward this direction have emerged (*e.g.*, Boudreau, 1992; Bosatta and Ågren, 1994; Ågren and Bosatta, 1996). This approach treats organic matter decomposition as both a loss of total carbon as well as a continuous change in litter composition along a quality continuum. It can incorporate both the influence of initial litter composition and the transformation of primary litter compounds into secondary materials and subsequent effects on the overall decomposition rate. As an alternative way in model development, this approach can help to address the shortcomings in the multicompartment models and improve our knowledge on soil organic matter dynamics.

References

Ågren, G.I. and Bosatta, E., 1996. Quality – a bridge between theory and experiment in soil organic matter studies. Oikos, 76: 522-528.

Amthor, J.S., Chen, J.M., Clein, J., Frolking, S.E., Grant, R.F., Kimball, J.S., King, A.W., McGuire, A.D., Nikolov, N.T., Potter, C.S., and Wang, S., 2000. Comparing hourly, daily, monthly, and annual CO_2 and water vapor exchange of a boreal forest predicted by nine ecosystem process models: Model results and relationships to measured fluxes. (to be published)

Baldocchi, D.D., and Vogel, C., 1996. Energy and CO_2 flux densities above and below a temperate broadleaved forest and a boreal pine forest. Tree Physiology, 16: 5-16.

Black, T.A., den Hartog, G., Neumann, H.H., Blanken, P.D., Yang, P.C., Russell, C., Nesic, Z., Lee, X., Chen, S.G., and Staebler, R., 1996. Annual cycles of water vapor and carbon dioxide fluxes in and above a boreal aspen forest. Global Change Biol. 2: 219-229.

Bonan, G.B. and Shugart, H.H., 1989. Environmental factors and ecological process in boreal forests. Annu. Rev. Ecol. Syst., 20: 1-28.

Bosatta, E. and Ågren, G.I., 1994. Theoretical analysis of microbial biomass dynamics in soils. Soil Biology and Biochemistry, 26: 143-148.

Boudreau, B.P., 1992. A kinetic model for microbic organic-matter decomposition in marine sediments. FEMS Microbiology Ecology, 102: 1-14.

Buyanovsky, G.A. and Wagner, G.H., 1983. Annual cycles of carbon dioxide level in soil air. Soil Sci. Soc. Am. J., 47: 1139-1145.

Buyanovsky, G.A., Wagner, G.H., and Gentzer, C.J., 1986. Soil respiration in a winter wheat ecosystem. Soil Sci. Soc. Am. J., 50: 338-344.

Campbell, C.A., 1978. Soil organic carbon, nitrogen, and fertility. p173-272. In: M. Schnitzer and S. U. Khan (ed.), Soil Organic Matter. Elsevier Scientific Publ. Co., Amsterdam.

Chen, W.J., Black, T.A, Yang, P.C., Barr, A.G., Neumann, H.H., Nesic, Z., Blanken, P.D., Novak, M.D., Eley, J., Ketler, R.J., and Cuenca, R., 1999. Effects of climatic variability on the annual carbon sequestration by a boreal aspen forest. Global Change Biology, 5: 41-53.

Christensen, B.T., 1996. Matching measurable soil organic matter fractions with conceptual pools in simulation models of carbon turnover: Revision of model structure. In: Powlson, D.S., Smith, P., and Smith, J.U. (eds.), Evaluation of soil organic matter models using existing long-term datasets. NATO ASI Series, Series I: Global Environmental Change, vol.38.

Ciais, P., Tans, P.P., White, J.W.C., Trolier, M., Francey, R.J., Berry, J.A., Randall, D.R., Sellers, P.J., Collatz, J.G., and Schimel, D.S., 1995. Partitioning of ocean and land uptake of CO_2 as inferred by $\delta^{13}C$ measurements from the NOAA Climate Monitoring and Diagnostics Laboratory Global Air Sampling Network. J. Geophys. Res., 100: 5051-5070.

Denning, A.S., Fung, I., and Randall, D.A., 1995. Strong simulated meridional gradient of atmospheric CO_2 due to seasonal exchange with the terrestrial biota. Nature, 376: 240-243.

Eswaran, H., Van Den Berg, E., and Reich, P., 1993. Organic carbon in soils of the world. Soil Science Society of America Journal, 57: 192-194.

Goulden, M.L., and Crill, P.M., 1997. Automated measurements of CO_2 exchange at the moss surface of a black spruce forest. Tree Physiology, 17: 537-542.

Hunt, H.W., 1977. A simulation model for decomposition in grasslands. Ecology, 58: 469-484.

IPCC, 1995. Climate Change 1994. Radiative Forcing of Climate Change and An Evaluation of the IPCC IS92 Emission Scenarios. Intergovernmental Panel on Climate Change. Cambridge University Press, Cambridge, UK.

Jenkinson, D.S., 1990. The turnover of organic carbon and nitrogen in soil. Phil. Trans. Royal Soc. London B, 329: 361-368.

Jenny, H., 1941. Factors of soil formation. McGraw-Hill, New York.

Juma, N.G. and Paul, E.A., 1981. Use of tracers and computer simulation techniques to assess mineralization and immobilization of soil nitrogen. In Simulation of Nitrogen Behaviour of Soil-Plant System - Papers of a workshop models for the behaviour of nitrogen in soil and uptake by plant. Wageningen, the Netherlands, Jan. 28-Feb.1.

Keeling, C.D., Whorff, T.P., Wahlen, M., and van der Piicht, J., 1995. Interannual extremes in the rate of rise of atmospheric carbon dioxide since 1980. Nature, 375: 666-670.

Kimmins, J.P., 1997. Forest Ecology: A foundation for sustainable management. Second Edition. Prentice-Hall, Inc., New Jersey.

McKane, R.B., Rastetter, E.B., Mellilo, J.M., Shaver, G.R., Hopkinson, C.S., and Fernandes, D.N., 1995. Effects of global change on carbon storage in tropical forests of South America. Global Biogeochemical Cycle, 9: 329-350.

McGill, W.B., Hunt, H.W., Woodmansee, R.G., and Reuss, J.O., 1981. PHOENIX, a model of the dynamics of carbon and nitrogen in grassland soils. Clark, F.E. and Rosswall, T. (eds): Terrestrial Nitrogen Cycles, Ecol. Bull. (Stockholm) 33: 49-115.

Molina, J.A.E., Clapp, C.E., Shaffer, M.J., Chichester, F.W., and Larson, W.E., 1983. NCSOIL, a model of nitrogen and carbon transformations in soil: Description, calibration and behaviour. Soil Sci. Soc. Am. J., 47: 85-91.

Parton, W.J., 1996. Ecosystem model comparison: science of fantasy world? In: Powlson, D.S., Smith, P., and Smith, J.U. (eds.), Evaluation of soil organic matter models using existing long-term datasets. NATO ASI Series, Series I: Global Environmental Change, vol.38.

Parton, W.J., Schimel, D.S., Cole, C.V., and Ojima, D.S., 1987. Analysis of factors controlling soil organic matter levels in Great Plains grasslands. Soil Sci. Soc. Am. J. 51:1173-1179.

Paustian, K., 1994. Modelling soil biology and biochemical processes for sustainable agriculture research. P 182-193, In: Soil biota management in sustainable farming systems. ZE Pankhurst, BM Doube, VVSR Gupta, and PR Grace (eds.) CSIRO Information Services, Melbourne.

Potter, C., Amthor, J., King, A., Nikolov, N., Chen, J., Frolking, S., Grant, R., Wang, S., Kimball, J., Running, S., McGuire, D., and Clein, J., 2000. Comparison of boreal ecossystem model sensitivity to variability in climate and forest site parameters. (To be published).

Powlson, D.S., Smith, P., and Smith, J.U. (editors), 1996. Evaluation of soil organic matter models. NATO ASI Series. Series I: Global Environmental Change, Vol. 38.

Rastetter, E.B., Ryan, M.G., Shaver, G.R., Melillo, J.M., Nadelhoffer, K.J., Hobbie, J.E., and Aber, J.D., 1991. A general biogeochemical model describing the responses of the C and N cycles in terrestrial ecosystems to changes on CO_2, climate, and N deposition. Tree Physiology, 9: 101-126.

Schlentner, R.E., Van Cleve, K., 1985. Relationship between CO2 evolution from soil, substrate temperature, and substrate moisture in four mature forest types in interior Alaska. Canadian Journal of Forest Research, 15: 97-106.

Schlesinger, W.H., 1991. Biogeochemistry: An analysis of global change. Academic Press Inc., San Diego, 443 p.

Šimůnek J. and Suarez, D.L., 1993a. Modeling of carbon dioxide transport and production in soil. 1. Model development. Water Resources Research, 29: 487-497.

Šimünek J. and Suarez, D.L., 1993b. Modeling of carbon dioxide transport and production in soil. 2. Parameter selection, sensitivity analysis, and comparison of model predictions to field data.

Swift, M.J., Heal, O.W., and Anderson, J.M., 1979. Decomposition in terrestrial ecosystems. Studies in Ecology, 5, p. 220-226. Blackwell, Oxford.

Tans, P.P., Fung, I.Y., and Takahashi, T., 1990. Observational constraints on the global atmospheric CO_2 budget. Science, 247: 1431-1438.

Trofymow, J.A., Preston, C.W., and Prescott, C.E., 1995. Litter quality and its potential effect on decay rates of materials from Canadian forests. Water, Air and Pollution, 82: 215-226.

van Veen, J.A. and Paul, E.A., 1981. Organic C dynamics on grassland soils. I. Background information and computer simulation. Can. J. Soil Sci., 61:185-201.

van Veen, J.A., Ladd, J.N., and Amato, M., 1985. Turnover of carbon and nitrogen through the microbial biomass in a sandy loam and a clay soil incubated with $[^{14}C(U)]$glucose and $[^{15}N](NH_4)_2SO_4$ under different moisture regimes. Soil Biol. Biochem., 17: 747-756.

Verberne, E.L.J., Hassink, J., de Willigen, P., Groot, J.J.R., and van Veen, J.A., 1990. Modelling organic matter dynamics in different soils. Netherland Journal of Agricultural Science, 38: 221-238.

Chapter 6 General Conclusions and Discussion

With the three modules described in detail in the previous three chapters, the energy balance and water simulations in the CLASS model have been improved by changing the original algorithms which were determined by the prescribed vegetation processes to those that are determined by plant self-constrained processes. CLASS has also been enhanced to include CO_2 flux between land surfaces and the atmosphere through implementing carbon and nitrogen dynamics in terrestrial ecosystems. Therefore CLASS has been upgraded to a version with fully coupled water and carbon dynamics which are proposed for developing the third-generation land surface schemes (Sellers et al., 1997).

Model behavior was studied when it was parameterized for deciduous trees which is one of the four broad vegetation groups (needleleaf trees, broadleaf trees, crops, and grass) recognized in CLASS. Meteorological variables recorded at SSA-OA of BOREAS in 1994 and 1996 were used to drive the model. Analyses of model predictions included energy balance, plant water relations, stomatal resistance, plant carbon exchange, soil carbon exchange, and ecosystem carbon budgets. These model outputs were compared with the corresponding measurements and estimations implemented by the scientific research groups of BOREAS at the SSA-OA site. In addition, model sensitivities of evapotranspiration, gross primary production, net primary production, autotrophic respiration, heterotrophic respiration, and net ecosystem carbon exchange to the variations of air temperature, precipitation, and atmospheric CO_2 concentration were also investigated.

Strategy for parameterization is determined by the modelling purpose. Since CLASS was developed for the global climate studies by coupling with GCMs, I tried to parameterize the model in this thesis research generally to a functional vegetation type of deciduous trees rather than focusing on some specific features of the particular ecosystem. Most of the parameters adopted in the model, as listed in Table 3.1, 4.1 and 5.1, were from corresponding investigations that are independent of the model used datasets. This independent parameterization strategy is important for modelling studies focused on extended applications. Parameters reveal the relationships between/among processes and they represent our knowledge of these processes. While some parameters in the model have been extensively tested by researchers and/or have solid physical background, some others are still quite empirical or limited by our understandings on the physical relationships. Optimization of parameters is always one of the main efforts for modelling studies and it can only be obtained from the improvement of our knowledge and understandings on the physical principles.

Energy partitioning between sensible and latent heat is the main concern in land surface schemes and the most important feedbacks to GCMs that can determine the simulated climate conditions. Tower measurements by the eddy correlation technique show that a seasonal shifting in energy partitioning between sensible and latent heat occurred as a function of the leaf development of the canopy (Blanken *et al.*, 1997). This seasonal change was successfully reproduced by the model (see Figure 3.3, 3.5 and 3.7) which showed that in the early growing season when the plant leaf area index (*LAI*) was small, most of the radiative energy received by the ecosystem was dissipated as sensible heat, and later when *LAI* grew high, most energy was dissipated as latent heat. Unlike radiation simulation which is of solid physical laws and has less parameters, water flow and evapotranspiration processes in the soil-plant-atmosphere system are much more complicated. Knowledge of some parameters (e.g. root and stem hydraulic resistance) and processes is still quite limited. Comparisons between modelled and tower measured daily evapotranspiration showed that the annual RMSE and linear correlation coefficient were 0.71 mm H_2O day^{-1} and 0.87, respectively. Compared with other model publications, this correlation is quite good with respect to water simulations on an annual basis, implying the success of implementing Ball-Berry method and the soil-plant water transfer dynamics in the land surface scheme. Even though, there are still about one-fourth in the variations of measured evapotranspiration needed to be explained by the model.

Further model development may include addressing the water vapor transport processes within canopy which affect the transpiration of underlying leaves and the evaporation of the ground surface. Another point for further model improvement in CLASS is the snow sublimation calculations under the "wood canopy" in winter. It was found that simulated water exchanges in winter brought significant amount of errors in the overall model evaluations. This part was not addressed in this research.

After CLASS was modified by the three modules, C dynamics in plant and in soil provide the basis for the energy and water calculations on the vegetated land surfaces. C influx by plant gross photosynthesis, or *GPP* of the ecosystem, plays the key roles in determining the canopy stomatal resistance, vegetation parameters such as the plant leaf area index, C and N transformations in soil through plant litterfall, and the overall C budgets of the ecosystem. Simulated annual *GPP* for this OA site in 1994 and 1996 was 1097 g C m^{-2} $year^{-1}$ on the average, which was close to the corresponding estimation of 1075 ± 60 g C m^{-2} $year^{-1}$ based on the eddy correlation measurements (Chen *et al.*, 1999). This result supported the Farquhar theory of leaf carbon fixation and the separating and scaling schemes of sunlit and shaded leaves. Daily *GPP* changed significantly, either due to the seasonal distributions or the short-term variations in weather conditions. Highest *GPP* occurred around July. Maximum daily *GPP* under good weather conditions reached above 12 g C m^{-2} day^{-1}. Solar radiation and air temperature were the most important environmental factors in determining the *GPP* of this old aspen ecosystem. Another factor that had significant effect on the annual accumulated *GPP* was the phenological index which controlled the growth length of plants. The measured annual *GPP* in 1996 was 90 g C m^{-2} less than that in 1994 which can be largely attributed to the cold spring in 1996 that led to a significant delay of about 20 days in leaf emergence. The evaluation of phenological progress in CLASS is still very simple. It failed to reproduce the difference in leaf emergence time between 1994 and 1996. As a result, simulated *GPP* in 1996 was only 13 g C m^{-2} lower than that in 1994. Further studies and refinements on the plant phenology simulations in CLASS are required.

Carbon efflux from ecosystems can be represented by two respiration processes: autotrophic respiration R_a, which was separated into plant growth respiration R_g and maintenance respiration R_m in the model, and heterotrophic respiration R_h. Growth respiration was simulated proportional to the plant growth rate. Therefore climate conditions only affected R_g indirectly through altering the growth rates of plants. Maintenance respiration, however, was strongly temperature dependent following the Q_{10} functions (equation 4.29). Temperature increase in summer thus greatly increased the plant carbon consumption. Heterotrophic respiration was strongly affected by both litterfall availability and environmental conditions such as soil temperature. Heterotrophic respiration was simulated lower than autotrophic respiration year round. This low heterotrophic respiration led to the large amount of organic matter accumulated in the soil ecosystem. Overall, of the 1097 g C m^{-2} total annual carbon influx (*GPP*) at this old aspen site, more than one half was consumed by plant autotrophic respiration and about one-fourth was consumed by microbial heterotrophic respiration in the model (see Table 4.2). These results from the model are close to the corresponding values estimated from field measurements (Ryan *et al.*, 1997; Chen *et al.*, 1999).

Difference between carbon influx and efflux, or the net ecosystem production *NEP*, represents the carbon source-sink relations of the ecosystem. It plays important roles in global carbon budget and climate changes studies. Since the total respiration (R_a + R_h) consumed much of the carbon fixed in this SSA-OA ecosystem, *NEP* accounted for only a small fraction of the annual *GPP*. According to the meteorological conditions recorded at the old aspen site, the model predicted this ecosystem as a net carbon sink of 164 g C m^{-2} $year^{-1}$ and 203 g C m^{-2} $year^{-1}$ for 1994 and 1996, respectively, which was only 17% of *GPP* on the average. The carbon source-sink relations of the ecosystem changed seasonally. The ecosystem reached its highest carbon sequestration rates around July. Maximum sink strength was simulated at around 7 g C m^{-2} day^{-1}. The ecosystem acted as a carbon source from mid-September through late May, with very low carbon loss rates in winter and two peak values in late September and mid-May. This annual course of net carbon source-sink strength and relations simulated by the model can be supported by the corresponding field measurements (see Figure 5.9). Therefore during only one-third of year did the ecosystem act as a net carbon sink. Comparisons of the model outputs with field measurements show that the RMSE and correlation coefficient between daily *NEP* in the two years were 1.1 g C m^{-2} day^{-1} and 0.93, respectively.

Sensitivity analyses of the model showed that this old aspen ecosystem was very sensitive to the variations in temperature, both in terms of energy balance and carbon dynamics. Decrease in temperature brought significant decrease in both evapotranspiration and carbon flows due to a reduction of physiological and biochemical activities and a shortening of the growing season. This sensitivity to temperature implies that the ecosystem was strongly temperature constrained. Modelled sensitivity to the variations of precipitation was smaller than those to temperature and CO_2 concentration, particularly in the case with increase in precipitation, indicating that this SSA-OA ecosystem was predicted as less constrained by water conditions. Application of model sensitivity results may be limited due to the unrealistic model initializations. For example, CLASS simulates soil layer to a depth of 4.1 m. Water held in this deep soil column could significantly diminish the model response to the prescribed lower precipitation conditions. Neglect of the covariance among driving variables can also cause unrealistic response in the model predictions. For example, more precipitation is often related to low solar radiation and high atmospheric humidity, high temperature is usually related to high solar radiation. While in the model sensitivity analyses, one variable was changed completely independent of other variables. Therefore the impacts of the covariance of variables were not accounted in the sensitivity results. The best way to analyze the model sensitivity to climate change may be coupling the model with GCMs and using the driving variables generated by the GCM model itself.

Compared with other model studies, the revised CLASS model behaves quite well in terms of energy, water and carbon exchange simulations between ecosystem and the atmosphere. Among the nine models that used in a BOREAS carbon model comparison tests, results[†] from CLASS showed the best correlations with the field measurements either on hourly evapotranspiration or on hourly and daily carbon exchanges (Amthor et al., 2000; Potter et al., 2000). This indicates that the strategy on the model algorithms and structure, such as the water transfer scheme in soil-plant system, Ball-Berry model for stomatal simulation, Farquhar model for photosynthesis simulation, Thornley theory for plant carbon and nitrogen dynamics, etc, was a successful choice and implementation.

Land surface schemes coupled with GCMs need to deal with different kinds of vegetation. Different plants may be very different in their physiological mechanisms, such as the photosynthesis pathways between C_3 and C_4 plants. Many of the research components of this thesis have been directed at implementing the algorithms for deciduous trees which is recognized as the second type of vegetation in the CLASS model. While research on model implementations for coniferous trees (the first vegetation type in CLASS) has also been finished but not included in this thesis, further studies on the developments of crop and grass modelling, which are the two other vegetation types, are required to follow.

Another area of interest in the land surface scheme studies is model validation under different climate conditions. It is very often the case that for an ecosystem model only part of the whole suite of algorithms in the model is tested under one specific ecosystem conditions. For example, very dry soil conditions at the SSA-OA site were not simulated to happen very often. Low soil water content can have significant effects on the model behavior, such as on the plant-water relations and on the microbial decomposition. Therefore it is very hard to validate these processes thoroughly in the model under these conditions. Further validations of the algorithms under different climate conditions are imperative to make the model more robust.

[†] Measured datasets from the Old Black Spruce (OBS) site in the Northern Study Area (NSA) of BOREAS were selected for the model comparison tests. Models were initialized, driven and tested by the similar datasets with those of SSA-OA used in this thesis but obtained at the NSA-OBS site.

References

Amthor, J.S., Chen, J.M., Clein, J., Frolking, S.E., Grant, R.F., Kimball, J.S., King, A.W., McGuire, A.D., Nikolov, N.T., Potter, C.S., and Wang, S., 2000. Comparing hourly, daily, monthly, and annual CO_2 and water vapor exchange of a boreal forest predicted by nine ecosystem process models: Model results and relationships to measured fluxes. (to be published)

Blanken, P.D., Black, T.A., Yang, P.C., Neumann, H.H., Nesic, Z., Staebler, R., den Hartog, G., Novak, M.D., and Lee, X., 1997. Energy balance and canopy conductance of a boreal aspen forest: Partitioning overstory and understory components. J. Geophysical Research, 102, No. D24: 28,915-28,927.

Chen, W.J., Black, T.A, Yang, P.C., Barr, A.G., Neumann, H.H., Nesic, Z., Blanken, P.D., Novak, M.D., Eley, J., Ketler, R.J., and Cuenca, R., 1999. Effects of climatic variability on the annual carbon sequestration by a boreal aspen forest. Global Change Biology, 5: 41-53.

Potter, C., Amthor, J., King, A., Nikolov, N., Chen, J., Frolking, S., Grant, R., Wang, S., Kimball, J., Running, S., McGuire, D., and Clein, J., 2000. Comparison of boreal ecosystem model sensitivity to variability in climate and forest site parameters. (To be published).

Ryan, M.G., Lavigne, M.B., and Gower, S.T., 1997. Annual carbon cost of autotrophic respiration in boreal forest ecosystems in relation to species and climate. Journal of Geophysical Research, 102, NO. D24: 28,871-28,883.

Sellers, P.J., Dickinson, R.E., Randall, D.A., Betts, A.K., Hall, F.G., Berry, J.A., Collatz, G.J., Denning, A.S., Mooney, H.A., Nobre, C.A., Sato, N., Field, C.B., and Henderson_Sellers, A., 1997b. Modeling the exchanges of energy, water, and carbon between continents and the atmosphere. Science, 275: 502-509.

Appendixes

A. Controlling Equations for the State Variables in the *PLANTC* Module

$$dC_{L,F}/dt = V_C - R_{g,F} - R_{m,F} - G_F^C - L_{L,F}^C - T_{F,S}^C$$

$$dC_{L,S}/dt = T_{F,S}^C - R_{g,S} - R_{m,S} - G_S^C - L_{L,S}^C - T_{S,R}^C$$

$$dC_{L,R}/dt = T_{S,R}^C - R_{g,R} - R_{m,R} - \sum_{i=1}^{IG} G_{R,i}^C - L_{L,R}^C - \sum_{i=1}^{IG} X_{C,i}$$

$$dC_{S,F}/dt = G_F^C - L_{S,F}^C$$

$$dC_{S,S}/dt = G_S^C - L_{S,S}^C - G_H^C$$

$$dC_{S,R}/dt = G_R^C - L_{S,R}^C$$

$$dC_{S,H}/dt = G_H^C - L_{S,H}^C$$

$$dN_{L,F}/dt = T_{S,F}^N - G_F^N - L_{L,F}^N - t_{L,F}^N$$

$$dN_{L,S}/dt = T_{R,S}^N - G_S^N - L_{L,S}^N - T_{S,F}^N + t_{L,F}^N + t_{S,F}^N + t_{L,R}^N + \sum_{i=1}^{IG} t_{S,R,i}^N + t_{S,S}^N$$

$$dN_{L,R}/dt = Q_N - \sum_{i=1}^{IG} G_{R,i}^N - T_{R,S}^N - L_{L,R}^N - t_{L,R}^N$$

$$dN_{S,F}/dt = G_F^N - L_{S,F}^N - t_{S,F}^N$$

$$dN_{S,S}/dt = G_S^N - L_{S,S}^N - G_H^N - t_{S,S}^N$$

$$dN_{S,R,i}/dt = G_{R,i}^N - L_{S,R,i}^N - t_{S,R,i}^N$$

$$dN_{S,H}/dt = G_H^N - L_{S,H}^N$$

B Controlling Equations for the State Variables in the *SOILC* Module

$dC_{E,i}/dt = F^C_{E,F} + F^C_{E,S} + F^C_{E,R,i} - D^C_{E,i}$

For $i = 0, 1, 2, 3$; if $i = 0$, $F^C_{E,R,i} = 0$; if $i = 1, 2, 3$, $F^C_{E,F} = F^C_{E,S} = 0$

$dC_{C,i}/dt = F^C_{C,F} + F^C_{C,S} + F^C_{C,R,i} - D^C_{C,i}$

For $i = 0, 1, 2, 3$; if $i = 0$, $F^C_{C,R,i} = 0$; if $i = 1, 2, 3$, $F^C_{C,F} = F^C_{C,S} = 0$

$dC_{L,i}/dt = F^C_{L,F} + F^C_{L,S} + F^C_{L,R,i} - D^C_{L,i} - T^C_{LS,i}$

For $i = 0, 1, 2, 3$; if $i = 0$, $F^C_{L,R,i} = 0$; if $i = 1, 2, 3$, $F^C_{L,F} = F^C_{L,S} = 0$

$dC_{A,i}/dt = T^C_{MA,i} - D^C_{A,i}$

For $i = 1, 2, 3$; if $i = 1$, $T^C_{MA,1} = T^C_{MA,0} + T^C_{MA,1}$

$dC_{S,i}/dt = T^C_{MS,i} + T^C_{LS,i} - D^C_{S,i} - T^C_{SH,i}$

For $i = 1, 2, 3$; if $i = 1$, $T^C_{MS,1} = T^C_{MS,0} + T^C_{MS,1}$, and $T^C_{LS,1} = T^C_{LS,0} + T^C_{LS,1}$

$dC_{H,i}/dt = T^C_{SH,i} - D^C_{H,i}$

For $i = 1, 2, 3$

$dC_{M,i}/dt = G^C_{M,i} - D^C_{M,i}$

For $i = 0, 1, 2, 3$; $G^C_{M,0} = \sum_{Y} \beta_Y D^C_Y$, (if $i = 0$, $Y = E, C, L$; if $i = 1, 2, 3$, $Y = E, C, L, A, S, H$)

$dN_{E,i}/dt = F^N_{E,F} + F^N_{E,S} + F^N_{E,R,i} - D^N_{E,i}$

For $i = 0, 1, 2, 3$; if $i = 0$, $F^N_{E,R,i} = 0$; if $i = 1, 2, 3$, $F^N_{E,F} = F^N_{E,S} = 0$

$dN_{C,i}/dt = F^N_{C,F} + F^N_{C,S} + F^N_{E,R,i} - D^N_{C,i}$

For $i = 0, 1, 2, 3$; if $i = 0$, $F^N_{C,R,i} = 0$; if $i = 1, 2, 3$, $F^N_{C,F} = F^N_{C,S} = 0$

$dN_{L,i}/dt = F^N_{L,F} + F^N_{L,S} + F^N_{L,R,i} - D^N_{L,i} - T^C_{LS,i}/\alpha_L$

For $i = 0, 1, 2, 3$; if $i = 0$, $F^N_{L,R,i} = 0$; if $i = 1, 2, 3$, $F^N_{L,F} = F^N_{L,S} = 0$

$dN_{A,i}/dt = D^C_{M,i}/\alpha_M - T^C_{MS,i}/\alpha_S - D^N_{A,i}$

For $i = 1, 2, 3$; if $i = 1$, $D^{C}_{M,1} = D^{C}_{M,0} + D^{C}_{M,1}$, and $T^{C}_{MS,1} = T^{C}_{MS,0} + T^{C}_{MS,1}$

$$dN_{S,i} / dt = T^{C}_{MS,i} / \alpha_S + T^{C}_{LS,i} / \alpha_S - D^{N}_{S,i} - T^{C}_{SH,i} / \alpha_S$$

For $i = 1, 2, 3$; if $i = 1$, $T^{C}_{MS,1} = T^{C}_{MS,0} + T^{C}_{MS,1}$, and $T^{C}_{LS,1} = T^{C}_{LS,0} + T^{C}_{LS,1}$

$$dN_{H,i} / dt = T^{C}_{SH,i} / \alpha_H - D^{N}_{H,i}$$

For $i = 1, 2, 3$

$$dN_{M,i} / dt = G^{N}_{M,i} - D^{N}_{M,i}$$

For $i = 0, 1, 2, 3$

$$dN_{I,i} / dt = D^{N}_{E,i} + D^{N}_{C,i} + D^{N}_{L,i} + D^{N}_{A,i} + D^{N}_{S,i} + D^{N}_{H,i} - T^{C}_{LS,i}(\frac{\alpha_L - \alpha_S}{\alpha_S \alpha_L}) - T^{C}_{SH,i}(\frac{\alpha_S - \alpha_H}{\alpha_H \alpha_S})$$
$$- G^{N}_{M,i} - Q_{N,i} - F_N + I_N - O_N$$

For $i = 0, 1, 2, 3$; if $i = 0$, $D^{N}_{A,i} = D^{N}_{S,i} = D^{N}_{H,i} = Q_N = O_N = 0$,

If $i = 1, 2$, $I_N = O_N = 0$,

If $i = 3$, $I_N = 0$